

**Investigation of BAP1's role in gene regulatory networks and  
epigenetic patterning in Uveal Melanoma**

Inaugural-Dissertation  
to obtain the academic degree  
*Doctor rerum naturalium* (Dr. rer. nat.)

submitted to the Department of Biology, Chemistry, Pharmacy  
of Freie Universität Berlin

by  
**Hasan Ozan Otaş**

Berlin, Germany  
September 2024

This work was conducted in Otto Warburg Laboratory Research Group “Gene Regulation and Systems Biology of Cancer” at the Max Planck Institute for Molecular Genetics under the supervision of Dr. rer. nat. Marie-Laure Yaspo between May 2020 and January 2024.

1<sup>st</sup> reviewer: Dr. rer. nat. Marie-Laure Yaspo

2<sup>nd</sup> reviewer: Prof. Dr. Petra Knaus

Date of defense: 27.01.2025

## Acknowledgments

Firstly, I would like to thank my doctoral supervisor Dr. Marie-Laure Yaspo for her support and contributions to me to accomplish this thesis providing insightful and scientific inputs to the project. I would like to thank my Thesis Advisory Committee (TAC) members Dr. Aydan Bulut-Karslıoğlu and Prof. Dr. Petra Knaus who is also the second reviewer for my thesis in the Institute of Chemistry and Biochemistry at the Department of Biology, Chemistry and Pharmacy of the Freie Universität Berlin.

I would like to express my sincere gratitude to Begüm Özemek-Güner for her contributions to the data analysis part on my project. I am grateful for her friendship, support, and discussions. I would like to extend my thanks to the present and former members of our research group for providing support to conduct my research work. I would like to thank my colleagues Alex, Anika, Chethan, Daniela, Maïa, Mathurin, Wanwan, and all Yaspo lab members.

I thank the Deutscher Akademischer Austauschdienst (DAAD) academic service for its extended funding support during my study. I also want to thank Prof. Dr. Martin Vingron who supported me for extra time to complete my thesis. I thank all MPIMG services including the Sequencing Core Facility and Imaging Facility.

Last but not least, I thank my parents Serpil and Osman, and my sister Gülşah, and her family. It would not have been easy to reach this point without their support, sacrifices, and encouragement. Thank you for being there with me throughout my life, for guiding me on the right path, for your belief in me, and for being supportive of all my decisions. I love you all. I'd love to thank my dear, Doğa. Thank you for being there during the critical phases of my life and for all your support and motivation. I would like to thank everyone including Misket who is involved in this wonderful journey.

I dedicate this thesis to all cancer patients, survivors, and to those who have lost their lives to this disease, all of whom faced the battle with strength, resilience, and never gave up hope.

## **Declaration of Authorship**

I hereby declare that I alone am responsible for the content of my doctoral dissertation and that I have only used the sources or references cited in the dissertation.

Berlin, 30.09.2024

Hasan Ozan Otaş



## Summary

Uveal melanoma (UM) is a challenging cancer which is a rare type of melanoma. It originates from the melanocytes, which bear *GNAQ/GNA11* mutations, localized in the ocular tract, and progress with a high risk of metastasis associated with poor prognosis and limited therapeutic options. When the primary cancer cells metastasize, the median survival is on average twelve months. There are two main UM subtypes differing by their genomic profile and metastatic properties in the literature. UMs with Monosomy 3 (M3) subtype which is characterized by the loss of chromosome 3 and *BAP1* mutation are associated with a worse prognosis. UMs with Disomy 3 (D3) do not show the loss of chromosome 3 yet, they carry mutually exclusive *EIF1AX* or *SF3B1* mutations and exhibit better prognosis. In contrast to the D3 subtype, the underlying reasons why the M3 subtype with *BAP1* mutations are linked to very high metastatic risk within the disease mechanisms are not fully understood. The low tumor mutation burden of UM suggests a contribution of epigenetic components to the disease mechanism. *BAP1* is a member of the Polycomb repressive deubiquitinase (PR-DUB) complex acting as a tumor suppressor and an epigenetic regulator.

Given the relevance of *BAP1* loss in UM, we hypothesized that repatterning in the epigenetic landscape and regulation might be affected by the absence of *BAP1*, causing novel TF interplay that contributes to reprogramming the cells towards malignancy. Thus, we compared the genome-wide patterns in *BAP1* wild-type versus *BAP1* mutant cases. Within this scope, this thesis aims to decipher the altered gene regulation networks investigating the effects of *BAP1* loss in UM. We set out to model *BAP1* loss in UM cell lines to better understand the molecular programs related to the subtype. Then, we investigated the differences between transcriptomic and epigenomic landscapes in an integrative manner. Our findings demonstrated that *BAP1* predominantly binds to active regulatory regions, particularly transcription start sites and enhancers. Its binding influences the chromatin landscape and facilitates interactions with pioneering transcription factors *TFAP2A* and *TFAP2C*, which may contribute to transcriptional reprogramming observed in *BAP1*-deficient UM cells. Furthermore, the loss of *BAP1* leads

to aberrations in the histone landscape, including alterations in H3K4me3, H3K4me1, H3K27ac, and H3K27me3, as well as chromatin remodeling at functional genomic elements, accompanied by changes in chromatin accessibility.

## Zusammenfassung

Das Uveale Melanom (UM) ist eine herausfordernde Krebsart und eine seltene Form des Melanoms. Es entsteht aus Melanozyten, die *GNAQ/GNA11*-Mutationen tragen, welche im Augenbereich lokalisiert sind und sich mit einem hohen Metastasierungsrisiko entwickeln, das mit einer schlechten Prognose und begrenzten therapeutischen Möglichkeiten verbunden ist. Wenn die Primärtumorzellen metastasieren, liegt die mittlere Überlebenszeit im Durchschnitt bei zwölf Monaten. In der Literatur werden zwei Hauptsubtypen des UM beschrieben, die sich durch ihr genomisches Profil und ihre metastatischen Eigenschaften unterscheiden. UMs des Subtyps Monosomie 3 (M3), die durch den Verlust von Chromosom 3 und eine *BAP1*-Mutation gekennzeichnet sind, weisen eine schlechtere Prognose auf. Im Gegensatz dazu zeigen UMs des Subtyps Disomie 3 (D3) keinen Verlust von Chromosom 3, tragen jedoch wechselseitig ausschließende *EIF1AX*- oder *SF3B1*-Mutationen und weisen eine bessere Prognose auf. Im Gegensatz zum D3-Subtyp sind die zugrunde liegenden Mechanismen, warum der M3-Subtyp mit *BAP1*-Mutationen mit einem sehr hohen Metastasierungsrisiko verbunden ist, noch nicht vollständig verstanden. Die niedrige Tumormutationslast von UM deutet auf die Beteiligung epigenetischer Komponenten am Krankheitsmechanismus hin. *BAP1* ist ein Mitglied des Polycomb Repressive Deubiquitinase (PR-DUB)-Komplexes und wirkt als Tumorsuppressor und epigenetischer Regulator.

Angesichts der Relevanz des *BAP1*-Verlustes im UM haben wir die Hypothese aufgestellt, dass Veränderungen in der epigenetischen Landschaft und Regulation durch das Fehlen von *BAP1* beeinflusst werden könnten, was eine neue Interaktion von Transkriptionsfaktoren (TF) verursacht, die zur Umprogrammierung der Zellen in Richtung Malignität beiträgt. Dementsprechend haben wir die genomweiten Muster von *BAP1*-Wildtyp- und *BAP1*-Mutantenfällen verglichen. In diesem Zusammenhang zielt diese Arbeit darauf ab, die veränderten Genregulationsnetzwerke zu entschlüsseln und die Auswirkungen des *BAP1*-Verlustes im UM zu untersuchen. Wir haben den *BAP1*-Verlust in UM-Zelllinien modelliert, um die molekularen Programme, die mit dem Subtyp in Zusammenhang stehen, besser zu verstehen. Anschließend untersuchten wir die

Unterschiede zwischen transkriptomischen und epigenomischen Landschaften auf integrative Weise. Unsere Ergebnisse zeigten, dass BAP1 hauptsächlich an aktiven regulatorischen Regionen, insbesondere an Transkriptionsstartstellen und Enhancern, bindet. Seine Bindung beeinflusst die Chromatinlandschaft und erleichtert die Interaktion mit den pionierhaften Transkriptionsfaktoren TFAP2A und TFAP2C, was zur beobachteten transkriptionellen Umprogrammierung in BAP1-defizienten UM-Zellen beitragen könnte. Darüber hinaus führt der Verlust von BAP1 zu Veränderungen in der Histonlandschaft, einschließlich Veränderungen in H3K4me3, H3K4me1, H3K27ac und H3K27me3, sowie zur Chromatinumgestaltung an funktionellen genomischen Elementen, begleitet von Änderungen in der Chromatinzugänglichkeit.

# Table of Contents

<b>Acknowledgments</b> .....	<b>III</b>
<b>Declaration of Authorship</b> .....	<b>IV</b>
<b>Summary</b> .....	<b>V</b>
<b>Zusammenfassung</b> .....	<b>VII</b>
<b>List of Figures</b> .....	<b>XIV</b>
<b>List of Tables</b> .....	<b>XX</b>
<b>List of Abbreviations and Symbols</b> .....	<b>XXII</b>
<b>Chapter 1: Introduction</b> .....	<b>1</b>
<b>1.1. Cancer genetics and gene expression</b> .....	<b>1</b>
1.1.1. <i>Cancer and malignancy</i> .....	1
1.1.2. <i>Hallmarks of Cancer</i> .....	2
1.1.3. <i>Genetic and epigenetic alterations in cancer</i> .....	3
1.1.3.1. Somatic mutations, oncogenes and tumor suppressor genes.....	4
1.1.3.2. Epigenetic dysregulation.....	7
<b>1.2. The routes to Melanoma</b> .....	<b>15</b>
1.2.1. <i>Melanocytogenesis and functions of the melanocytes</i> .....	15
1.2.2. <i>Process of melanogenesis</i> .....	18
1.2.3. <i>Roles and differences of cutaneous and uveal melanocytes</i> .....	21
1.2.4. <i>Melanoma and variety of its subtypes</i> .....	25
<b>1.3. Uveal Melanoma</b> .....	<b>30</b>
1.3.1. <i>Genetic landscape, somatic mutations, and subtypes of UM</i> .....	34
1.3.1.1. Primary (driver) mutations in the G $\alpha$ q pathway .....	37
1.3.1.2. Secondary mutations .....	39
1.3.1.3. Copy Number Alterations (CNAs) .....	42
1.3.1.4. Evolutionary routes of the tumor.....	46
1.3.2. <i>Transcriptomic and epigenetic features</i> .....	47
1.3.3. <i>BRCA-1 associated protein 1 (BAP1)</i> .....	50
1.3.3.1. <i>BAP1</i> gene and protein structure .....	51
1.3.3.2. Gene regulatory roles of BAP1 in UM.....	51
<b>Chapter 2: Aims</b> .....	<b>54</b>

<b>Chapter 3: Materials and Methods .....</b>	<b>56</b>
<b>3.1. Materials .....</b>	<b>56</b>
3.1.1. <i>Antibodies</i> .....	56
3.1.2. <i>Equipment and chemicals</i> .....	57
3.1.3. <i>Kits</i> .....	60
3.1.4. <i>Plasmids and primers</i> .....	60
<b>3.2. Methods .....</b>	<b>63</b>
3.2.1. <i>Cell Culture</i> .....	63
3.2.2. <i>CRISPR/Cas9 mediated gene knockout</i> .....	64
3.2.2.1. Design of the single guide RNAs .....	64
3.2.2.2. Restriction digestion, UV-free gel extraction, and purification of the plasmid backbone .....	65
3.2.2.3. Molecular cloning of the gRNAs into LentiCRISPRv2GFP backbone .	68
3.2.2.4. Bacterial transformation by electroporation .....	68
3.2.2.5. Bacterial culture .....	69
3.2.2.6. Plasmid DNA purification .....	69
3.2.2.7. Cell transfection and production of lentiviral particles .....	70
3.2.2.8. Lentiviral transduction .....	72
3.2.2.9. Fluorescence Activated Cell Sorting (FACS) .....	72
3.2.3. <i>siRNA-mediated gene knockdown</i> .....	73
3.2.3.1. Preparation of the siRNAs .....	73
3.2.3.2. Cell seeding and reverse transfection of the siRNAs .....	74
3.2.4. <i>Western blot</i> .....	74
3.2.4.1. Sample Preparation .....	74
3.2.4.2. BCA Assay for protein quantification .....	75
3.2.4.3. Protein separation by sodium dodecyl-sulfate polyacrylamide gel electrophoresis (SDS-PAGE) and blotting .....	77
3.2.4.4. Imaging of the membrane .....	78
3.2.5. <i>Immunofluorescence (IF) staining</i> .....	78
3.2.5.1. Coverslip preparation and cell seeding .....	78
3.2.5.2. Formaldehyde fixation .....	78
3.2.5.3. Permeabilization and Blocking .....	79
3.2.5.4. Primary and secondary antibody incubations .....	79
3.2.6. <i>Confocal Microscopy</i> .....	79
3.2.7. <i>Bulk RNA sequencing</i> .....	79
3.2.8. <i>Assay for Transposase-Accessible Chromatin (ATAC) sequencing</i> .....	80
3.2.8.1. Cell sample preparation .....	80
3.2.8.2. Tagmentation reaction and purification .....	81
3.2.8.3. PCR amplification of tagmented DNA .....	82
3.2.9. <i>Chromatin Immunoprecipitation (ChIP) sequencing</i> .....	84

3.2.9.1.	Cell culture cross-linking and sample preparation .....	84
3.2.9.2.	Nuclei preparation and chromatin digestion.....	84
3.2.9.3.	Analysis of chromatin digestion and concentration .....	85
3.2.9.4.	Chromatin Immunoprecipitation .....	85
3.2.9.5.	Elution of chromatin from Antibody/Protein G magnetic beads and reversal of cross-links.....	86
3.2.9.6.	DNA purification using spin columns .....	87
3.2.9.7.	NG-Sequencing library construction .....	87
3.2.10.	<i>Cleavage Under Targets and Release Using Nuclease (CUT&amp;RUN)</i> .....	88
3.2.10.1.	Live Cell Preparation .....	88
3.2.10.2.	Binding of Concanavalin A Beads and Primary Antibody .....	89
3.2.10.3.	Binding of pAG-MNase Enzyme .....	89
3.2.10.4.	DNA Digestion and Diffusion.....	90
3.2.10.5.	Preparation of the Input Sample.....	90
3.2.10.6.	DNA Purification.....	90
3.2.11.	<i>Data Analysis</i> .....	91

## **Chapter 4: Results..... 93**

<b>4.1.</b>	<b>Characterization of the MEL202 cell line as a UM model .....</b>	<b>93</b>
<b>4.2.</b>	<b>Genome-wide binding characteristics of BAP1 in MEL202 cells .....</b>	<b>95</b>
4.2.1.	<i>BAP1 mainly associates with TSS (88%) and enhancer (10%) sites in MEL202 cells .....</i>	<i>96</i>
4.2.2.	<i>BAP1 binding sites are associated with CpG regions, genic regions, and accessible chromatin in MEL202 cells.....</i>	<i>99</i>
<b>4.3.</b>	<b>Strategies for BAP1 loss in MEL202 cells.....</b>	<b>102</b>
4.3.1.	<i>CRISPR/Cas9 knockout strategy for BAP1 gene .....</i>	<i>102</i>
4.3.2.	<i>BAP1 is knocked down via siRNA-mediated strategy .....</i>	<i>104</i>
<b>4.4.</b>	<b>Modification of Gene Expression Profiles upon BAP1 loss in MEL202 cells and UM tumors.....</b>	<b>106</b>
<b>4.5.</b>	<b>Pathway enrichment analysis of the differentially expressed genes and integration with BAP1-binding sites .....</b>	<b>112</b>
4.5.1.	<i>Loss of BAP1 depleted DNA replication and cell cycle-related processes in MEL202 BAP1 KD cells.....</i>	<i>112</i>
4.5.2.	<i>Transcription factor activity, DNA-binding, and cell-adhesion-related processes are enriched upon BAP1 loss .....</i>	<i>116</i>
4.5.3.	<i>Integration of BAP1-binding sites with altered gene expression profiles in MEL202 WT and BAP1-KD cells.....</i>	<i>119</i>
4.5.4.	<i>DNA replication and repair pathways of BAP1-bound genes are suppressed upon BAP1 loss .....</i>	<i>122</i>

4.5.5.	<i>BAP1 loss upregulates BAP1-bound genes related TF activity, cis-regulation, DNA-binding of transcription factors, and RNA polymerase II</i> .....	124
<b>4.6.</b>	<b>Impact of BAP1 loss through enrichment of TF binding motifs for TFAP2 family and DNA methylation in MEL202 cells</b> .....	<b>127</b>
<b>4.7.</b>	<b>Interplay between BAP1 and TFAP2A/TFAP2C pioneering transcription factors in UM</b> .....	<b>133</b>
4.7.1.	<i>Loss of BAP1 changes TFAP2A/TFAP2C occupancies at their target sites</i> ... ..	135
4.7.2.	<i>Modulation of TFAP2A and TFAP2C pioneering TF binding on BAP1-bound genes in UM cells</i> .....	139
4.7.3.	<i>Signature of novel TFAP2C-bound genes stratify UM patients based on BAP1 status</i> .....	143
<b>4.8.</b>	<b>Chromatin accessibility changes in response to BAP1 loss</b> .....	<b>145</b>
4.8.1.	<i>Chromatin accessibility decreases at BAP1-bound TSS and enhancer regions</i> .....	146
4.8.2.	<i>Genome-wide accessibility reductions in Bivalent enhancers following BAP1 loss</i> .....	148
<b>4.9.</b>	<b>Impact of BAP1 loss on genome-wide histone mark landscape</b> .....	<b>150</b>
4.9.1.	<i>H3K27ac: Divergent effects at TSS and enhancers regions</i> .....	150
4.9.2.	<i>H3K4me3: Active mark suppression at promoters and enhancers</i> .....	153
4.9.3.	<i>H3K4me1: Reductions predominantly at enhancer sites</i> .....	157
4.9.4.	<i>H3K27me3: Subtle increases at bivalent promoters</i> .....	159
<b>4.10.</b>	<b>Antagonistic effect of PRC1 member RING1B reveals differential genome-wide occupancy</b> .....	<b>161</b>
<b>Chapter 5: Discussion</b> .....	<b>165</b>	
<b>5.1.</b>	<b>Aim 1: Genome-wide effects of BAP1 loss on gene expression, chromatin accessibility and histone mark profiles in UM cells</b> .....	<b>166</b>
5.1.1.	<i>Modulation of gene expression and transcriptomic programs in BAP1-deficient UM</i> .....	167
5.1.2.	<i>Gene expression changes annotated with BAP1-binding</i> .....	172
5.1.3.	<i>Chromatin accessibility, histone modification landscape and repressive chromatin states</i> .....	173
5.1.4.	<i>Impact on the enhancer subtypes</i> .....	174
<b>5.2.</b>	<b>Aim 2: BAP1 modifies the interplay of TFs in UM</b> .....	<b>175</b>
5.2.1.	<i>Enriched TF binding motifs based on the transcriptional regulation in BAP1-deficient UM cells</i> .....	175
5.2.2.	<i>Altered TFAP2A and TFAP2C binding upon BAP1 loss</i> .....	177



5.2.3.	<i>The role of ELK1 in the BAP1-TFAP2C axis.....</i>	178
5.2.4.	<i>Novel TFAP2C-bound genes and patient stratification .....</i>	179
<b>5.3.</b>	<b>Aim 3: Potential contribution of molecular changes to the disease progression observed in BAP1-mutant UM.....</b>	<b>179</b>
<b>5.4.</b>	<b>Clinical implications and future directions.....</b>	<b>181</b>
<b>5.5.</b>	<b>Conclusions.....</b>	<b>182</b>
<b>Bibliography .....</b>		<b>183</b>
<b>Appendix.....</b>		<b>213</b>

## List of Figures

Figure 1: Updated concept of the emerging hallmarks and enabling characteristics of the cancer. ....	3
Figure 2: Somatic mutations detected by genome-wide sequencing studies in the representative human cancers. ....	5
Figure 3: Epigenetic regulations in cancer. ....	8
Figure 4: Epigenetic changes in cancer. ....	9
Figure 5: Difference of DNA methylation patterns on TSGs between normal and cancerous states. ....	11
Figure 6: Changes in the chromatin structure between normal and cancer cells. ....	13
Figure 7: Overview of the histone modifications. ....	14
Figure 8: Lineage determination of the Melanocytes from the NCCs. ....	17
Figure 9: Melanin biosynthesis pathways in melanocytes during melanogenesis. ....	19
Figure 10: Production of Melanin after UV Exposure in cutaneous melanocytes. ....	20
Figure 11: Formation and maturation stages of a melanosome in a melanocyte. ....	21
Figure 12: UVA and UVB have different penetrances and effects on the skin. ....	22
Figure 13: Anatomy of the eye. ....	23
Figure 14: Multiple anatomical types and the location distributions of melanoma. ....	26
Figure 15: Sites for the UM tumor development. ....	31
Figure 16: Kaplan-Meier curve showing the correlation between the survival rate and the tumor size. ....	32
Figure 17: Comparisons of the somatic mutation profiles ....	35
Figure 18: Driver mutations on <i>GNAQ</i> , <i>GNA11</i> , <i>PLCB4</i> and <i>CYSLTR2</i> genes constitutively activating the $G\alpha q$ pathway and its downstream signal transduction pathways. ....	38
Figure 19: Kaplan-Meier plot of the three groups of UM patients (n=185) with the secondary gene mutations: <i>EIF1AX</i> (n = 33), <i>SF3B1</i> (n = 63), <i>BAP1</i> (n = 89). ....	40
Figure 20: Recurrent copy number alterations (CNAs) based risk groups proposed to define the molecular subtypes for prognostication of UM. ....	43

Figure 21: Chromosomal alterations of a primary UM patient particularly showing M3 and 8q gain.....	45
Figure 22: Proposed order of the mutational and cytogenetic events during the tumor evolution from melanocytes to UM metastasis. ....	47
Figure 23: UM subtype characterization scheme based on DecisionDX-UM gene expression profile classification. ....	49
Figure 24: Structure of BAP1 protein with domains of its interaction partners. ....	51
Figure 25: Summary of the functional and regulatory roles of BAP1.....	52
Figure 26: Impacts of the loss of BAP1 on the chromatin involving altered deposition of H2AK119ub by PRC1. ....	53
Figure 27: Schematic representation for the design of the study (created with BioRender). ....	55
Figure 28: Target sites of the two guides (sgBAP1_1 and sgBAP1_3) on the different locations of exons on the BAP1 gene.....	65
Figure 29: Restriction digestion of LentiCRISPRv2GFP plasmid using SapI and SphI enzymes. ....	66
Figure 30: UV-free gel run of the digested products of LentiCRISPRv2GFP by BsmBI enzyme.....	67
Figure 31: Strategy for the application of the lentiviral transduction system. ....	71
Figure 32: Experimental design of the FACS using lentivirally transduced MEL202 cells. ....	73
Figure 33: Solution colors as a function of pH.....	81
Figure 34: Shortlist of cell line selection based on UM-lineage subtype having BAP1 expression.....	93
Figure 35: Confirmation of the presence and localization of BAP1. ....	94
Figure 36: Overview of the 18 chromatin states based on histone marks, accessibility scores and other genomic features.....	95
Figure 37: Distribution of the BAP1 binding sites throughout the chromatin states. ....	97
Figure 38: Peaks coming from BAP1 binding sites are distributed mainly to the CpG sites. ....	100

Figure 39: BAP1 binds mainly promoter and 5' UTRs (>%90).....	101
Figure 40: 77% of the BAP1 binding sites are accessible. ....	102
Figure 41: Growth of the FACS-sorted monoclonal MEL202 cells in a 96-well plate.....	103
Figure 42: Western blot results showing the BAP1 status of the FACS-sorted monoclonal MEL202 cells with were transduced with either sgBAP1_1 or sgBAP1_3. ....	104
Figure 43: Validation of the BAP1 knockdown experiment with MEL202 cells using (A) Western blot, (B) RNA-seq experiments. ....	105
Figure 44: MA plot showing the differentially ( $ \logFC  > 1$ ) upregulated (red) and downregulated (blue) genes upon BAP1 loss in MEL202 cells. ....	107
Figure 45: Correlation of the DEGs between MEL202 / BAP1 KD conditions (X-axis) and D3 / M3 UM patient cohort (Y-axis).....	109
Figure 46: Expression (TPM) differences of <i>FGF2</i> , <i>GATA4</i> , <i>MIA</i> , <i>RASD1</i> and <i>HTN1</i> genes from MEL202 / BAP1 KD conditions. ....	110
Figure 47: Expression (TPM) differences of <i>RAPGEF4</i> , <i>MAP2</i> , <i>GNAT3</i> and <i>CLIC2</i> genes from MEL202 WT / KD conditions. ....	111
Figure 48: Fold enrichment analysis of the genes in pathways related to GO Biological process.....	113
Figure 49: Fold enrichment analysis of the genes in pathways related to GO Molecular function.....	114
Figure 50: Fold enrichment analysis of the genes in pathways related to GO Cellular component.....	115
Figure 51: Effect of BAP1 knockdown on cell proliferation in MEL202 cells.....	116
Figure 52: Fold enrichment analysis of the genes in pathways related to GO Biological process.....	117
Figure 53: Fold enrichment analysis of the genes in pathways related to GO Molecular function.....	118
Figure 54: Fold enrichment analysis of the genes in pathways related to GO Cellular component.....	119

Figure 55: Sankey diagram shows our filtering strategy for the BAP1-bound DEGs of MEL202 BAP1 WT / BAP1 KD condition. .... 120

Figure 56: Scatter plot shows the BAP1-bound DEGs after BAP1 loss in MEL202 cells. .... 121

Figure 57: GO Molecular function pathway enrichment analysis of the differentially downregulated genes (which were annotated with BAP1-binding in MEL202 WT condition). .... 122

Figure 58: Network of the enriched gene clusters (annotated with BAP1-binding in MEL202 WT condition) downregulated after BAP1 loss. .... 123

Figure 59: GO Molecular function pathway enrichment analysis of the differentially upregulated genes (which were annotated with BAP1-binding in MEL202 WT condition). .... 125

Figure 60: Network of the enriched gene clusters (annotated with BAP1-binding in MEL202 WT condition) upregulated after BAP1 loss. .... 126

Figure 61: Genome-enrichment representation of the differentially downregulated genes upon BAP1 loss in MEL202 cells. .... 127

Figure 62: Genome-enrichment representation of the differentially upregulated genes after BAP1 loss in MEL202 cells. .... 131

Figure 63: Positive correlation between *BAP1* and *TFAP2A* gene expressions. .... 134

Figure 64: Negative correlation between *BAP1* and *TFAP2C* gene expressions. .... 135

Figure 65: Heatmaps showing the binding profiles of (A) *TFAP2A* and (B) *TFAP2C* between MEL202 WT / BAP1 KD conditions. .... 137

Figure 66: Change in the TPM gene expressions of *TFAP2C* between MEL202 WT / BAP1 KD conditions. .... 138

Figure 67: Heatmaps showing the differences of *TFAP2A/TFAP2C* binding patterns on the BAP1bound genes in MEL202 BAP1 WT / KD conditions. .... 140

Figure 68: Distribution of *TFAP2C* peaks (A) across the chromatin states and (B) ATAC-seq peaks. .... 141

Figure 69: Clustered heatmap of 80 TCGA uveal melanoma patients based on BAP1-dependent, *TFAP2C*-bound genes. .... 144

Figure 70: Chromatin accessibilities decreased at active TSS and Enhancer sites when BAP1 is KD.....	147
Figure 71: Chromatin accessibilities shown for the Bivalent Enhancers. ....	149
Figure 72: H3K27ac histone mark profile differences at (A) active enhancers (B) flanking TSS and (C) active TSS sites upon BAP1 loss in MEL202 cells.....	151
Figure 73: H3K4me3 histone mark landscapes at active, flanking, and bivalent TSS regions upon BAP1 loss in MEL202 cells.....	153
Figure 74: H3K4me3 histone mark landscapes at genic enhancers. ....	155
Figure 75: Representative image from the IGV browser showing ChIP-seq (H3K4me3, H3K27ac, H3K4me1, BAP1, TFAP2A, TFAP2C), RNA-seq and ATAC-seq results of <i>DNMT1</i> gene in MEL202 WT and BAP1 KD conditions.....	156
Figure 76: H3K4me1 histone mark profiles show decreased patterns at enhancers upon BAP1 loss.....	158
Figure 77: H3K27me3 repressive histone mark profile showing a decrease at bivalent TSS upon BAP1 loss. ....	160
Figure 78: Distribution of RING1B peaks (A) across the chromatin states, (B) ATAC-seq peaks. ....	162
Figure 79: Counteracting binding patterns of PRC1-member RING1B in the antagonism of BAP1 in MEL202 cells. ....	163
Figure 80: Location of the BAP1 binding sites majorly at CGIs compared to CpG shore, shelf, and inter CGI regions on the genome. ....	168
Figure 81: Schematic representation of the roles of BAP1 along with TFAP2C in regulation of the target genes. ....	181
Figure 82: Plasmid map of LentiCRISPRv2GFP vector.....	213
Figure 83: Plasmid map of pMD2.G vector.....	214
Figure 84: Plasmid map of pMDLg/pRRE vector. ....	215
Figure 85: Plasmid map of pRSV-Rev vector. ....	216

Figure 86: Antibody manufacturer’s Western blot result for BAP1 (C-4 clone) expression in (A) KNRK, (B) PC-3, (C) A-431, (D) MCF7, (E) Jurkat and (F) THP-1 whole cell lysates. .... 217

Figure 87: Antibody manufacturer’s Western blot result of BAP1 (C-4 clone) in (A) KNRK and (B) PC-3 whole cell lysates and (C) A-431, (D) HeLa, (E) MCF7 and (F) Jurkat nuclear extracts..... 217

Figure 88: FACS settings and gating strategy for the untransduced MEL202 cells as negative control..... 218

Figure 89: FACS settings and gating strategy for the transduced MEL202 cells with sgBAP1\_1-Cas9-GFP construct. .... 219

Figure 90: FACS settings and gating strategy for the transduced MEL202 cells with sgBAP1\_3-Cas9-GFP construct. .... 220

Figure 91: Monoclonal growth after one month of the transduced MEL202 cells with sgBAP1\_1-Cas9-GFP construct. .... 221

Figure 92: Western blot result for replicates of siRNA-mediated BAP1 knockdown experiment in MEL202 cells, showing the effects of two different siRNAs targeting BAP1 and optimization of their amounts. .... 222

Figure 93: Different replicates of the siRNA-mediated BAP1 knockdown experiment in MEL202 cells, showing two different replicates using optimized siRNA amount. .... 223

Figure 94: Changes in the TPM gene expressions of *TFAP2A* and *RING1B* between MEL202 WT / BAP1 KD conditions. .... 224

Figure 95: Chromatin accessibilities shown for the all Enhancer site groups..... 225

## List of Tables

Table 1: Frequency of the four main types of melanoma subtypes.....	29
Table 2: Antibodies used in the study. ....	56
Table 3: Equipment and chemicals used in this study. ....	57
Table 4: Kits used in this study. ....	60
Table 5: Plasmids used in this study.....	60
Table 6: ATAC-seq i7 and i5 index primers used in this study. ....	61
Table 7: ChIP-seq and CUT&RUN dual index primers for Illumina systems used in this study.....	61
Table 8: Cell lines used in this study. ....	63
Table 9: Features of the single guide RNAs designed to target the BAP1 gene. ....	64
Table 10: Restriction digestion conditions of SapI and SphI-HF enzymes. ....	65
Table 11: Sequencing primers used for LentiCRISPRv2GFP plasmid for Sanger sequencing. ....	66
Table 12: Digestion conditions of BsmBI with LentiCRISPRv2GFP plasmid. ....	67
Table 13: Gibson assembly protocol to clone sgRNAs into the LentiCRISPRv2GFP backbone fragment.....	68
Table 14: Composition of the lentivirus packaging medium without any antibiotics.....	70
Table 15: Preparation of the transfection mix for lentivirus production. ....	70
Table 16: siRNAs used in this study.....	73
Table 17: Preparation of 1X RIPA Lysis Buffer.....	75
Table 18: Sonication settings of the Covaris S2 sonicator used for the Western blot. ....	75
Table 19: Dilution scheme of BSA for the standard test tube protocol for the working range.....	76
Table 20: Preparation of Tagmentation Master Mix.....	81
Table 21: i7 and i5 indexed primers of the ATAC-seq kit.....	82
Table 22: Mixture for the PCR amplification reaction of the tagmented DNA.....	82
Table 23: PCR program to amplify the tagmented DNA for ATAC-seq.....	83
Table 24: Conditions of the PCR enrichment of the adaptor-ligated ChIP DNA.....	88



Table 25: Mutational status of MEL202 cell line.....	94
Table 26: HOMER de novo motif analysis results for BAP1-binding sequences. ....	97
Table 27: Number of genes differentially expressed (upregulated and downregulated) when $ \log_{2}FC  > 1$ after BAP1 loss in MEL202 cells.....	106
Table 28: Correlations of the DEGs from MEL202 / BAP1 KD cell condition and up / down regulated genes of the UM patient cohort. ....	108
Table 29: Enriched TF binding motifs at promoters (600 bp upstream) of the differentially downregulated genes upon BAP1 loss in MEL202 cells.....	129
Table 30: Enriched TF binding motifs at promoters (600 bp upstream) of the differentially upregulated genes upon BAP1 loss in MEL202 cells.....	132
Table 31: HOMER <i>de novo</i> motif analysis results for TFAP2C-binding sequences. ....	142

## List of Abbreviations and Symbols

µg	Microgram
µL	Microliter
µm	Micrometer
µM	Micromolar
ATAC-seq	Assay for Transposase-Accessible Chromatin sequencing
ATCC	American Type Culture Collection
BAP1	BRCA1 Associated Protein 1
BRCA1	Breast Cancer gene 1
°C	Centigrade / Degree Celcius
CaCl <sub>2</sub>	Calcium Chloride
CGI	CpG island
ChIP-seq	Chromatin Immunoprecipitation sequencing
CNV	Copy number variation
CpG	5'—C—phosphate—G—3'
CRISPR	Clustered Regularly Interspaced Short Palindromic Repeats
CUT&RUN	Cleavage Under Targets and Release Using Nuclease
CYSLTR2	Cysteinyl leukotriene receptor 2
D3	Disomy 3
DAR	Differentially accessible region
DMSO	Dimethyl sulfoxide
DNA	Deoxyribonucleic acid
DNMT	DNA methyltransferase
EIF1AX	Eukaryotic Translation Initiation Factor 1A X-Linked
FACS	Fluorescence Activated Cell Sorting
FBS	Fetal Bovine Serum
g	Grams
GDP	Guanosine diphosphate
GEP	Gene expression profile

GNA11	Guanine nucleotide-binding protein subunit alpha-11
GNAQ	Guanine nucleotide-binding protein G(q) subunit alpha
GPCR	G-protein-coupled receptor
GTP	Guanosine triphosphate
HDAC	Histone deacetylase
KD	Knockdown
kDa	Kilodalton
KO	Knockout
L	Liter
LB	Luria Bertani
LOH	Loss of heterozygosity
LVP	Lentiviral particles
m	Meter
M	Molarity
M3	Monosomy 3
Mb	Megabase
MITF	Microphthalmia-associated transcription factor
mL	Milliliter
NC	Neural crest
NCS	Neural crest cells
ng	Nanogram
NGS	Next-generation sequencing
NT	Neural tube
OS	Overall survival
PBS	Phosphate Buffered Saline
PcG	Polycomb group
pH	Power of Hydrogen
PIC	Protease Inhibitor Cocktail
PLCB4	Phospholipase C Beta 4

PRAME	Preferentially expressed antigen of melanoma
PRC1	Polycomb repressive complex 1
PRC2	Polycomb repressive complex 2
PR-DUB	Polycomb repressive deubiquitinase
PTM	Posttranslational modification
RCC	Renal cell carcinoma
RING1B	Really interesting new gene 1B
RIPA	Radioimmunoprecipitation assay
RNA	Ribonucleic acid
ROS	Reactive oxygen species
RPE	Retinal pigment epithelium
RPKM	Reads Per Kilobase Million
RPM	Revolutions per minute
SCP	Schwann cell precursors
SF3B1	Splicing factor 3B subunit 1
siRNA	Small interfering RNA
SNV	Single nucleotide variant
SPRI	Solid-phase reversible immobilization
TCGA	The Cancer Genome Atlas
TF	Transcription factor
TFAP2A	Transcription Factor AP-2 alpha
TFAP2C	Transcription Factor AP-2 gamma
TMB	Tumor mutation burden
TME	Tumor microenvironment
TSG	Tumor suppressor gene
TSS	Transcription start site
UM	Uveal Melanoma
UV	Ultraviolet
UVR	Ultraviolet radiation

V	Volt
WES	Whole exome sequencing
WGBS	Whole-genome bisulfite sequencing
WGS	Whole-genome sequencing
WT	Wild type

# **Chapter 1: Introduction**

## **1.1. Cancer genetics and gene expression**

Cancer fundamentally arises as a genetic disease and is rooted in alterations to crucial genes known as cancer driver genes. These alterations include both mutations and epigenetic modifications that persist as cancer cells proliferate. Together with environmental influences, tumor formation, and progression were catalyzed by these genetic changes caused by disruption of the normal regulation of genes vital for cellular functioning. This disruption is central to the hallmark abilities of cancer, including unrestrained cell proliferation, survival advantage, apoptosis evasion, impaired differentiation, cell cycle abnormalities, and enhanced angiogenic and metastatic potential. While many cancer-causing mutations are acquired during a person's lifetime (somatic mutations), a fraction are inherited from one generation to the next (germline mutations), underscoring the role of heredity in cancer risk (Mancarella and Plass, 2021, Youn et al., 2018).

### **1.1.1. Cancer and malignancy**

Cancer is distinguished from benign growths by its malignant nature, which is characterized by uncontrolled cell proliferation and the potential to invade other tissues. This invasive ability marks the transition from a localized tumor to a cancer capable of affecting distant organs through metastasis. Malignant tumors disrupt normal body functions either by invading and destroying adjacent structures or by spreading to non-adjacent sites through the lymphatic system and bloodstream. Understanding the biological basis of malignancy is essential for the development of targeted cancer therapies (Ganesh and Massague, 2021, Gupta and Massague, 2006, Valastyan and Weinberg, 2011).

### 1.1.2. Hallmarks of Cancer

A set of functional capabilities that are acquired by human cells in order to make the transition from normal state to neoplastic growth states were proposed as the “Hallmarks of Cancer” (Hanahan and Weinberg, 2000). This initial proposal of the six hallmarks provided a logical framework for understanding the diversity of neoplasms. Eleven years later, conceptual progress in cancer research expanded the six original hallmarks to ten adding two new “emerging hallmarks” and two new “enabling characteristics” highlighting the effects of genomic instability, mutational burden, cellular energetics and TME (Hanahan and Weinberg, 2011).

Rationalization of the complex phenotypes from diverse human tumor types within the limited hallmark designation yielded broad engagement across the large spectrum of cancers. Nevertheless, the hallmark traits needed to be updated to address the intricacy of the cancer pathogenesis. Eleven years after the update, four more new concepts were recognized as “new dimensions” in the updated version of the Hallmarks of Cancer (Hanahan, 2022). According to the new dimensions, phenotypic plasticity and senescence were classified as emerging hallmarks while non-mutational epigenetic reprogramming and microbiomes were described as enabling characteristics as shown in **Figure 1**.

Recognition of the non-mutational epigenetic reprogramming as an enabling characteristic is a compelling argument for a distinct type of genome reprogramming that operates through purely epigenetic mechanisms to alter gene expression. The proposed model suggests that cancer cells can evolve without genetic mutations, relying on epigenetic modifications to program its hallmark traits. The idea was introduced nearly a decade ago and it has been gaining attention in recent cancer research (Darwiche, 2020, Nam et al., 2021, Baylin and Jones, 2016).

The principle of non-mutational epigenetic regulation has an effect as a well-recognized driver of embryonic development, differentiation, and organogenesis. In adults, the formation of long-term memories involves alterations in gene and histone modifications, changes in chromatin structure, and activation of gene expression switches. These

changes are maintained over time through complicated feedback loops. There is also increasing evidence that comparable epigenetic modifications play crucial roles in enabling tumors to develop capabilities of the cancer hallmarks (Goldberg et al., 2007, Kim and Kaang, 2017, Zeng and Chen, 2019).

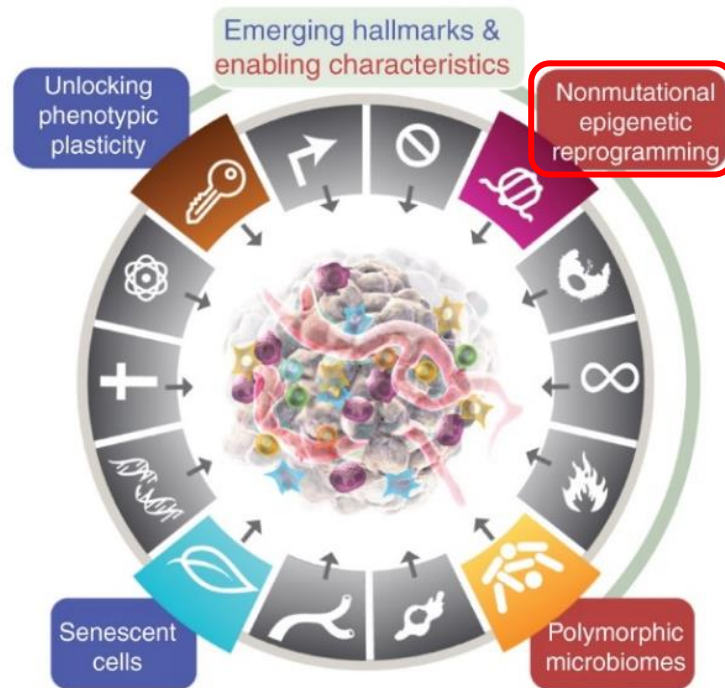


**Figure 1: Updated concept of the emerging hallmarks and enabling characteristics of the cancer.** (Hanahan, 2022).

### 1.1.3. Genetic and epigenetic alterations in cancer

The complex interplay of genetic and epigenetic alterations characterizes the cancer. Initiation, progression, and diversification of the cancer phenotypes are shaped by this interplay. Genetic mutations in cancer can activate oncogenes or inactivate tumor suppressor genes, while epigenetic changes such as DNA methylation, histone modification, and chromatin remodeling may regulate the gene expression without changing the DNA sequence (Mancarella and Plass, 2021, Costa et al., 2023). These epigenetic alterations are dynamic and can be influenced by environmental factors. Epigenetic dysregulation also contributes to cancer heterogeneity and the evolution of drug resistance (Wajapeyee and Gupta, 2021).



#### 1.1.3.1. Somatic mutations, oncogenes and tumor suppressor genes

Somatic mutations are known to accumulate in all dividing cells including both normal and cancerous cells at a consistent rate in each division. Despite this constancy, there is a big variability in the number of somatic mutations observed across different cancer types and even within the same cancer type. This variability is caused by several factors including exposure to both intrinsic and extrinsic mutagens, the type of the cell, the presence of rare hereditary diseases and possibly an increased mutation rate in cancer cells following neoplastic transformation. As shown in **Figure 2**, while some cancers exhibit accelerated mutation rates and significant genomic instability, others do not require such conditions for cancer development (Greenman et al., 2007, Stratton et al., 2009, Bodmer et al., 2008, Vogelstein et al., 2013). In tumors, over 97% of these somatic mutations do not offer any selective advantage to cancer cells and accumulate over time without directly contributing to the cancerous process. These mutations are termed "passenger" mutations, as opposed to "driver" mutations. Driver mutations occur in specific genes and play a direct role in cancer development by providing selective growth advantages or enhancing tumor fitness (Vogelstein et al., 2013).

Driver mutations in the cancer can have an "activating" effect on oncogenes, leading to various alterations in the cellular functions. These activating effects include the production of hyperactive proteins via structural modification, gene amplification, increased gene expression through various mutations which enhance transcriptional activity from permanently active promoters or the creation of fusion proteins with oncogenic properties resulting from chromosomal translocations. An oncogene can be activated by a mutation in just one of its alleles, which is enough to provide a growth advantage to the cell and manifest a gain-of-function phenotype. Since the initial identification of an oncogene (*c-src*) in the 1970s from retrovirus studies, numerous oncogenes have been identified (Stehelin et al., 1976). These oncogenes include growth factors like *c-Sis*, *EGF* and *FGF*; growth factor receptors such as *EGFR*, *HER2* and *VEGFR*; signal transducers like *KRAS*, *GNAQ* and *HRAS*; transcription factors including *MYC*; and apoptosis regulators such as

*BCL-2*, each playing distinct roles in the cellular pathways influencing cancer progression (Vogelstein and Kinzler, 2004).

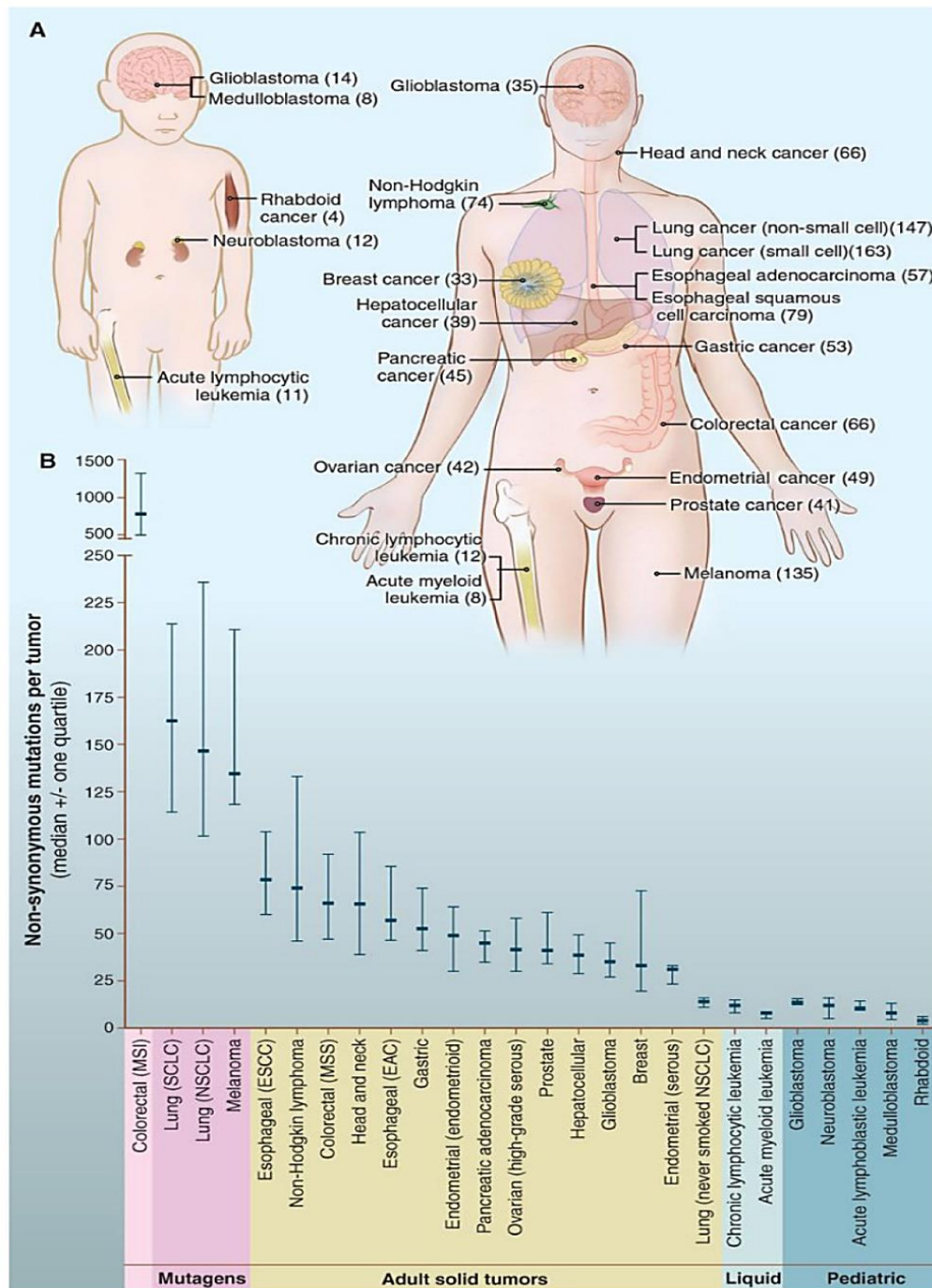


**Figure 2: Somatic mutations detected by genome-wide sequencing studies in the representative human cancers. (A)** Various pediatric (left) and adult (right) cancer genomes were analyzed. The numbers in the parentheses show the median number of nonsynonymous mutations per tumor. **(B)** The median number of nonsynonymous mutations per tumor across various tumor types. The 25<sup>th</sup> and 75<sup>th</sup> quartiles are indicated by the horizontal bars (Vogelstein et al., 2013).

On the other side of genetic alterations, tumorigenesis can also arise from loss-of-function events which lead to the inactivation of tumor suppressor genes (TSGs). These mutations often take the form of stop-gain or missense mutations, indels of a few nucleotides or larger rearrangements which disrupt gene splicing. While oncogenes often harbor mutations at specific 'hotspot' positions, TSG mutations are more dispersed and can occur throughout the gene. To fully deactivate a tumor suppressor gene, a secondary event is typically needed to occur which results in the loss of the other allele. This might include the loss of an entire chromosomal arm or a segment which includes the TSG (Vogelstein et al., 2013).

Knudson's two-hit hypothesis is elucidated when two loss-of-function events are usually necessary to see the phenotype associated with tumor growth. These events can be a combination of mutations affecting both alleles or a mix of genetic and chromosomal alterations. An example of the investigation into this phenomenon is the search for 'loss of heterozygosity' (LOH), that detects the loss of an allele in tumor cells compared to normal tissue. In some instances, even the inactivation of just one allele (haploinsufficiency) of a TSG is enough to confer a selective advantage to the tumor cell. This is because the remaining wild-type allele produces insufficient protein levels to maintain normal cell function leading to tumorigenesis (Knudson, 2001, Knudson, 2002, Johnson et al., 2019, Inoue and Fry, 2017). For example, the TSG *TP53*, which is often mutated in various cancers and associated with Li-Fraumeni syndrome or *53BP1* in glioblastoma can exhibit this pattern where LOH may not always be present (Venkatachalam et al., 1998, Squatrito et al., 2012).

TSGs function almost as biological brakes: they regulate and inhibit uncontrolled cell division, and DNA replication or trigger apoptosis in case it is necessary. Some of the known proteins produced by TSGs which have critical roles in these cases are p53, p16, APC and RB. The TSGs are generally described as 'gatekeepers' of the cell cycle but another category related to TSGs is 'caretakers' or stability genes which ensure the genomic stability and provide minimum levels of the DNA damage (Vogelstein and Kinzler, 2004). These genes are crucial in DNA repair pathways such as the mismatch repair (MMR), nucleotide excision repair (NER) and homologous recombination (HR). Mutations

in caretaker genes can lead to a higher mutation rate in other genes, accelerating the tumorigenesis. Some of the caretakers are mismatch repair proteins MLH1, MSH2, pleiotropic repair protein BRCA1 and double-stranded DNA break repair protein ATM whose dysfunction can lead to a cascade of DNA damage and subsequent mutations in oncogenes and TSGs. This complex interplay of the genetic and chromosomal events indicates the complexity of the cancer development and highlights the critical balance maintained by both oncogenes and tumor suppressor genes in cellular homeostasis and regulation (Friedberg, 2003).

#### 1.1.3.2. Epigenetic dysregulation

Classical genetics has argued that DNA sequences dictate cellular phenotypes from the reveal of DNA's structure as a double helix. DNA within the cell is structured into chromatin, composed primarily of nucleosomes that consist of an octamer of four core histones (H2A, H2B, H3, and H4) wrapped by a 147-base-pair segment of DNA, with linker DNA segments of 10–60 base pairs separating each nucleosome. Within the genetic studies, scientists observed organisms with identical genetic codes, but which differ in phenotypes. These findings suggested a role beyond DNA sequence in determining the cellular function. This observation led to the proposal of the term "epigenetics" by Conrad Waddington in 1942 to describe the study of the additional layer of genetic control which links genotype to the phenotype (Waddington, 2012).

Epigenetics encompasses mechanisms which are able to modify gene expressions without altering the DNA sequence itself. This concept of epigenetics was further expanded by Arthur Riggs and colleagues who described it in the context of inheritable phenotypic changes observable in both mitosis and meiosis (Riggs, 1975). Holliday also suggested the inheritability of epigenetics without any alteration of the DNA sequences (Holliday, 1987). It encircles a range of processes including cell growth, differentiation, and disease progression. The epigenetic regulations are generalized within the concepts of DNA methylations and histone modifications which are manipulated by enzymatic "writers" and "erasers" that add or remove chemical groups, and "readers" that interpret these chemical

modifications resulting in change of chromatin remodeling and expression of noncoding RNAs as the readout (Bird, 2007, Shen and Laird, 2013).

The regulation of gene expression by the epigenome is influenced by a variety of factors, including transcription factors and noncoding RNAs. Intracellular signals and external stimuli are also players in this regulation. This dynamic and reversible modification of the epigenome highlights its critical role in cellular function and disease particularly in cancer in which aberrant epigenetic changes can be the critical factors in the formation and progression of the cancer as shown in **Figure 3**. Understanding these complex mechanisms offers insights into the cancer development and provides avenues for novel therapeutic approaches.

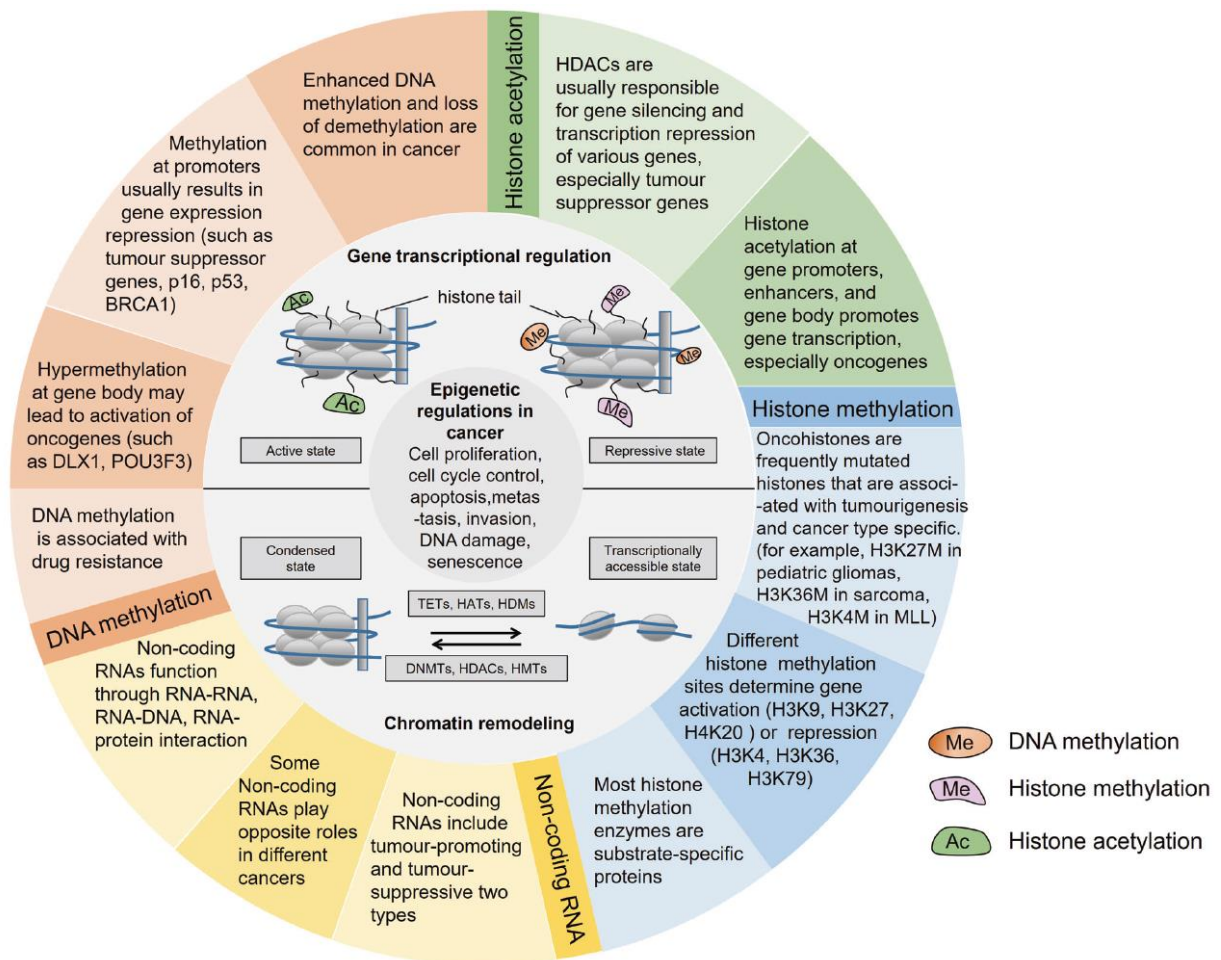


**Figure 3: Epigenetic regulations in cancer.** (Cheng et al., 2019).

In cancerous tissues, the patterns of histone modification vary significantly among different tumor cells, both genome-wide and within the specific genes. This demonstrates a level of epigenetic diversity at the cellular level. The variation can also support the use of molecular biomarkers to categorize cancer patients into distinct groups for more targeted treatment approaches. Tumorigenesis often results from the interplay of multiple epigenetic modifications. Commonly, the suppression of tumor suppressor genes involves the methylation of DNA within CpG islands, which is typically associated with a reduction in histone acetylation and an increase in histone methylation (Seligson et al., 2005, Fahrner et al., 2002). Key epigenetic markers identified during gene silencing include hypoacetylation of histones H3 and H4, methylation of histone H3K9 and cytosine methylation. The complex epigenetic landscape offers a framework for the mechanisms driving cancer phenotypes as illustrated in **Figure 4**.

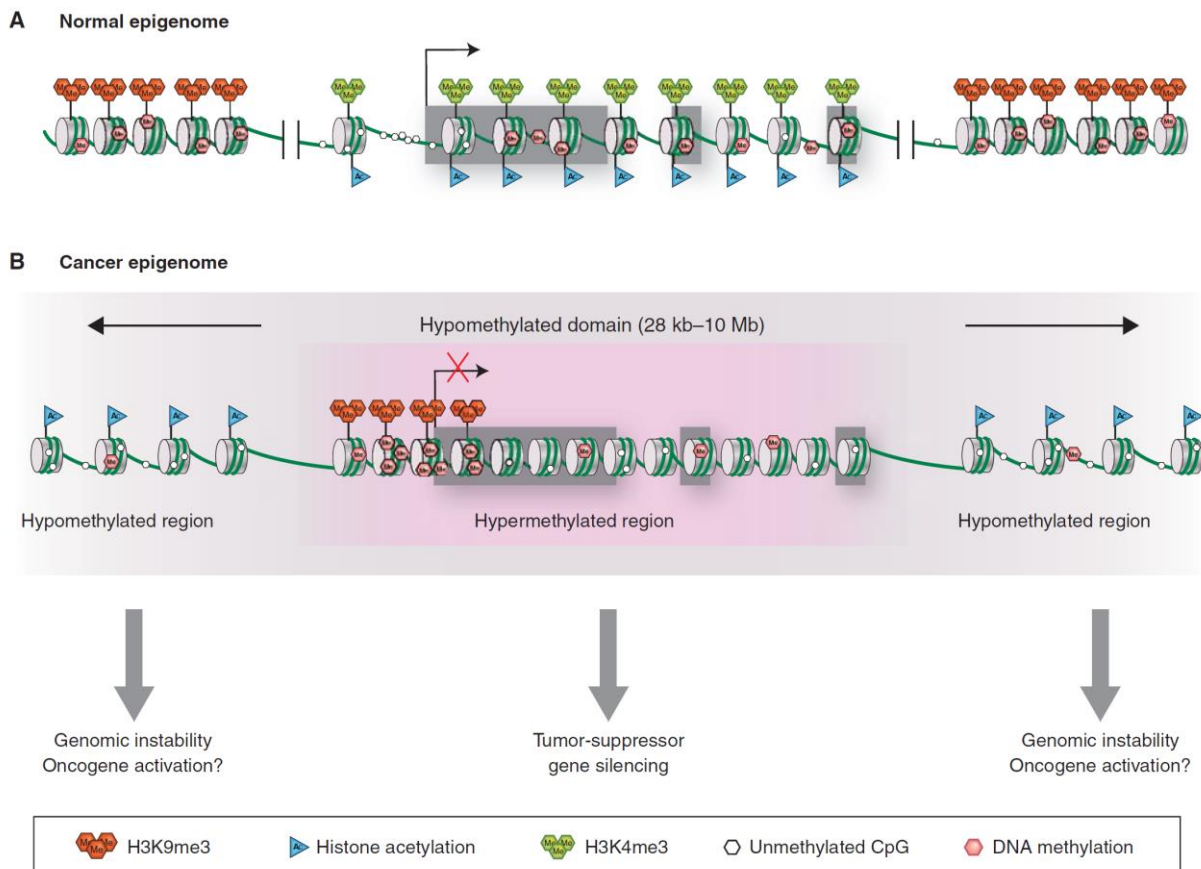


**Figure 4: Epigenetic changes in cancer.** (Baylin and Jones, 2016).

Roles of epigenetics in cancer were studied in two critical areas: DNA methylation and histone modifications including histone acetylation and histone methylation each having a pivotal role in the regulation of gene expression and the progression of cancer (Ben-Porath and Cedar, 2001, Richards and Elgin, 2002).

**DNA methylation** is a dynamic epigenetic process that is catalyzed by DNA methyltransferases (DNMTs) that function by adding the methyl group on the Carbon (C5) position of cytosine to yield C5-methyl-cytosine (5mC). The DNMTs are studied in two major types such as *de novo* methyltransferases and maintenance methyltransferases. *De novo* DNMTs are DNMT3A and DNMT3B and are responsible for binding to non-methylated DNA through which generating the new methylation patterns and has a role especially during embryonic development. Maintenance DNMT is DNMT1 which has a role in hemimethylated CpG dinucleotide sites that occurred during the DNA replication (Quintero-Ronderos and Montoya-Ortiz, 2012, Mehdipour et al., 2021, Razin and Riggs, 1980).

DNA methylation patterns in mammals are governed by specific biological principles. During embryogenesis, germ cells undergo a systematic process of demethylation to facilitate global gene repression and appropriate gene regulation. Most CpG sites are subject to *de novo* methylation, post-implantation. Except for those sites, the remaining are protected (Cedar and Bergman, 2012). Typically, dynamic changes in DNA methylation and demethylation correlate with aging due to the levels of changing enzyme expressions. At the same time, inappropriate methylation can lead to several diseases such as inflammatory diseases, precancerous changes, and cancer as illustrated in **Figure 5**. In cancer, *de novo* methylation mainly serves to maintain the suppression of already repressed genes in normal cells, rather than to induce gene expression (Kulis and Esteller, 2010, Valentini et al., 2016, Easwaran et al., 2014).

Aberrant DNA methylation is a recognized characteristic of cancer which impacts the transcription of genes and stability of the chromatins via silencing genes or by repressing transcription (Ito et al., 2010). The relationship between DNA methylation and chromatin



structure has complex mechanisms in which methylation is typically associated with tighter and less active chromatin structures.

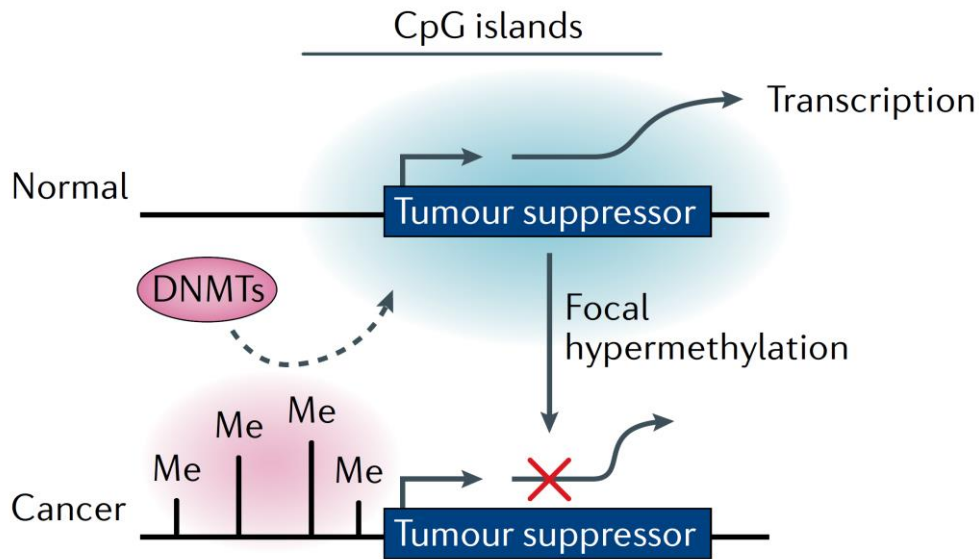


**Figure 5: Difference of DNA methylation patterns on TSGs between normal and cancerous states.** (Hogg et al., 2020).

In cancers, it is common for promoter regions of especially key tumor suppressor genes to be hypermethylated. In normal tissues, these regions are contrastingly unmethylated. For example, the tumor suppressor gene *CDKN2A* which encodes p16 tumor suppressor shows significant *de novo* methylation in around 20% of several primary neoplasms (Keshet et al., 1986, Baylin and Jones, 2011). Further studies have linked higher levels of methylations with larger tumor sizes which is observed in comprehensive genome-wide methylation studies in breast cancer. It is also shown that increased methylation at specific genes correlates with advanced tumor stages (Christensen et al., 2010). In the HCT116 human colon cancer cell line, the genes *MLH1* and *CDKN2A* are typically affected by both genetic mutations and hypermethylation of one allele which leads to the suppression of the key TSGs. In bladder cancer, *CDKN2A*, *CDKN2B* and *PAX6* genes frequently exhibit abnormal methylation and a hypermethylation pattern is observed in the cell culture conditions (Baylin and Ohm, 2006, Markl et al., 2001).



Contrasting with the suppressive effects of promoter methylation, gene body methylation generally enhances transcriptional activity. This event particularly happens in CpG-sparse regions, prompting a base transition from cytosine to thymine. In cancer cells, the hypermethylation of specific CpG islands, compared to their unmethylated state in normal tissues, can indicate potential mutations. An example of this situation is the *GSTP1* gene. It is the commonly altered gene in human prostate cancer through methylation (Wolf et al., 1984, Jones, 2012, Lee et al., 1994). Recently studies on DNA methylation patterns in cancer have also been linked to drug resistance and the ability to predict responses to treatments (Wilting and Dannenberg, 2012).

**Histone modifications** are another epigenetic factor. In eukaryotic cells, chromatin is structured into nucleosomes which consist of a histone octamer wrapped by DNA. These structures are very crucial for the dynamic behavior of the chromatin due to histone posttranslational modifications (PTMs) together with DNA methylation that introduce variability in chromatin structures. Not only the canonical histones (H2A, H2B, H3, and H4) but also other histone variants can integrate into nucleosomes independently of DNA replication. There is a variety of histone PTMs especially methylations on histone H3 and H4 at specific lysine residues such as H3K4, H3K9, H3K27, H3K36, H3K79 and H4K20 which can present in several forms ranging from unmodified to trimethylated as well as acetylated resulting in the occurrence of a complex regulatory landscape (Zhao et al., 2021, Strahl and Allis, 2000, Jenuwein and Allis, 2001).

Homeostasis of this regulatory landscape is important in normal cells and dysregulation of the interplay has a role particularly in cancer where the cancer cells usually show abnormal histone modifications, not just at specific gene sites but also globally and observable even at the single-nuclei level (Seligson et al., 2005, Seligson et al., 2009). These aberrations in PTMs are linked to cancer development and progression as shown in **Figure 6**.

Histone modifications can take place not only on the flexible tails but also within the core domain of histones, even at sites that are covered by DNA. The flexible tails which are rich in basic amino acids such as Lysine - Arginine and hydroxyl bearing Serine – Threonine -

Tyrosine are the primary targets for the key histone modifications because of their accessibility for the PTMs. These PTMs that involve adding or removing the chemical groups play essential roles in gene regulation by activating or silencing gene expression. They include acetylation and methylation of Lysine and Arginine residues, phosphorylation of Serine and Threonine residues and other modifications such as ubiquitylation and sumoylation (Kouzarides, 2007, Audia and Campbell, 2016).

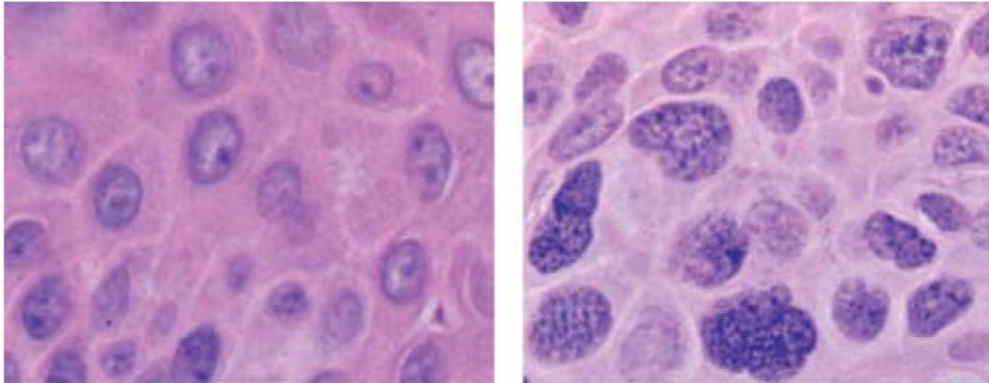


**Figure 6: Changes in the chromatin structure between normal and cancer cells.** The left panel shows the healthy epidermal cells. The right panel shows the squamous cell carcinoma of the skin. Chromatin was stained purple using hematoxylin (Baylin and Jones, 2016).

Beyond the well-known modifications, histone tails can also undergo citrullination, ADP-ribosylation, deamination, formylation, O-GlcNAcylation, propionylation, butyrylation, crotonylation and proline isomerization which may affect over 60 different amino acid residues as shown in **Figure 7** (Yang et al., 2022).

Histone modifications at the critical genomic regions such as promoters and enhancers are typically stable. These modifications at the other sites may remain dynamic and contribute to the regulation of gene expression. To note, H3K4me1 and H3K27ac are the essential histone marks which are associated with active enhancers, whereas H3K4me3, H3K9ac and H3K9me3 frequently occur at the promoters. Epigenetic studies to understand the complex nature of these modifications which marks the active, repressive, bivalent sites such as H2AK119ub, H3K27me3, H4K20me3 or H4K16ac can provide more insights into the mechanisms of the tumorigenesis offering potential strategies for cancer diagnosis and therapy (Hawkins et al., 2011, Heintzman et al., 2009, Hon et al., 2009).

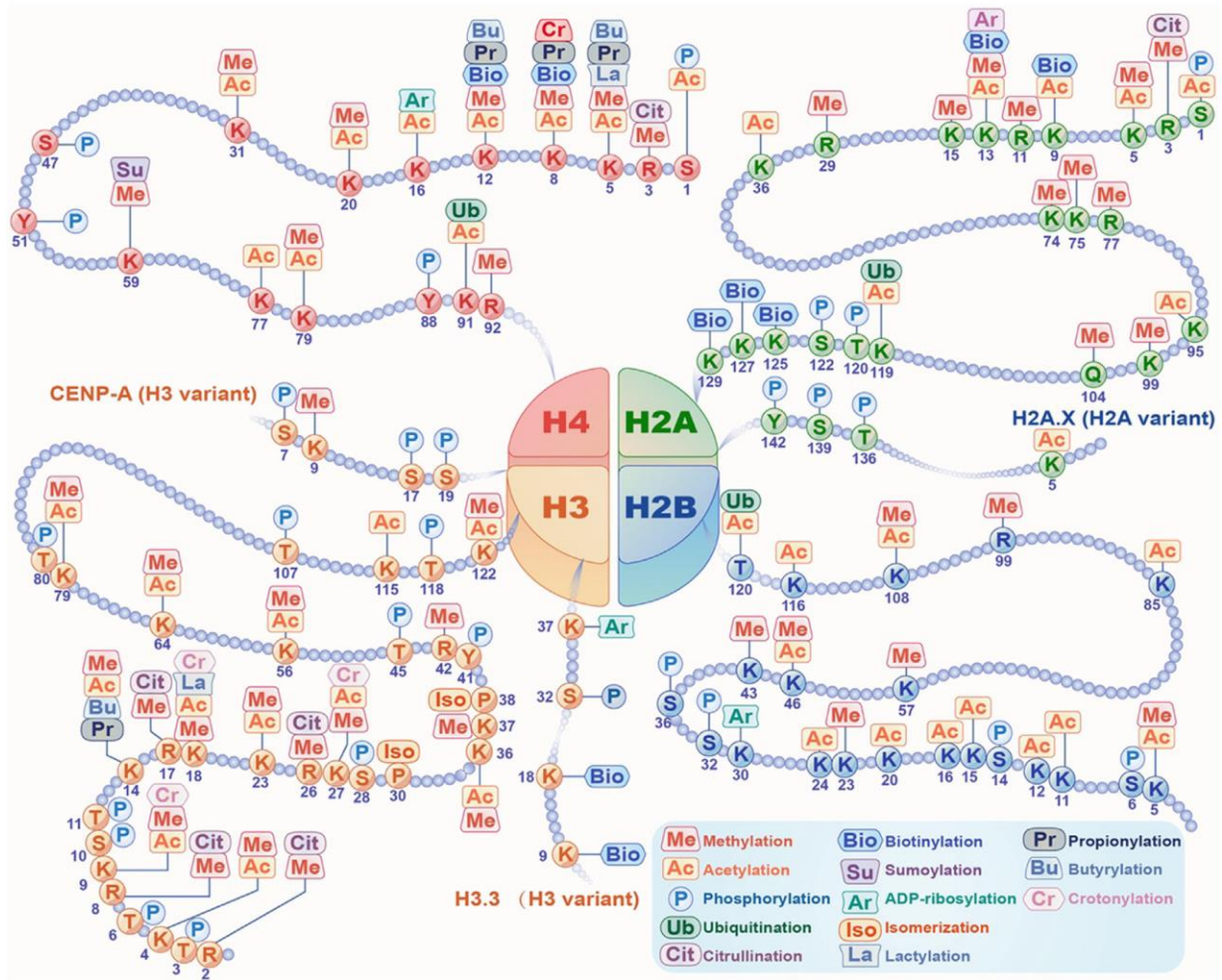


Figure 7: Overview of the histone modifications. (Yang et al., 2022).

Further downstream effects of the histone PTMs are altering the physical characteristics of nucleosomes, enhancing accessibility of the DNA, altering the charge of histones and acting as binding sites for the various chromatin-associated proteins such as chromatin modifiers. The interplay between these chromatin modifiers is based on mechanisms such as self-propagation, cooperation and competition. Gene regulatory mechanisms are also affected also by this interplay of the modifiers. Ongoing cancer research about the roles of chromatin modifications highlights how dysregulation can influence cancer initiation and progression. Understanding these epigenetic processes in depth can lead to uncovering the roles of chromatin modifications in the gene regulation networks of cancer (Biggar and Li, 2015, Narita et al., 2019, Farria et al., 2015).

## **1.2. The routes to Melanoma**

The research shown in this thesis is centered on uveal melanoma, which develops from the transformation of the melanocytes in the eye. To enhance the understanding of the progression of melanoma and the function of melanocytes in the uveal melanoma, the next chapters of the introduction outline the essential processes involved in melanocytogenesis, melanogenesis, melanoma subtypes and uveal melanoma progression.

### **1.2.1. Melanocytogenesis and functions of the melanocytes**

Melanocytes of humans originate from neural crest cells (NCCs). The precursor cells of melanocytes are known as melanoblasts which also originate from the neural crest (NC) during the neurulation process and migrate post-neural tube closure to various parts of the body differentiating into melanocytes. When they are differentiated, they begin producing melanin and fulfill distinct roles based on their locations. While melanocytes are primarily recognized for their presence in the epidermis, hair follicles and eyes, they are also found in less commonly discussed sites such as the cochlea's stria vascularis contributing to balance and hearing and in the brain in which they play a role in neuroendocrine functions and produce neuromelanin helping protection against oxidative damages. Additionally, melanocytes are present in the heart, influencing the mechanical properties of heart valves, and in the meninges, although their function there remains unclear (Takeda et al., 2007, Zecca et al., 2008, Carneiro et al., 2015, Goldgeier et al., 1984, Haass et al., 2005, Slominski et al., 2004, Mort et al., 2015, Aoki et al., 2009).

The principal role of the melanocytes is to produce melanin pigment, operating the color of the skin, hair and eyes. Also, some other cell types such as certain epithelial cells in the iris and retina, some neurons and adipocytes have the capability to produce melanin pigment. Current studies in melanocytes have primarily focused on skin melanocytes. As a result, most of our understanding of melanocyte differentiation and biological function is based on studies of epidermal melanocytes and melanin (Hu et al., 2008, Randhawa et al.,

2009). On the other hand, epidermal melanocytes might serve as the model for exploring melanocytic development and melanin synthesis thereby setting the stage for the investigation of the specific characteristics and functions of uveal melanocytes and iris pigmentation.

The current understanding of melanocyte development has mostly derived from the mice studies. It has been further enriched by research on chicken and zebrafish models that offered unique embryological and genetic insights (Lamoreux et al., 2001, Wilson et al., 2004, Higdon et al., 2013). The development and differentiation process of melanocytogenesis and melanogenesis involves several key stages: the emergence of melanocyte precursors (melanoblasts) from the neural crest, migration of these melanoblasts to various body sites and their maturation into melanocytes which function to synthesize melanin within specialized organelles called melanosomes (Loring and Erickson, 1987, Baxter and Pavan, 2003, Mort et al., 2015).

The neural crest (NC) is a transient embryonic structure that emerges from neuroectoderm, under the control of the notochord (O'Rahilly and Muller, 2007). Neural crest cells (NCCs) are the pluripotent cells originating in the neural tube then they migrate and differentiate into not only melanocytes but also neuronal and glial cells within the peripheral nervous system (PNS). The dorsolateral migratory pathway primarily generates melanocytes as illustrated in **Figure 8**. The process begins with the specification of melanoblasts around embryonic days 8.5 to 9.5 (Bonaventure et al., 2013, Cichorek et al., 2013b, Theveneau and Mayor, 2012). The development of melanocytes from SOX10-positive precursors through to mature melanocytes involves complex molecular signaling involving receptors like c-kit, transcription factors such as SOX10, PAX3 and MITF and enzymes such as TYR, TYRP2 crucial for melanin production (Cichorek et al., 2013b).

The signaling pathways like MAPK, along with growth factors such as ephrins and stem cell factor (SCF) play significant roles in the early stages of melanoblast development and migration. Notch and Wnt pathways are critical for the later stages of melanocyte maturation, influencing activity of key transcription factors. MITF is such a TF that has been

considered a master regulator of melanocyte development and essential for the proliferation, differentiation and survival of these cells within mechanisms together *KIT*, *EDN3* and *EDN3* (Bonaventure et al., 2013). Sustained expression of MITF is known to activate other proteins such as BCL-2 and TYR that are crucial for the survival of melanocytes and production of melanin together with melanosome formation, respectively.

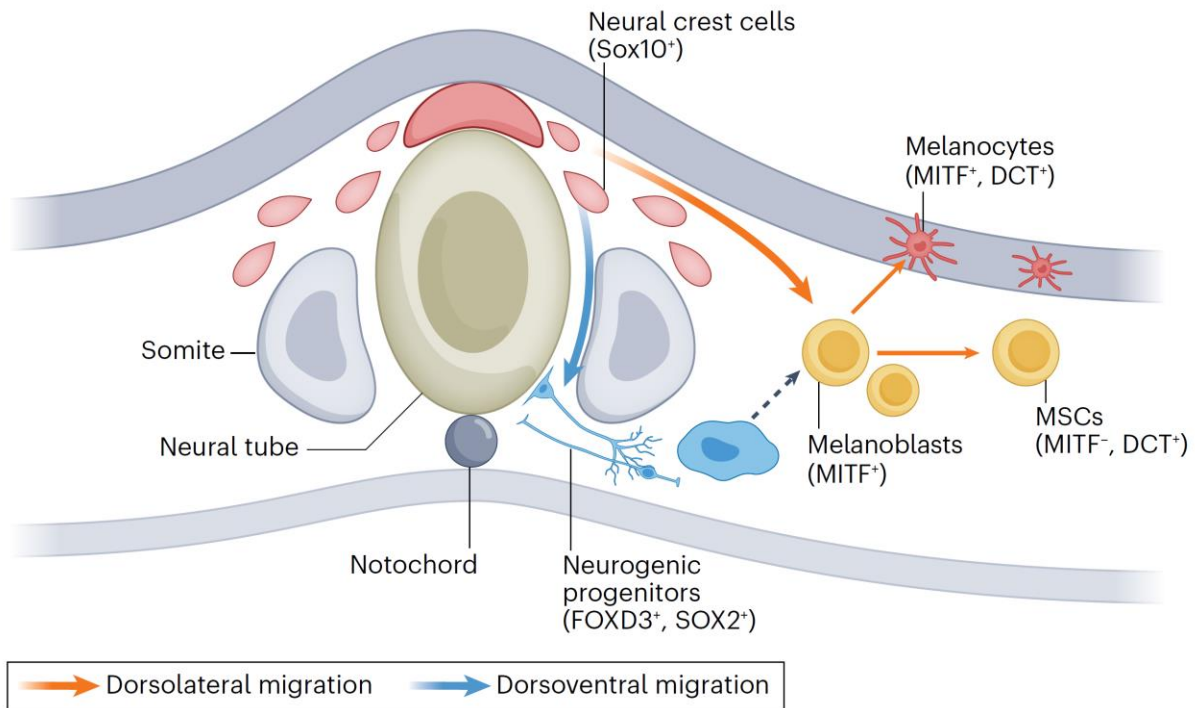


**Figure 8: Lineage determination of the Melanocytes from the NCCs.** (Centeno et al., 2023).

There are ongoing studies on neural crest-derived cell migration and differentiation as well as the timing and determination of their final differentiation into melanocytes. Models suggest varying timings and influences, ranging from environmental factors to inherent developmental programming (Dupin et al., 2007, Harris and Erickson, 2007). The transition of melanoblasts to their ultimate locations involves additional phases of proliferation and differentiation, significantly influenced by the expression of factors like *KIT*, *MITF* and *DCT*. After settling in locations like the epidermis and hair follicles, some melanocytes may dedifferentiate to form nests of melanocyte stem cells capable of repopulating pigment cells (Mort et al., 2015, Cichorek et al., 2013b).

### 1.2.2. Process of melanogenesis

Melanogenesis is the process by which melanocytes synthesize melanin which is the primary pigment in these cells. This synthesis occurs within the melanosomes which are specialized organelles that are found in the cytoplasm of melanocytes. Melanin production occurs during the later stages of melanosome maturation after which the melanin pigment is transferred to neighboring keratinocytes in the epidermis and hair follicles (Cichorek et al., 2013b, Wiriyasermkul et al., 2020). Melanocytes produce two types of melanin pigment: the brown-black eumelanin and the red-yellow pheomelanin, each having distinct physical characteristics regarding granule density and packaging (D'Mello et al., 2016, Lin and Fisher, 2007).

The production of these melanin types is controlled by a network of biochemical pathways facilitated by a group of enzymes that includes tyrosinase (TYR), tyrosinase-related protein 1 (TYRP1) and tyrosinase-related protein 2 (TYRP2). These enzymes work together to convert L-tyrosine into L-DOPA and then to dopaquinone which is a precursor shared by both types of melanin. The synthesis routes diverge for eumelanin and pheomelanin based on the availability of specific substrates and the action of these enzymes as drawn in **Figure 9**. Eumelanin synthesis involves a feedback mechanism where the precursor dopachrome enhances TYR activity, promoting further synthesis of L-DOPA and thus, sustaining melanin production (Slominski et al., 2012). Conversely, pheomelanin production depends on the presence of L-cysteine in melanosomes. This event directs dopaquinone towards producing cysteinyl-DOPA rather than dopachrome. This enzymatic regulation is crucial for determining the pigmentation of skin and hair because the ratio of eumelanin to pheomelanin and the overall concentration of eumelanin influence the coloration (D'Mello et al., 2016). High levels of eumelanin typically result in darker skin tones and darker hair colors. On the other hand, higher concentrations of pheomelanin lead to lighter skin, blonde or red hair and the presence of freckles (Simon et al., 2009).



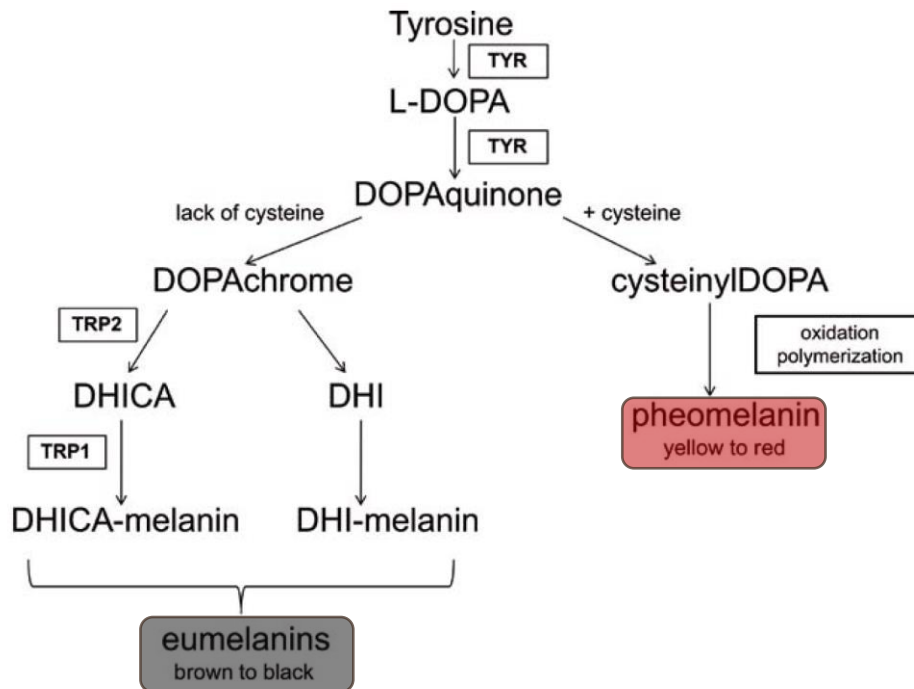


**Figure 9: Melanin biosynthesis pathways in melanocytes during melanogenesis.** (Cichorek et al., 2013a).

The production of melanin involves multiple molecular pathways, signaling cascades, and transcription factors which regulate the expression of critical genes within the melanogenesis pathway. Melanocortin-1 receptor (MC1R) is a G-protein coupled receptor and has a central role in this process. When this receptor is activated by agonists, it stimulates cyclic AMP (cAMP) production and this event activates important transcription factors such as MITF which regulates both pigmentation and melanocyte development, binding to E-box sequences on various pigmentation-related genes, promoting the transcription of genes involved in melanin production, such as *TYR*, *TYRP1* and *TYRP2*, as well as genes related to melanocyte differentiation such as *PMEL* and other cellular functions (D'Mello et al., 2016, Lin and Fisher, 2007).

Different agonists of MC1R can influence the synthesis of the two types of melanin, driving the preference for either eumelanin or pheomelanin. For example, in epidermal melanocytes,  $\alpha$ -melanocyte stimulating hormone ( $\alpha$ -MSH) and adrenocorticotrophic hormone (ACTH) bind to MC1R and stimulate eumelanin production by enhancing cAMP levels as shown in **Figure 10**. On the other hand, the MC1R antagonist agouti signaling



protein (ASP) can block  $\alpha$ -MSH binding, reduce MITF expression thereby reducing the activation of TYR, TYRP1 and TYRP2 and promoting a shift towards the pheomelanin production (Nasti and Timares, 2015, Videira et al., 2013).

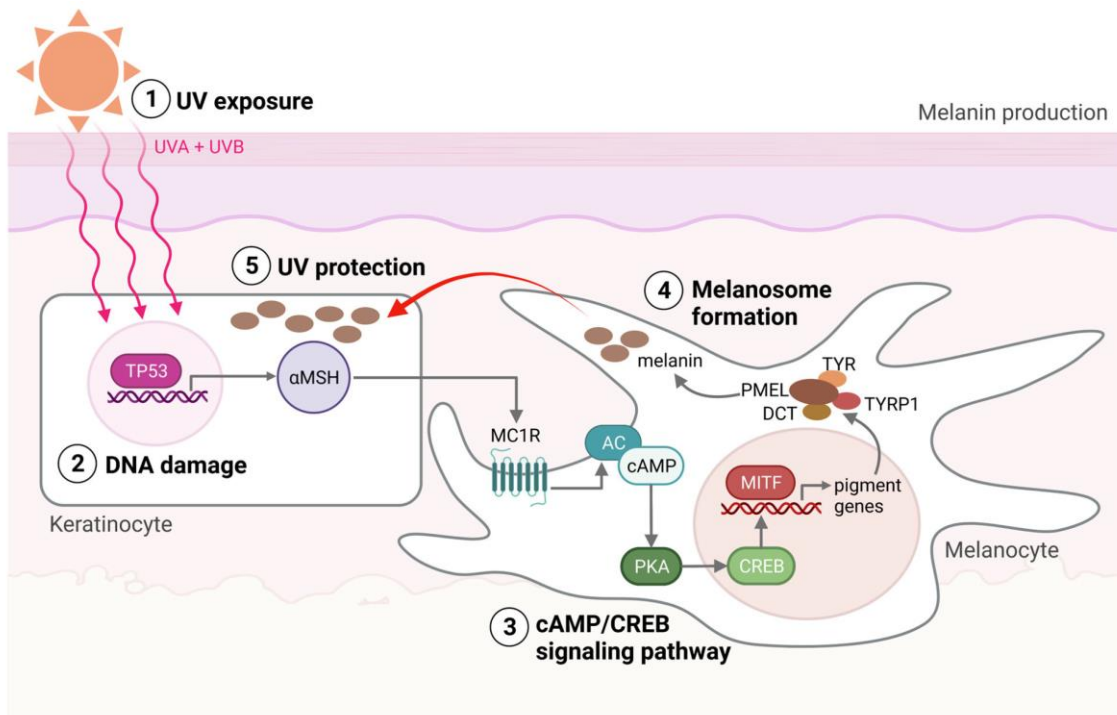


**Figure 10: Production of Melanin after UV Exposure in cutaneous melanocytes.** (Kuras, 2023).

While these enzymes, receptors and TFs are essential in melanin synthesis and the switch between eumelanin and pheomelanin, the regulation of melanogenesis also involves numerous other pathways that are mostly dependent on MITF. These pathways include the Wnt, CREB, MAPK-ERK and PKC pathways, as well as the SOX family of transcription factors which are crucial in melanocyte development (Harris et al., 2010, D'Mello et al., 2016).

Melanin synthesis is closely linked to the development of melanosomes which have four stages of biogenesis as illustrated in **Figure 11**. Firstly, pre-melanosomes which are the non-pigmented precursor of the melanosomes derive from early endosomes and produce pre-melanosome protein (PMEL) protein fibrils. Second, these fibrils elongate and arrange themselves setting the structure within the developing pre-melanosome having the

ellipsoidal shape. In the third step, melanin synthesis is started by the arrival of TYR, TYRP1 and TYRP2 melanogenic enzymes and membrane ion transport proteins from the Trans-Golgi network to the melanosomes. In the fourth step, the transition from an acidic to a neutral pH allows the TYR enzyme to become functional, initiating melanin synthesis which accumulates on the PMEL matrix. At the end of this last step, the melanosome is fully mature and capable of transferring pigment to keratinocytes, effectively dispersing color throughout the skin and hair (Wiriyasermkul et al., 2020).

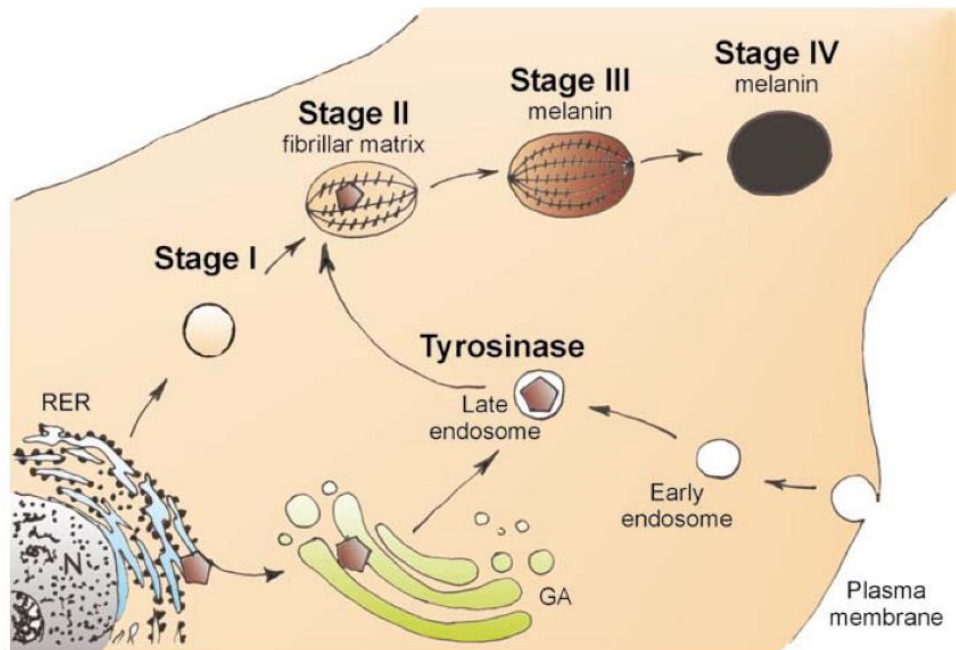


**Figure 11: Formation and maturation stages of a melanosome in a melanocyte.** (Cichorek et al., 2013a).

### 1.2.3. Roles and differences of cutaneous and uveal melanocytes

Melanocytes are the specialized cell types that are responsible for melanin pigment production. Dysregulated transformation of the melanocytic cells during their developmental stages results in melanoma pathogenesis (Centeno et al., 2023). There are various types of melanocytes depending on their placement throughout the body such as cutaneous, uveal, oral, cochlear, meningeal, nasal and esophageal melanocytes (Yamaguchi and Hearing, 2014).

**Cutaneous melanocytes** have the role of dispersing the melanin-rich melanosomes to keratinocytes across the skin. Therefore, the cutaneous melanocytes serve as a crucial defense mechanism against ultraviolet radiation (UVR) from the sunlight. Exposure to UVR can damage cells via the carcinogenic effects of UVA which generate reactive oxygen species (ROS) and UVB which directly causes DNA mutations (Nasti and Timares, 2015) as illustrated in **Figure 12**.

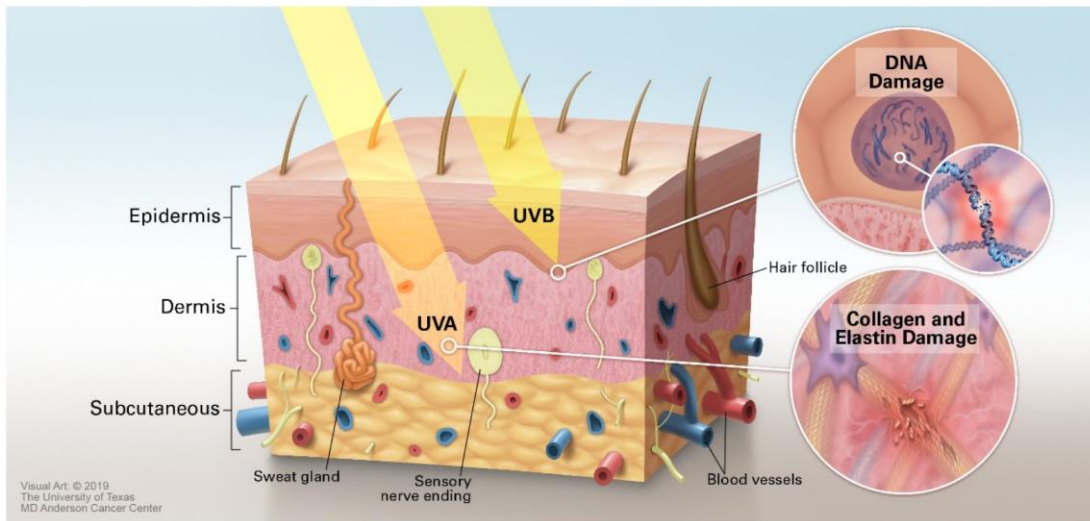


**Figure 12: UVA and UVB have different penetrances and effects on the skin.** (Alexander, 2019).

The skin's pigmentation that is enhanced by the distribution of melanin from melanocytes to keratinocytes acts as a protective barrier by absorbing UVR and shielding the deeper skin layers such as the dermis from that damage. Consequently, melanin production increases following the UVR exposure which then leads to the tanned skin. Some studies showed melanin as a free-radical scavenger due to its anti-oxidant capabilities (Lin and Fisher, 2007, Brenner and Hearing, 2008). Eumelanin is denser than pheomelanin providing superior protection against UVR and oxidative stress. In contrast, pheomelanin can play a phototoxic and pro-oxidant role contributing to ROS production through stimulated lipid peroxidation pathways (Wiriyasermkul et al., 2020, Houtzagers et al., 2020, Fujiwara et al., 2018). Therefore, individuals who typically has lower levels of eumelanin and has lighter skin encounter a higher risk of developing cutaneous melanoma (CM) compared to individuals having darker skin. While the direct link between UVR exposure and CM risk is still being studied, frequent sun exposure and resulting sunburns are

considered as well-established risk factors for this type of skin cancer (Schadendorf et al., 2018).

**Uveal melanocytes** are the cells that originate from the NCCs, located in the inner and middle layers of the ocular tract of the eye and provide continuous melanin production during the lifetime. The human eye comprises various layers as illustrated in **Figure 13**; firstly, the outermost cornea and sclera, secondly the pigmented and vascular uveal tract (including the iris, ciliary body, and choroid), thirdly the retina that consists of the neural retina for visual processing and the retinal pigment epithelium (RPE).

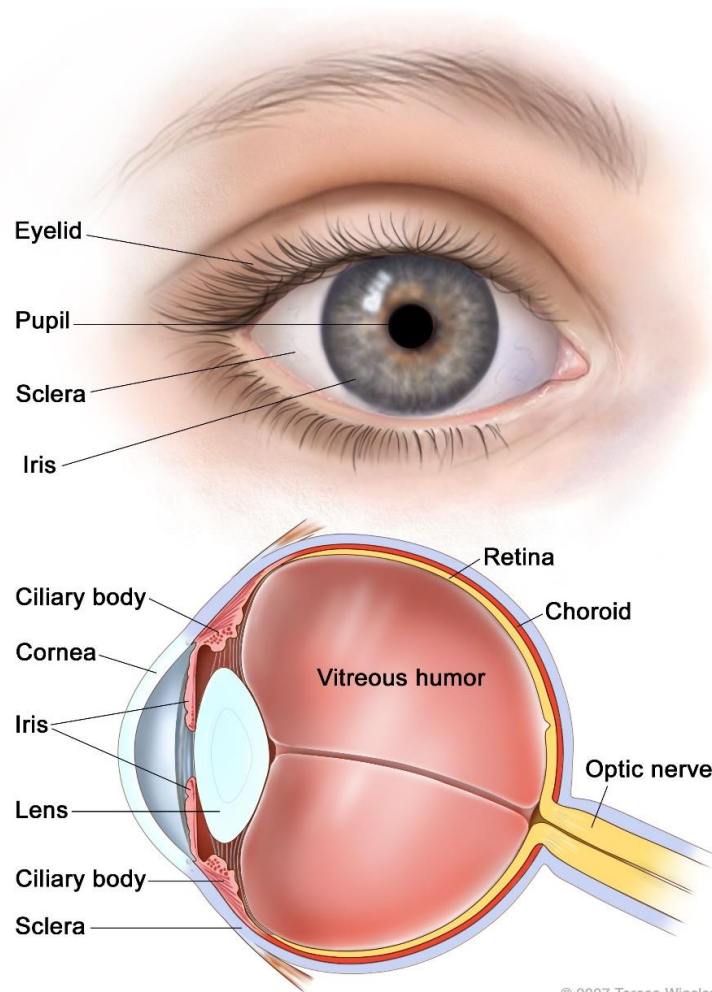


**Figure 13: Anatomy of the eye.** (Winslow, 2007).

Both the uveal melanocytes and RPE contribute to the eye's pigmentation. On the other hand, they differ based on some aspects such as uveal melanocytes originate from the

neural crest and constantly produce melanin during the lifetime whereas, RPE cells originate from the neural ectoderm and they cease melanosome production early in childhood and do not continue melanin production constantly (Sarna et al., 2003, Lopes et al., 2007, Jager et al., 2020).

Although uveal and cutaneous melanocytes both originate from the neural crest (NC), their developmental pathways and roles separate significantly. Uveal melanocytes, unlike their cutaneous counterparts, follow a unique developmental trajectory characterized by distinct timing, distinct migration patterns and specific gene expression profiles that reflect their adaptation to the eye's specific needs (Rodrigues et al., 2019, van der Kooij et al., 2019, Pandiani et al., 2017). Uveal and cutaneous melanocytes both originate from the cervical trunk and midbrain-hindbrain junction of the NC, but they follow a distinct path. Uveal melanocytes migrate towards the uveal tract of eyes which includes the choroid and the stroma of the iris and ciliary body. This process is followed by the start of melanin production by the uveal melanocytes. During the development, the process of uveal melanogenesis typically spans from the 20<sup>th</sup> week to about six months after birth which can lead to variations in iris color during this period. On the other hand, this constant melanin production process contrasts with the cutaneous melanocytes which react dynamically to environmental factors like UVR thus, being involved in skin pigmentation (Wilson et al., 2004, Griewank et al., 2018, Sitiwin et al., 2019, Hu, 2000).

While the ratio of eumelanin to pheomelanin in iridal melanocytes affects eye color similarly to its impact on skin and hair pigmentation, other significant differences exist between uveal and cutaneous melanocytes in their biological characteristics and functions. In contrast to cutaneous melanocytes, uveal melanocytes are mostly in contact with each other, and they do not transfer the melanin pigment to the keratinocytes. Also, uveal melanocytes do not modify their melanin pigment production in response to environmental factors such as UVR. On the other hand, cutaneous melanocytes in the skin actively transfer melanin to the keratinocytes to shield deeper skin layers from UVR damage. This protective mechanism is not observed in uveal melanocytes. Uveal melanocytes do not alter the pigment density to enhance photoprotection or do not change the iris color upon

sunlight exposure. Moreover, RPEs that are situated anterior to the uvea, do not produce melanin in adulthood, contrasting with the dynamic melanin production occurs in cutaneous melanocytes (Wade and Finger, 2001, Sliney, 2002).

While uveal melanocytes in the iris are considered to provide photoprotective benefits by absorbing and scattering the light and quenching the reactive oxygen species (ROS), the role of uveal melanocytes placed in the posterior parts of the eye such as the choroid and ciliary body which are not exposed to UVR remains less clear (Cichorek et al., 2013b, Houtzaggers et al., 2020, Hu, 2000). Uveal melanocytes located at the posterior site of the uvea are hypothesized to act as free radical scavengers due to potential exposure to highly oxidative stress conditions (Hu et al., 2008, Hong et al., 2006). Furthermore, studies suggest that uveal melanocytes might play broader roles in maintaining the eye's homeostasis through immune regulation and involvement in inflammatory and angiogenic processes. Still, further research is necessary to fully understand the functions of the uveal melanocytes situated in different locations in the uveal tract (Mochizuki et al., 2013).

#### **1.2.4. Melanoma and variety of its subtypes**

Melanoma is a cancer type which is the major cause of death from skin diseases that involve the largest organ in humans. Melanoma has the highest prevalence in the United States and other Western countries, having the incidence jump by 270% from 1973 to 2002 and with an enhanced climb (Rastrelli et al., 2014). This cancer type originates from the malignant transformation of the melanocytes that normally produce melanin pigment. This malignant transformation is caused by various factors in different subtypes having the accumulated mutations causing abnormal proliferation, driver events and epigenetic dysregulation (Castro-Perez et al., 2023).

The initial classification mainly focusing on the cutaneous melanoma was majorly based on the morphological characteristics of the initial growth phase and the primary site of the melanocytic lesions. This classification had identified four main types: superficial spreading melanoma (SSM), lentigo malignant melanoma (LMM), nodular melanoma



(NM), and acral-lentiginous melanoma (ALM) (Clark et al., 1986). On the other hand, modern classifications of the melanocytic neoplasms consider factors such as chronic sun damage exposure and lesion locations. The 2018 World Health Organization classification of cutaneous, uveal and mucosal melanomas defines nine distinct subtypes based on their epidemiology, clinical and histological features and genetic profiles (Elder et al., 2020). However, recent reports (Castro-Perez et al., 2023) indicate that some tumors may not even clearly fit these broad categories, depending on the origin and distribution of melanocytes and their properties as shown in **Figure 14**.

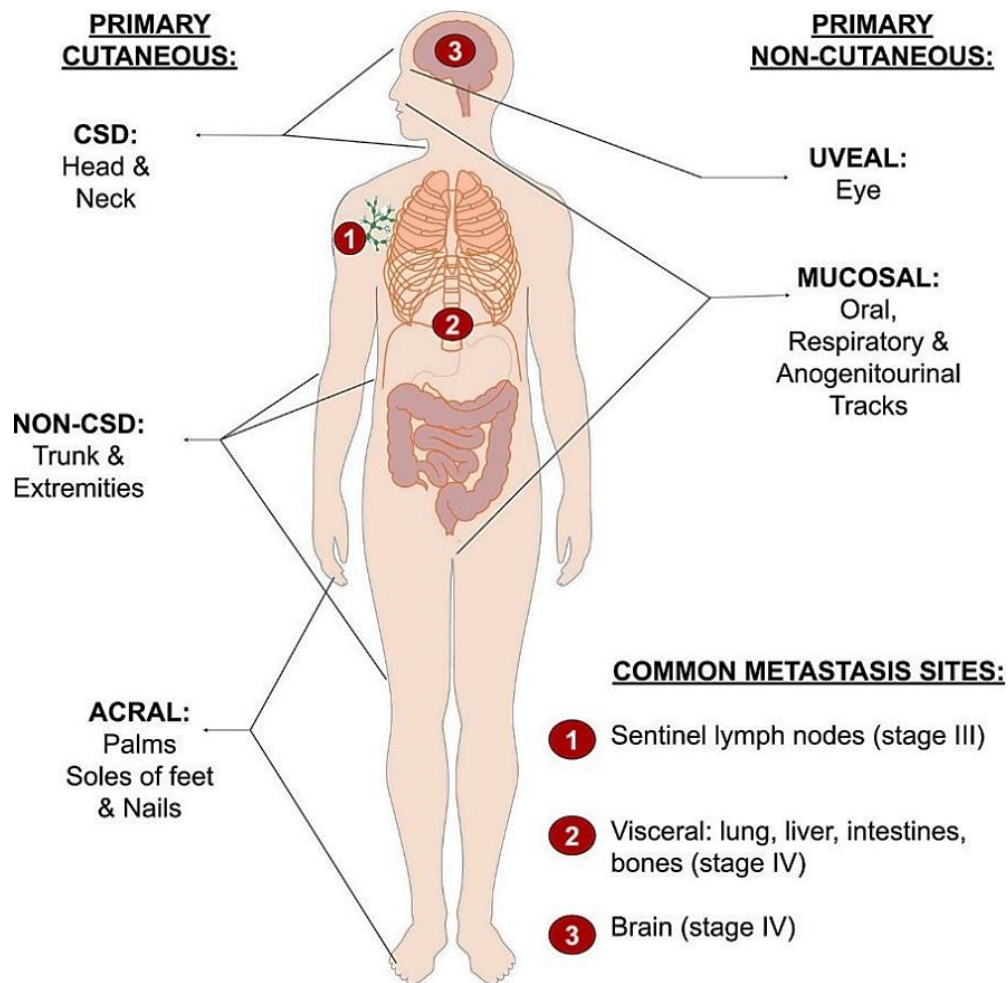


**Figure 14: Multiple anatomical types and the location distributions of melanoma.** (Castro-Perez et al., 2023).

The exact developmental stage of melanocytes from which these histologically unique lesions arise remains unclear. Further research is needed to clarify whether melanocytes

in different skin substructures, such as follicular and interfollicular regions, or from varying precursor cells such as skin-resident melanocyte precursors, melanocyte stem cells, or fully differentiated melanocytes serve as a source for these lesions to originate (Grichnik et al., 2014, Yu et al., 2010, Kulesa et al., 2006). Typically, cutaneous melanomas are most found on hair-bearing skin. Yet, melanomas can also develop on non-hair bearing glabrous skin like the palms, soles, and under the nails, as well as on ocular sites such as the choroid, ciliary body and iris and other sites like mucosal surfaces (Shain and Bastian, 2016). Different types of melanocytic neoplasms may arise from specific susceptibilities to oncogenic transformation. However, whether these diverse melanocytic lesions all stem from mature, differentiated melanocytes or from various precursors within the melanocytic lineage is yet to be clarified (Grichnik et al., 2014). A deeper understanding is needed to uncover how different melanoma subtypes originate from various cellular backgrounds and to enhance the accuracy of melanoma classification, diagnosis, and prognosis.

Distinct clinical and histopathological melanocytic lesions exhibit unique patterns of oncogenic driver mutations (Bastian, 2014). In cutaneous melanoma, these driver mutations categorize the cancer into four main subclasses based on their prevalence and association with chronic sun damage (CSD). Over 60% of these melanomas involve *BRAF* mutations and are typically found in non-CSD cases. About 28% involve *NRAS* mutations and 14% *NF1* mutations, both more commonly associated with CSD. Additionally, about 15% of cases are categorized as triple-wild type lacking mutations in *BRAF*, *NRAS*, or *NF1* and these are predominantly observed in CSD melanomas. Interestingly, these triple-wild type melanomas often exhibit mutations in the *GNA11*, *GNAQ*, *SF3B1*, or *KIT* genes, which are also significant drivers in uveal melanoma (Cancer Genome Atlas, 2015, Hayward et al., 2017, Lawrence et al., 2013, Cirenajwis et al., 2017, Beadling et al., 2008, Torres-Cabala et al., 2009).

In uveal melanoma, the most frequently occurring mutations involve genes such as *GNAQ*, *GNA11*, *BAP1*, *EIF1AX*, and *SF3B1*. Specifically, mutations in the *GNAQ* and *GNA11* genes are identified in approximately 33% and 39% of uveal melanoma cases, respectively and both have the position of Q209L (Moore et al., 2018, Reddy et al., 2017, Shoushtari



and Carvajal, 2014). Melanocytes are also present in the conjunctiva, which is the thin mucous membrane lining the inside of the eyelids and covering the sclera, or white part of the eye. These cells can develop into conjunctival melanoma. Like their counterparts in the uvea and skin, conjunctival melanocytes originate from the neural crest but migrate during different developmental stages (Hu et al., 2007, Iwamoto et al., 2002). While further population studies are needed, existing research indicates that conjunctival melanoma commonly involves mutations in the *BRAF*, *NF1*, *NRAS*, and *c-KIT* genes. These mutations predominantly activate the MAPK pathway and may also trigger the PI3K/AKT/mTOR signaling pathway, crucial for cell growth and survival (Gkiala and Palioura, 2020). Thus, these genetic alterations summarized in **Table 1** are the significant factors for understanding the molecular mechanisms driving melanoma subtypes.

Metastasis mechanisms for melanomas are uncovered to be influenced by both the oncogenic drivers involved and the origin of the cell type. For example, cutaneous melanomas with *BRAF* mutations are notably more likely to metastasize to the brain compared to those without such mutations (Ribas and Flaherty, 2011). On the other hand, uveal melanomas particularly those with mutations in *GNAQ* or *GNA11* genes, tend to spread hematogenously to the liver, lung and bone being the most common metastatic sites. This distinction in metastatic behavior and the sites affected between cutaneous and uveal melanomas raises interesting questions, especially given that the anatomical position of uveal melanomas would intuitively suggest the brain as a more likely site for metastasis compared to *BRAF* mutant cutaneous melanomas (Harbour, 2012, Reddy et al., 2017). Partly answering these questions, it has been indicated that the tendency of melanomas to metastasize to specific tissues and organs may not only reflect the influence of specific driver oncogenes but might also relate to inherent biological characteristics of the melanocyte lineages from which the melanomas originate. This suggests that the cellular origin and genetic background of melanomas play a crucial role in determining their metastatic behavior and target locations (Taube et al., 2009, Holt et al., 2004).

**Table 1: Frequency of the four main types of melanoma subtypes.** (Castro-Perez et al., 2023).

Subtype	Incidence (%)	Mutation	Frequency (%)	Common variants	Exclusive mutations
Cutaneous	91.2	<i>BRAF</i>	60	V600E (80–90%)	<i>NRAS/NF1</i>
		<i>NRAS</i>	28	Q61K, Q61R	<i>BRAF/PTEN</i>
		<i>NF1</i>	14	Deletion/inactivation	<i>BRAF</i>
		Triple WT	15	<i>GNAQ/GNA11/KIT</i>	<i>BRAF/NRAS/NF1</i>
		<i>KIT</i>	28	L576P (70%)	<i>BRAF/NRAS</i>
		<i>PTEN</i>	14	Deletion/inactivation	Unk/ND
		<i>MITF</i>	10	Amplification/activation	Unk/ND
		<i>CDKN2A</i>	2	Deletion/inactivation	Unk/ND
		<i>TERT</i>	29 (all)	Amplification/activation	Unk/ND
		<i>TP53</i>	20 (all)	Deletion/inactivation	Unk/ND
Uveal	5.2	<i>GNAQ</i>	33	Q209L (90%)	<i>BRAF/NRAS/GNA11</i>
		<i>GNA11</i>	39	Q209L (90%)	<i>BRAF/NRAS/GNAQ</i>
		<i>BAP1</i>	45	Del/inactivation	<i>EIF1AX/SF3B1</i>
		<i>EIF1AX</i>	14-20	A11T, N4S	<i>SF3B1/BAP1</i>
		<i>SF3B1</i>	22	R625C/H/L	<i>EIF1AX/BAP1</i>
Acral	2.3	<i>CCND1</i>	45	Amplification	Unk/ND
		<i>KIT</i>	36	L576P, activation	<i>BRAF/NRAS</i>
		<i>PDGFRA</i>	7	Amplification/activation	<i>KIT</i>
Mucosal	1.3	<i>KIT</i>	39	L576P, K642E	<i>BRAF/NRAS/PDGFRA</i>
		<i>PDGFRA</i>	4	Amplification/activation	<i>KIT</i>
		<i>GNAQ</i>	4.6	Q209L (92%)	<i>GNA11</i>
		<i>GNA11</i>	4.9	Q209L (92%)	<i>GNAQ</i>
		<i>SF3B1</i>	20-35	R625H/S/C	Unk/ND

The next chapter focuses more specifically on uveal melanoma, a subtype of melanoma that arise uniquely within the uveal tract of the eye and presents many complex biological and clinical challenges which distinct it apart from the cutaneous counterpart.

### 1.3. Uveal Melanoma

Uveal melanoma (UM) is recognized as the most prevalent primary intraocular tumor in adults having an estimated incidence of about 4.3 cases per million people globally, even though it is accepted as a rare type of cancer. UM accounts for approximately 5% of all melanoma cases. Despite its melanocytic roots that have some shared similarities to cutaneous melanoma, UM has major differences in terms of its causes, genetic profile and progression of the disease (Mahendraraj et al., 2016, Singh et al., 2011, Rodrigues et al., 2019, Pandiani et al., 2017).

The historical context of UM traces back to the early 19<sup>th</sup> century around 1809-1812. One of the first known cases was documented by Scottish surgeons Allan Burns and James Wardrop. Burns involved Wardrop in the enucleation of a woman's eye and the patient later understood to have UM. The presence of intraocular tumors had previously been detected by Wardrop in young children. According to the initial observations of Wardrop, he thought the tumor to originate from the retina, and he considered enucleation as a potential treatment for the disease (Wardrop, 1809). Unlike the typically white retinoblastoma tumors, the tumor in the woman patient was black which is attributed to pigmentation from the choroid. This situation only became apparent after the eye's removal about 1.5 years later from the initial symptoms occurred. Initially, the patient suffered progressive vision loss, ending in total blindness four months before surgery. Tragically, she had liver metastasis which is a common site for UM spread one year following the enucleation procedure of the eye (Burns, 1811, Kivela, 2018).

UM originates from an overgrowth of melanocytes located in the uveal tract, including the iris, ciliary body, and choroid. Statistically, the majority of UM cases (approximately 90%) originate in the choroid, while a smaller percentage develop in the ciliary body (5-7%) or the iris (3-5%) (Shields et al., 2012, Mahendraraj et al., 2016, Lamas et al., 2021) as illustrated in **Figure 15**.

UM symptoms often include the blurred vision and the loss of visual field. On the other hand, many cases are asymptomatic and this situation causes delayed diagnoses. This

delay is because the tumors typically develop in regions that are not visible on the surface of the eye such as occurring between the sclera and retina. While primary tumors are generally treated the methods like brachytherapy, external radiation therapy or enucleation for the particularly large tumors, metastasis event occurs in 30 to 50% of the cases. The liver is the primarily affected organ in about 90% of these metastasis cases. Despite recent advances, metastatic UM leads to poor outcomes having the median survival rates ranging from 9 to 16 months (Carvajal et al., 2018, Augsburger et al., 2009).

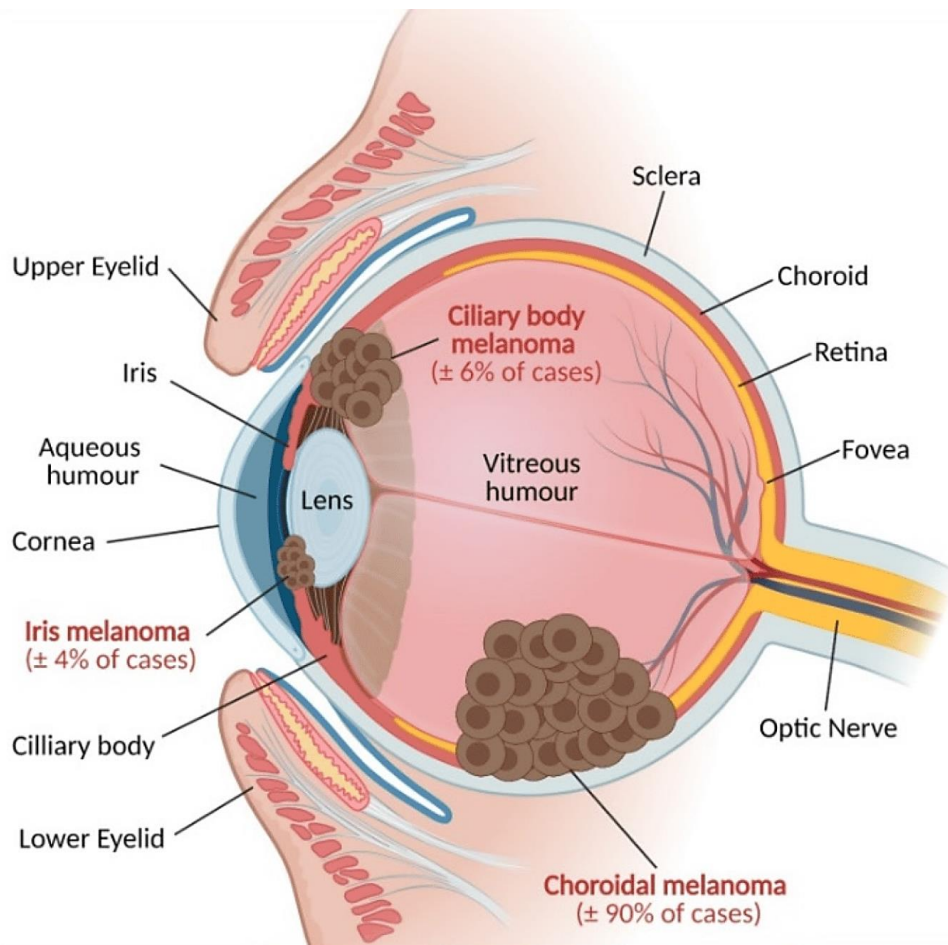


**Figure 15: Sites for the UM tumor development.** (Lamas et al., 2021).

Most cases of UM are unilateral and unifocal. Also, extremely rare bilateral cases have been reported. The estimated lifetime risk of developing bilateral UM is extremely low, it is about 1 in 50 million with a 0.2% chance of a bilateral occurrence after an initial diagnosis (Sturm and Richard, 2007, Singh et al., 1996). Unilateral and multifocal UMs in which a

second tumor develops are even rarer and typically associated with ocular melanocytosis or germline *BAP1* mutations which are the significant risk factors (Echegaray et al., 2019).

UM tumors can differ greatly in terms of size, shape, location and color influencing their detectability (Rodriguez et al., 2016). Notably, a strong negative correlation between the survival rate of the UM patients and their basal tumor size is observed (Damato and Coupland, 2009a, Damato, 2010) as shown in **Figure 16**.

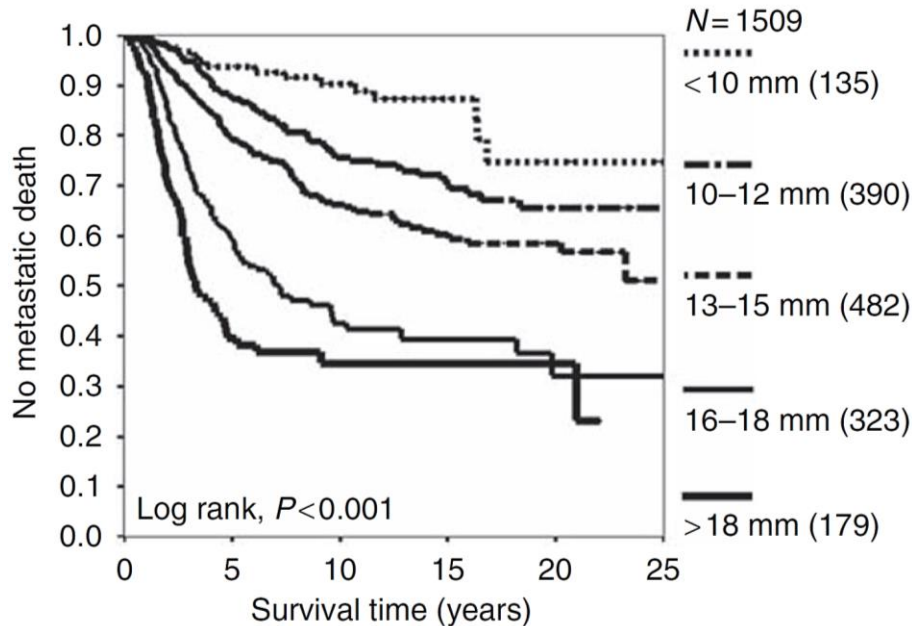


**Figure 16: Kaplan-Meier curve showing the correlation between the survival rate and the tumor size.** (Damato, 2010).

Their pigmentation can range from the non-pigmented to the highly pigmented with multiple pigmentation levels even within the same tumor. Melanotic UMs generally produce both eumelanin and pheomelanin due to active melanosomes but amelanotic tumors that are characterized by low tyrosinase activity primarily produce pheomelanin (Houtzagers et al., 2020).

Management strategies: Primary tumors are locally treated based on their size, location, retinal invasion and detachment. Classical treatments are radiotherapy and enucleation surgery. Radiotherapy options such as plaque brachytherapy and proton beam therapy have the benefits of preserving the eye. Brachytherapy is used for small, easily accessible tumors but larger or more posterior tumors are treated with proton beam therapy or

enucleation (Jager et al., 2020, Shields and Shields, 2015, Dogrusoz et al., 2017b). Enucleation involves the removal of the entire eyeball and the process is generally applied for cases where other treatments are not suitable. Adjuvant chemotherapy with fotemustine has been tested in UM patients carrying high risks of metastasis whereas it did not result in improved survival (Shields and Shields, 2015, Rodriguez-Vidal et al., 2020). The preferred treatment for the primary tumors varies by country (Jager et al., 2020).

Nearly 50% of UM patients develop metastases lacking curative treatment options and are associated with very poor prognosis. Overall survival (OS) after a metastatic diagnosis has not improved more than the past 30 years and it remains at about 12 months. Chemotherapy agents that are used for cutaneous melanoma have been tested in metastatic UM but the response rates are significantly low because of a high chemoresistance. Survival rates stayed between 4 to 17 months (Rodriguez-Vidal et al., 2020). Drugs such as dacarbazine, cisplatin, temozolomide, fotemustine, bendamustine and others have also shown very poor response rates and no clinical improvement (Carvajal et al., 2017, Bhatia et al., 2012, Homsy et al., 2010, Kivela et al., 2003). Also, modern chemotherapy agents like paclitaxel, vincristine, or docosahexaenoic acid have not yielded better results (Pons et al., 2011).

UM metastasized to the liver in nearly 90% of the cases. Thus, liver-directed therapies including surgical resection, intra-arterial chemotherapy and hepatic chemoembolization have been attempted but the clinical trials comparing intravenous and intra-arterial administration of the chemotherapeutic agents such as fotemustine or melphalan have not improved the OS (Leyvraz et al., 2014, Hughes et al., 2016). Also, trials with MAPK inhibitors like sorafenib, imatinib or sunitinib have resulted in a median overall survival of 6 months (Rodriguez-Vidal et al., 2020). Combined inhibition of Gαq downstream effectors MEK and PI3K, PI3K and mTOR, and Mdm2 and PKC have shown promise in cell lines but have not performed as well in clinical settings (Carvajal et al., 2018, Heijkants et al., 2018, Sacco et al., 2024, Wespiser et al., 2023).

Immunotherapy approaches such as immune checkpoint blockade have been tried in UM but they have been less successful than in cutaneous melanoma. Agents like ipilimumab

which targets CTLA-4 have shown response rates less than 5% with the OS less than 6 months (Khattak et al., 2013, Wolchok et al., 2013). PD-1 inhibitors have also resulted in low response rates and the OS less than 1 year which is significantly lower than in cutaneous melanoma. Recent research revealed that PD-1 and CTLA-4 are not always particularly expressed in the tumor-infiltrating immune cells on the other hand, LAG3 negative checkpoint inhibitor is prevalent in CD8+ T-cells which would offer new strategies for the immune checkpoint blockade in the UM (Durante et al., 2020). T-cell redirection strategies have recently shown a high potential in treating metastatic UM (Smith et al., 2019). Very recently, trials of a cutting-edge bi-specific immunotherapy drug named Tebentafusp has improved OS to 21.7 months in phase III clinical trials. Tebentafusp (IMCgp100) is a bispecific fusion protein that targets the gp100 (Premelanosome protein, *PMEL*) antigen on melanoma cells with a high-affinity and then, redirects T-cells specifically to the UM cells via an antibody portion targeting CD3. This shows a partial promise in increasing OS for the patients and it could become the first standard treatment for metastatic UM (Boutros et al., 2024, Carvajal et al., 2023, Eteghadi et al., 2024, Middleton et al., 2020, Damato et al., 2019).

These overall poor clinical results including low OS and disease-free survival of this dismal disease point out the urgent need for a better understanding of the molecular programs deciphering the mechanisms of the genomic, transcriptomic and epigenetic regulations.

### **1.3.1. Genetic landscape, somatic mutations, and subtypes of UM**

UM tumors present a genetic stability with minimal structural variants and one of the lowest tumor mutation burdens (TMB) among all cancer types. The tumors display an average mutation rate of 0.5 single nucleotide variants (SNVs) per megabase (Mb). This is significantly less than what is observed in other melanoma subtypes (Johansson et al., 2016, Furney et al., 2013) as illustrated in **Figure 17**.

Although whole genome sequencing (WGS) studies, including those by Furney and colleagues found no evidence of UV-related mutations in UM (Furney et al., 2013), some studies suggest that exposure to blue light (peak 475 nm) may increase mitotic division in

human UM cell lines (Marshall et al., 2006, Di Cesare et al., 2009). While the exact mechanism remains unclear, shorter wavelengths of visible light such as blue light, are known to induce cell death in retinal pigment epithelial cells through mitochondrial ROS production (Logan et al., 2015, King et al., 2004).

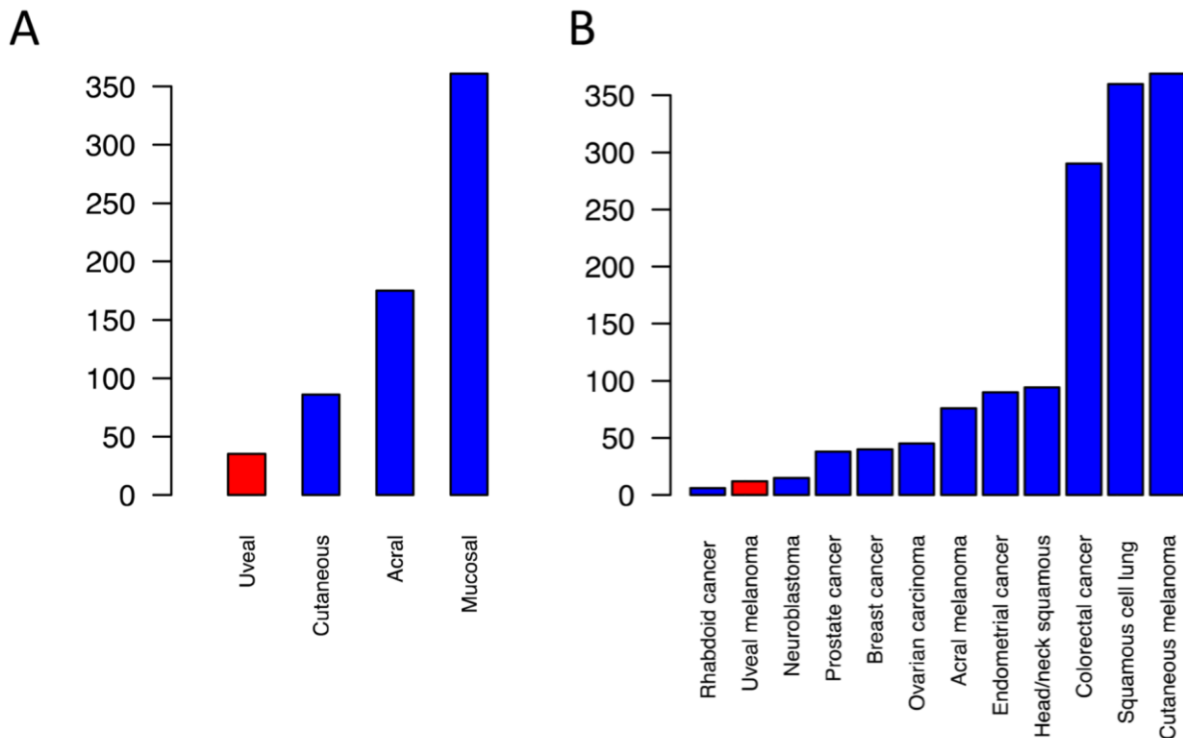


**Figure 17: Comparisons of the somatic mutation profiles** within (A) melanoma subtypes, (B) various solid tumor types (Furney et al., 2013).

UVR-induced mutations are usually marked by C>T transitions in pyrimidine dinucleotides and they are common (80-90% of the mutations) in cutaneous melanoma (Robertson et al., 2017, Royer-Bertrand et al., 2016, Ikehata and Ono, 2011, Berger et al., 2012, Cancer Genome Atlas, 2015). Unlike other UM subtypes, iris melanoma presents a clear UVR mutation signature, despite being a small percentage of UM cases. This subtype, which also harbors *GNAQ/GNA11* and *BAP1* alterations, is directly exposed to sunlight unlike the more shielded posterior parts of the eye. This highlights the genetic differences between the front (anterior) and back (posterior) parts of the eye in UM (Johansson et al., 2020).



The absence of a UVR-induced mutational landscape in most UM cases is important for understanding how this cancer develops.

In UM, two primary genetic changes occur 1) “activating” mutations in the genes of Gαq G-protein coupled receptor signaling pathway including *GNAQ*, *GNA11*, *PLCB4*, or *CYSLTR2* and 2) secondary mutations in *BAP1*, *SF3B1* or *EIF1AX* genes.

Over 90% of UMs bear mutations in either *GNAQ* (Guanine nucleotide-binding protein G(q) subunit alpha) or *GNA11* (Guanine nucleotide-binding protein subunit alpha-11) genes. Fewer cases involve mutations in *CYSLTR2* (Cysteinyl leukotriene receptor 2) at around 4% and *PLCB4* (1-phosphatidylinositol 4,5-bisphosphate phosphodiesterase beta-4) at around 2.5% (Chua et al., 2017, Van Raamsdonk et al., 2010, Robertson et al., 2017). These mutations are mutually exclusive and result in the constant activation of the Gαq signaling pathway. This situation causes the dysregulation and over-activation of several downstream pathways including the MAP-kinase (RAS/RAF/MEK/ERK) cascade as illustrated in **Figure 18** (Vivet-Noguer et al., 2019). This cascade is triggered by the activation of phospholipase Cβ (PLCβ), which cleaves phosphatidylinositol (PIP2) into diacylglycerol (DAG) and inositol triphosphate (IP3). The resulting increase in cytoplasmic calcium along with DAG then activates protein kinase C (PKC) which is a key initiator of the MAPK pathway. RAS guanyl-releasing protein 3 (RASGRP3) in the MAPK pathway is found to be highly expressed in *GNAQ/GNA11*-mutated tumors and cell lines. Although MAPK signaling is overactivated in UM, the precise mechanism by which oncogenic *GNAQ/GNA11* triggers this MAPK pathway remains unclear. (Chen et al., 2017, Moore et al., 2018). Dysregulated downstream pathways of UM include the overactivation of a PLCβ-independent pathway involving the activation of Yes-associated protein (YAP) via Rho small GTPase, mediated by TRIO downstream of Gαq. Other pathways dysregulated in UM include the β-catenin pathway, activated by Gαq through small GTPase ARF6 and the PI3K/Akt/mTOR signaling cascade (Lapadula and Benovic, 2021).

The second set of the critical mutations in UM include alterations in *BAP1* (BRCA1 Associated Protein 1), *SF3B1* (Splicing Factor 3b Subunit 1), and *EIF1AX* (Eukaryotic

translation initiation factor 1A, X-chromosomal), and occur in a mutually exclusive pattern within UM cases (Gentien et al., 2023). These exclusive mutations are also associated with different prognostic outcomes. Specifically, loss-of-function mutations in *BAP1* are generally connected with Monosomy of chromosome 3 (Monosomy 3, M3) and an increased risk of early metastasis. On the other hand, mutations in *SF3B1* are often associated with Disomy of chromosome 3 (Disomy 3, D3) and a higher likelihood of late-onset metastasis. In addition, *EIF1AX* mutations are also linked to Disomy 3 and a reduced metastatic risk (Khan et al., 2024, Mastronikolis et al., 2021, Jager et al., 2020).

#### 1.3.1.1. Primary (driver) mutations in the Gαq pathway

Mutations in the *GNAQ*, *GNA11*, *PLCB4*, or *CYSLTR2* genes function to increase gene activity, occur in a mutually exclusive manner and cause the continuous activation of the Gαq signaling pathway thereby dysregulation of the downstream signal transduction pathways as illustrated in **Figure 18**. These mutations represent a "first set" of the driving events in all cases of the UM. These mutually exclusive driver mutations emerge very early in the cancer process and present at all stages of the malignant progression. They are found to initiate the tumorigenesis however, these "driver", "first set" Gαq mutations alone are not sufficient to cause a malignant transformation (Field et al., 2018, Onken et al., 2008).

*GNAQ* and *GNA11* are GPCR subunit genes that encode the Gα subunits of the Gαq heterotrimeric proteins consisting of α, β, and γ subunits. These proteins have roles as essential membrane-bound signal transducers carrying on the GTPase activity and acting downstream of the GPCRs. In their inactive state, GPCRs are bound to the Gα subunit which is linked to guanosine diphosphate (GDP) and the Gβγ partners that form an inactive G protein trimer. Activation occurs when an extracellular ligand binds to the GPCR and causes a conformational change. This conformational change prompts Gα to release GDP and bind guanosine triphosphate (GTP) in turn and activates it. The activated Gα-GTP then dissociates from Gβγ and allows both to initiate their respective downstream signaling pathways (Van Raamsdonk et al., 2010, Silva-Rodriguez et al., 2022, Babchia et al., 2010).

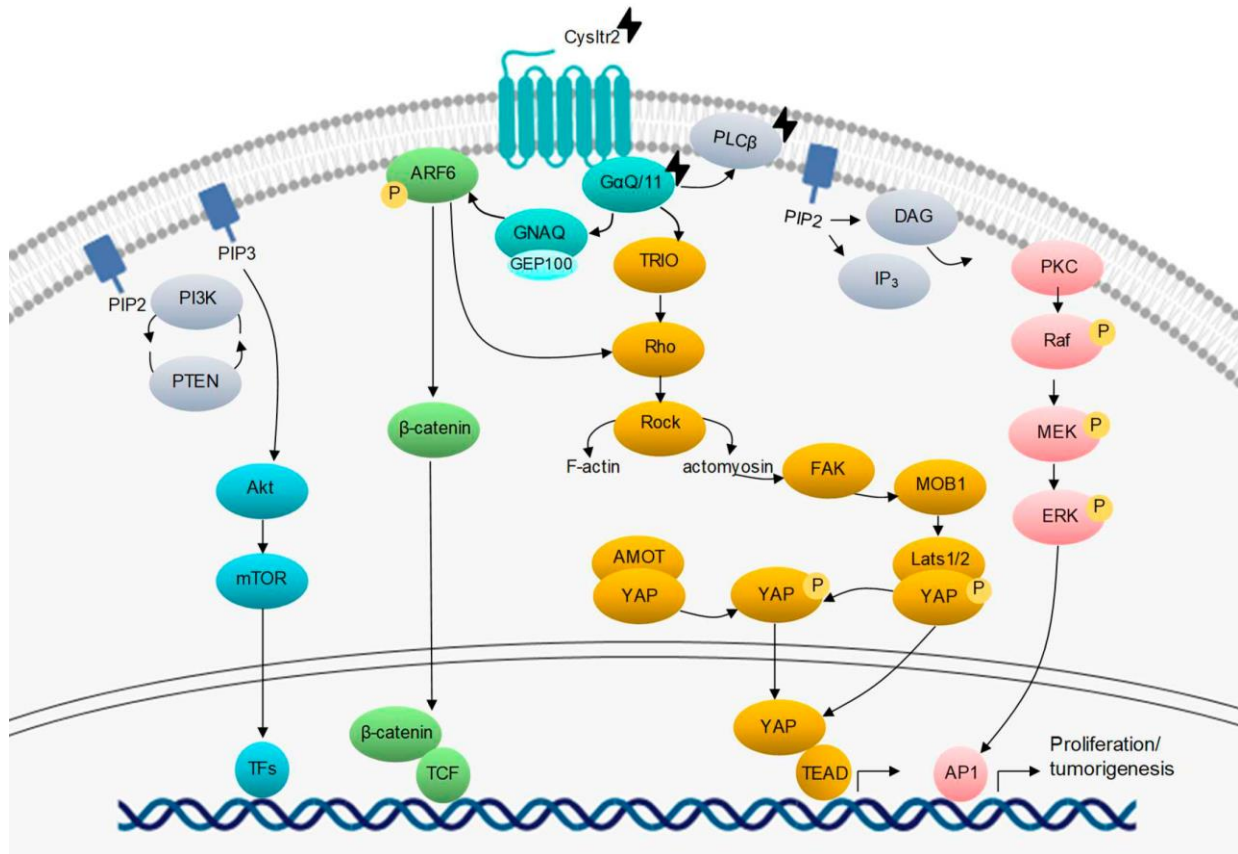


**Figure 18: Driver mutations on *GNAQ*, *GNA11*, *PLCB4* and *CYSLTR2* genes constitutively activating the Gαq pathway and its downstream signal transduction pathways.** (Vivet-Noguer et al., 2019).

*GNAQ* and *GNA11* are oncogenes that are paralogous with each other and they are mutated in approximately 85% to 90% of all UM cases. It makes these mutations the most common in the Gαq signaling pathway for this cancer type. These genes are almost identical having 90% amino acid homology and they are widely expressed across different tissues (Van Raamsdonk et al., 2010, Van Raamsdonk et al., 2009). The activating mutations primarily occur at two specific hotspots: 1) mutation predominantly at codon Q209 in exon 4 which accounts for 95% of cases, 2) mutation less frequently at the R183 position in exon 5, observed in 5% of cases. In addition, mutations may also arise at the G48 hotspot. These somatic mutations are not limited to UM and they also occur in nevi of Ota, which manifest as facial hyperpigmentation, where these oncogenes play a role in evolving into melanoma (Robertson et al., 2017, Amaro et al., 2017, Gerami et al., 2010, Hitchman et al., 2021). Also, the *GNAQ* R183Q somatic mosaic mutation is linked to the

development of port-wine stains and Sturge-Weber syndromes (Shirley et al., 2013). However, the impact of this mutation varies depending on the specific timing of its occurrence during developmental stages. To note, nearly all choroidal nevi possess a clonal mutation in either *GNAQ* or *GNA11* which supports the theory that UM may arise from the malignant transformation of a pre-existing nevus with mutations in *GNAQ/GNA11* serving as the initial driving event in UM development (Vader et al., 2017).

Although the exact mechanisms through which the Gαq signaling pathway causes oncogenesis are not fully defined, the initial driver event in UM tumorigenesis appears to involve these mutually exclusive mutations as observed in nearly all UM cases. These mutations are considered the primary triggers for the development of UM (Amaro et al., 2017). Research showed that these genetic alterations are linked more to tumor initiation than to metastatic progression. These mutations do not result in differing prognoses or clinical outcomes which indicates their primary role in the early stages of tumor formation (Robertson et al., 2017, Koopmans et al., 2013, Onken et al., 2008, Silva-Rodriguez et al., 2022, Moore et al., 2016).

#### 1.3.1.2. Secondary mutations

Relatively low frequency of the choroidal nevi which progresses into melanoma compared to the incidence of UM shows that an additional critical mutation is necessary for the malignant transformation in UM. These secondary and nearly exclusive mutations occur in *BAP1*, *SF3B1* and *EIF1AX* (Harbour et al., 2010, Yavuzyigitoglu et al., 2016b, Furney et al., 2013, Martin et al., 2013, Harbour et al., 2013). The presence of these mutations is closely linked with the prognosis of the disease (Robertson et al., 2017, Royer-Bertrand et al., 2016) as shown with the survival plot in **Figure 19**.

**BRCA-1 associated protein 1 (*BAP1*)** gene mutation is the major secondary mutation in UM. Bi-allelic inactivation of *BAP1* is evident in about 50% of the primary UM and 85% of the metastatic UM cases. *BAP1* functions as a tumor suppressor gene (TSG) in UM but the loss-of-function mutations occur along the exons of the gene. Its bi-allelic inactivation follows Knudson's two-hit involving a deleterious mutation in one allele and loss of

heterozygosity (LOH) of the other allele through Monosomy 3 or less commonly Isodisomy 3. This cytogenetic alteration is commonly linked with a poor prognosis (Amaro et al., 2017, Harbour et al., 2010, Prescher et al., 1996). UM tumors with deactivated *BAP1* are known to have a significantly higher risk of tumor progression and metastatic relapse. Also, they are associated with the poorest outcomes (Robertson et al., 2017).

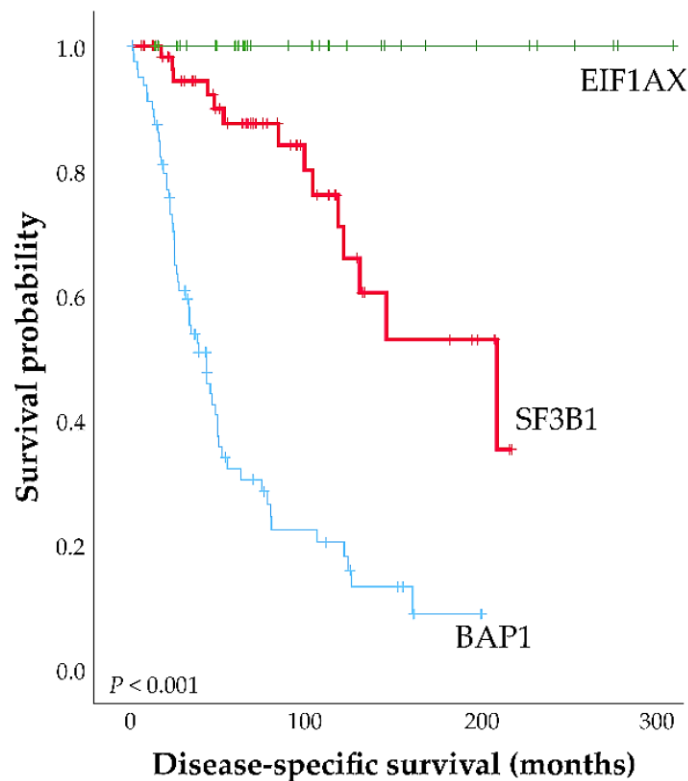


**Figure 19: Kaplan-Meier plot of the three groups of UM patients (n=185) with the secondary gene mutations: *EIF1AX* (n = 33), *SF3B1* (n = 63), *BAP1* (n = 89).** (Nguyen et al., 2020).

Somatic inactivation of *BAP1* plays a role also in various other cancers including mesothelioma, clear renal cell carcinoma (RCC) and some cutaneous melanocytic tumors. Germline mutations in *BAP1* occur in 2–4% of all UM cases and strongly predispose individuals to UM (Murali et al., 2013, Gupta et al., 2015, Aoude et al., 2013, Singh et al., 2021). These germline mutations act as the first of the two required hits for the complete gene inactivation and they are prevalent in multiple cancer types defining the “*BAP1* Tumor Predisposition Syndrome” (*BAP1*-TPDS). It includes UM, mesothelioma, RCC, melanocytic tumors and basal cell carcinoma. This syndrome is also linked with aggressive

tumors and poor prognosis (Abdel-Rahman et al., 2011, Walpole et al., 2018, Popova et al., 2013, Testa et al., 2011, Wiesner et al., 2011, Carbone et al., 2012, Pilarski et al., 2014). Further details on BAP1 and its functions in UM are explained in the section “1.3.3. BRCA-1 associated protein 1 (BAP1)” in this thesis.

**Splicing factor 3B subunit 1 (*SF3B1*)** gene mutation occurs in 25% of the primary UMs. The missense mutations typically occur at hotspots R625, H666 and less commonly at K700 that is found as more often mutated in myelodysplastic syndrome and chronic lymphocytic leukemia (Furney et al., 2013, Harbour et al., 2013, Visconte et al., 2012, Cazzola et al., 2013, Yoshida et al., 2011). In UM, *SF3B1* mutations are almost mutually exclusive with mutations in *BAP1* and *EIF1AX*. It is linked to a lower to moderate risk of metastasis compared to *BAP1* mutations but longer patient follow-up studies have shown a higher rate of late-onset metastases (more than 5-10 years after UM diagnosis) (Yavuziyigitoglu et al., 2016a). *SF3B1* gene encodes splicing factor 3B subunit 1 which is a key component of the U2 small nuclear ribonucleoprotein (snRNP) complex within the spliceosome. It plays a crucial role in early RNA splicing stages by recognizing the branch point (BP) upstream of the 3' splice site and recruiting U2 snRNP having the interaction with intronic RNA and U2AF that is essential for correct splicing. *SF3B1* change-of-function mutations cause to the recognition of alternative BPs which disrupt normal splicing at about 1% of splicing junctions and cause the use of cryptic 3' splice sites. This contributes to transcriptomic and proteomic diversity in tumors (Furney et al., 2013, Gozani et al., 1998, Alsafadi et al., 2016, Darman et al., 2015, DeBoever et al., 2015, Jayasinghe et al., 2018). The exact mechanisms by which *SF3B1*-related splicing defects drive UM malignancy remain unclear. Potential outcomes of cryptic splice site usage include mRNA degradation if the intronic insertion is out-of-frame but, in about one-third of abnormal transcripts where the insertions are in-frame could lead to the production of altered or activated proteins (Jager et al., 2020).

**Eukaryotic Translation Initiation Factor 1A X-Linked (*EIF1AX*)** is the third secondary and mutually exclusive mutation in UM. Somatic mutations in *EIF1AX* were first identified in UM by Martin and colleagues (Martin et al., 2013). These mutations generally occur in

the absence of *BAP1* or *SF3B1* mutations, primarily in tumors with Disomy 3 and rarely in the Monosomy 3 cases. UM cases with somatic *EIF1AX* mutations are associated with a good prognosis and have very low metastatic risk (Ewens et al., 2014, Robertson et al., 2017). Missense mutations and small deletions in *EIF1AX* appear in about 15–20% of UMs, particularly within the unstructured N-terminal tail (NTT) of eIF1A (Martin et al., 2013, Amaro et al., 2017). As a key part of the 43S preinitiation complex, eIF1A facilitates the transfer of methionyl initiator tRNA to the small 40S ribosomal subunit which is essential for the translation initiation. The functional impact of *EIF1AX* mutations in UM is not fully understood. It has been suggested that these mutations might cause the use of alternative start codons to compensate for a weak recruitment of the ternary complex at the first start site and potentially lead to the different ratios of protein isoforms (Saini et al., 2010, Martin et al., 2013). The specific protein targets and the mechanisms through which *EIF1AX* mutations contribute to tumorigenesis without significantly affecting metastatic risk remain to be uncovered (Johnson et al., 2017).

#### 1.3.1.3. Copy Number Alterations (CNAs)

Compared to many other cancers, most UMs exhibit relatively low genomic instability and aneuploidy. Primary UM is characterized by recurrent chromosomal aberrations in chromosomes 1, 3, 6, 8, 9 and 16 and these are strongly linked to prognosis. Also, they are used to classify patients into risk groups as illustrated in **Figure 20**. The most common chromosomal changes in the primary UM include 1p loss (28–34%), 1q gain (24%), 3 loss (50–61%), 6p gain (28–54%), 6q gain (28–54%), 6q loss (25–38%), 8p loss (17–28%), 8q gain (36–63%), 9p loss (24%) and 16q loss (16%) (Kilic et al., 2006, Coupland et al., 2013). These abnormalities were initially detected using standard karyotypic analyses (Wiltshire et al., 1993, Prescher et al., 1995) and later confirmed by fluorescence in situ hybridization (FISH) (Patel et al., 2001), comparative genomic hybridization (CGH) (Aalto et al., 2001, Hughes et al., 2005, Ehlers et al., 2008), spectral karyotyping (Naus et al., 2001), microsatellite analysis (MSA) (Scholes et al., 2003), multiplex ligation-dependent probe amplification (MLPA) (Damato et al., 2010), and single-nucleotide polymorphism (SNP) analysis (Onken et al., 2007). Among these cytogenetic changes, Monosomy 3 and 8q

gain are particularly significant as they are strongly associated with poor prognosis and a high risk of metastasis (Robertson et al., 2017, Royer-Bertrand et al., 2016, Field et al., 2018).

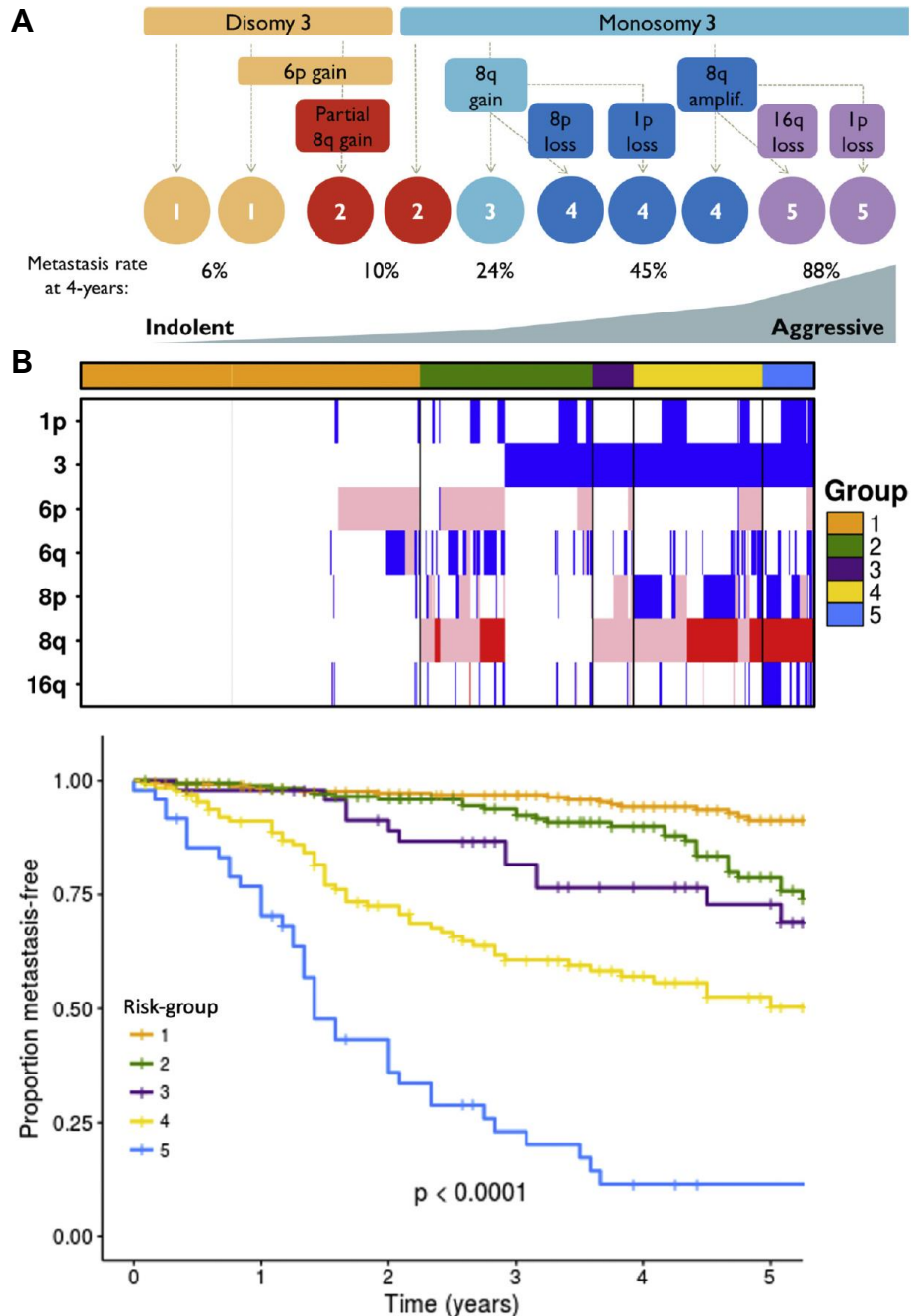


**Figure 20: Recurrent copy number alterations (CNAs) based risk groups proposed to define the molecular subtypes for prognostication of UM. (A) Scheme of the classification (B) Metastasis-free survival plot based on the proposed scheme. The log-rank P value is shown. (Lalonde et al., 2022).**



**Monosomy 3 (M3):** The most frequent chromosomal alteration in UM is the loss of one copy of chromosome 3 which is known as Monosomy 3 (M3). This aberration occurs in about 50% of cases and it is highly specific to UM (Scholes et al., 2003, Sisley et al., 1990). For more than twenty-five years it has been consistently shown that there is a strong correlation between M3 and the development of metastasis (Prescher et al., 1996). *BAP1* gene that is located at the 3p21.1 region on the genome plays a crucial role in UM progression thus and M3 is associated with poor prognosis and it is the strongest predictor of high metastatic risk. Thus, this poor prognosis is reasonably attributed to the alterations in the *BAP1* gene (Aalto et al., 2001, Damato and Coupland, 2009b, Prescher et al., 1996). In addition, M3 is strongly associated with several clinical and histopathological features such as epithelioid cell type, closed vascular patterns, large tumor size and involvement of the ciliary body (Aalto et al., 2001, Scholes et al., 2003, Prescher et al., 1996). It is suggested that M3 happens as an early event in the tumorigenesis because it often co-occurs with other chromosomal abnormalities. In 5–10% of cases, one copy of chromosome 3 is lost while the remaining copy is duplicated. This results in a state known as chromosome 3 isodisomy and it has a prognosis like M3 (Prescher et al., 1995, Onken et al., 2007).

**8q gain:** Chromosome 8 alterations are common in the UM cases (Dogrusoz and Jager, 2018). Gain in the long arm of chromosome 8 (8q) is observed in 37% - 63% of the primary UM patients and it is associated with the poor prognosis (Kilic et al., 2006, Ewens et al., 2013, van den Bosch et al., 2012, Dogrusoz et al., 2017a). This gain is an important factor in predicting shorter survival and mostly occurs together with M3 either as an 8q gain or isodisomy (Hughes et al., 2005, Sisley et al., 1997, White et al., 1998, Cassoux et al., 2014) as shown in **Figure 21**. This combination correlates with higher metastatic rates compared to a single alteration. Abnormalities in chromosomes 3 and 8 are more frequent in UMs which are in the ciliary body. Alterations specifically in 8q are more frequent in UMs derived from choroid (Prescher et al., 1995, Aalto et al., 2001, Sisley et al., 2000). While 8q abnormalities correlate with larger tumor diameter, there is no significant relationship

between 8q gain and metastasis from univariate analysis. This suggests that 8q gain occurs later after following monosomy 3 (Kilic et al., 2006).

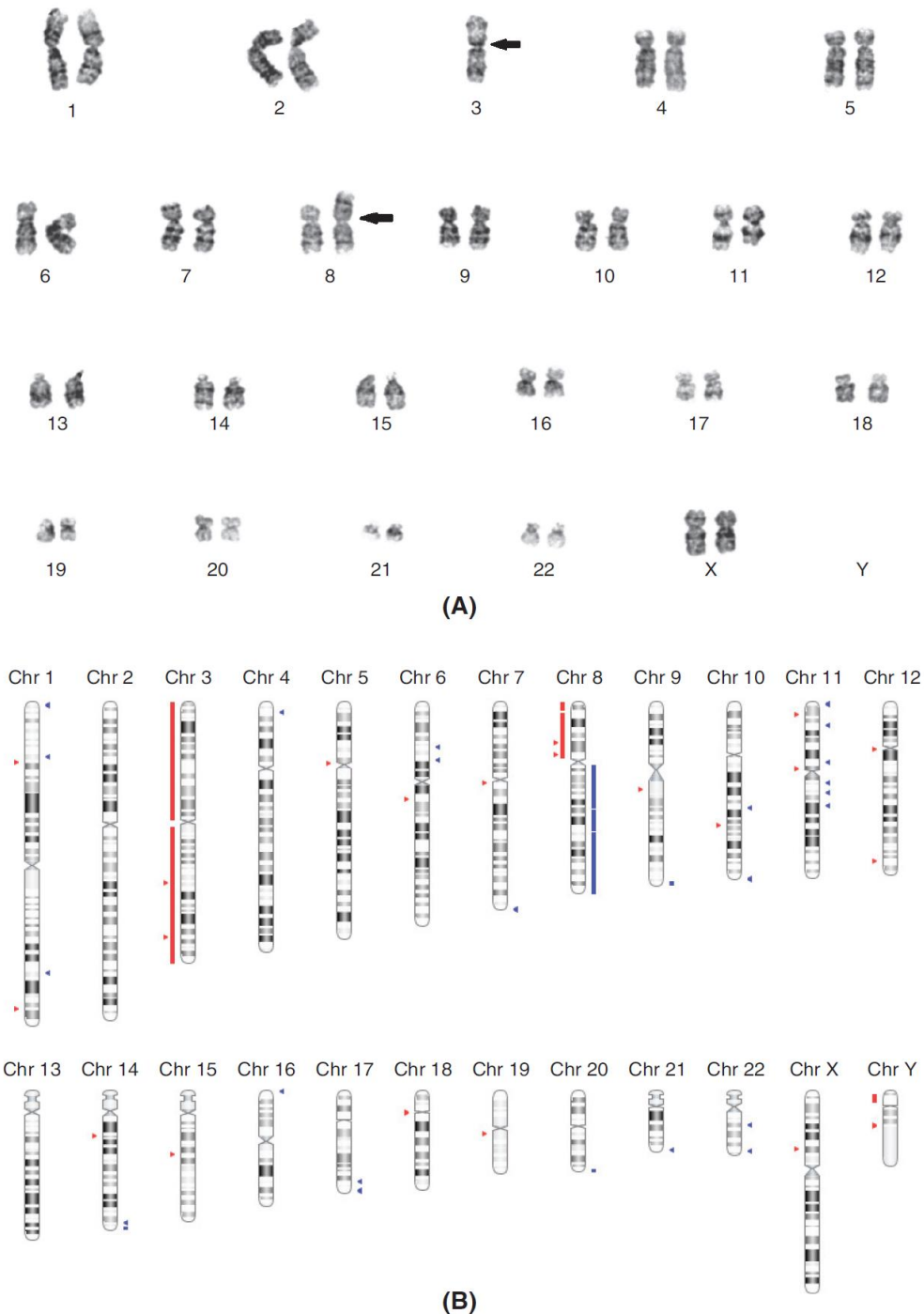


**Figure 21: Chromosomal alterations of a primary UM patient particularly showing M3 and 8q gain. (A)** Loss of chromosome 3 (M3) and aberrations in chromosome 8 shown with arrows on the karyotype **(B)** Array CGH profile shows the loss (chromosome 3, chromosome 8p) in red and the gain (chromosome 8q) in blue. (Doherty et al., 2018).

The 5-year mortality rate is 66% for the cases with both monosomy 3 and 8q gain, 40% for monosomy 3 alone, and 31% for 8q gain alone (Fallico et al., 2021, Scholes et al., 2003). Research indicated that the status of chromosome 3 and 8q can improve the prognostic value of the AJCC staging system in which tumors with both alterations had an increased risk of metastatic death (Dogrusoz et al., 2017a). Oncogenes on chromosome 8q such as *MYC*, *NBS1/NBN* and *DDEF1/ASAP1* are thought to be potential factors in UM (Parrella et al., 2001, Ehlers and Harbour, 2005, Ehlers et al., 2005). In 50% of the UMs, the *NBN* gene is overexpressed having its protein involved in the DNA repair potentially promoting tumor progression. Also, high expression of *DDEF1/ASAP1* may contribute to metastasis by increasing cell motility (Ehlers and Harbour, 2005, Ehlers et al., 2005).

#### 1.3.1.4. Evolutionary routes of the tumor

Tumor evolution in the UM is presented by the contribution of the mutational waves and clonal expansions which lead to the development of malignant tumors. Uveal melanocytes are thought to gradually evolve into pre-neoplastic nevi through an early oncogenic event involving activating mutations in the Gαq signaling pathway on the other hand, these Gαq alterations are insufficient alone to direct the tumorigenesis. These mutations, found in *GNAQ/GNA11* are also present in uveal nevi and benign blue nevi unlike the secondary mutations (Van Raamsdonk et al., 2010, Vader et al., 2017). Then, the most recent common ancestor (MRCA) of the UM would possess *GNAQ/GNA11* mutations and begin to accumulate sub-clonal somatic mutations. Eventually, a second oncogenic event involving combinations of *BAP1*, *SF3B1* and *EIF1AX* mutations and cytogenetic changes such as CNAs would occur and drive further progression of the tumor including transcriptional and epigenetic changes. These changes include events like *BAP1* bi-allelic inactivation through mutation of one allele and loss of chromosome 3 or M3 associated with the large-scale methylation repatterning (Field et al., 2019), high risk of metastasis and death. Nevertheless, the exact timing and sequence of these events in the transition from benign nevi to UM remains unclear. The overall process of primary and secondary hits with CNAs would be proposed as in **Figure 22** (Jager et al., 2020, Vader et al., 2017, Zhilnikova et al., 2024, Shain et al., 2019).

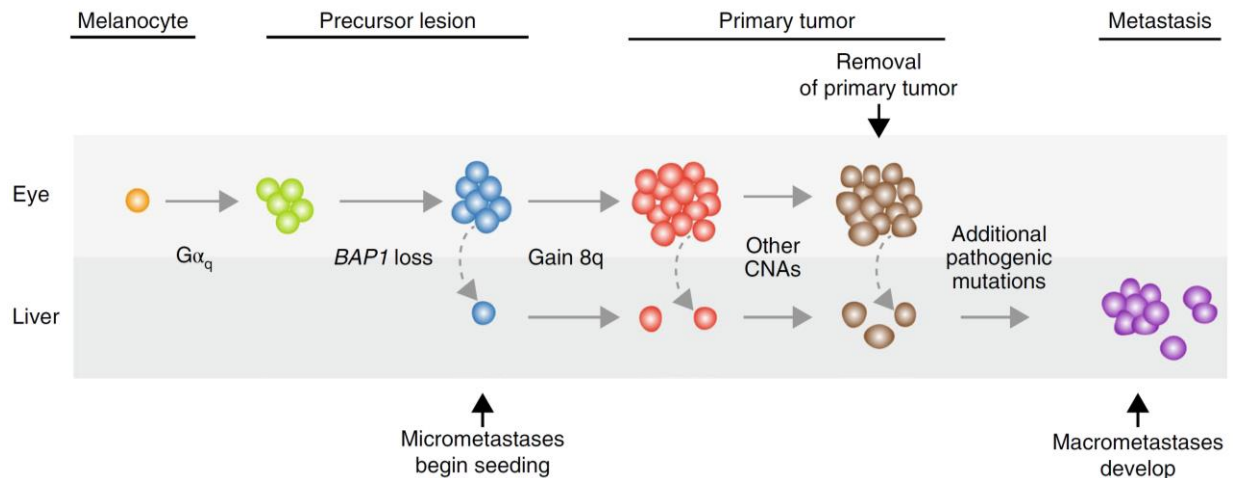


**Figure 22: Proposed order of the mutational and cytogenetic events during the tumor evolution from melanocytes to UM metastasis.** (Shain et al., 2019).

### 1.3.2. Transcriptomic and epigenetic features

**Transcriptomic features** of the UM groups majorly include the gene expression profile (GEP) classification which initially identified two molecular groups based on specific mRNA levels. These groups are class 1 which has a lower risk of metastasis and a better prognosis and class 2 which has a high metastatic rate (Onken et al., 2004, Tschentscher et al., 2003, Onken et al., 2010b). Initially, 62 genes were used to differentiate these classes. Class 2 was marked by decreased expression of genes on chromosome 3 and increased expression of genes on chromosome 8 that reflect the cytogenetic differences between the high-risk and the low-risk UMs (Onken et al., 2004). Then, this list has been updated to include 12 discriminative key genes (*HTR2B*, *ECM1*, *RAB31*, *CDH1*, *FXR1*, *LTA4H*, *EIF1B*, *ID2*, *ROBO1*, *LMCD1*, *SATB1*, *MTUS1*) and 3 least-variable control genes (*MRPS21*, *RBM23*, *SAP130*) (Onken et al., 2010b). From this research, the “DecisionDx-UM” test is developed and widely used in the United States to evaluate the risks in UM patients (Harbour and Chen, 2013, Plasseraud et al., 2016).

Again, many of the genes that differentiate class 1 and class 2 UM are on chromosome 3 and to a lesser extent chromosome 8 (Onken et al., 2010a). This suggests that the global expression changes observed in class 2 GEP tumors may reflect copy number variations

rather than indicating specific mechanistic pathways in UM progression (Onken et al., 2012).

According to the GEP classification, class 1 tumors are like differentiated uveal melanocytes in the gene expression while class 2 tumors show stem-like behavior reverting to the primitive neural crest-like progenitors. This indicates that the deregulation of differentiation transcriptomic programs may play a role in tumor progression (Onken et al., 2006, Chang et al., 2008, Lamas et al., 2021). Supporting this, it has recently been found methylation changes that are class 2 specific triggered by BAP1 loss which then leads to the downregulation of genes involved in the axon guidance and melanogenesis (Field et al., 2019). This aligns with previous findings on the impact of *BAP1* mutations in class 2 tumors (Harbour et al., 2010).

Class 1 UM has been further divided into subclasses 1a and 1b. Class 1b has been determined to have an intermediate prognosis between class 1a and class 2 (Correa, 2016). Preferentially expressed antigen of melanoma (*PRAME*) has also been identified as a prognostic biomarker within class 1 tumors but its exact mechanism remains unknown (Field et al., 2016). Additionally, high metastatic risk UM tumors namely class 2 have been further subdivided into classes 2a and 2b by other research groups based on large immune infiltration found only in class 2b. These two subclasses are distinguished molecularly by the gain of chromosome 8q in class 2b, which corresponds with the expression of certain immune genes located on chromosome 8q.

Combining various prognostic factors such as mRNA GEP and cytogenetic changes, UM tumors are classified into four subsets and each of them is associated with different metastatic potentials also aligning with the main UM "BSE" events as illustrated in **Figure 23** (de Lange et al., 2015, Carvajal et al., 2023).

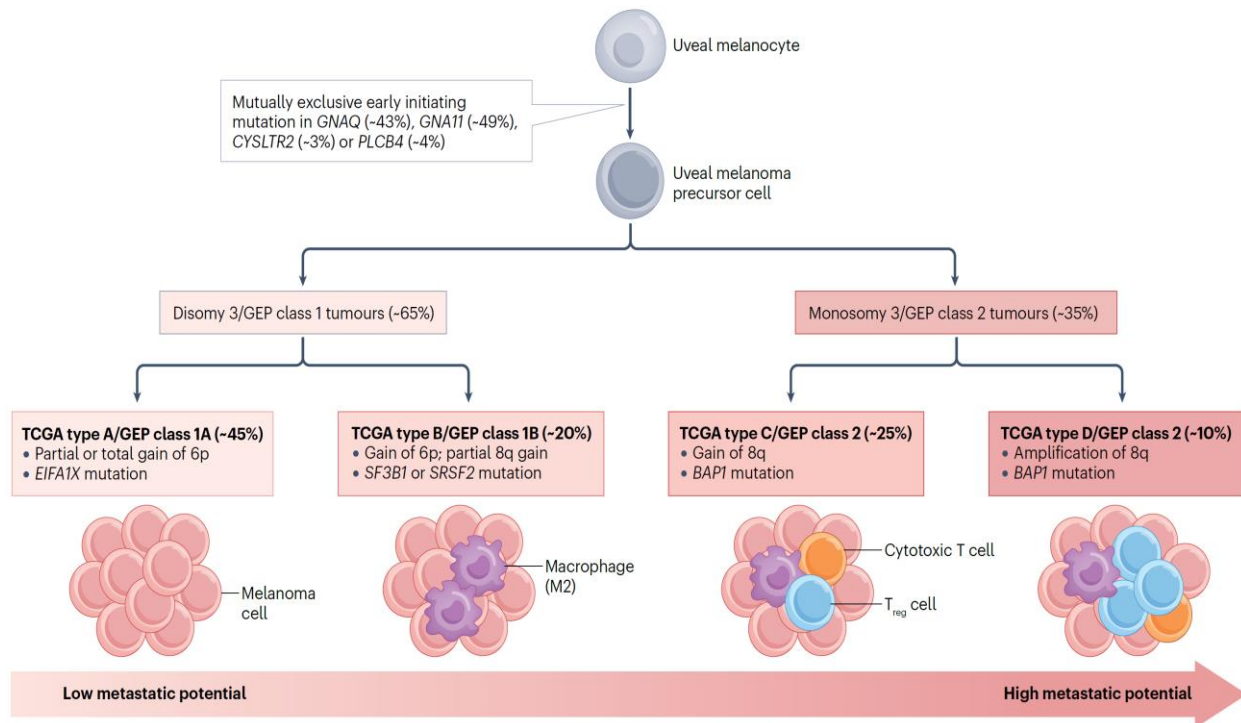


**Figure 23: UM subtype characterization scheme based on DecisionDX-UM gene expression profile classification.** (Carvajal et al., 2023).

**Epigenetic factors** have a crucial role in UM progression and metastatic risk determination. Some key oncogenic epigenetic mechanisms contributing to UM tumorigenesis include aberrant DNA methylations and histone modifications (Li et al., 2017, Chokhachi Baradaran et al., 2020).

Aberrant DNA hypermethylation events at the CpG islands in the promoters of genes result in the silencing of some TSGs in cancer. In UM, this event has been reported for genes such as *RASSF1A* (on chromosome 3p), *p16*, *TIMP3*, *RASSF1A*, *RASEF*, *hTERT* and *EFS* (Chokhachi Baradaran et al., 2020, Maat et al., 2007, van der Velden et al., 2001, Merhavi et al., 2007). Widespread hypermethylation has been found particularly on chromosome 3 in UM tumors with *BAP1* inactivation being associated with high metastatic risk (Field et al., 2019). This epigenetic regulation of *BAP1* can be related to the loss of melanocytic differentiation in this UM subgroup. Also, DNA hypomethylation is observed at specific CpG sites of the *PRAME* gene and it correlates with the tumor progression and metastasis

in UM being associated with the 8q gain and serves as an epigenetic biomarker for the metastatic UM (Field et al., 2016).

Histone modifications are other epigenetic factors involved in dysregulated mechanisms associated with UM progression. *BAP1* is also an epigenetic player and displays deubiquitylating enzymatic activity (described in detail in the section “1.3.3 BRCA-1 associated protein 1 (BAP1)”). Loss of this enzyme leads to the acquisition of stem-like properties by hyper-ubiquitination of histone 2A (H2A) at the Lysine 119 site (Conway et al., 2021, Fursova et al., 2021, Matatall et al., 2013). Histone deacetylases (HDACs) are enzymes that play an important role in histone modifications regulating gene expression by removing acetyl groups from histones, leading to a more condensed chromatin structure and reduced gene transcription (Audia and Campbell, 2016). In some studies, loss of BAP1 in UM cell lines resulted in a shift from a differentiated Class 1 to a more aggressive Class 2 transcriptomic profile. Histone deacetylase inhibitors (HDACi) have been identified as potential therapeutic agents to counteract these effects by increasing histone acetylation and promoting a more open chromatin state thereby reprogramming the gene expression. HDAC inhibition reduces H2A hyperubiquitination, prevents cell proliferation and shifts Class 2 cells toward a less aggressive phenotype in BAP1-deficient UM cells which suggests a potential therapeutic role for HDAC inhibitors in high-risk UM cases (Matatall et al., 2013, Landreville et al., 2012, Chokhachi Baradaran et al., 2020, Ny et al., 2021). Also, a recent phase 2 clinical trial of combined epigenetic and immunotherapy employing HDAC inhibition showed tumor regression in a small subset of metastatic UM cases (Ny et al., 2021).

### **1.3.3. BRCA-1 associated protein 1 (BAP1)**

BAP1 was originally discovered as a new ubiquitin carboxy-terminal hydrolase in 1998 (Jensen et al., 1998). It functions as a tumor suppressor and contributes to chromatin remodeling via its deubiquitylation activity. It has also roles in DNA damage repair, TF regulation, cell cycle, cell proliferation and cell death mechanisms (Scheuermann et al., 2010, Machida et al., 2009, Caporali et al., 2022).

### 1.3.3.1. *BAP1* gene and protein structure

*BAP1* gene is located on the short (p) arm of the chromosome 3 at position 21.1 (3p21.1) and covers approximately 9 kilobases. It contains 17 exons which encode for a 729 amino acid, 90 kDa BAP1 protein (Harbour et al., 2010, Wang et al., 2016). As illustrated in **Figure 24**, the main catalytic domain of the BAP1 protein is a ubiquitin carboxy-terminal hydrolase domain which is placed at its N-terminal region.

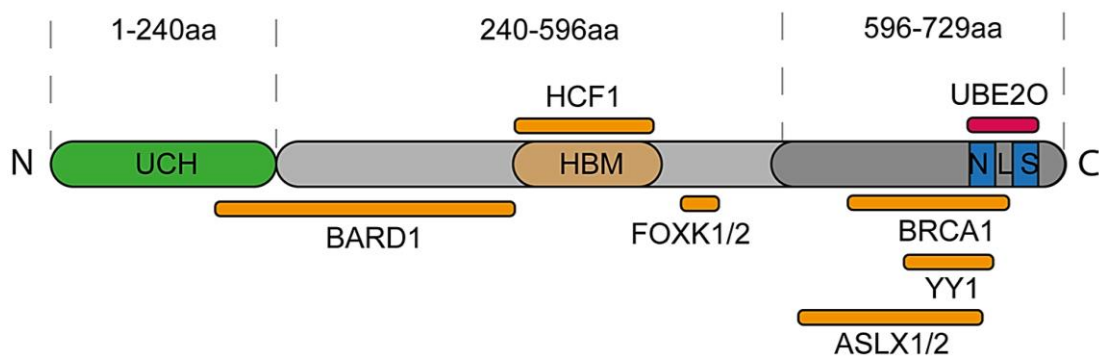


**Figure 24: Structure of BAP1 protein with domains of its interaction partners.** Ubiquitin carboxy hydrolase (UCH) domain (1–250); BARD1-binding region (182–365); HCF1 binding (HBM) domain (365–385); FoxK1/K2 binding region (477–526); BRCA1 binding region (596–721); ASXL1/2 binding domain (635–693); Nuclear localization signals (NLS) (656–661 and 717–722); Yin Yang 1 (YY1) binding domain (642–686) (Caporali et al., 2022).

This domain enables BAP1 to perform its primary function of removing ubiquitin marks from its substrates. While ubiquitination was initially associated with directing proteins for proteasomal degradation, it is now recognized as a complex multifunctional cell signaling system (Jensen et al., 1998, Welchman et al., 2005). BAP1 features protein-binding motifs for Host Cell Factor 1 (HCF1), BRCA1, ASXL1/2, FoxK1/K2, and YY1 indicating its involvement in the regulation of the several cellular functions. In the C-terminal region, BAP1 has two nuclear localization signals which direct its primary activities within the cell nucleus (Ventii et al., 2008).

### 1.3.3.2. Gene regulatory roles of BAP1 in UM

BAP1 has several functions in the cells and it has a significant role in the epigenetic modifications and remodeling of the chromatin which is particularly involved in cancer progression as summarized in **Figure 25** (Louie and Kurzrock, 2020).



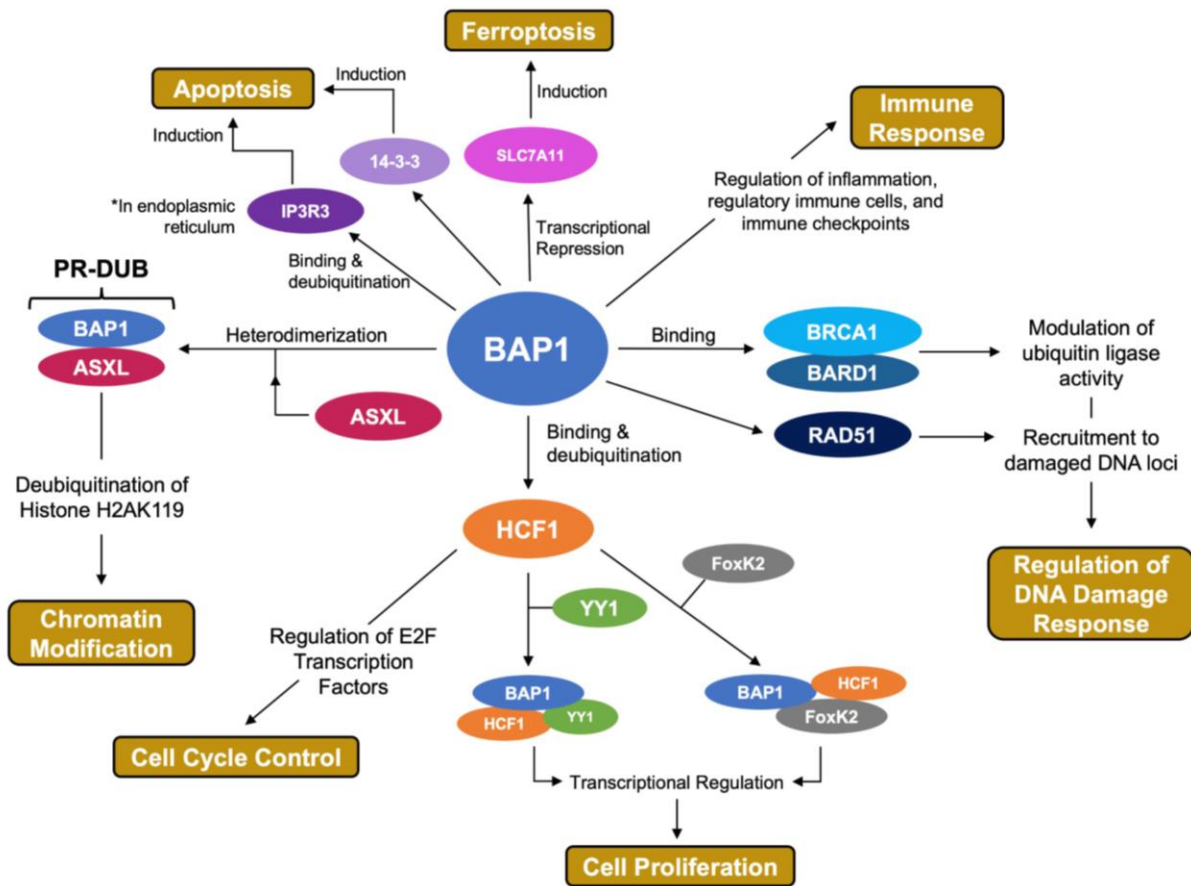


**Figure 25: Summary of the functional and regulatory roles of BAP1.** (Louie and Kurzrock, 2020).

Scheuermann et al. identified the Polycomb group (PcG) protein *Calypso* in *Drosophila* in 2010. That protein is a homolog of BAP1 and binds with additional sex combs (ASX, the homolog of ASXL1/2/3 in mammals) to form the Polycomb repressive deubiquitinase (PR-DUB) complex (Scheuermann et al., 2010). This PR-DUB complex uses the catalytic power of BAP1 to regulate chromatin by removing monoubiquitin from the histone H2A at lysine 119 (H2AK119ub1). This activity which is conserved in mammalian cells was shown to counteract the function of PcG protein complex “Polycomb repressive complex 1 (PRC1)” (Campagne et al., 2019).

PRC1 acts as an E3 ligase which adds monoubiquitin to histone H2AK119 and results in chromatin modification and gene silencing. Thus, PR-DUB opposes PRC1 by deubiquitinating H2A and alters chromatin structure preventing PRC1-mediated gene silencing. Polycomb group proteins are well-known transcriptional regulators targeting

genes essential for embryonic development, self-renewal, pluripotency and differentiation (Scheuermann et al., 2010, Campagne et al., 2019, Di Croce and Helin, 2013). Consequently, BAP1's role in the PR-DUB complex's deubiquitination of histone H2A directly influences chromatin modification and the transcription of vital PcG target genes. Furthermore, ubiquitination of histone H2AK119 is a tightly regulated modification that has an impact on transcription initiation, elongation and gene silencing. BAP1-mediated deubiquitination plays a significant role in maintaining the balance of H2A ubiquitination and influences chromatin architecture and gene expression (Conway et al., 2021) as illustrated in **Figure 26** (Barbour et al., 2020).

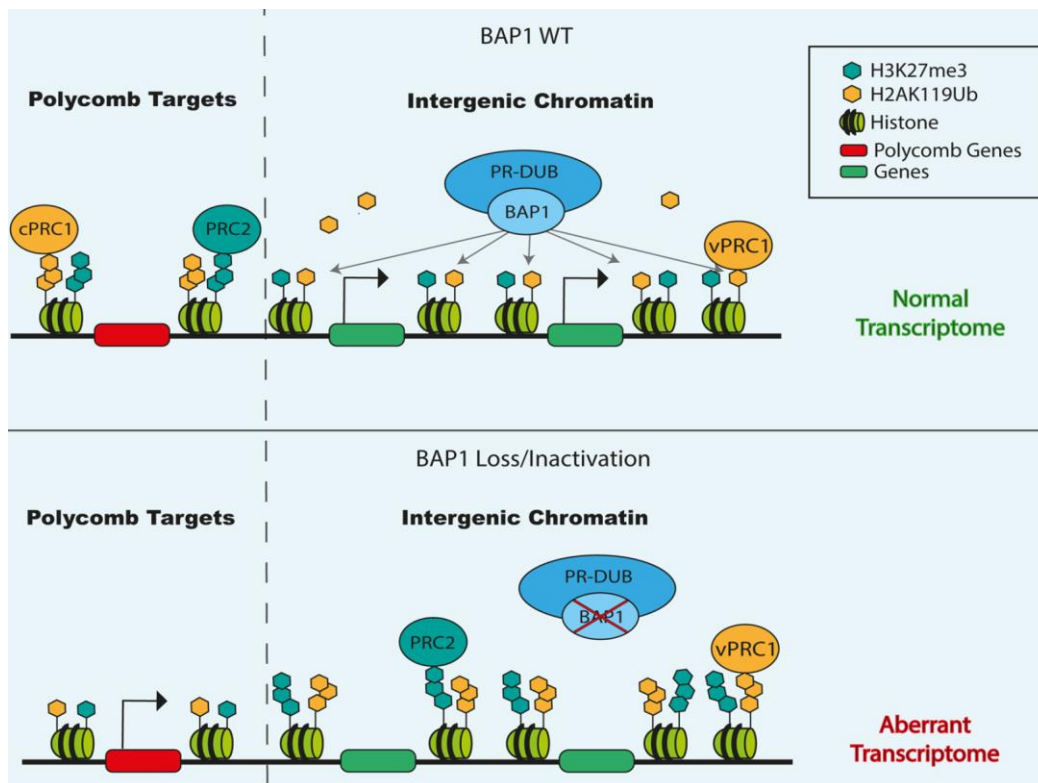


**Figure 26: Impacts of the loss of BAP1 on the chromatin involving altered deposition of H2AK119ub by PRC1.** (Caporali et al., 2022).

Field and colleagues showed that BAP1 inactivation in UM tumors with high metastatic risk results in significant methylation changes leading to the dysregulation of multiple genes. (Field et al., 2019). Thus, BAP1 loss in UM might contribute to cancer progression by disrupting the gene regulation in UM. However, the molecular mechanisms through which BAP1 promotes UM progression are still unclear (Field et al., 2019, Smit et al., 2022).

## Chapter 2: Aims

This thesis aims to contribute to deciphering the molecular mechanisms associated with BAP1 loss in UM and to analyze altered gene regulation networks in this process. This research seeks to address several key questions:

- 1) What are the genome-wide effects of BAP1 loss on gene expression, chromatin accessibility and histone mark profiles in UM cells?
- 2) Does the loss of BAP1 modify the interplay of TFs in UM?
- 3) How do these molecular changes potentially influence the disease progression observed in BAP1-mutant UM?

To answer these questions, we designed a strategy represented in **Figure 27** which involves the modeling of BAP1 loss in a previously established UM cell line creating a BAP1 knockdown model using siRNA in MEL202 to mimic the loss of BAP1 observed in high-risk UM patients.

In this study, we set out to investigate the impact of BAP1 in terms of changes in transcriptomic and epigenomic landscapes using bulk RNA sequencing and ATAC sequencing. To help map and understand the changes in chromatin states and gene regulatory network potentially influenced by BAP1 loss, we performed ChIP-seq for active and repressive histone marks (H3K4me3, H3K4me1, H3K27ac, H3K27me3), for key proteins including BAP1 and RING1B, as well as the pioneer transcription factors TFAP2A and TFAP2C involved in melanogenesis.

With this research, we aim to provide new insights shedding light into the molecular mechanisms such as transcriptional reprogramming associated with aggressive UM pathogenesis.

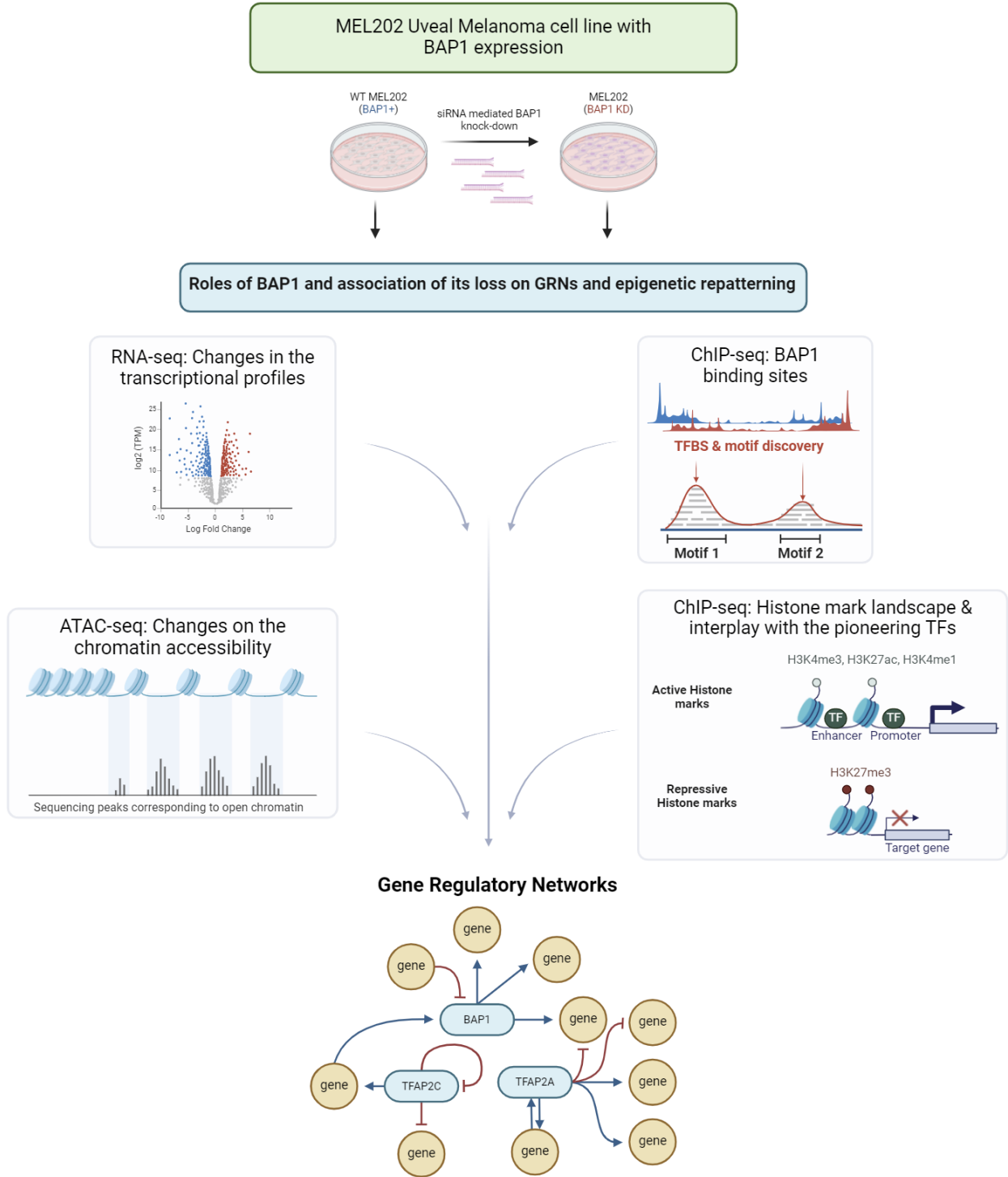


**Figure 27: Schematic representation for the design of the study (created with BioRender).**

# Chapter 3: Materials and Methods

## 3.1. Materials

### 3.1.1. Antibodies

**Table 2: Antibodies used in the study.** (ChIP: Chromatin Immunoprecipitation, IF: Immunofluorescence, WB: Western blot, mAb/pAb: monoclonal/polyclonal Antibody)

Name of the Antibody	Number and Provider	Application and Dilution
BAP1 mouse mAb	C-4 clone, Santa Cruz	ChIP: 1:50 IF: 1:200 WB, 1:250
Cas9 mouse mAb (Alexa Fluor 488 Conjugate)	7A9-3A3, Invitrogen	IF: 1:100
CTCF rabbit mAb	D31H2, Cell Signaling	IF: 1:200
GAPDH mouse mAb	D4C6R, Cell Signaling	WB, 1:1000
H2AK119ub rabbit mAb	D27C4, Cell Signaling	ChIP: 1:100
H3K27ac rabbit mAb	D5E4, Cell Signaling	ChIP: 1:100 CUT&RUN: 1:100
H3K27me3 rabbit mAb	C36B11, Cell Signaling	ChIP: 1:50
H3K4me1 rabbit mAb	D1A9, Cell Signaling	ChIP: 1:50
H3K4me3 rabbit mAb	C42D8, Cell Signaling	ChIP: 1:50 CUT&RUN: 1:50
IgG (Goat) - HRP, mouse secondary pAb	62-6520, Invitrogen	WB: 1: 5000
IgG isotype control rabbit mAb	DA1E, Cell Signaling	ChIP: 1:250
MITF rabbit mAb	D3B4T, Cell Signaling	ChIP: 1:50 IF: 1:200
RING1B rabbit mAb	D22F2, Cell Signaling	ChIP: 1:50
RNA pol II subunit B1 (phospho CTD Ser-2)	3E10, Sigma-Aldrich	ChIP: 1:250
SATB1 rabbit pAb	ab70004, Abcam	ChIP: 1:250
SMARCC1 rabbit mAb	D7F8S, Cell Signaling	ChIP: 1:100
TFAP2A rabbit pAb	PA5-17359, Invitrogen	ChIP: 1:50 IF: 1:100 WB: 1:1000
TFAP2C rabbit pAb	PA5-17330, Invitrogen	ChIP: 1:50 IF: 1:200 WB: 1:1000

### 3.1.2. Equipment and chemicals

**Table 3: Equipment and chemicals used in this study.**

<b>Name of the Material</b>	<b>Provider</b>
2100 Bioanalyzer Instrument	Agilent
2-position ClearLine® cell scraper - 25 cm	Kisker
5424 Centrifuge	Eppendorf
5810R Centrifuge	Eppendorf
5815R Centrifuge	Eppendorf
-80 °C Freezers	EWALD
Agarose	Sigma-Aldrich
AMPure XP beads	Beckman Coulter
Axiovert 40 CFL Microscope	Carl Zeiss
Bovine Serum Albumin (BSA)	Sigma-Aldrich
Buffer EB	QIAGEN
Carbenicillin	CARL ROTH
C-Chip Disposable Hemacytometers	INCYTO
Cell culture dishes (100-mm, 150-mm)	Sarstedt
Cell culture flasks (T-25, T-75)	Sarstedt
Cell culture cabinet (HERA safe / HSP 12)	Thermo Scientific
Cell culture plates (6-well, 12-well, 24-well, 48-well, 96-well)	Sarstedt
Chemical fume hood	Hohenloher
Clarity™ Western ECL Substrate	Bio-Rad
cOmplete™, Mini, EDTA-free Protease Inhibitor Cocktail	Roche
CoverGrip™ Coverslip Sealant	Biotium
Cryogenic Vial	VWR
Dimethyl sulfoxide (DMSO) sterile	Sigma-Aldrich
DNA Gel Loading Dye (6X)	Thermo Scientific
DNA LoBind Tubes	Eppendorf
DNase I	Invitrogen
Dulbecco's Modified Eagle Medium (DMEM)	Gibco
Electroporation cuvettes, 1 mm, orange lid, sterile	Biozym
Electroporation system	BTX
EndoFree Plasmid Maxi Kit	QIAGEN
Endura ElectroCompetent Cells (DUOS)	Lucigen/BioCat

Falcon tubes (15 ml, 50 ml)	Corning
Fetal Bovine Serum (FBS)	Gibco
Fluoromount-G™ Slide Mounting Medium	Invitrogen
Formaldehyde solution	Sigma-Aldrich
Freezers and fridges	Bosch
GeneRuler 1 kb DNA ladder	Thermo Fischer
Hoechst Nucleic Acid Stain	Thermo Scientific
Inoculation loop sterile, 1 µL, 0.9 mm	CARL ROTH
Laemmli Sample Buffer 4x	Bio-Rad
LB Broth (Miller)	Sigma-Aldrich
Lipofectamine™ 3000 Transfection Reagent	Invitrogen
Lipofectamine™ RNAiMAX Transfection Reagent	Invitrogen
Low-range Ultrapure Agarose Powder	Bio-Rad
Mini Protean III electrophoresis unit	Bio-Rad
Mini-PROTEAN® Cassette Opening Lever	Bio-Rad
Mini-PROTEAN® TGX™ 4-15% Precast Protein Gels, 12-well	Bio-Rad
Mr. Frosty™ Freezing Container	Thermo Scientific
NEBuffer™ r3.1	New England Biolabs
NEBuilder® HiFi DNA Assembly Master Mix	New England Biolabs
NEBuilder® Positive Control	New England Biolabs
Nuclease Free Water	Ambion
Nunc™ Square BioAssay Dish	Thermo Scientific
Opti-MEM™ Reduced-Serum Medium, GlutaMAX™ Supplement	Gibco
PageRuler™ Plus Prestained Protein Ladder (10 – 180 kDa)	Thermo Fisher Scientific
PBS, pH: 7.4	Gibco
PCR clean, 8-tube strips	Eppendorf
PCR tubes	Eppendorf
Penicillin-Streptomycin (5,000 U/mL)	Gibco
Plasmid Plus Midi Sample Kit	QIAGEN
Polybrene (Hexadimethrine bromide)	Sigma-Aldrich
Positively Charged Microscope Slides, 1 mm thick, white Marking Region	THORLABS
Powdered milk (Blotting Grade)	CARL ROTH
Precision Cover Glasses, #1.5H Thickness, Ø12 mm	THORLABS

Protein LoBind Tubes	Eppendorf
PTC-200 Peltier Thermocycler	MJ Research
Q5® Hot Start High-Fidelity 2X Master Mix	New England Biolabs
Qubit 3.0 Fluorometer	Life Technologies
Qubit tubes, 0.5 ml	Corning
rCutSmart™ Buffer	New England Biolabs
Real-Time PCR System	Applied Biosystems
Restriction enzyme BamHI-HF®	New England Biolabs
Restriction enzyme BsmBI-v2	New England Biolabs
Restriction enzyme EcoRI-HF®	New England Biolabs
Restriction enzyme Sapl	New England Biolabs
Restriction enzyme SphI-HF®	New England Biolabs
RIPA Lysis Buffer 10x	Millipore
RNAse A (10 mg/ml)	Cell Signaling
RPMI 1640 Medium	Gibco
Safety containers DuraPorter®, transparent	CARL ROTH
Select agar	Sigma-Aldrich
SOC Outgrowth Medium	New England Biolabs
Sodium Pyruvate (100 mM)	Gibco
SYBR® Select Master Mix	Applied Biosystems
Syringe filter, 0.45 µm	VWR
Trans-Blot Turbo Midi 0.2 µm PVDF Transfer Packs	Bio-Rad
Tris Buffered Saline (TBS) 10x	Bio-Rad
Tris/Glycine/SDS (TGS) 10x	Bio-Rad
Triton™ X-100	Sigma-Aldrich
Trypan Blue	Merck
Trypsin/EDTA (0.025%) solution	Lonza
TWEEN® 20	Sigma-Aldrich
UltraPure™ DNA Typing Grade™ 50X TAE Buffer	Invitrogen
Vortex-Genie 2T	Scientific Industries
Water bath WNB	Memmert GmbH
Western Lightning Ultra, Chemiluminescent Substrate	PerkinElmer



### 3.1.3. Kits

**Table 4: Kits used in this study.**

Name of the Kit	Provider
AllPrep DNA/RNA/miRNA Universal Kit	QIAGEN
ATAC-Seq Kit (16 rxns)	Active Motif
DNA Library Prep Kit for Illumina Systems (ChIP-seq, CUT&RUN)	Cell Signaling
DNA Purification Buffers and Spin Columns (ChIP, CUT&RUN, CUT&Tag)	Cell Signaling
Gibson Assembly® Cloning Kit	New England Biolabs
High Sensitivity DNA Analysis Kit (Bioanalyzer)	Agilent
Multiplex Oligos for Illumina Systems (Dual Index Primers) (ChIP-seq, CUT&RUN)	Cell Signaling
NucleoSpin RNA Virus, Mini kit for viral RNA from cell-free fluids	MACHEREY-NAGEL
Pierce™ BCA Protein Assay Kit	Thermo Scientific
S.N.A.P.™ UV-Free Gel Purification Kit	Invitrogen
SimpleChIP® Plus Enzymatic Chromatin IP Kit (Magnetic Beads)	Cell Signaling
TruSeq Stranded Total RNA Kit	Illumina
Venor®GeM Classic Mycoplasma Detection Kit for PCR	Minerva Biolabs
Zymoclean Gel DNA Recovery Kit (capped)	Zymo Research

### 3.1.4. Plasmids and primers

**Table 5: Plasmids used in this study.**

Name of the plasmid	Source
LentiCRISPRv2GFP	Addgene plasmid # 82416 ; <a href="http://n2t.net/addgene:82416">http://n2t.net/addgene:82416</a> ; RRID:Addgene_82416
LentiCRISPRv2GFP-sgBAP1_1	Produced cloning sgBAP1_1 to LentiCRISPRv2GFP backbone for this study
LentiCRISPRv2GFP-sgBAP1_3	Produced cloning sgBAP1_3 to LentiCRISPRv2GFP backbone for this study
pMD2.G	Addgene plasmid # 12259 ; <a href="http://n2t.net/addgene:12259">http://n2t.net/addgene:12259</a> ; RRID:Addgene_12259

pMDLg/pRRE	Addgene plasmid # 12251 ; <a href="http://n2t.net/addgene:12251">http://n2t.net/addgene:12251</a> ; RRID:Addgene_12251
pRSV-Rev	Addgene plasmid # 12253 ; <a href="http://n2t.net/addgene:12253">http://n2t.net/addgene:12253</a> ; RRID:Addgene_12253

**Table 6: ATAC-seq i7 and i5 index primers used in this study.**

<b>i7 Index</b>	<b>i7 Sequence</b>	<b>Sample Sheet</b>
N701	TCGCCTTA	TAAGGCGA
N702	CTAGTACG	CGTACTAG
N703	TTCTGCCT	AGGCAGAA
N704	GCTCAGGA	TCCTGAGC
<b>i5 Index</b>	<b>i5 Sequence</b>	<b>Sample Sheet (NovaSeq v1.5 reagent kits, NextSeq, HiSeq 3000 / 4000)</b>
N501	TAGATCGC	GCGATCTA
N502	CTCTCTAT	ATAGAGAG
N503	TATCCTCT	AGAGGATA
N504	AGAGTAGA	TCTACTCT

**Table 7: ChIP-seq and CUT&RUN dual index primers for Illumina systems used in this study.**

<b>Index 7 Primer</b>	<b>Sequence</b>
Index 701 Primer	ATTACTCG
Index 702 Primer	TCCGGAGA
Index 703 Primer	CGCTCATT
Index 704 Primer	GAGATTCC
Index 705 Primer	ATTCAGAA
Index 706 Primer	GAATTCGT
Index 707 Primer	CTGAAGCT
Index 708 Primer	TAATGCGC
Index 709 Primer	CGGCTATG
Index 710 Primer	TCCGCGAA
Index 711 Primer	TCTCGCGC
Index 712 Primer	AGCGATAG

<b>Index 5 Primer</b>	<b>Sequence</b>
Index 501 Primer	TATAGCCT
Index 502 Primer	ATAGAGGC
Index 503 Primer	CCTATCCT
Index 504 Primer	GGCTCTGA
Index 505 Primer	AGGCGAAG
Index 506 Primer	TAATCTTA
Index 507 Primer	CAGGACGT
Index 508 Primer	GTACTGAC

## 3.2. Methods

### 3.2.1. Cell Culture

For the passaging of the cells (**Table 8**) using T75 flasks, full RPMI media (supplemented with 10% FBS and 1% Penicillin-Streptomycin), Trypsin/EDTA and a 1×PBS falcons were warmed in the water bath for 20 minutes. All the tubes were wiped with %70 Ethanol before placing them inside the cell culture hood. The old media inside of the flask was removed, and 5 ml 1×PBS was added to the corner slowly. The flask was gently swirled and the PBS washing was removed. 1.5 ml Trypsin/EDTA was added to the flask and placed back in the incubator waiting for detachment of the cells from the surface of the flask for around 1-2 minutes. 5 ml of full RPMI was transferred to the flask. After gentle pipetting a couple of times, the mixture was transferred to a new, empty falcon and centrifuged at 300 g for 3 minutes. Then, the supernatant was removed and the cell pellet was dissolved with 10 ml RPMI. For the counting of the cells, 10 µL from the cell suspension (in 10 ml RPMI) was taken and mixed with 10 µL of Trypan blue, next the mixture was transferred on a cell counting chip and an average number of the cells from the four corners of the chip calculated.  $5 \times 10^5 - 1 \times 10^6$  cells were seeded to a new T75 flask. The flask was gently shaken up-down and right-left about five times to distribute the cells evenly through the flask. The cells were controlled under the light microscope and the flask was returned to the incubator. All cells were frequently tested for mycoplasma contamination using a PCR-based mycoplasma detection kit.

**Table 8: Cell lines used in this study.**

Cell lines	Source	Provider
MEL202	Uveal Melanoma	Curie Institute
MP46	Uveal Melanoma	ATCC, CRL-3298
HEK293T	Embryonic Kidney	ATCC

For freezing, cells were collected as previously described. After the centrifugation, the cell pellet was resuspended in 1 ml of freezing medium composed of 90% complete medium and 10% DMSO. The cells were aliquoted into cryovial tubes and placed in a Mr. Frosty container, which was then stored in a -80°C freezer for at least 48 hours. Subsequently,

the frozen cells were transferred to a liquid Nitrogen tank for long-term storage. For thawing, the frozen cell vial was taken from the liquid Nitrogen tank on dry ice to transfer to the cell culture and quickly placed in a 37 °C-water bath until the medium was completely melted. The cells were then centrifuged and resuspended as previously described, then the cells were seeded to a plate containing an adequate amount of the respective medium. After one day, the medium was replenished with fresh medium to remove any residual DMSO.

### 3.2.2. CRISPR/Cas9 mediated gene knockout

#### 3.2.2.1. Design of the single guide RNAs

Design of the single guide RNAs to select the optimal CRISPR/Cas9 target sequences for the BAP1 gene was done using the CHOPCHOP tool (Labun et al., 2019, Labun et al., 2016). After the selection of the guides based on their target efficiency scores, GC contents, self-complementarity scores, and off-targets, two guides were determined to be selected and annotated as sgBAP1\_1 and sgBAP1\_3 as shown in **Table 9**.

**Table 9: Features of the single guide RNAs designed to target the BAP1 gene.**

Guide	Spacer sequence (5'-3')	Genomic location	GC content (%)	Efficiency
sgBAP1_1	CACGGACGTATCATCCACCAAGG	chr3:52408516	55	71.56
sgBAP1_3	TCTACCCCATTGACCATGGTAGG	chr3:52407169	50	63.86

Target sites of the guides selected to be efficient in introducing cleavage to the prior coordinates on the gene to ensure the maximum knock-out yield as represented in **Figure 28**.

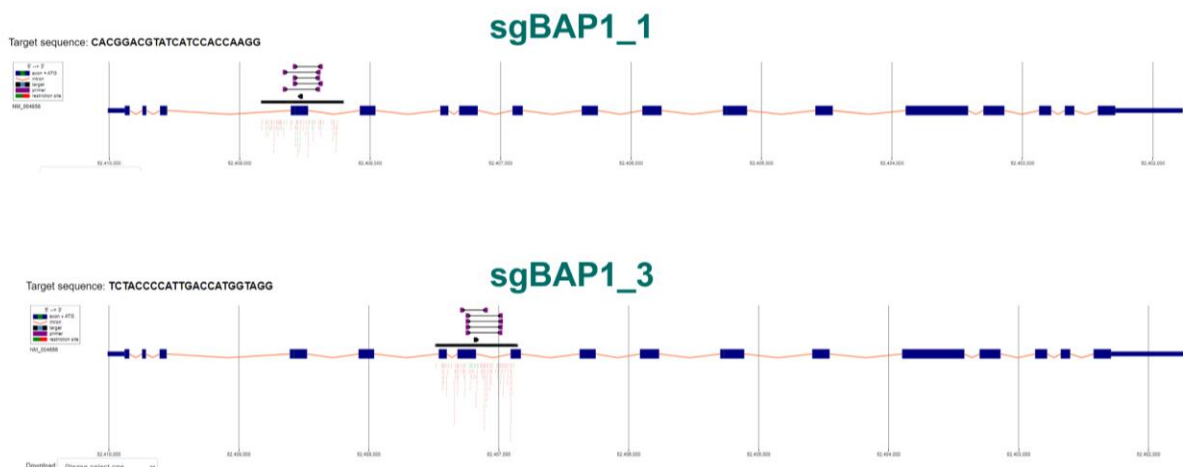


**Figure 28:** Target sites of the two guides (sgBAP1\_1 and sgBAP1\_3) on the different locations of exons on the BAP1 gene.

### 3.2.2.2. Restriction digestion, UV-free gel extraction, and purification of the plasmid backbone

LentiCRISPRv2GFP plasmid (Appendix **Figure 82**) was obtained from Addgene in the standard format where the plasmid is sent in bacteria as agar stab. Single colonies were obtained and the plasmid purification was done according to the protocols in sections 3.2.2.4, 3.2.2.5, and 3.2.2.6. Its plasmid length was controlled by restriction digestion using Sapl and SphI-HF enzymes (**Table 10**). The digestion was done by incubating the mixture at 37 °C for 1 hour. Inactivation of the enzyme was done by incubating the mixture at 65 °C for 20 minutes in the thermocycler machine.

**Table 10: Restriction digestion conditions of Sapl and SphI-HF enzymes.**

	<b>Sapl</b>	<b>SphI-HF</b>
Plasmid DNA	1 µg	1 µg
10× Buffer	CutSmart, 5 µl	CutSmart, 5 µl
Enzyme	1 µl	1 µl
Nuclease Free Water	Complete to 50 µl	Complete to 50 µl

After the restriction digestion, the cut products and uncut plasmid were loaded and run on 1% Agarose gel electrophoresis as in **Figure 29**.

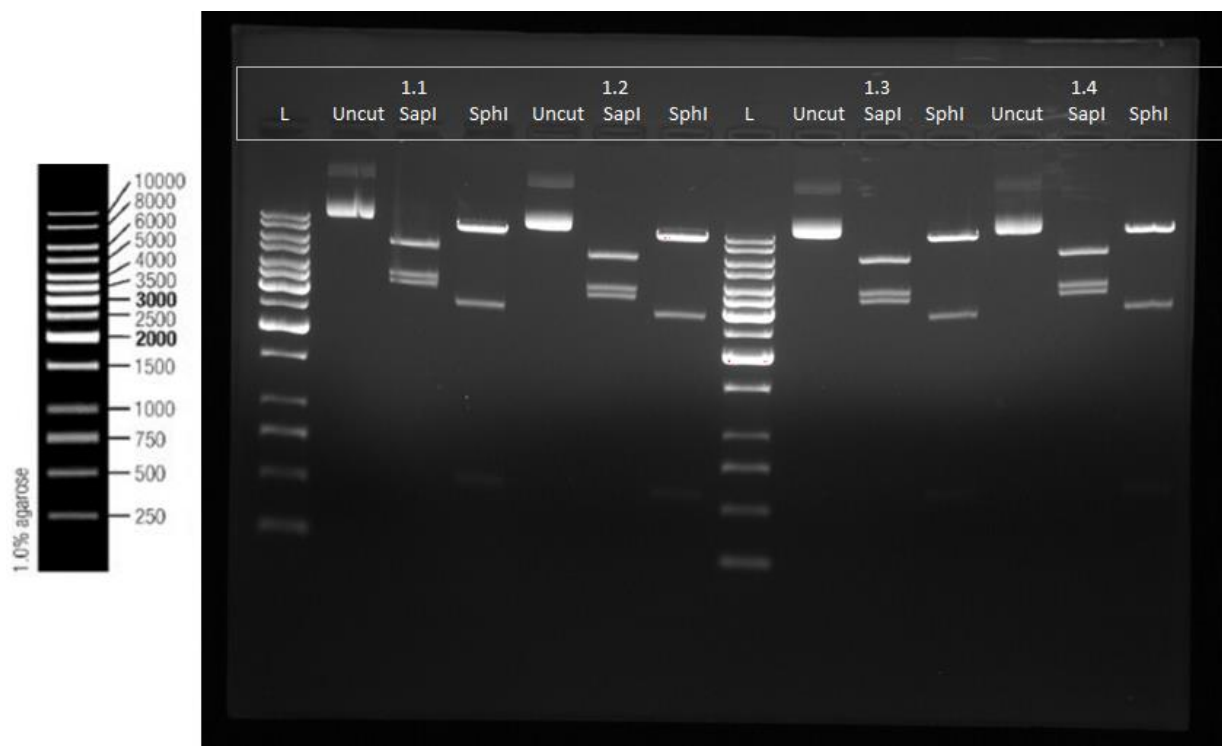


**Figure 29: Restriction digestion of LentiCRISPRv2GFP plasmid using SapI and SphI enzymes.** Four colonies were selected to analyze. The uncut plasmid length is 13,131 bp. Product sizes after SapI digestion: 6015, 3704, and 3412 bp. Product sizes after SphI digestion: 9649, 2836, 574, and 72 bp (invisible).

Also, the plasmid sequence was validated by Sanger sequencing using the primers in **Table 11**.

**Table 11: Sequencing primers used for LentiCRISPRv2GFP plasmid for Sanger sequencing.**

Primer Name	Sequence (5'-3')	Binding sites (bp)	Length (bases)
CMV-F	CGCAAATGGGCGGTAGGCGTG	154 - 174	21
hU6-F	GAGGGCCTATTTCCCATGATT	1990 - 2010	21
WPRE-R	CATAGCGTAAAAGGAGCAACA	9400 - 9420	21
M13 Reverse	CAGGAAACAGCTATGAC	12101 - 12117	17

After the confirmation of the length and sequence of the plasmid, it was digested with BsmBI enzyme (**Table 12**) to linearize the plasmid preparing the guide RNA site. The digestion was done by incubating the mixture at 55 °C for 3 hours. Inactivation of the enzyme was done by incubating the mixture at 80 °C for 20 minutes in the thermocycler machine.

**Table 12: Digestion conditions of BsmBI with LentiCRISPRv2GFP plasmid.**

Component	Amount
Plasmid DNA (LentiCRISPRv2GFP)	1 µg
10× NEB Buffer 3.1	5 µl
BsmBI (10 U)	1 µl
Nuclease Free Water	Complete to 50 µl

For the UV-free gel extraction of the digested plasmid by BsmBI, firstly 0.8% Agarose gel was prepared with 1x TAE buffer containing 1.8 µg/ml Crystal Violet. 0.4 g agarose was dissolved in 50 ml TAE, after waiting for 3 minutes to cool down, 40 µl of 2 mg/ml Crystal Violet Solution was added to the mixture. The thin comb was used for more intense bands. 16 µl (8 µg) of regular DNA ladder (0.5 µg/µl without any loading dye) was loaded. 3.2 µL of 6x Crystal Violet Loading Dye was added. Proper dilution of 6x Crystal Violet Loading Dye was added to the samples and they were loaded. The gel was run at 80 V and the separation of the bands was observed with the naked eye for 20 min. Once the bands were sufficiently resolved, the electrophoresis was stopped and the 12931 bp fragment was cut with a clean razor blade as shown in **Figure 30**.

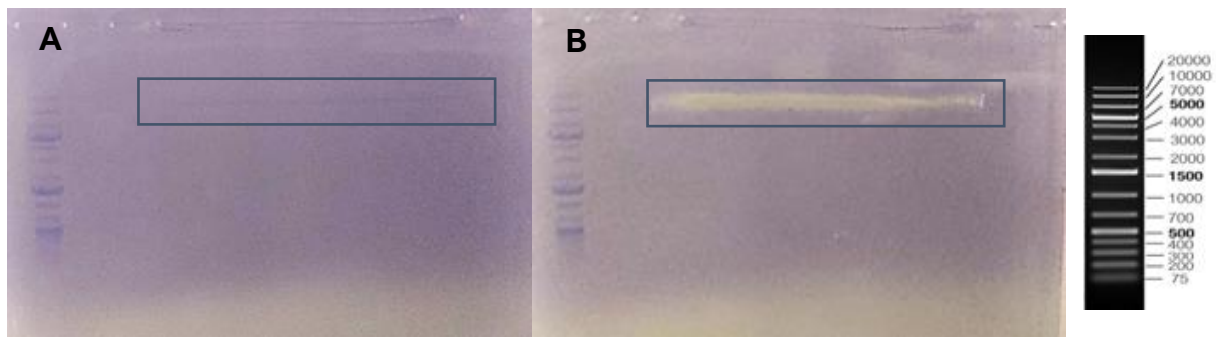


**Figure 30: UV-free gel run of the digested products of LentiCRISPRv2GFP by BsmBI enzyme. (A)** After the digestion, the product sizes are 13,111 (indicated by the blue rectangle) and 20 bp (invisible). The gel image is before cutting the gel. **(B)** The gel image was taken after cutting the gel at the band of interest positioned around the 10,000 bp level of the ladder.

After the fragment of interest had been excised from the gel, the Zymoclean Gel DNA Recovery kit was used to obtain the plasmid backbone purifying from the gel. The manufacturer's protocol was used to elute the DNA. After the elution, DNA concentration was measured using Qubit HS DNA reagents.



### 3.2.2.3. Molecular cloning of the gRNAs into LentiCRISPRv2GFP backbone

Assembly of sgRNA-encoding ssDNA oligonucleotides into the LentiCRISPRv2GFP vector backbone was done using the Gibson assembly method (Gibson et al., 2009). The cloning reaction was set up as described in **Table 13**. Gibson assembly of sgBAP1\_1, sgBAP1\_3, as well as controls (only backbone fragment, NEB positive control pUC19, and no DNA negative control), were done incubating the reactions at 50 °C for 1 hour.

**Table 13: Gibson assembly protocol to clone sgRNAs into the LentiCRISPRv2GFP backbone fragment.**

Component	Amount
LentiCRISPRv2GFP backbone fragment	100 ng
sgRNA	100 nM
NEBuilder HiFi DNA Assembly Master Mix 2×	10 $\mu$ l (1×
Nuclease Free Water	Complete to 20 $\mu$ l

Then, desalting of the Gibson assembly was done by filling a 6-cm cell culture dish with NFW, placing a membrane filter on top transferring 20  $\mu$ l of the Gibson assembly reaction, and letting it float on top of the filter for 30 minutes. After this desalting step, about 10  $\mu$ l of the Gibson assembly reaction could be recovered and the DNA concentrations were measured using Qubit HS DNA assay. After the cloning of the sgRNAs into the backbone fragment, the new sequences were annotated as LentiCRISPRv2GFP-sgBAP1\_1 and LentiCRISPRv2GFP-sgBAP1\_3.

### 3.2.2.4. Bacterial transformation by electroporation

Lucigen electrocompetent bacterial cells were thawed on ice for 20 minutes as one vial of bacteria per two electroporations. One 1 mm electroporation cuvette and one empty 2 mL tube were pre-chilled on ice per electroporation. Lucigen recovery medium was warmed at 37 °C. LB-agar plates containing 100  $\mu$ g/ml Carbenicillin were warmed at RT. 25  $\mu$ l of bacteria was transferred into pre-chilled 2 ml tubes and kept on ice. 10  $\mu$ l of de-salted Gibson Assembly mixture was added to the bacteria and the tube was mixed gently. Each electroporation was performed sequentially transferring the mix to the electroporation cuvette, tapping to bring contents to the bottom, and checking for air bubbles. A

micropipette capable of transferring 1 ml was pre-filled with 1 ml of Lucigen recovery medium. Electroporation was done with the settings: 25  $\mu$ F, 200-ohm, 1.5 kV, 5 milliseconds. Immediately after the pulse, the prepared Lucigen recovery medium was added and the cells were resuspended. The mix was pipetted up and down two times and then transferred to round-bottom tubes. The cells in the tubes were incubated for 1 hour in a shaking incubator at 37 °C with 150 RPM for recovery. Different dilutions such as 1:50, and 1:100 of bacteria to SOC medium ratios were prepared, and different amounts such as 50  $\mu$ l, and 100  $\mu$ l from these dilutions were transferred to the LB-agar plates. The agar plates were incubated at 37 °C overnight ensuring the bacterial growth. The next day, the colonies were counted and the plate having the colony number between 50-300 were selected.

#### 3.2.2.5. Bacterial culture

To isolate the single bacterial colonies, sterile inoculation loops were used and all the work was done near the flame ensuring the aseptic condition. Marked single colonies were picked using the sterile loops and dipped into starter cultures of 5 mL LB media inside the round-bottom tubes. 5  $\mu$ l of the 1000 $\times$  Carbenicillin antibiotic solution was added to keep the selection for the cells carrying the plasmids. The starter culture was incubated at 37 °C for 8 hours on a shaker at 250 RPM. The starter culture was used to expand the bacterial growth to the main culture diluting with 1:1000 LB-media in a large flask with 1 $\times$  Carbenicillin antibiotics incubating at 37 °C overnight at 250 RPM. The proportions were adjusted depending on the goal in the next plasmid DNA isolation step in terms of mini, midi, maxi or mega prep of the plasmids.

#### 3.2.2.6. Plasmid DNA purification

Plasmid DNA purifications were done according to the Manufacturer's (QIAGEN Plasmid Plus) Midi, Maxi and Mega prep kit protocols. The kit principle followed pelleting the bacteria, lysing the cells, clearing the lysate by filtration, binding the plasmid DNA to columns, washing the impurities and eluting the plasmid. 25, 100 and 250 ml of LB media

were used for midi, maxi and mega preps, respectively. After the elution, plasmid DNA concentrations were measured using Qubit HS DNA reagents.

### 3.2.2.7. Cell transfection and production of lentiviral particles

In this study, 3<sup>rd</sup> generation lentiviral transduction system was used including the plasmids of pMD2.G (Appendix **Figure 83**), pMDLg/pRRE (Appendix **Figure 84**) and pRSV-Rev (Appendix **Figure 85**) were obtained from Addgene in bacterial agar stabs. Selection, bacterial growth and purification of these plasmids were done as previously described in sections 3.2.2.5 and 3.2.2.6. After all the required plasmids were purified and their concentrations were determined, lentivirus packaging medium (LPM) was prepared with Opti-MEM, 5% FBS, and 200  $\mu$ M sodium pyruvate without any antibiotics as in **Table 14**. Then,  $7 \times 10^6$  Human Embryonic Kidney (HEK293T) cells were seeded to 10-cm cell culture dishes in 12 ml lentivirus packaging medium.

**Table 14: Composition of the lentivirus packaging medium without any antibiotics.**

Component	Volume (Total 50 ml)
Opti-MEM I	47,5 ml
5% FBS	2,5 ml
200 $\mu$ M Sodium Pyruvate (stock: 100 mM)	100 $\mu$ L

Transfection is done on the following day when the cells are 60-80% confluent. The transfection mixtures were prepared as in **Table 15**.

**Table 15: Preparation of the transfection mix for lentivirus production.**

Transfection mix	Component	Amount
<b>A</b>	LentiCRISPRv2GFP-sgBAP plasmids	10.2 $\mu$ g
	pMDLg/pRRE	5.4 $\mu$ g
	pRSV-Rev	5.4 $\mu$ g
	pMD2.G	5.4 $\mu$ g
	Opti-MEM	1.5 ml
	P3000 enhancer reagent	36 $\mu$ l
<b>B</b>	Opti-MEM	1.5 ml
	Lipofectamine 3000 reagent	42 $\mu$ l

Lipid-DNA complexes were prepared by combining transfection mixes A and B, incubating for 20 min at RT. 6 ml medium was removed from the HEK293T cells during the incubation time. All the mix of lipid-DNA complexes was added to the HEK293T cells and agitated gently. After 6 hours of incubation at 37 °C, the medium was changed to 12 ml of fresh lentivirus packaging medium.

Lentivirus collection was done two times, firstly after 24 hours of collecting the lentivirus-containing medium and storing at 4 °C, adding 12 ml of fresh lentivirus packaging medium. Secondly, after 48 hours, the lentivirus-containing medium was pooled with the supernatant obtained on the previous day and filtered all through a 0.45 µm filter to remove any cells. The preparation of the lentiviral system and obtaining the LVPs are summarized in **Figure 31**. The lentiviruses were aliquoted into cryotubes having 500 µl each and placed on dry ice to snap-freeze them. The tubes were kept at -80 °C freezer.

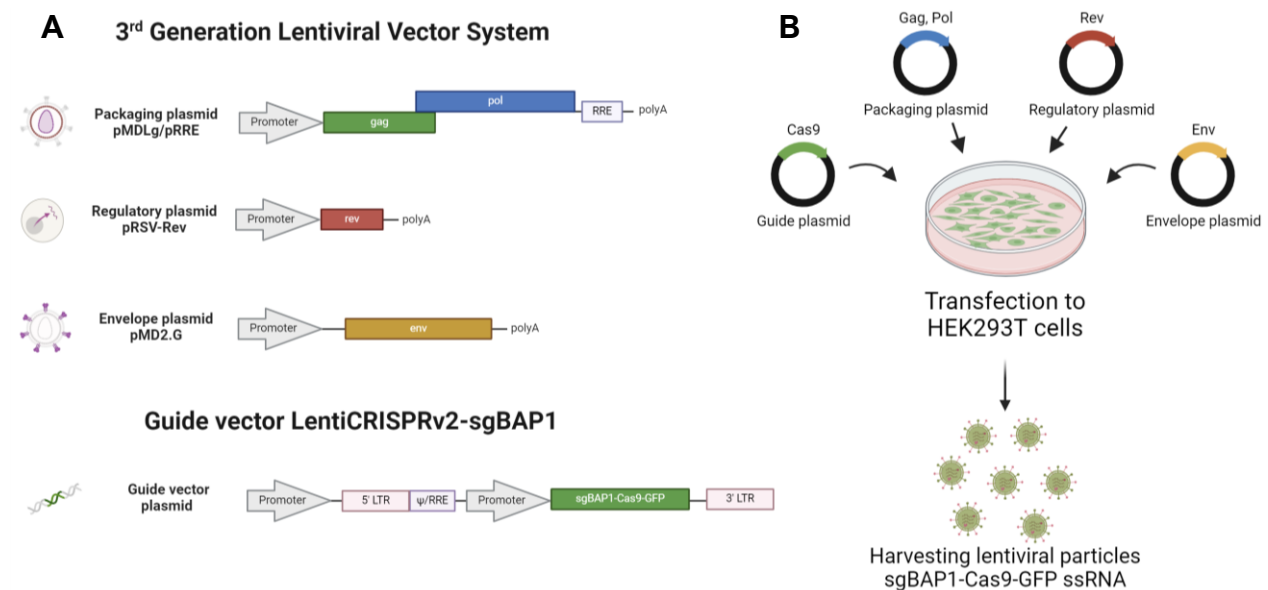


**Figure 31: Strategy for the application of the lentiviral transduction system. (A)** 3<sup>rd</sup> generation lentiviral vector system with guide plasmid which contains Cas9 and GFP sequences. **(B)** Transfection of the vectors into HEK293T cells to produce lentiviral particles.

#### 3.2.2.8. Lentiviral transduction

$5 \times 10^5$  MEL202 cells were seeded in 24-well plates. To transduce LentiCRISPRv2GFP-BAP1\_1 and BAP1\_3 LVPs, polybrene with the final concentration of 8  $\mu\text{g}/\text{ml}$  was used. In the initial experiment, the optimum amount of the LVPs was determined by having the titration range of 1:1, 1:10, 1:50, 1:250, and 1:1250 including negative control and only polybrene control to assess whether polybrene has any negative effect on the cells. After the transduction, in order to sort the cells using FACS, PBS washings were done to ensure there were no detectable LVPs from which, no ssRNA could be probed to quantify using qRT-PCR. That step makes the process safe to continue with the next step.

#### 3.2.2.9. Fluorescence Activated Cell Sorting (FACS)

Fresh cells were harvested from the cell culture and gently dissociated. Then, cells were collected and centrifuged at 300 g for 5 minutes and resuspended in PBS with 5% FBS. Then, the cells were filtered through a 35  $\mu\text{m}$  mesh cell strainer and counted to obtain a single cell suspension of  $10 \times 10^6$  cells per ml for the cell sorting. Cell viabilities were determined using trypan blue dye to ensure viability above 80% before the sorting. Cell sorting was done with FACSAria™ II (BD Biosciences) using a 100  $\mu\text{m}$  nozzle.

As in the representation of the experimental setup in **Figure 32**, only GFP-positive cells were sorted as single cells to a single well of a 96-well plate. To obtain the best condition for the sorted cells, fresh media, and conditioned media from the mix of fresh and incubated media were used. For sorting, the FACSDiva software (BD Biosciences) was used and the fluorescence was determined by the analysis and gating against the negative control cells. Flow cytometry forward (FSC) versus side scatter (SSC) density plots were first used to exclude debris. Then, singlets were selected based on FSC-area versus FSC-width and SSC-area versus SSC-width. Untransduced cells were used as negative controls to set the appropriate negative gates.

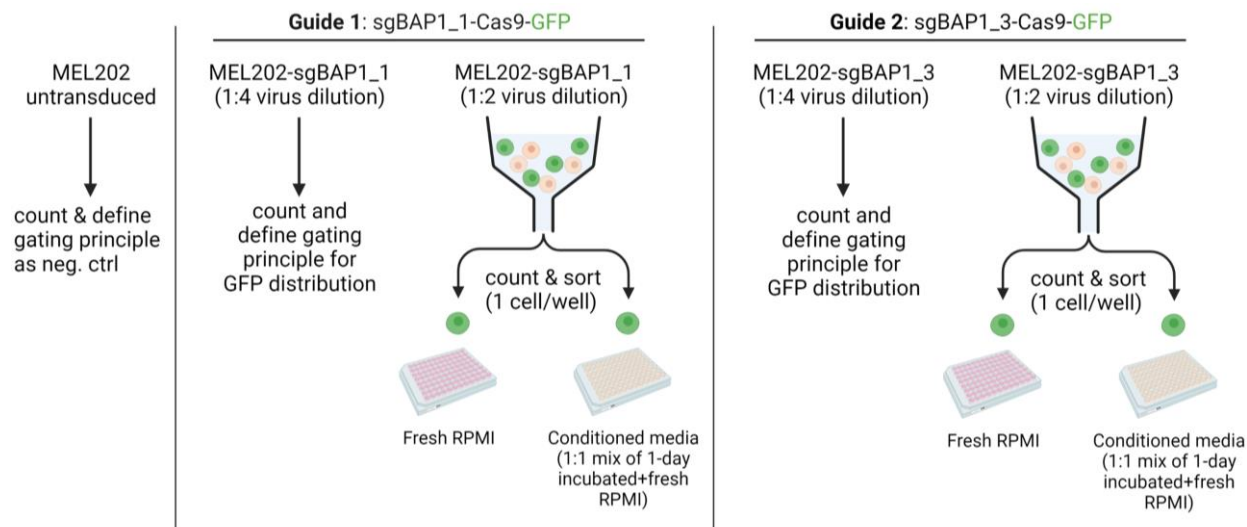


**Figure 32: Experimental design of the FACS using lentivirally transduced MEL202 cells.**

### 3.2.3. siRNA-mediated gene knockdown

#### 3.2.3.1. Preparation of the siRNAs

Two siRNAs specific for BAP1 and one siRNA as a negative control as in **Table 16** were obtained in lyophilized format.

**Table 16: siRNAs used in this study.**

siRNAs	Target
Silencer® Select Pre-Designed siRNA, Standard 5 nmol, ID: s15820	BAP1
Silencer® Select Pre-Designed siRNA, Standard 5 nmol, ID: s15822	BAP1
Silencer™ Select Negative Control No. 1 siRNA, 5 nmol	Negative control

First, the tubes were briefly centrifuged to ensure that the dried siRNA was at the bottom of the tube. Then, the siRNAs were dissolved with nuclease-free water (NFW) resuspending the 5 nmol siRNA using 50  $\mu$ L of NFW to obtain the final concentration of 100  $\mu$ M. This main stock solution was further diluted to 10  $\mu$ M for immediate use as aliquots to prevent freeze-thaw cycles. A 10  $\mu$ M stock of siRNA duplex is equivalent to 10 pmol/ $\mu$ L. The aliquots were stored at  $-20$   $^{\circ}$ C in a freezer.

### 3.2.3.2. Cell seeding and reverse transfection of the siRNAs

In reverse transfection, the complexes are prepared inside the well then, cells and medium are added. Reverse transfection is faster to perform than forward transfections and yields high-throughput transfection. For each well to be transfected, RNAi duplex-Lipofectamine RNAiMAX complexes were prepared. 30 pmol (3  $\mu$ L of 10  $\mu$ M working stock) RNAi duplex was diluted in 500  $\mu$ l Opti-MEM I Medium without serum in the well of the cell culture plate, and gently mixed. Lipofectamine RNAiMAX reagent was pipetted before use, and then 5  $\mu$ l Lipofectamine RNAiMAX was added to each well containing the diluted RNAi molecules. Gently mixed and incubated for 15 minutes at RT.

Cells were diluted in a complete growth medium but without antibiotics so that 3 ml contains the appropriate number of cells to give 30-50% confluence 24 hours after plating.  $5 \times 10^5$  MEL202 cells/well was optimized.

To each well with RNAi duplex - Lipofectamine RNAiMAX complexes, 2.5 ml of the diluted cells were added having a final volume of 3 ml and a final RNA concentration of 10 nM. The plate was mixed gently by rocking back and forth. The cells were incubated for 72 hours at 37 °C in a cell culture incubator for the gene knockdown. The cell pellets were collected on the 3<sup>rd</sup> day of the transfection. The cell pellets in clean 1.5 ml tubes were snap-frozen on dry ice and placed in a -80 °C freezer for Western blot validation and RNA-seq preparation.

## 3.2.4. Western blot

### 3.2.4.1. Sample Preparation

All the steps for the protein extraction from cells were carried out at 2-8 °C. Medium in culture flask was discharged, washed with 1X PBS, trypsinized, neutralized, centrifuged and the supernatant was removed. The pellet was resuspended with ice-cold PBS, the tube was centrifuged, and the PBS-containing supernatant was removed. Then any liquid on the cell pellet was removed, and the tubes were located on dry ice to snap-freeze the cell pellets and stored at -80 °C. To use the pellets, the samples were taken from the freezer

on ice and 100  $\mu$ L ice-cold RIPA lysis buffer with protease inhibitor cocktail (PIC) (**Table 17**) was added. The cells were lysed on ice for 15 min.

**Table 17: Preparation of 1X RIPA Lysis Buffer.**

1X RIPA Lysis Buffer	
10X RIPA Lysis Buffer (stock)	1 ml
dH <sub>2</sub> O	9 ml
cOmplete mini EDTA-free PIC	one tablet

Sonication: The samples were sonicated 3 times with Covaris S2 sonicator with the optimized settings (**Table 18**) to complete the cell lysis and to shear the DNA to reduce sample viscosity. The samples were centrifuged at 16,000 g for 20 min at 4°C. The centrifuged tubes were gently removed and placed on ice. The supernatants were transferred to a fresh tube on ice, the pellets were discharged.

**Table 18: Sonications settings of the Covaris S2 sonicator used for the Western blot.**

Sonication program	Western-blot_shearing_Ozan
1x Duty cycle	2%
Intensity	3
Cycles/Burst	200
Time	20 seconds

1  $\mu$ L from each sample was taken to perform a BCA protein quantification assay. The protein concentration for each cell lysate was determined. If necessary, the protein samples were aliquoted for storage at -20 °C.

#### 3.2.4.2. BCA Assay for protein quantification

Preparation of diluted Bovine serum albumin (BSA) standards: The contents of the one BSA ampule were diluted into several clean vials using the same diluent as the samples using **Table 19** as a guide for preparation of a set of protein standards. Each 1 mL ampule of 2 mg/mL Albumin Standard is enough to prepare the set of diluted standards.



**Table 19: Dilution scheme of BSA for the standard test tube protocol for the working range.**

Vial	Volume of Diluent (µL)	Volume and Source of BSA (µL)	Final BSA Concentration (µg/mL)
A	0	300 of Stock	2000
B	125	375 of Stock	1500
C	325	325 of Stock	1000
D	175	175 of vial B dilution	750
E	325	325 of vial C dilution	500
F	325	325 of vial E dilution	250
G	325	325 of vial F dilution	125
H	400	100 of vial G dilution	25
I	400	0	0 = Blank

BCA working reagent (WR) was prepared using **Equation 1** to determine the total volume of WR required:

**Equation 1: Formula of the WR preparation for BCA assay.**

$$\begin{aligned} & (\# \text{ standards} + \# \text{ unknowns}) \times (\# \text{ replicates}) \times (\text{volume of WR per sample}) \\ & = \text{total volume WR required} \end{aligned}$$

WR was prepared by mixing 50 parts of BCA Reagent A with 1 part of BCA Reagent B (50:1, Reagent A: B). For one experiment, combining 15 mL of Reagent A with 0.3 mL of Reagent B. Test-tube procedure (sample to WR ratio = 1:20) was applied for the protein samples pipetting 50 µL of each standard and unknown sample into a test tube, adding 1 mL of the WR to each tube and mixing well, covering and incubating the tubes at 37 °C heater for 30 minutes (working range = 20–2000 µg/mL) as in the standard procedure. All the tubes were cooled to RT. The spectrophotometer was set to measure BCA assay at 562 nm, the blank measurement was done, samples were transferred into cuvettes and the absorbance of all the samples was measured within 10 minutes.

### 3.2.4.3. Protein separation by sodium dodecyl-sulfate polyacrylamide gel electrophoresis (SDS-PAGE) and blotting

20 ug of each sample was taken and an equal volume of 4x Laemmli sample buffer (containing  $\beta$ -mercaptoethanol). Each cell lysate in the sample buffer was boiled at 95 °C for 5 minutes. Equal amounts of protein (20 ug) were loaded into the wells of the SDS-PAGE gel. 5  $\mu$ L of PageRuler Prestained protein ladder was used. The gel was run for 1 hour at 100 V. After the bands of the ladder were separated, trans blot turbo transfer system packs were used to blot the gel. First, the bottom part of the wiping was placed, having the shiny face of the membrane looking upwards and the dotted face looking at the bottom of the wet paper. The cassette was opened, and the unnecessary top and bottom parts of the gel were removed. The gel was placed on the membrane having the gel and membrane wet in each step. The blotting sandwich was assembled by placing the top part, rolling on the top (with 15 ml falcon or roller) to remove any air bubbles, and then placing the top of the cassette. The cassette was inserted into the Trans-Blot Turbo instrument. The protocol for the mixed molecular weight was chosen from the list and the transfer was started. After the finish of the transfer, the cassette was opened and the membrane was directly placed in a container to block in the blocking solution (5% milk powder in TBS-T) at RT for 1 hour. For one membrane, 20 ml of blocking solution was used. Then, the membrane was incubated in the primary antibody solution (blocking solution + primary antibody) for the target protein at 4 °C overnight placing the membranes facing the shiny/blotted face and contacting the solution inside of the 50 ml falcon tube. The falcon was placed on a falcon roller device at 4 °C room. After the overnight incubation, the membranes were rinsed 3 times for 5 mins with TBS-T. The HRP-conjugated secondary antibody is diluted in 20 ml 5% milk/TBS-T as a 1:5000 dilution. The membranes were incubated for 1 hour on the roller at RT. The membranes were rinsed 3 times for 10 mins with TBS-T.

#### 3.2.4.4. Imaging of the membrane

ECL was applied by mixing substrate kit components in a 1:1 ratio. 0.1 ml of solution/cm<sup>2</sup> of the membrane was prepared. ECL was working for GAPDH but did not detect BAP1 as sensitive. Ultra substrate was used to detect BAP1. 250 µL of the solution was mixed on the membrane inside of a transparent plastic bag covering the region of interest on the membrane. During the imaging, firstly the membrane was positioned, and then a Custom-white image was taken to have the ladders. Then Blot-Chemiluminescence HS was taken arranging for faint bands with a time series of exposure. Each file was saved as .scn then, two images were merged to have the ladder and bands on the same image saving both as .scn and .jpeg files.

### 3.2.5. Immunofluorescence (IF) staining

#### 3.2.5.1. Coverslip preparation and cell seeding

Coverslips were placed into an ethanol bath in a 3.5 cm dish within the cell culture hood. The ethanol wash was applied for at least 1 hour. After the ethanol wash, coverslips were held with tweezers to remove residual ethanol and placed vertically in a well of a cell culture plate to allow evaporation of the remaining ethanol on both sides. After drying, the coverslips were laid horizontally at the bottom of the wells. The UV light of the cell culture hood was turned on for at least 30 minutes for further sterilization. Following the ethanol wash and UV exposure,  $1 \times 10^5$  cells were seeded in 500 µl of medium into the wells. The plate was placed in the incubator overnight.

#### 3.2.5.2. Formaldehyde fixation

All formaldehyde-related steps were performed under the chemical hood, with freshly prepared Formaldehyde on the same day using the protocol modified from (Rinderle et al., 1999). 24 hours later the cell seeding, 500 µL of medium was removed. 400 µL of %3.7 PFA was added to each well, and incubated for 10 minutes at RT. After 10 minutes, the PFA solution was completely removed. The wells were washed 3 times with 400 µl 1x PBS. The experiment continued with the permeabilization step.

#### 3.2.5.3. Permeabilization and Blocking

500  $\mu$ L of PBS + 0.2 % Triton X-100 was transferred to the wells. The cells were incubated for 10 min at RT, then washed 3 times with 1x PBS. After this permeabilization step, 500  $\mu$ L PBS + 3% BSA was added to each well for blocking and incubated for 1 hour at RT.

#### 3.2.5.4. Primary and secondary antibody incubations

Primary antibodies were diluted at determined ratios in 1% BSA + 0.1% Triton-X 100 (A new antibody was tested at 1:400, 1:200, and 1:100 ratios). After 1 hour of blocking, the blocking solution was removed and the primary antibody mixture was directly added into the wells having around 200  $\mu$ L mix per well. The plate was sealed with parafilm and placed at 4 °C for the overnight incubation. After the overnight incubation, the primary antibody solution was removed from the wells and washed 3 times with 500  $\mu$ L 1x PBS. A secondary antibody was prepared in 1% BSA + 0.1% Triton-X 100 at a 1:500 ratio and added into the wells after the PBS washes. The plate was covered with aluminum foil and incubated for 1 hour at RT. Then, washed 3 times with 500  $\mu$ L 1x PBS. Hoechst (0.1-12  $\mu$ g/ml) was prepared in 1x PBS at a 1:1000 ratio and added to the wells to stain the nucleus for 10 min. Then, the wells were washed 2 times with 1x PBS, for 5 min each. The coverslips were taken out from the wells using the tweezers, mounted on the slides using 10  $\mu$ L mounting medium, left for 3-4 hours for stabilization of the coverslip on the slides before the imaging. The slides were stored at 4 °C in a dark environment until imaging.

#### 3.2.6. Confocal Microscopy

Fixed cells from section 3.2.5 were visualized using confocal laser scanning microscopes LSM700 (Carl Zeiss Inc.) and the obtained data were processed and analyzed with the Zeiss ZEN 2011 software (Carl Zeiss Inc.). Further analysis of the images was done using ImageJ software.

#### 3.2.7. Bulk RNA sequencing

Cells were obtained from the cell culture and washed with cold PBS. After centrifugation, the cell pellet containing  $1 \times 10^6$  cells in 1.5 ml safe-lock tubes was placed onto dry-ice to

snap-freeze and placed in a  $-80^{\circ}\text{C}$  freezer until further use. To obtain the RNA content from the cells, the tubes were taken from the  $-80^{\circ}\text{C}$  freezer then, total DNA and RNA isolations were done using AllPrep DNA/RNA/miRNA Universal Kit. The protocol of “Simultaneous Purification of Genomic DNA and Total RNA, including miRNA, from Cells” was applied according to the kit manufacturer’s instructions. This kit protocol included the steps of cell lysis, and separation of genomic DNA by binding to a column while flowing the total RNA through as the eluate. Then, the DNA and RNA contents were transferred to separated tubes, and in parallel setup, they were washed, Proteinase K digestion was applied to remove bound proteins. DNA samples are eluted and stored in a freezer. RNA samples were precipitated in the presence of ethanol and all the impurities were removed by washing, DNase I digestion was done to eliminate any DNA inside and finally eluted after the washes. The RNA samples were quantified, aliquoted, and stored in the freezer.

To process the RNA samples obtained from the cells, a TruSeq Stranded Total RNA kit was used. The protocol of the “TruSeq® Stranded Total RNA Sample Preparation Guide” was applied according to the kit manufacturer’s instructions. This kit protocol included the steps of depleting the rRNA (RiboZero) and fragmenting the DNA content, first and second strand cDNA synthesis, adenylation of 3' ends, ligation of adapters, PCR amplification, validation, normalization and pooling of the libraries before the NG-sequencing. Sequencing was performed as  $2\times 100$  bp, paired-end on a NovaSeq 6000 instrument.

### **3.2.8. Assay for Transposase-Accessible Chromatin (ATAC) sequencing**

#### **3.2.8.1. Cell sample preparation**

Fresh cells were trypsinized to detach and washed with cold 1xPBS.  $1\times 10^5$  cells were counted and aliquoted into 1.5 ml centrifuge tubes for each sample. The tubes containing  $1\times 10^5$  cells were centrifuged at  $500\times g$  for 5 mins at  $4^{\circ}\text{C}$ . The supernatant was removed without disturbing the cell pellet, and 100  $\mu\text{l}$  of ice-cold PBS was added and centrifuged at  $500\times g$  for 5 mins at  $4^{\circ}\text{C}$ . The supernatant was removed, and the cell pellet was resuspended in 100  $\mu\text{l}$  ice-cold ATAC Lysis Buffer. After the resuspension, the sample was centrifuged at  $500\times g$  for 10 mins at  $4^{\circ}\text{C}$ . During this centrifugation step, Tagmentation

Master Mix per sample in **Table 20** was prepared. Then, the supernatant of the samples was removed without disturbing the cell pellet, and the protocol was continued with “tagmentation reaction and purification” steps.

**Table 20: Preparation of Tagmentation Master Mix.**

Reagents	Volume (per sample)
2X Tagmentation Buffer	25 $\mu$ L
10X PBS	2 $\mu$ L
1.0% Digitonin	0.5 $\mu$ L
10% Tween 20	0.5 $\mu$ L
H <sub>2</sub> O	12 $\mu$ L
Assembled Transposomes	10 $\mu$ L

### 3.2.8.2. Tagmentation reaction and purification

50  $\mu$ L of Tagmentation Master Mix was added to each sample, the nuclei were resuspended. The tagmentation reaction was incubated at 37 °C for 30 minutes in a thermomixer working at 800 rpm. After the tagmentation reaction, each sample was transferred to a clean 1.5 mL tube. 250  $\mu$ L DNA Purification Binding Buffer and 5  $\mu$ L 3 M sodium acetate were added to each sample. If the color of the sample is anything other than bright yellow, an additional 3 M sodium acetate was added in 5  $\mu$ L increments until the correct color in **Figure 33** is achieved.

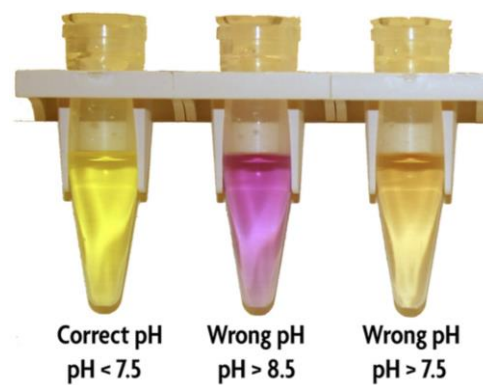


**Figure 33: Solution colors as a function of pH.**

The sample was only applied to the column when the solution was bright yellow (tube on the left) which indicated a pH under 7.5 to ensure DNA binds to the column. Each sample

was mixed. For each sample, a labeled DNA purification column was placed into a collection tube. Each sample was transferred to its corresponding column, its cap was closed, and centrifuge at 17,000 x g for 1 minute. The flow-through was discharged and the collection tube was returned to the column. 750  $\mu$ L of Wash Buffer (having 80% ethanol) was added to the column and they were capped. Centrifuged at 17,000 x g for 1 minute, the flow-through was discharged and the column was returned to the collection tube. With the column cap open, they were centrifuged at 17,000 x g for 2 minutes to remove any residual Wash Buffer from the column. Each column was transferred to a new microcentrifuge tube. 35  $\mu$ L of DNA Purification Elution Buffer was added to the center of the column matrix, the columns were capped and incubated for 1 minute at RT. Centrifuged at 17,000 x g for 1 minute. The columns were discharged and the DNA purification step was completed. The experiment continued with the following “PCR Amplification of Tagmented DNA” steps.

### 3.2.8.3. PCR amplification of tagmented DNA

The PCR reactions were set up by choosing the primers as dual-indexed from **Table 21** and adding the components in **Table 22**. Libraries to be multiplexed for sequencing on the same flow cell were ensured to have unique i5 and i7 index combinations for each.

**Table 21: i7 and i5 indexed primers of the ATAC-seq kit.**

<b>i7 Indexed Primer</b>	<b>i5 Indexed Primer</b>
i7 Indexed Primer 1 = i7 N701	i5 Indexed Primer 1 = i5 N501
i7 Indexed Primer 2 = i7 N702	i5 Indexed Primer 2 = i5 N502
i7 Indexed Primer 3 = i7 N703	i5 Indexed Primer 3 = i5 N503
i7 Indexed Primer 4 = i7 N704	i5 Indexed Primer 4 = i5 N504

**Table 22: Mixture for the PCR amplification reaction of the tagmented DNA.**

<b>Reagents</b>	<b>Volume (per reaction)</b>
Tagmented DNA	33.5 $\mu$ L
i7 Indexed Primer (25 $\mu$ M)	2.5 $\mu$ L
i5 Indexed Primer (25 $\mu$ M)	2.5 $\mu$ L
dNTPs (10 mM)	1 $\mu$ L

5X Q5 Reaction Buffer	10 $\mu$ L
Q5 Polymerase (2 U/ $\mu$ L)	0.5 $\mu$ L

PCR was performed using the program in **Table 23** on a thermal cycler with a heated lid.

**Table 23: PCR program to amplify the tagged DNA for ATAC-seq.**

Step 1:	72 °C for 5 minutes
Step 2:	98 °C for 30 seconds
Step 3: <b>10-cycles</b>	98 °C for 10 seconds 63 °C for 30 seconds 72 °C for 1 minute
Step 4:	Hold at 10°C

After the PCR reaction finished, SPRI clean-up was done with 60  $\mu$ L SPRI bead solution (1.2X the sample volume), eluting in 20  $\mu$ L DNA Purification Elution Buffer. To do this step, initially, 60  $\mu$ L well-mixed SPRI Beads at RT were added to each sample. The samples were vortexed briefly and incubated for 5 minutes at RT to provide the beads to bind. The tubes were placed on a magnetic rack to collect the beads. Once the solution was clear, the supernatant was aspirated. With the magnet still applied to the sample, 180  $\mu$ L 80% ethanol was added to each sample without mixing. Incubation was done for 30 seconds at RT. The supernatant was aspirated. Another (second) ethanol wash was done. The tubes were allowed to sit at RT to evaporate the residual ethanol. Once the beads transitioned from shiny to matte (2-5 minutes), 20  $\mu$ L DNA Purification Elution Buffer was added while the tubes separated from the magnetic rack. The tubes were capped and vortexed to mix. The samples were incubated for 5 minutes at RT. Tubes were placed on the magnetic rack to collect beads. Once the solution was clear, each supernatant containing the eluted DNA was transferred to a fresh tube. At this stage, the ATAC-seq libraries were ready for quantification and sequencing. PCR amplified libraries were analyzed to assess size distribution with a Bioanalyzer before the pooling and sequencing.



### **3.2.9. Chromatin Immunoprecipitation (ChIP) sequencing**

#### **3.2.9.1. Cell culture cross-linking and sample preparation**

Cells were seeded in 15 cm cell culture dishes with 20 ml of media and grown until the desired confluency had been reached. For each immunoprecipitation (IP), approximately  $4 \times 10^6$  cells were used. To crosslink proteins to DNA, 540  $\mu$ l of 37% formaldehyde was added to each 15 cm culture dish containing 20 ml of medium. The mixture was briefly swirled and incubated at RT for 10 minutes. The final formaldehyde concentration was 1% and color change in the medium was observed upon the addition of formaldehyde. Then, 2 ml of 10X glycine was added to each 15 cm dish containing 20 ml of medium, briefly mixed, and incubated at RT for 5 minutes. Another color change in the medium was observed after the addition of glycine to stop the reaction. The medium was removed and the cells were washed twice with 20 ml of ice-cold 1X PBS, any residues from the washes were completely removed each time. Then, 2 ml of ice-cold PBS + 10  $\mu$ l 200X PIC was added to each 15 cm dish, and the cells were scraped into the cold buffer. The cells from all dishes were combined into a single 15 ml falcon tube. The cells were centrifuged at 2,000 g for 5 minutes at 4 °C. The supernatant was discarded and the process continued with Nuclei Preparation and Chromatin Digestion.

#### **3.2.9.2. Nuclei preparation and chromatin digestion**

The cells were resuspended in 1 ml of ice-cold 1X Buffer A + DTT + PIC per IP preparation and incubated on ice for 10 minutes, inverting the tube every 3 minutes. The nuclei were pelleted by centrifugation at 2,000 g for 5 minutes at 4 °C. The supernatant was removed, and the pellet was resuspended in 1 ml of ice-cold 1X Buffer B + DTT per IP. The centrifugation was repeated, the supernatant removed and the pellet resuspended in 100  $\mu$ l of 1X Buffer B + DTT per IP. The sample was then transferred to a 1.5 ml microcentrifuge tube having up to 1 ml per tube. 0.5  $\mu$ l Micrococcal Nuclease was added per IP, the tube was mixed and incubated for 20 minutes at 37 °C with frequent mixing (3-5 mins) to digest the DNA to lengths of approximately 150-900 bp. The precise amount of Micrococcal Nuclease required to achieve optimal DNA length was determined empirically. The

digestion was stopped by adding 10  $\mu$ l of 0.5 M EDTA per IP preparation and placing the tube on ice for 1-2 minutes. The nuclei were pelleted by centrifugation at 16,000 g for 1 minute at 4  $^{\circ}$ C and the supernatant was removed. The nuclear pellet was resuspended in 100  $\mu$ l of 1X ChIP Buffer + PIC per IP and incubated on ice for 10 mins. Up to 500  $\mu$ l of lysate per 1.5 ml microcentrifuge tube was sonicated with several pulses to break the nuclear membrane. The lysates were clarified by centrifugation at 9,400 g for 10 minutes at 4  $^{\circ}$ C. The supernatant was transferred to a new tube. This cross-linked chromatin preparation was stored at -80  $^{\circ}$ C until further use. A 50  $\mu$ l sample of the chromatin preparation was removed for Analysis of Chromatin Digestion and Concentration.

#### 3.2.9.3. Analysis of chromatin digestion and concentration

To the 50  $\mu$ l chromatin sample from the previous step, 100  $\mu$ l of NFW, 6  $\mu$ l of 5 M NaCl, and 2  $\mu$ l of RNase A were added. The mixture was vortexed and incubated at 37 $^{\circ}$ C for 30 mins. Then, 2  $\mu$ l of Proteinase K was added to each RNase A-digested sample. The mixture was vortexed and incubated at 65  $^{\circ}$ C for 2 hours. DNA was purified from the samples using DNA purification spin columns as described in “3.2.9.6. DNA purification using spin columns”. After the purification, a 10  $\mu$ l sample of DNA was removed to determine fragment size by electrophoresis on a 1% agarose gel with a 100 bp DNA marker. The DNA was expected to be digested to lengths of approximately 150-900 bp (1 to 5 nucleosomes). DNA concentration was measured using Qubit HS.

#### 3.2.9.4. Chromatin Immunoprecipitation

10  $\mu$ g of digested, cross-linked chromatin was used per IP. In one tube, enough 1X ChIP Buffer for diluting the digested chromatin into the desired number of IPs was prepared. For one IP, 400  $\mu$ l of 1X ChIP Buffer (40  $\mu$ l of 10X ChIP Buffer + 360  $\mu$ l water) and 2  $\mu$ l of 200X PIC was prepared. The IPs included positive control H3K4me3 and negative control Rabbit IgG samples and the mixture was placed on ice. To the prepared 1X ChIP Buffer, 10  $\mu$ g of the digested, cross-linked chromatin preparation was added per IP. 10  $\mu$ l sample of the diluted chromatin was removed and transferred to a microfuge tube as a 2% Input sample which was stored at -20  $^{\circ}$ C until further use. For each IP, 500  $\mu$ l of the diluted

chromatin was transferred to a 1.5 ml microcentrifuge tube and the immunoprecipitating antibody was added. IP samples were incubated overnight at 4 °C with rotation. ChIP-Grade Protein G Magnetic Beads were resuspended by gently vortexing then, 30 µl of Protein G Magnetic Beads was added to each IP reaction and incubated for 2 hours at 4 °C with rotation.

Protein G magnetic beads in each IP were collected by placing the tubes in a magnetic separation rack. The solution was allowed to clear 2 minutes before removing the supernatant. The protein G magnetic beads were washed by adding 1 ml of low salt wash to the beads and incubating at 4 °C for 5 minutes with rotation. These steps were repeated two additional times for a total of 3 low-salt washes. Next, 1 ml of high salt wash was added to the beads and incubated at 4 °C for 5 minutes with rotation. Finally, the protein G magnetic beads in each IP were collected by placing the tubes in a Magnetic Separation Rack. The solution was allowed to clear for 2 minutes before removing the supernatant. The process proceeded to the elution step.

#### 3.2.9.5. Elution of chromatin from Antibody/Protein G magnetic beads and reversal of cross-links

Initially, to the 2% input sample tube, 150 µl of the 1X ChIP Elution Buffer was added and set aside at room temperature. Then, 150 µl of 1X ChIP Elution Buffer was added to each IP sample. Chromatin was eluted from the antibody/protein G magnetic beads by incubating for 30 minutes at 65 °C with vortexing. Protein G magnetic beads were collected by placing the tubes in a magnetic separation rack, allowing the solution to clear for 2 minutes. The eluted chromatin supernatant was transferred to a new tube. To all tubes, including the 2% input sample, 6 µl of 5M NaCl and 2 µl of Proteinase K were added to reverse cross-links. The samples were incubated for 2 hours at 65 °C. The process proceeded to the DNA purification step.

#### 3.2.9.6. DNA purification using spin columns

To each DNA sample, 750  $\mu$ l of DNA Binding Buffer was added and vortexed. Five volumes of DNA Binding Buffer were used for every volume of sample. 450  $\mu$ l of each sample were transferred to a DNA spin column in a collection tube. The samples were centrifuged at 18,500 g for 30 seconds. The spin column was then removed from the collection tube, and the liquid was discarded. The spin column was replaced in the collection tube. The remaining 450  $\mu$ l of each sample were transferred to the spin column in the collection tube and these steps were repeated. 750  $\mu$ l of DNA Wash Buffer was added to the spin column in the collection tube. The samples were centrifuged at 18,500 g for 30 seconds. The spin column was then removed from the collection tube, and the liquid was discarded. The spin column was replaced in the collection tube and centrifuged again at 18,500 g for 30 seconds. The collection tube and liquid were discarded, but the spin column was retained. 50  $\mu$ l of DNA Elution Buffer were added to each spin column which was then placed into a clean 1.5 ml microcentrifuge tube. The samples were centrifuged at 18,500 g for 30 seconds to elute the DNA. The DNA spin column was then removed and discarded. The eluate was the purified DNA. The concentration of the samples was measured using a Qubit HS kit.

#### 3.2.9.7. NG-Sequencing library construction

The purified DNA samples were processed according to the kit instruction protocol of “DNA Library Prep Kit for Illumina Systems (ChIP-seq, CUT&RUN)” to be prepared for obtaining high throughput next-generation sequencing (NG-seq) results. The steps that were followed during the library construction were end preparation, adaptor Ligation, cleanup of adaptor-ligated ChIP DNA without size selection, PCR Enrichment of Adaptor-ligated ChIP DNA (PCR conditions were based on **Table 24**, dual index primers in **Table 7** were used in combinational way ensuring the color balance during the sequencing of the bases), cleanup of PCR amplification and pooling the samples based on  $C_t$  values from qPCR amplification results.

**Table 24: Conditions of the PCR enrichment of the adaptor-ligated ChIP DNA.**

<b>Initial Denaturation</b>	98 °C for 30 sec
<b>Denaturation</b>	98 °C for 10 sec
<b>Anneal and Extension</b>	65 °C for 15 sec
For starting material of <b>50 ng</b> ChIP DNA, <b>6 cycles</b> , For starting material of <b>5 ng</b> ChIP DNA, <b>10 cycles</b> , For starting material of <b>0.5 ng</b> ChIP DNA, <b>13 cycles</b> were applied for denaturation, annealing and extension steps.	
<b>Final Extension</b>	65 °C for 3 min
<b>Hold</b>	4 °C

### **3.2.10. Cleavage Under Targets and Release Using Nuclease (CUT&RUN)**

To probe protein-DNA interactions within the natural chromatin context of the cells using a low number of the cells, the CUT&RUN technique was applied according to the manufacturer's kit instruction protocol with optimizations and modifications as described.

#### **3.2.10.1. Live Cell Preparation**

Fresh adherent cells from cell culture were harvested as 100,000 cells for each reaction, including an additional sample for input, positive control (H3K4me3) and negative control (IgG isotype control). Detachment of the cells was done using Trypsin avoiding scraping to prevent cell stress or lysis. Cells were centrifuged at 600 g for 3 min at RT, supernatant was removed. The cell pellet was resuspended in 1 mL of 1X Wash Buffer (+ spermidine + PIC), centrifuged again and the supernatant was removed. This wash step was repeated totally twice. Each cell pellet was resuspended in 100 µL of 1X Wash Buffer (+ spermidine + PIC). 100 µL of the resuspended cells were transferred to a new safe-lock tube and stored at 4 °C as the input sample.

### 3.2.10.2. Binding of Concanavalin A Beads and Primary Antibody

Concanavalin A Magnetic Beads were resuspended by pipetting, and 10  $\mu$ L of the bead suspension per CUT&RUN reaction were transferred to a new 1.5 mL microcentrifuge tube. 100  $\mu$ L Concanavalin A Bead Activation Buffer was added per 10  $\mu$ L of beads and mixed. The tube was placed on a magnetic rack until the solution became clear, the liquid was removed. The tubes were removed from the magnetic rack, the beads were washed a second time by repeating the addition of Concanavalin A Bead Activation Buffer and removal of the liquid. 10  $\mu$ L Concanavalin A Bead Activation Buffer was added to the initial bead suspension. The activated beads were mixed well into the solution and 10  $\mu$ L of the bead suspension per reaction was added to the washed cell suspension. The samples were mixed by pipetting and incubated for 5 minutes at RT. The tubes were placed on the magnetic rack until the solution turned clear and the liquid was removed. The tube was then removed from the stand, 100  $\mu$ L of Antibody Binding Buffer (with spermidine, PIC, and digitonin) per reaction was added, and the mixture was placed on ice. 100  $\mu$ L of the cell suspension was aliquoted into separate 1.5 mL tubes for each reaction and placed on ice. Antibodies were added to each reaction and mixed. 2  $\mu$ L of the positive control, and 5  $\mu$ L of the negative control antibodies were added. The tubes were incubated at 4  $^{\circ}$ C for 2 hours.

### 3.2.10.3. Binding of pAG-MNase Enzyme

For each reaction, a pAG-MNase pre-mix was prepared by adding 50  $\mu$ L of Digitonin Buffer and 1.5  $\mu$ L of pAG-MNase Enzyme to a new tube. The tubes from the previous section were placed on a magnetic rack until the solution turned clear and the liquid was removed. The tubes were then removed from the magnetic rack and 1 mL of Digitonin Buffer (+ spermidine + PIC + digitonin) was added. The beads were resuspended. The tubes were placed back on the magnetic rack until the solution turned clear, and the liquid was removed. The tubes were then removed from the magnetic rack and 50  $\mu$ L of the pAG-MNase pre-mix was added to each tube and the samples were mixed. The tubes were incubated at 4  $^{\circ}$ C for 1 hour.

#### 3.2.10.4. DNA Digestion and Diffusion

The tubes from the previous section were placed on a magnetic separation rack and the liquid was removed. The tubes were taken from the rack and 1 mL of Digitonin Buffer (+ spermidine + PIC + digitonin) was added. The beads were resuspended. This washing step was repeated totally twice. Then, 150  $\mu$ L of Digitonin Buffer (+ spermidine + PIC + digitonin) was added to each tube and mixed. The tubes were placed on ice for 5 minutes to cool down before digestion.

pAG-MNase was activated by adding 3  $\mu$ L of cold  $\text{CaCl}_2$  to each tube and mixed. The samples were incubated at 4  $^\circ\text{C}$  for 30 minutes. Then, 150  $\mu$ L of 1X Stop Buffer (+ digitonin + RNase A) was added to each sample and mixed. The tubes were incubated at 37  $^\circ\text{C}$  for 10 minutes to release the DNA fragments into the solution. The samples were centrifuged at 4  $^\circ\text{C}$  for 2 minutes at 16,000 g and placed on a magnetic rack. Enriched chromatin in the supernatant were transferred to new 2 mL microcentrifuge tubes.

#### 3.2.10.5. Preparation of the Input Sample

200  $\mu$ L of DNA Extraction Buffer (+ Proteinase K + RNase A) was added to the 100  $\mu$ L input sample, mixed. The tube was placed at 55  $^\circ\text{C}$  for 1 hour with shaking. Then, the tube was placed on ice for 5 minutes to cool the sample. The cells were lysed and chromatin fragmented by sonicating the input sample. The lysate was clarified by centrifugation at 18,500 g for 10 minutes at 4  $^\circ\text{C}$ . The supernatant was transferred to a new 2 mL microcentrifuge tube.

#### 3.2.10.6. DNA Purification

Purification of the DNA was done according to the manufacturer's kit instruction protocol from "DNA Purification Buffers and Spin Columns (ChIP, CUT&RUN) Kit" and applied as previously described in "3.2.9.6 DNA purification using spin columns" with modifications at the start of the protocol. 1.5 mL of DNA Binding Buffer was added to each input and enriched chromatin samples and mixed thoroughly. Thus, five volumes of DNA Binding Buffer were used for every 1 volume of sample. Then, 600  $\mu$ L of each sample was

transferred to a DNA spin column in a collection tube and the rest of the protocol was applied in the same way as previously described.

#### 3.2.10.7. NG-Sequencing library construction

The purified DNA samples were processed according to the kit instruction protocol of “DNA Library Prep Kit for Illumina Systems (ChIP-seq, CUT&RUN)” to be prepared for obtaining high throughput next-generation sequencing (NG-seq) results. The conditions previously described in the section “3.2.9.7. NG-Sequencing library construction” were applied.

### 3.2.11. Data Analysis

RNA-seq data processing was done aligning the RNA reads to hg19 using STAR for gene expression quantification. Mapped reads were annotated with htseq using Ensembl v75. Gene expression levels were quantified in transcripts per million (TPM). Non-expressed genes in any of the samples (TPM < 0.5) were filtered out for further analysis. Differentially expressed genes were detected using R package edgeR “Generalized Linear Models” (GLM) model (Robinson et al., 2010, McCarthy et al., 2012, Chen et al., 2016). The genes with absolute logFC greater than 1 (logFC>1) are considered "differentially expressed".

ATAC-seq data processing was done subjecting the raw reads to adapter and quality trimming using the bbdduk tool from the BBTools package [BBMap - Bushnell B. - sourceforge.net/projects/bbmap/] (version 37.90; parameters: minlen=25 qtrim=rl trimq=10 ktrim=r k=25 mink=11 hdist=1 overwrite=t)(Bushnell et al., 2017). The adaptors were removed using Cutadapt (version 4.4)(Martin, 2011). The processed reads were aligned to the human genome (hg19) using Bowtie2 (version 2.5.0; parameters: --end-to-end --very-sensitive --no-mixed --no-discordant -q --phred33 -l 10 -X 700) (Langmead and Salzberg, 2012). Genrich tool [Genrich - Gaspar J. M. - github.com/jsh58/Genrich] is used to remove PCR duplicates, mitochondrial reads, as well as peak calling (version 0.6.1; parameters: -j -R -r -e chrM -q 0.05). Called peaks are further filtered by having a read count per million > 2. Differential accessibility analysis for four MEL202 WT, and two MEL202 BAP1 KD samples are done doing differentially accessible region (DAR) analysis.



The analysis is carried out using the R package DiffBind (version 3.8.4)(Stark, 2013, Ross-Innes et al., 2012). Blacklisted regions are removed from the previously called peak sets, an overall set of candidate accessible regions are obtained, normalized for the library size and differential binding affinity analysis is performed both using DESeq2 (Love et al., 2014) and edgeR (Robinson et al., 2010, McCarthy et al., 2012, Chen et al., 2016). For the sake of robustness, we took the regions that were detected to be differentially accessible with a p-value < 0.05 in both DESeq2 and edgeR analyses. Gained (when BAP1 is knocked down) and lost peaks are reported separately for the downstream analysis. Annotation of DARs is done. Gene annotations for the differentially accessible regions were generated using the ChIPseeker (version 1.34.1) package in R (Yu et al., 2015). Known gene annotation for hg19 is downloaded from UCSC. annotatePeak function is used for retrieving the annotation of the genes, as well as genic regions. Chromatin states are annotated as described.

ChIP-seq and CUT&RUN data analysis were done processing the data subjecting the raw reads to adapter and quality trimming using the bbdup tool from the BBTools package [BBMap - Bushnell B. - sourceforge.net/projects/bbmap/] (version 37.90; parameters: minlen=25 qtrim=rl trimq=10 ktrim=r k=25 mink=11 hdist=1 overwrite=t) (Bushnell et al., 2017). The adaptors were removed using Cutadapt (version 4.4) (Martin, 2011). The processed reads were aligned to the human genome (hg19) using Bowtie2 (version 2.5.0; parameters: --end-to-end --very-sensitive --no-mixed --no-discordant -q --phred33 -I 10 -X 700)(Langmead and Salzberg, 2012). PCR duplicates were removed using Picard's MarkDuplicates tool (VALIDATION\_STRINGENCY=SILENT)(GitHub, 2018). Replicates are merged using samtools merge (Danecek et al., 2021). Before peak calling, the blacklisted regions are filtered out (Nordin et al., 2023). Since IgG negative control samples turned out to have zero concentration on Bioanalyzer, peaks were called without a background, using SEACR in stringent mode with a p-value threshold of 0.01 (Meers et al., 2019). Common and condition-specific peaks are identified using bedtools intersect (Quinlan and Hall, 2010). Plots are generated using the PlotProfile and PlotHeatmap functions of Deeptools (Ramirez et al., 2016).

## Chapter 4: Results

In this study, we aimed to understand the transcriptomic and gene regulatory roles of BAP1 in UM. To achieve this, we conducted a search to identify well-established UM cell lines with BAP1 expression. **Figure 34** shows the result of the “Cell Line Selector” tool from the Dependency Map (DepMap) (Tsherniak et al., 2017) portal filtering the UM cells. Among the identified UM cell lines, MEL202 was selected due to its well-characterized genetic profile, including mutations in the *GNAQ* gene (Q209L and R210K) and its relevance to the study of BAP1-related molecular mechanisms (Jager et al., 2016). Additionally, MEL202 exhibits loss of heterozygosity (LOH) for BAP1 which, despite retaining some BAP1 expression, makes it a relevant system to study certain aspects of BAP1 function in UM particularly in the context of epigenetic and transcriptomic alterations.

Cell Line	Lineage	Lineage Subtype	Lineage Sub-subtype	BAP1 (UCLH2, hucep-6, KIAA0272) Expression Public 24Q2
921	Eye	Ocular Melanoma	Uveal Melanoma	4.56
MEL202	Eye	Ocular Melanoma	Uveal Melanoma	5.24
MEL270	Eye	Ocular Melanoma	Uveal Melanoma	5.21
MEL285	Eye	Ocular Melanoma	Uveal Melanoma	4.09
MEL290	Eye	Ocular Melanoma	Uveal Melanoma	5.15
MP41	Eye	Ocular Melanoma	Uveal Melanoma	
MP46	Eye	Ocular Melanoma	Uveal Melanoma	0
OMM1	Eye	Ocular Melanoma	Uveal Melanoma	4.98
OMM25	Eye	Ocular Melanoma	Uveal Melanoma	4.95
UPMD1	Eye	Ocular Melanoma	Uveal Melanoma	5.30
UPMM3	Eye	Ocular Melanoma	Uveal Melanoma	5.26
WM3772F	Eye	Ocular Melanoma	Uveal Melanoma	4.70

**Figure 34: Shortlist of cell line selection based on UM-lineage subtype having BAP1 expression.** Cell line selector tool of DepMap portal showing the filtered cell lines ([www.depmap.org/portal/](http://www.depmap.org/portal/)).

### 4.1. Characterization of the MEL202 cell line as a UM model

We obtained the MEL202 adherent cell line (from the Curie Institute, Paris, Stern team), which was originally derived from a primary uveal melanoma patient (Griewank et al.,

2012). We performed whole exome sequencing to confirm the somatic mutational profile of the MEL202 cell line. The mutational profile of MEL202 is summarized in **Table 25**.

**Table 25: Mutational status of MEL202 cell line.** (L: Leucine, R: Arginine, P: Proline, Q: Glutamine, K: Lysine, G: Glycine)

Gene	Status
<i>GNAQ</i>	Missense Mutations: Q209L and R210K
<i>SF3B1</i>	Missense Mutation: R625G
<i>CDKN2A</i>	Frameshift Mutations: L65R*52 and P80

According to the result, this cell line carries two activating *GNAQ* mutations (Q209L and R210K) which are known to be the primary mutations for the UM.

To confirm the presence of BAP1 protein, we cultured the MEL202 cells and performed Western blot analysis using GAPDH as a loading control. The Western blot results verified the expression of BAP1 in the MEL202 cells as presented in **Figure 35**. The band for BAP1 is obtained as intact without a smear or traces of degradation, and the size of the band located slightly above 100 kDa according to the ladder we used which was in alignment with the antibody manufacturer's results (Appendix **Figure 86** and Appendix **Figure 87**).

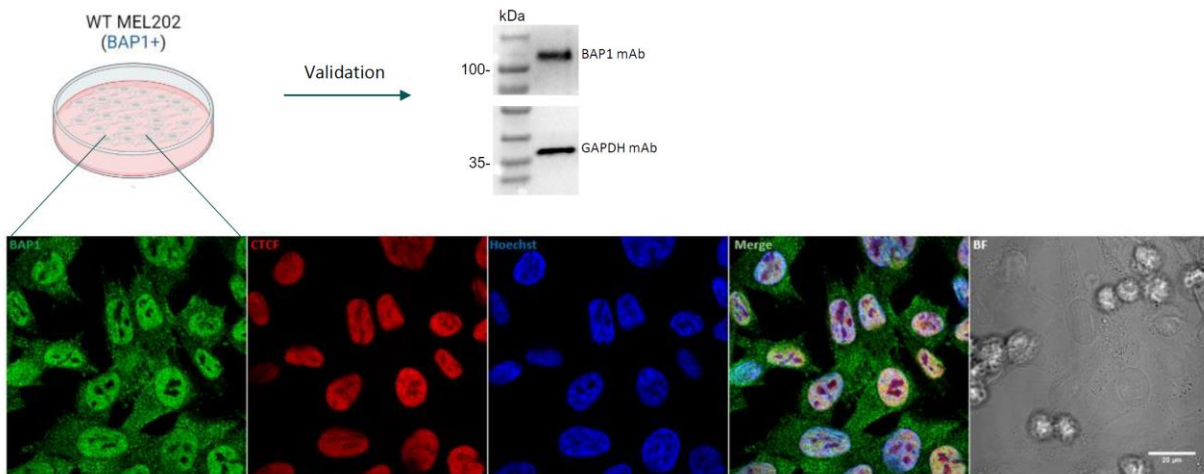


**Figure 35: Confirmation of the presence and localization of BAP1.** Green: BAP1, Red: CTCF, Blue: Hoechst. Scale bar = 20 μm.

Additionally, we utilized immunofluorescence (IF) staining to determine the localization of BAP1 within the cells. The staining revealed that BAP1 predominantly accumulates in the nucleus. For validation, we used CTCF as a positive control in the IF staining experiment. The images from the IF staining confirmed the nuclear localization of BAP1, as shown in **Figure 35**.

#### 4.2. Genome-wide binding characteristics of BAP1 in MEL202 cells

We performed ChIP-seq experiments to identify the genome-wide binding characteristics of BAP1 in MEL202 cells. Afterwards, we used ChromHMM algorithm (van der Velde et al., 2021) in order to annotate the binding characteristics of our ChIP-seq experiments to 18 chromatin states as summarized in **Figure 36**.

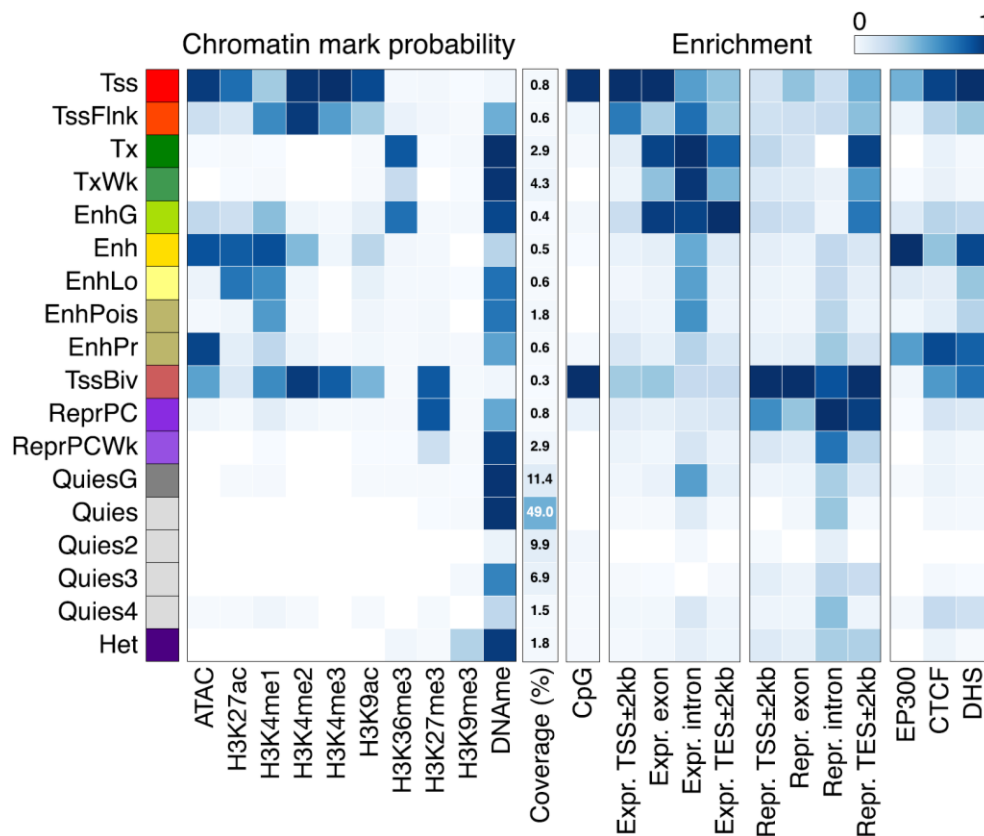


**Figure 36: Overview of the 18 chromatin states based on histone marks, accessibility scores and other genomic features.** Adapted from (van der Velde et al., 2021).

We identified key genomic regions where BAP1 was associated. According to our findings, BAP1 primarily associates with transcription start sites (TSS) and enhancer regions, suggesting that BAP1 may have roles in gene regulation, potentially through modulating transcriptional activities at these loci. Additionally, we observed that BAP1 binding sites overlap with CpG-rich regions, genic regions, and areas of accessible chromatin. While these observations do not confirm direct involvement of BAP1 in maintaining the epigenetic landscape, they indicate that BAP1 is present at critical genomic regions that are known to be involved in gene expression regulation and chromatin accessibility (Masclaf et al., 2021, Conway et al., 2021, Fursova et al., 2021). The following sections reveal our findings in greater detail.

#### **4.2.1. BAP1 mainly associates with TSS (88%) and enhancer (10%) sites in MEL202 cells**

Our ChIP-seq results revealed that BAP1 predominantly binds to TSS and enhancer regions in MEL202 cells. **Figure 37A** shows the distribution of BAP1 binding sites across various chromatin states. The majority of BAP1 peaks (87.79%) were found at TSS, with a second biggest fraction (10.01%) associated with enhancer regions. Other chromatin states, including bivalent/poised TSS, transcription, and repressed PolyComb regions, had minimal BAP1 binding.

To further understand the relevance of BAP1 binding, we analyzed its relative distribution over the genomic background (**Figure 37B**). This analysis confirmed the significant enrichment of BAP1 binding at active TSS and enhancer regions, indicating a strong association of BAP1 with transcriptionally active regions over the genomic background.

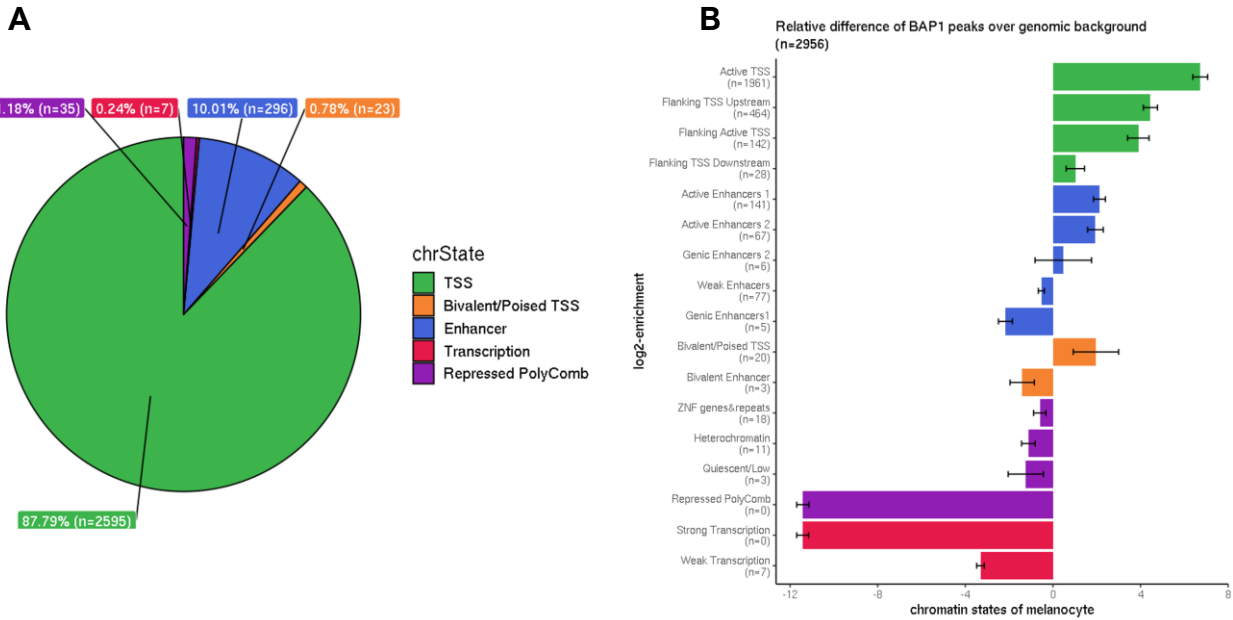


**Figure 37: Distribution of the BAP1 binding sites throughout the chromatin states.**

As a next step, we analyzed the binding motif of BAP1 in the MEL202 cells to understand the characteristics of its binding patterns. **Table 26** lists the *de novo* motif enrichment result obtained from the HOMER tool (Heinz et al., 2010).

**Table 26: HOMER de novo motif analysis results for BAP1-binding sequences.** Cutoff for the p-value set to  $< 1 \times 10^{-15}$ .

Motif	p-value	% of targets	Match
	$1 \times 10^{-83}$	34.97%	ELK1 (ETS family TF)
	$1 \times 10^{-27}$	31.12%	YY2 (C2H2 zinc finger)
	$1 \times 10^{-21}$	34.58%	DMRTA2 (DM-type zinc finger)
	$1 \times 10^{-16}$	10.18%	ZNF711 (C2H2 zinc finger)

The motif analysis highlights the presence of specific transcription factor (TF) motifs in BAP1-bound regions. According to our results, ELK1 stands out with the strongest

enrichment ( $p$ -value =  $1 \times 10^{-83}$ ), suggesting a prominent role in the regulatory network influenced by BAP1. The ELK1 motif is an ETS family TF. It is highly enriched in BAP1-binding regions, presenting 34.97% of the target sequences. The extremely low  $p$ -value underscores the significant association between BAP1 and ELK1 motif presence. This suggests that BAP1 may regulate or interact with genes modulated by ELK1 which is a TF known for roles in proliferation, differentiation, and survival pathways (Yang and Sharrocks, 2006). Also, the strong enrichment may imply that ELK1 could function as a regulatory partner of BAP1 and potentially influence gene expression in the context of UM. ELK1 is known to act downstream of the MAPK pathway and plays a role in cell growth and differentiation. Given its strong enrichment in BAP1-binding sites, it is plausible that BAP1 might facilitate or enhance ELK1's recruitment to chromatin, thereby regulating transcriptional programs critical for cellular proliferation and tumorigenesis. Alternatively, BAP1 might act to stabilize chromatin in a way that either permits or competes with ELK1 binding, suggesting a more complex regulatory interplay. This potential dual role of BAP1 in facilitating or displacing ELK1 could provide a further mechanistic link to the transcriptional dysregulation observed in BAP1-deficient UM. Considering BAP1's role in opposing Polycomb-mediated repression, BAP1 may prevent excessive repression at ELK1-bound loci, balancing gene activation and repression.

YY2, DMRT2, and ZNF711 were also identified among the significantly enriched ( $p$ -value set to  $< 1 \times 10^{-15}$ ) binding motifs of BAP1. YY2 (Yin Yang 2) is known to regulate gene expression involved in cell proliferation and differentiation. It is a homolog of YY1 (Yin Yang 1), shares considerable functional overlap with YY1 in gene regulation and transcriptional repression. YY1 is known to interact with various chromatin remodelers, including BAP1, to modulate chromatin structure and influence gene expression. Given the structural and functional similarities between YY1 and YY2, the presence of YY2 binding motifs in the BAP1-bound regions suggests that YY2 may play a role in the regulatory networks governed by BAP1, potentially affecting transcriptional programs controlled by both YY1 and YY2, and its interaction with BAP1 may contribute to the transcriptional regulation (Wu et al., 2017). DMRT2 (Doublesex and Mab-3 Related Transcription Factor 2) a key regulator

in somitogenesis differentiation, also SOX9-inducible gene involved in promoting chondrocyte hypertrophy. Epigenetic studies have shown that SOX9 regulates DMRT2 expression through an active enhancer during cell differentiation. It may suggest a potential targets for differentiation pathways whose motif are shared with BAP1 (Ono et al., 2021) in the UM cells. ZNF711 (Zinc Finger Protein 711) is a transcription factor involved in gene regulation, particularly in brain development and neurogenesis. It has been linked to the transcriptional control of X-linked genes and may play a role in neurological disorders. The presence of ZNF711 binding motifs within BAP1-associated regions suggests a potential regulatory interaction between BAP1 and ZNF711 indicating that BAP1 influences the expression of ZNF711 target genes, potentially affecting pathways related to cell differentiation and growth (Ni et al., 2020).

These results suggest that BAP1 plays a crucial role in regulating gene expression by predominantly associating with promoter and enhancer regions and the ELK1 motif appears to be the major target in MEL202 UM cells.

#### **4.2.2. BAP1 binding sites are associated with CpG regions, genic regions, and accessible chromatin in MEL202 cells**

To further investigate the genome-wide binding preferences of BAP1, we performed additional analyses focusing on its distributions throughout the CpG regions, genic regions, and chromatin accessibility in MEL202 cells.

Firstly, we examined the distribution of BAP1 binding sites across CpG regions. As shown in **Figure 38**, the majority of BAP1 peaks (96.67%) were found in CpG regions, with a small fraction distributed in CpG islands (3.17%) and even fewer in CpG shelves and shores. This indicates a strong preference for BAP1 for CpG-rich areas, suggesting its role in DNA methylation regulation.



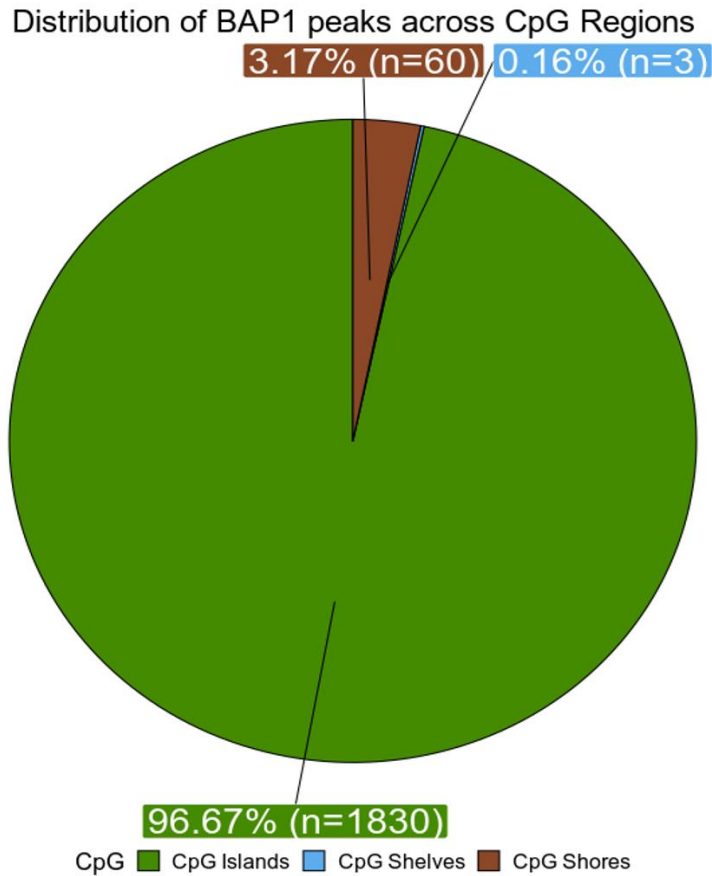


**Figure 38: Peaks coming from BAP1 binding sites are distributed mainly to the CpG sites.**

Secondly, we analyzed the distribution of BAP1 binding sites within the genic regions. **Figure 39** shows that BAP1 predominantly binds to promoter regions (61.12%) and 5' UTRs (32.45%), with minimal binding in introns, exons, and other regions. This enrichment at the promoter and 5' UTR regions indicates BAP1's role in transcription regulation.

Then, we assessed the chromatin accessibility of BAP1 binding sites using the ATAC-seq experiment. As shown in **Figure 40**, 76.82% of BAP1 binding sites were located in accessible chromatin regions, indicating that BAP1 preferentially binds to regions of open chromatin, which are typically associated with active transcription.

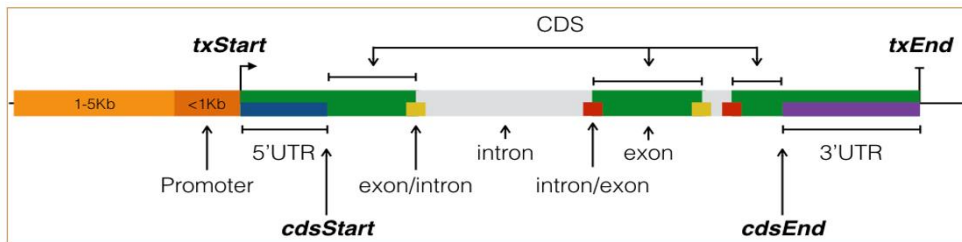
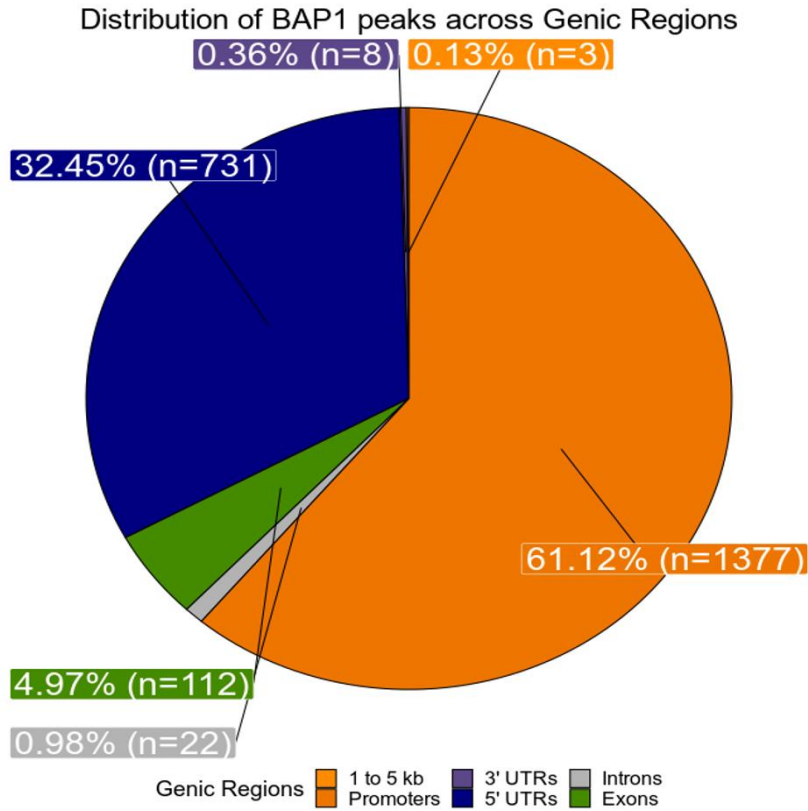


**Figure 39: BAP1 binds mainly promoter and 5' UTRs (>90%).**

These results collectively demonstrate that BAP1 binding sites are primarily associated with CpG-rich regions, promoter and 5' UTR regions, and accessible chromatin, highlighting its significant role in regulating gene expression and chromatin structure in MEL202 WT cells.

Distribution of BAP1 peaks across ATAC-Seq peaks

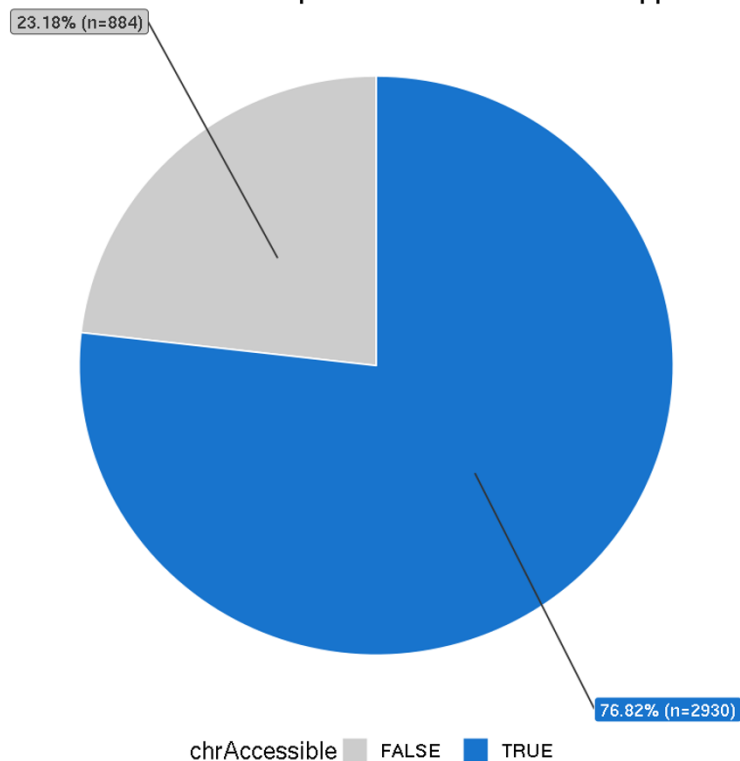


**Figure 40: 77% of the BAP1 binding sites are accessible.**

### 4.3. Strategies for BAP1 loss in MEL202 cells

#### 4.3.1. CRISPR/Cas9 knockout strategy for BAP1 gene

To investigate the effects of BAP1-loss in MEL202 cells, we first employed the CRISPR/Cas9 gene knockout (KO) system. We aimed to establish BAP1 KO monoclonal MEL202 uveal melanoma cells using the LentiCRISPRv2GFP system to integrate our guide RNA. Following transduction with 3<sup>rd</sup> generation lentiviral vectors, the transduced cells were sorted based on their GFP signal levels using fluorescence-activated cell sorting (FACS) into 96-well plates to ensure the isolation of monoclonal colonies. **Figure 41** shows the growth of FACS-sorted monoclonal MEL202 cells in a 96-well plate.

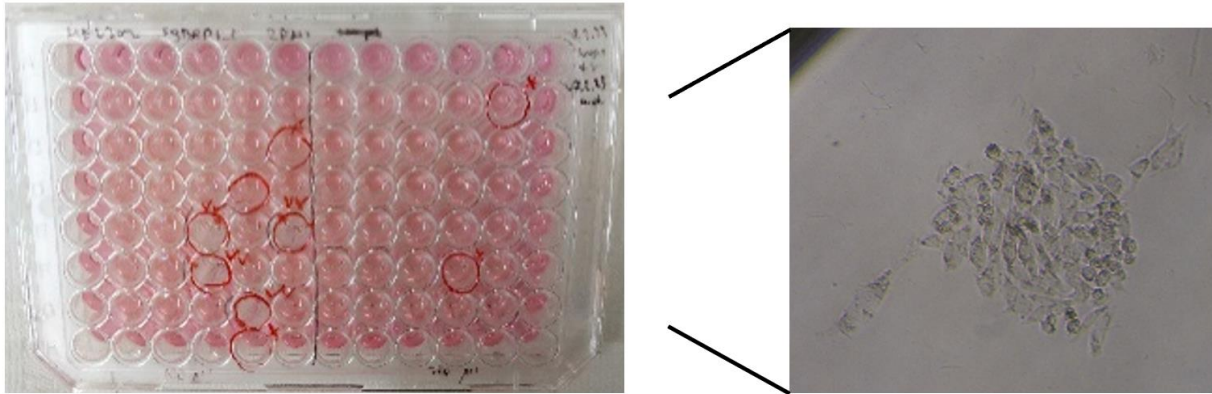


**Figure 41: Growth of the FACS-sorted monoclonal MEL202 cells in a 96-well plate.**

According to the cell sorting strategy, untransduced MEL202 cells were used as a negative control to determine the threshold for GFP expression to set the gating strategy (Appendix **Figure 88**). MEL202 cells that were transduced with sgBAP1\_1 and sgBAP1\_3 were first tested to obtain their threshold levels of GFP-negative and GFP-positive populations comparing the negative control. Then, the GFP-positive populations of each transduction were sorted with the established gating strategy for each MEL202 transduction group either transduced with sgBAP1\_1 or sgBAP1\_3 (Appendix **Figure 89** and Appendix **Figure 90**, respectively). The sorted single cells were incubated for approximately one month to allow the proliferation of monoclonal colonies (Appendix **Figure 91**). Healthy colonies were subsequently amplified in T25 cell culture flasks. Once sufficient cell proliferation was achieved, samples were collected for Western blot analysis to assess BAP1 protein levels.

The Western blot results, shown in **Figure 42**, indicated that the surviving monoclonal cell clones retained detectable levels of BAP1 protein. This finding suggests that cells with complete BAP1 depletion were likely eliminated during the monoclonal selection process, possibly due to the essential role of BAP1 in cell viability. According to the supporting evidence obtained in a recent study (Yu et al., 2022), colony formation was strongly inhibited in BAP1-deficient MEL202 cells, in a proportional manner to the knockout efficiency. Thus, the presence of BAP1 protein in the surviving colonies suggests that BAP1-deficient cells were negatively selected during the monoclonal selection process.

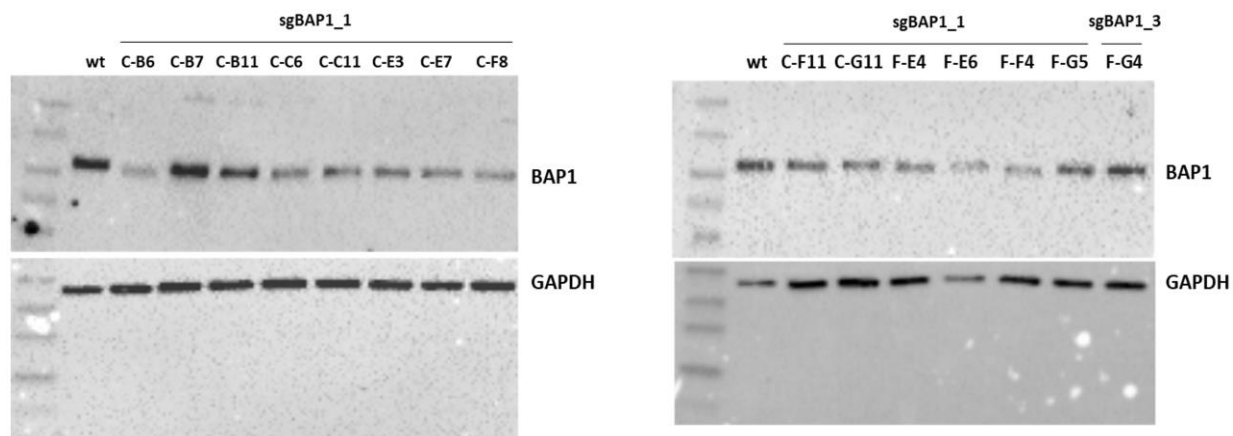


**Figure 42: Western blot results showing the BAP1 status of the FACS-sorted monoclonal MEL202 cells with were transduced with either sgBAP1\_1 or sgBAP1\_3.**

As a result of the incomplete knockout of BAP1 protein in the colonies obtained through the CRISPR/Cas9 strategy, we were prompted to explore an alternative method, specifically the siRNA-mediated knockdown of BAP1.

#### **4.3.2. BAP1 is knocked down via siRNA-mediated strategy**

After attempting to knock out the *BAP1* gene, we switched to a siRNA-mediated knockdown (KD) approach to achieve more effective suppression of BAP1 protein levels in MEL202 cells. Two siRNAs targeting *BAP1* were synthesized and transiently transfected into MEL202 cells, followed by a three-day incubation period. To ensure the reliability of our results, we independently repeated the KD experiment three times and each experiment yielded consistent results, as confirmed by Western blot analysis (Appendix **Figure 92** and Appendix **Figure 93**). We initially tested the efficiency of two siRNAs alongside a negative control siRNA. Also, we tested two different concentrations (30 pmol and 60 pmol) of the siRNAs to optimize the KD efficiency using the minimum amount of siRNA. As detailed in Appendix **Figure 92**, only the siRNA2 effectively targeted BAP1, leading to a significant reduction in BAP1 protein levels comparing the WT sample. The negative control siRNA showed no effect on BAP1 expression, confirming the specificity of the KD experiment.

Following the incubation, Western blot analysis was performed to assess the protein levels of BAP1. As shown in **Figure 43A**, the BAP1 protein levels were almost completely depleted in the siRNA-transfected cells compared to the wild-type controls. GAPDH was used as the loading control to ensure equal protein quantity loading.

To further validate the knockdown efficiency, RNA sequencing (RNA-seq) was conducted to measure the mRNA levels of BAP1. The results, shown in **Figure 43B**, indicated a massive reduction in BAP1 mRNA levels, with TPM values of the expression levels dropping from 99.7 in WT to 2.2 in the BAP1 KD sample.

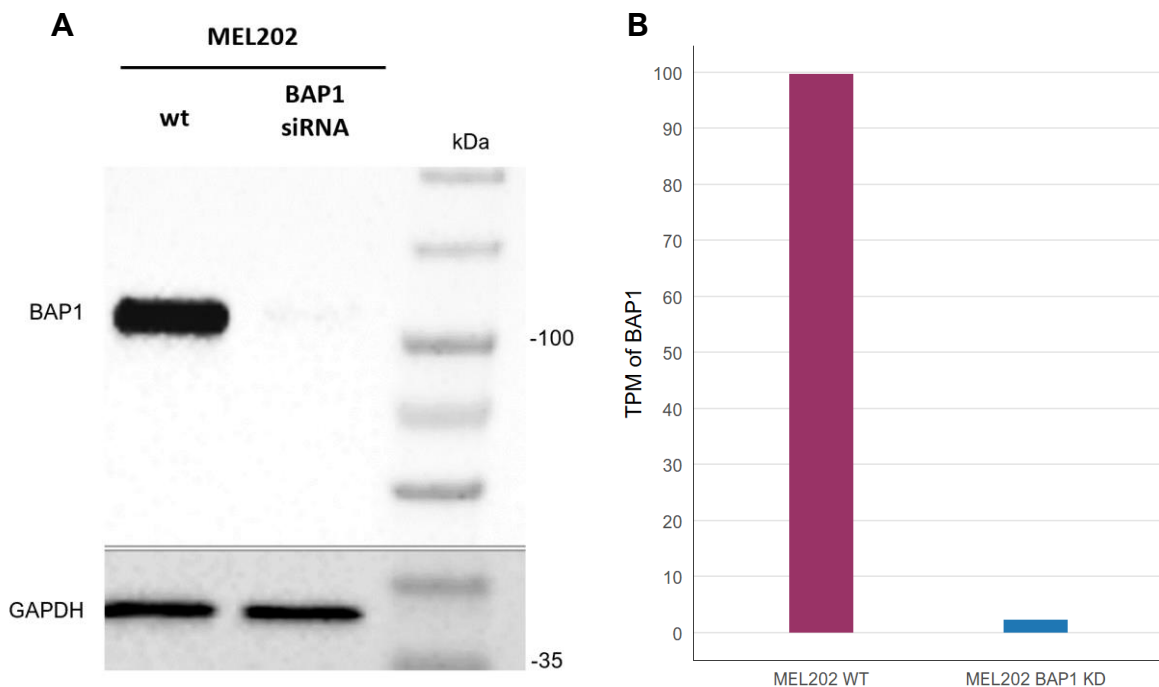


**Figure 43: Validation of the BAP1 knockdown experiment with MEL202 cells using (A) Western blot, (B) RNA-seq experiments.**

These findings confirm that the siRNA-mediated knockdown strategy effectively silenced BAP1 expression at both the protein and mRNA levels in MEL202 cells to further proceed with our experimental design in WT / BAP1 KD comparative way.

#### 4.4. Modification of Gene Expression Profiles upon BAP1 loss in MEL202 cells and UM tumors

To investigate the impact of BAP1 loss on the gene expression profiles, we performed RNA-seq experiments using deep-sequencing (aimed at least 60 million fragments/120 million paired-end reads per sample) on two MEL202 and one MEL202 BAP1 KD samples. To ensure reliable gene expression measurements, we filtered out genes whose expression values (TPM) were “0” in both MEL202 and BAP1 KD conditions. Additionally, we excluded genes that had less than 0.5 TPM ( $TPM < 0.5$ ) in both conditions, further refining the dataset to include only genes with sufficient expression levels for downstream analysis. After the rigorous filtering processes, we had a total of 12529 genes remaining for comparative analysis between MEL202 and BAP1 KD conditions in our cell culture system. Then, we identified differentially expressed genes (DEGs) using the edgeR package with the absolute log<sub>2</sub> fold change greater than 1 ( $\log_{2}FC > 1$  for the genes differentially upregulated and  $\log_{2}FC < -1$  for the genes differentially downregulated in the BAP1 KD condition).

As a result, after the knockdown of BAP1 in MEL202 cells, we found that 2784 genes were differentially expressed in total. From these DEGs, 1445 genes were upregulated and 1339 genes were downregulated in the MEL202 BAP1 KD condition as shown in **Table 27**.

**Table 27: Number of genes differentially expressed (upregulated and downregulated) when  $|\log_{2}FC| > 1$  after BAP1 loss in MEL202 cells.**

Upregulated Genes	Downregulated Genes
1445	1339

The overall range of log<sub>2</sub>FC values of the DEGs varied from +5.391 (*TXNIP* gene, TPM value of WT: 1.922, KD: 81.456) to -5.465 (*BAP1* gene, TPM value of WT: 99.750, KD: 2.239). We show the DEGs after BAP1 KD condition in MA plot, highlighting the upregulated genes in red and downregulated genes in blue in **Figure 44**.

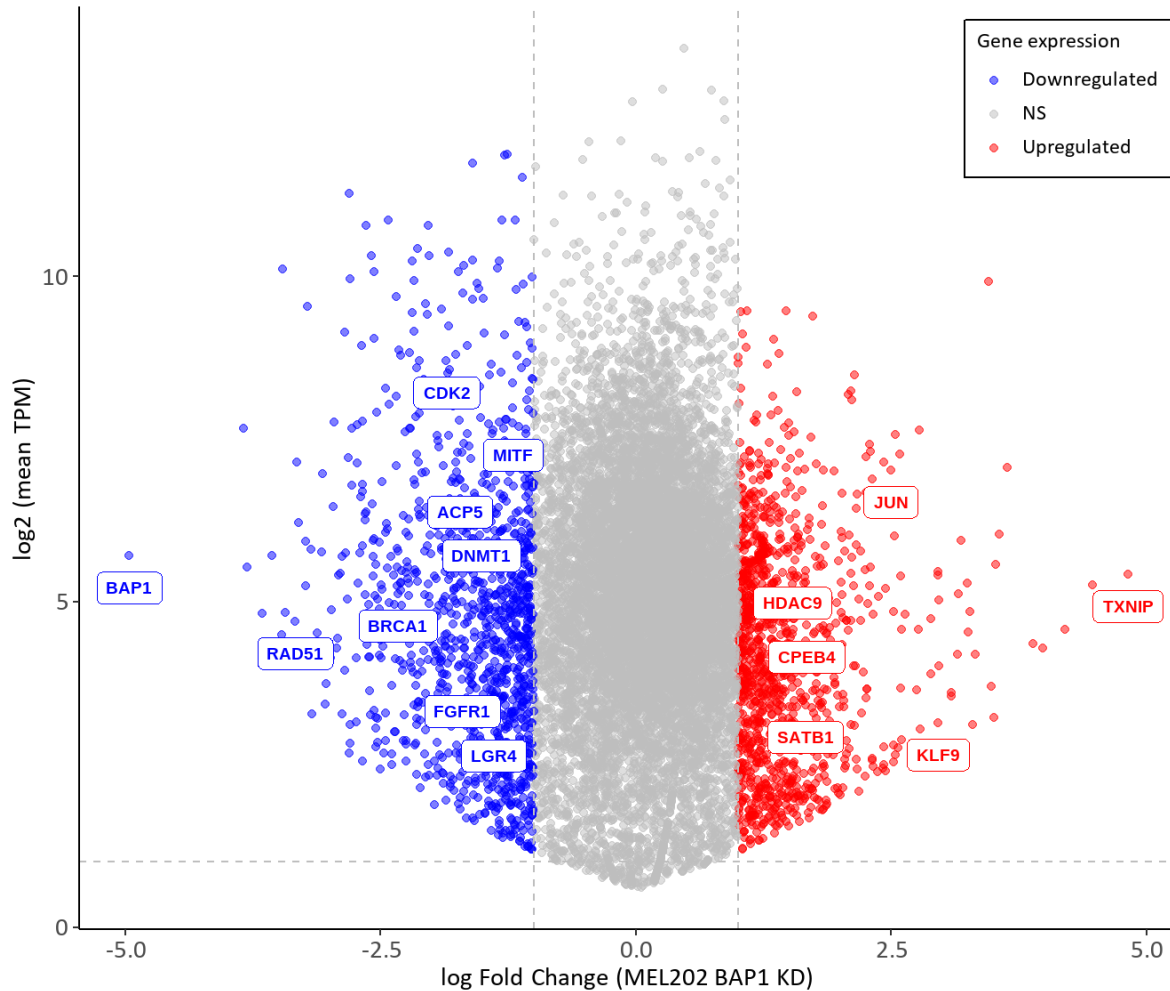


**Figure 44: MA plot showing the differentially ( $|\log\text{FC}| > 1$ ) upregulated (red) and downregulated (blue) genes upon BAP1 loss in MEL202 cells. NS: Non-significant. Vertical and horizontal gray lines show  $|\log\text{FC}|=1$ .**

Next, we compared these DEGs obtained from our MEL202 UM cell culture system with those identified in our uveal melanoma patient cohort. This UM patient cohort samples had been recruited by the Charité Comprehensive Cancer Center (Prof. Dr. med. Keilholz and Leyvraz) for the “Treat20 melanoma project” coordinated by our research group in a larger study (unpublished). Our lab performed WGS, WES, and bulk RNA-seq for this cohort. The somatic mutation profile of the patient cohort mainly showed a typical pattern with low tumor mutation burden and harboring mutually exclusive *GNAQ/GNA11* mutations. The cohort is composed of 41 metastatic UM cases recruited at relapse from 37 UM patients. 14 samples are Disomy 3 (D3) and BAP1 positive. 27 samples are



Monosomy 3 (M3) and BAP1 mutated. Three of the tumors are BAP1 WT of which, two of them carry *SF3B1* mutation.

We first set out to understand the biological consequences of BAP1 loss at the transcriptional level in the cell line. Thus, we compared the DEGs from the cell culture to the all upregulated / downregulated genes from data of the UM patient cohort. The result is summarized in **Table 28**.

**Table 28: Correlations of the DEGs from MEL202 / BAP1 KD cell condition and up / down regulated genes of the UM patient cohort.**

Up / down correlations of UM patient cohort \ DEGs of MEL202 cells	Differentially downregulated genes in MEL202 / BAP1 KD cells	Differentially upregulated genes in MEL202 / BAP1 KD cells
Upregulated genes in D3 / M3 patient cohort	646	702
Downregulated genes in D3 / M3 patient cohort	693	743

According to our results, 1445 differentially upregulated genes from the MEL202 BAP1 KD condition overlapped with 702 upregulated and 743 downregulated genes in the BAP1-deficient Monosomy 3 case (compared to Disomy 3). Also, 1339 differentially downregulated genes from MEL202 BAP1 KD overlapped with 646 upregulated and 693 downregulated genes in the Monosomy 3 condition.

We further refined our analysis by comparing the DEGs identified in the cell line model (MEL202 BAP1 KD) with only the DEGs observed in the patient cohort (D3 / M3).

This two-step comparison first focused on correlating gene expression changes between cell line and patient samples, followed by a direct overlap analysis to identify shared DEGs. As shown in **Figure 45**, the scatter plot illustrates how gene expression patterns change under BAP1 loss in both the cell line and patient cohorts.

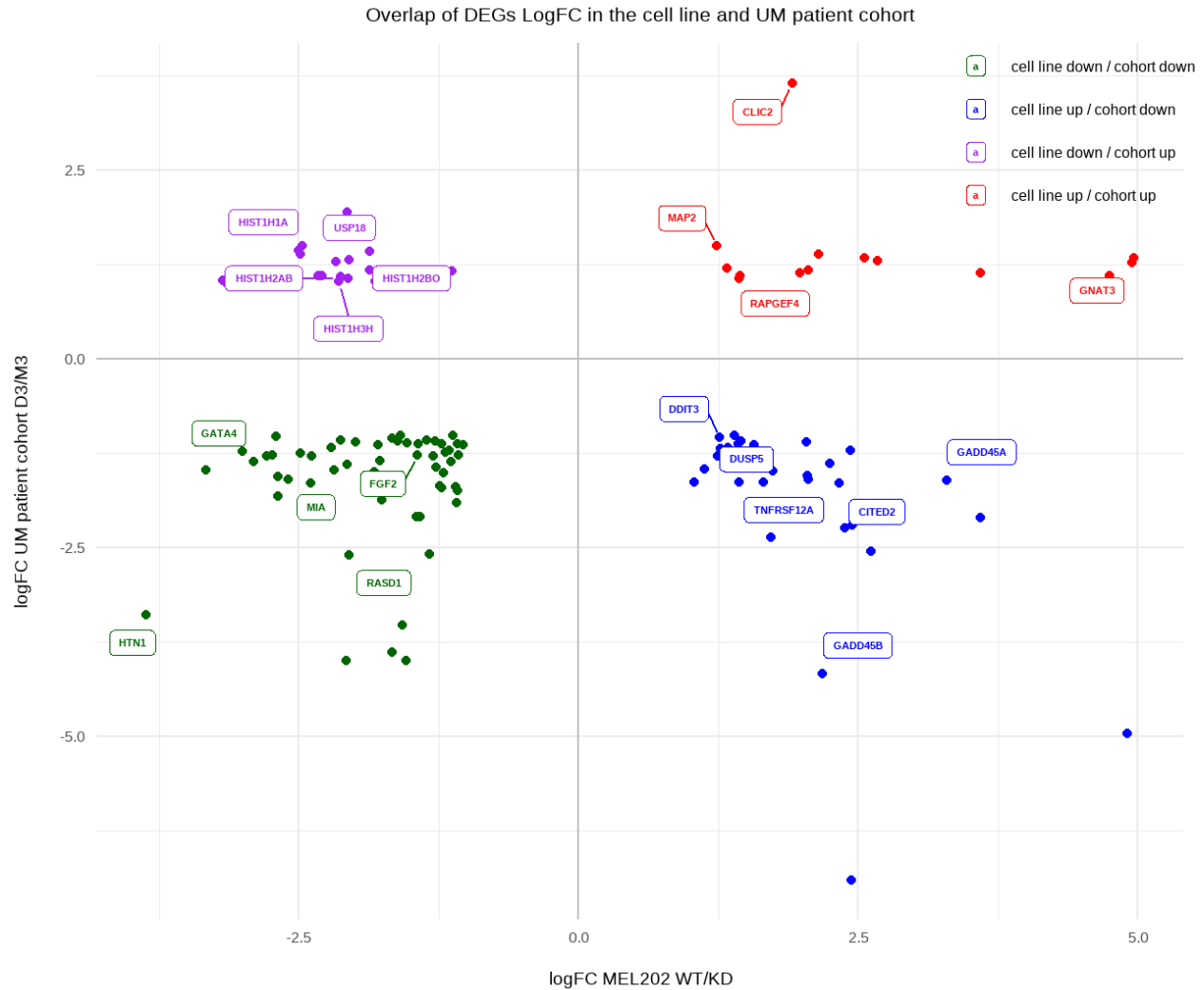


**Figure 45: Correlation of the DEGs between MEL202 / BAP1 KD conditions (X-axis) and D3 / M3 UM patient cohort (Y-axis).** Scatter plot shows the DEGs with  $|\logFC| > 1$ , commonly upregulated (top-right, red), commonly downregulated (bottom-left, green), upregulated in cell line but downregulated in the cohort (bottom-right, blue), and downregulated in cell line but upregulated in the cohort (top-left, purple).

This approach allowed us to categorize the overlapping DEGs into four distinct groups based on their expression patterns in both models. Specifically:

- 15 genes were upregulated in both the cell line and patient cohort (**Figure 45**, top-right quadrant).
- 55 genes were downregulated in both the cell line and patient cohort (**Figure 45**, bottom-left quadrant).

- 33 genes were upregulated in the cell line but downregulated in the patient cohort (**Figure 45**, bottom-right quadrant).
- 23 genes were downregulated in the cell line but upregulated in the patient cohort (**Figure 45**, top-left quadrant).

This categorization highlights the varying effects of BAP1 loss on gene expression between the cell line and patient samples, providing deeper insights into the transcriptional reprogramming associated with BAP1 deficiency in UM.

Commonly downregulated genes from **Figure 45** (bottom-left) include *FGF2*, *GATA4*, *MIA*, *RASD1*, *HTN1* each of which has been previously reported to play critical roles in key biological processes such as growth signaling (*FGF2*; (Wang et al., 2022)), cell differentiation (*GATA4*; (Gong et al., 2018)) and inhibition of melanoma progression (*MIA*; (Sasahira et al., 2018)). Furthermore, *RASD1* is implicated in MAPK signaling and stress response pathways (Gao et al., 2017), while *HTN1* is involved in cell migration and tissue healing (Torres et al., 2018). Their respective expression values are shown in **Figure 46**.

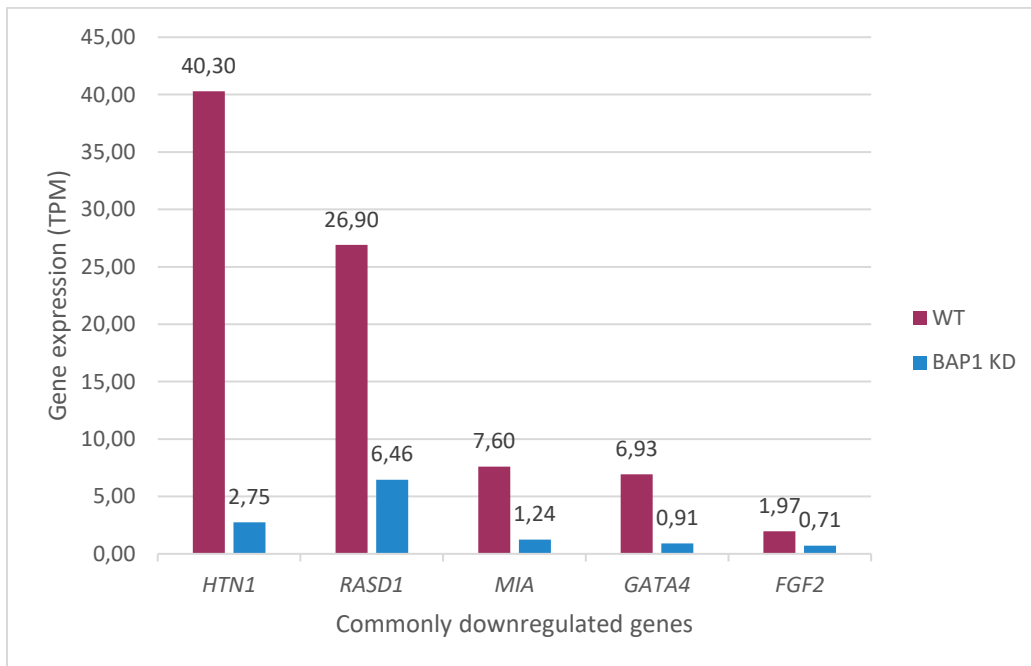


**Figure 46: Expression (TPM) differences of *FGF2*, *GATA4*, *MIA*, *RASD1* and *HTN1* genes from MEL202 / BAP1 KD conditions.** These genes are commonly downregulated DEGs from the cell line (WT / KD) and the patient cohort (D3 / M3).

In contrast, commonly upregulated genes from **Figure 45** (top-right) include *RAPGEF4*, *MAP2*, *GNAT3*, and *CLIC2*. *RAPGEF4* is involved in cAMP signaling, which is known to regulate cell proliferation and differentiation (Sugawara et al., 2016). *MAP2* is a structural protein linked to cytoskeletal stability and cell motility (Dehmelt and Halpain, 2005). *GNAT3* and *CLIC2* are implicated in signal transduction and ion transport, processes that may contribute to altered cellular homeostasis in tumor cells (Hoffman et al., 2021, Ozaki et al., 2022). These expression changes suggest that BAP1 loss may trigger signaling pathways and structural reprogramming in UM, potentially influencing tumor progression. **Figure 47** shows their expression values.

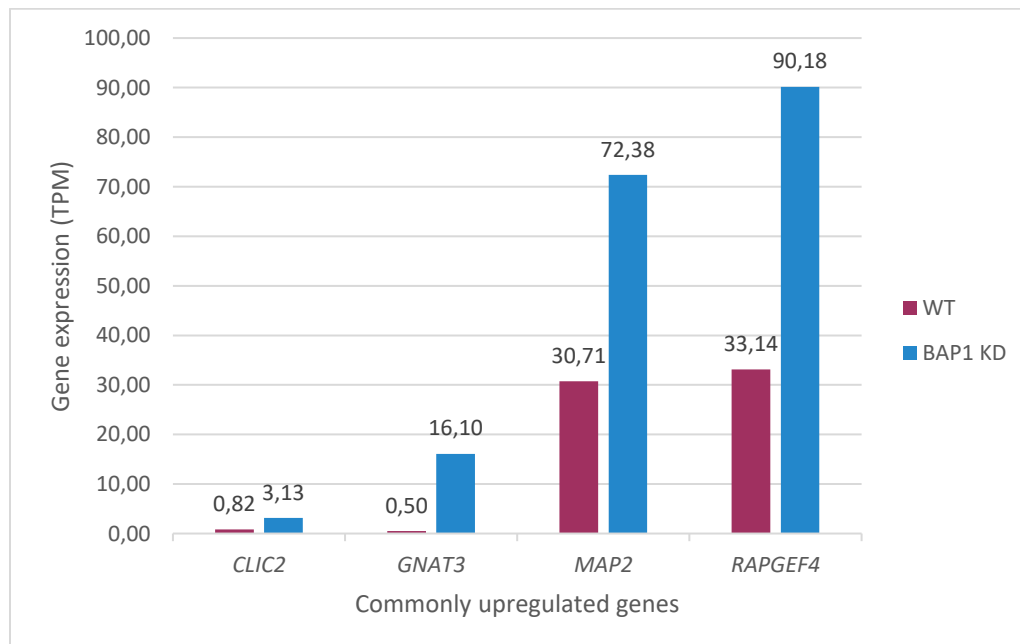


**Figure 47: Expression (TPM) differences of *RAPGEF4*, *MAP2*, *GNAT3* and *CLIC2* genes from MEL202 WT / KD conditions.** These genes are commonly upregulated DEGs from the cell line (WT / KD) and the patient cohort (D3 / M3).

These results highlight the correlated gene expression changes observed in MEL202 BAP1 KD cells and the BAP1-negative (M3) patient cohort. The common downregulation of genes like *FGF2* and *MIA* suggests that the loss of BAP1 compromises critical growth-inhibitory and differentiation pathways. Similarly, the upregulation of genes like *RAPGEF4* and *MAP2* indicates a shift towards tumor-promoting signaling cascades and cellular motility.

As a summary, loss of BAP1 leads to a slightly higher number of differentially upregulated genes (1445) compared to differentially downregulated genes (1339) in the MEL202 UM cells. The gene expression changes through TPM values in both settings strengthens the hypothesis that BAP1 loss play roles in UM progression by dysregulating critical signaling and structural pathways. These findings provide a foundation for future exploration of the pathways associated with these DEGs to further understand BAP1's role in UM pathogenesis.

#### **4.5. Pathway enrichment analysis of the differentially expressed genes and integration with BAP1-binding sites**

Following the RNA-seq analysis of MEL202 and BAP1 KD cells, we identified lists of differentially upregulated and downregulated genes from these conditions. To further understand the biological processes and pathways affected by BAP1 loss, we utilized ShinyGO (version 0.77) (Ge et al., 2020) graphical gene-set enrichment tool. The analyses were performed with a false discovery rate (FDR) cutoff set at 0.05 to ensure the robustness of our findings.

##### **4.5.1. Loss of BAP1 depleted DNA replication and cell cycle-related processes in MEL202 BAP1 KD cells**

We performed the pathway enrichment analysis to explore the biological processes most affected by BAP1 loss in MEL202 cells focusing on the 1339 differentially downregulated genes identified through the RNA-seq analysis. Our pathway enrichment analysis included the key Gene Ontology (GO) terms for “Biological processes”, “Molecular functions”, and “Cellular components” affected by the loss of BAP1. **Figure 48**, **Figure 49**, and **Figure 50** depict the fold enrichment of the downregulated gene sets (in BAP1 KD) across these categories.

In **Figure 48**, we show that the most significantly affected biological processes are associated with cell cycle regulation, DNA replication and chromosome segregation. The downregulation of genes involved in DNA replication are compatible with the BAP1's role

in maintaining proper cell proliferation and genomic integrity. Specifically, key genes governing the initiation and elongation of DNA replication, such as those encoding components of the MCM complex and DNA polymerase, were among the downregulated genes.

The involvement of BAP1 in the cell cycle is further underscored by the downregulation of genes involved in the G1/S transition and mitotic checkpoints. These findings align with BAP1's known function as a tumor suppressor and its role in safeguarding against inappropriate cell division. The loss of BAP1 disrupts cell cycle checkpoints, potentially leading to chromosomal instability and increased risk of malignancy particularly in UM.

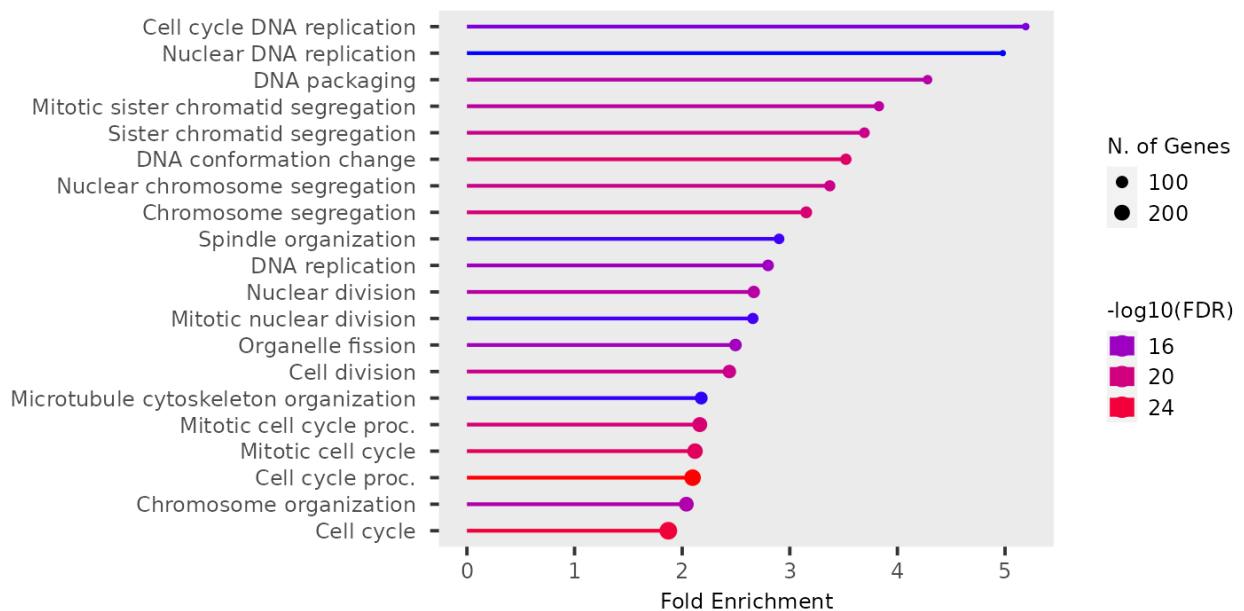


**Figure 48: Fold enrichment analysis of the genes in pathways related to GO Biological process.** The plot shows the enriched pathways from the differentially downregulated genes from the MEL202 BAP1 KD condition.

Molecular function enrichment analysis in **Figure 49** reveals a significant depletion of genes involved in DNA-binding, helicase activity, and chromatin binding. These molecular activities are crucial for orchestrating the replication and repair processes within the cell. BAP1's role in chromatin modulation could explain why the loss of this gene causes a widespread downregulation of genes that interact with the DNA replication machinery.

The depletion of helicase-related genes suggests that the unwinding of DNA necessary for replication and transcription is impaired, further supporting the notion that BAP1 KD leads to profound replication stress.

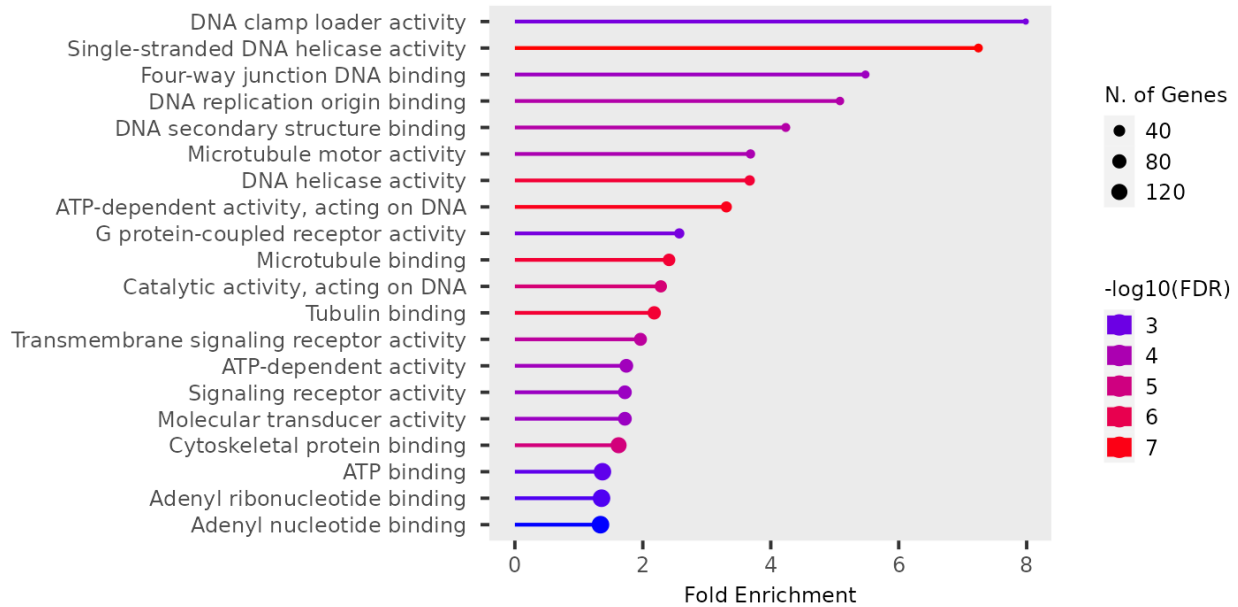


**Figure 49: Fold enrichment analysis of the genes in pathways related to GO Molecular function.** The plot shows the enriched pathways from the differentially downregulated genes from the MEL202 BAP1 KD condition.

In the cellular component enrichment in **Figure 50**, there is a significant depletion in genes associated with chromosomal regions, replication forks, and nucleoplasmic compartments. These findings reinforce the critical role of BAP1 in maintaining the structure and function of chromatin during replication. Loss of BAP1 likely disrupts the accessibility and proper organization of the replication machinery, leading to a cascade of transcriptional downregulation across multiple pathways.

The depletion of DNA replication and cell cycle-related processes can be attributed to BAP1's dual role as a deubiquitinase and chromatin remodeler. BAP1 is involved in regulating chromatin dynamics, particularly at replication origins and key checkpoint genes. The downregulation of replication-associated genes may stem from BAP1's loss, leading to the accumulation of DNA damage, genomic instability, and replication stress, hallmarks of cancer progression (Han et al., 2021).

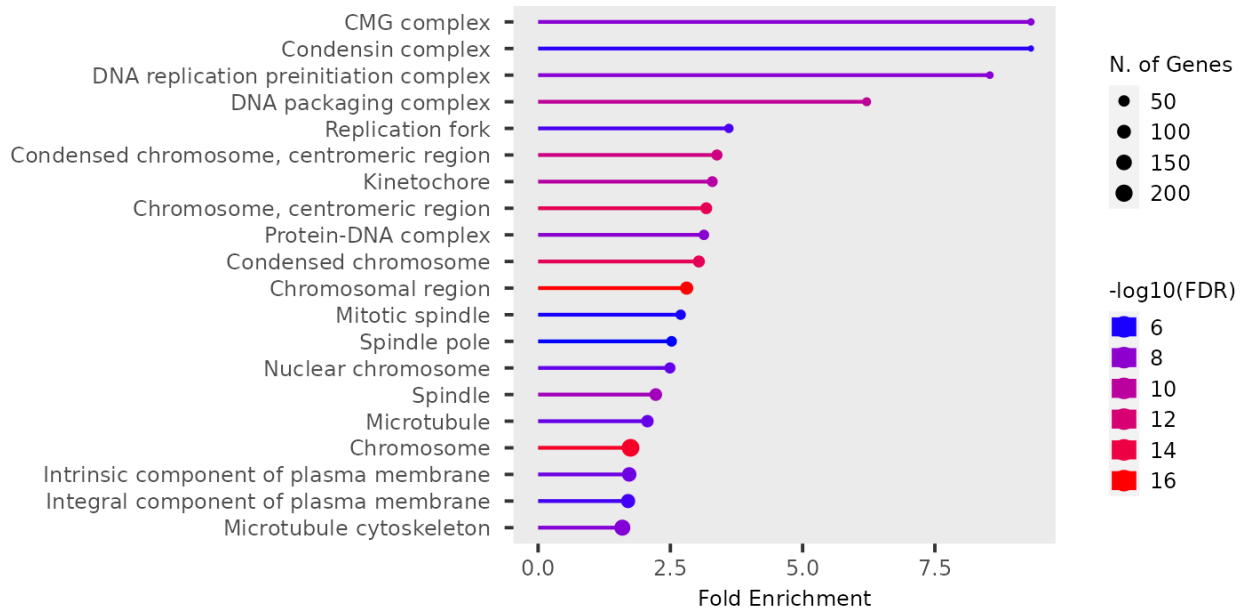


**Figure 50: Fold enrichment analysis of the genes in pathways related to GO Cellular component.** The plot shows the enriched pathways from the differentially downregulated genes from the MEL202 BAP1 KD condition.

In conclusion, our RNA-seq results revealed a significant downregulation of genes involved in cell cycle regulation and DNA replication upon BAP1 knockdown in the MEL202 UM cells.

Additionally, we measured cell confluences over a 72-hour incubation period counting the living cells with Trypan blue dye in both BAP1 KD and control conditions. As shown in **Figure 51**, all experimental conditions started with an initial seeding density of  $5 \times 10^5$  cells. After 72 hours, MEL202 control cells (Control 1 and Control 2) exhibited an increase in cell number with final cell counts of  $1.56 \times 10^6$  and  $1.55 \times 10^6$ , representing approximately a 3-fold increase in cell number. Similarly, MEL202 cells transfected with a negative control siRNA reached a final cell count of  $1.3 \times 10^6$ , showing an approximately 2.6-fold increase in proliferation. In contrast, cells transfected with siRNAs targeting BAP1 (siRNA-BAP1) demonstrated markedly reduced proliferation rates. The final cell counts for siRNA-BAP1 transfected cells were  $8.8 \times 10^5$  (Replicate 1) and  $9.2 \times 10^5$  (Replicate 2), corresponding to only a 1.6- to 1.8-fold increase in cell number. This reduction in cell proliferation upon BAP1 KD aligns with the result of our RNA-seq data where cell cycle-related genes were significantly downregulated. The diminished growth rate observed in BAP1-deficient cells



validates that BAP1 plays a crucial role in regulating cell cycle progression and maintaining normal rates of cell division. These findings further support the hypothesis that BAP1 loss leads to impaired cell cycle regulation and contributes to the reduced proliferative capacity.

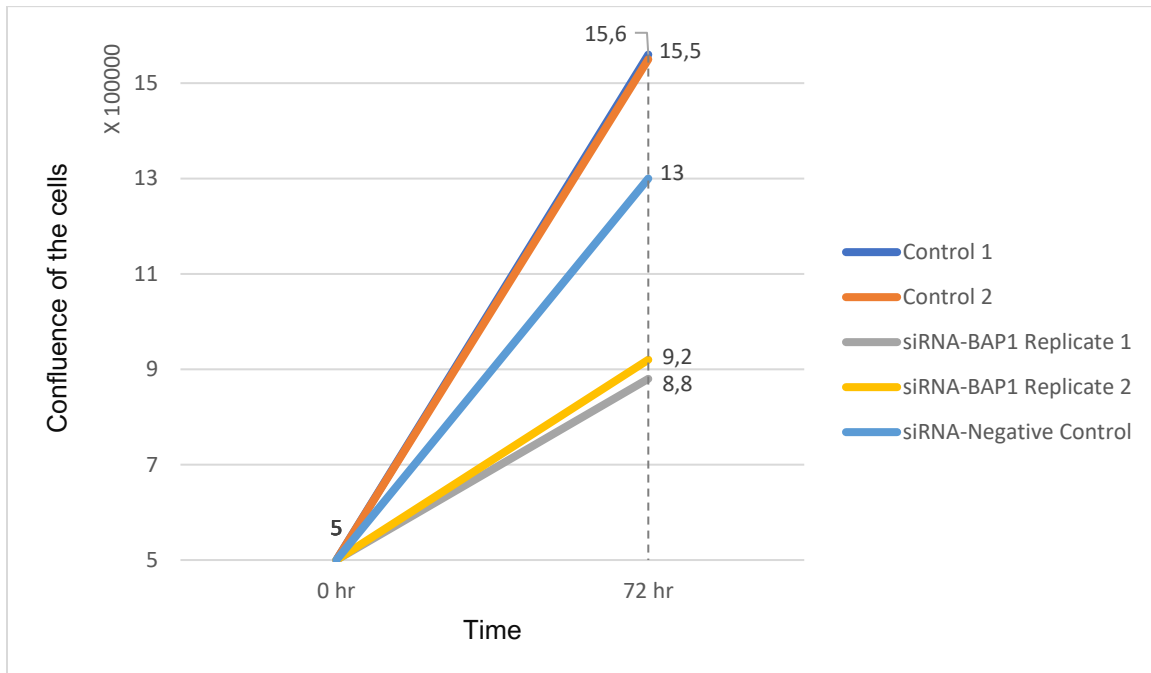


**Figure 51: Effect of BAP1 knockdown on cell proliferation in MEL202 cells.** Cell confluence was measured at 0 and 72 hours after transfection with siRNAs targeting BAP1 (siRNA-BAP Replicate 1 and 2), negative control siRNA and control MEL202 cells (Control 1 and Control 2).

#### **4.5.2. Transcription factor activity, DNA-binding, and cell-adhesion-related processes are enriched upon BAP1 loss**

In this section, we further investigated the consequences of BAP1 loss by focusing on 1445 differentially upregulated genes identified in the MEL202 BAP1 KD cells. The pathway enrichment analyses were conducted through the key Gene Ontology (GO) terms for “Biological processes”, “Molecular functions”, and “Cellular components” using the differentially upregulated genes to identify the most significantly impacted biological programs by the loss of BAP1.

As shown in **Figure 52**, the most prominently enriched biological processes upon BAP1 loss include cell-cell adhesion, extracellular matrix (ECM) organization, and extracellular structure organization.

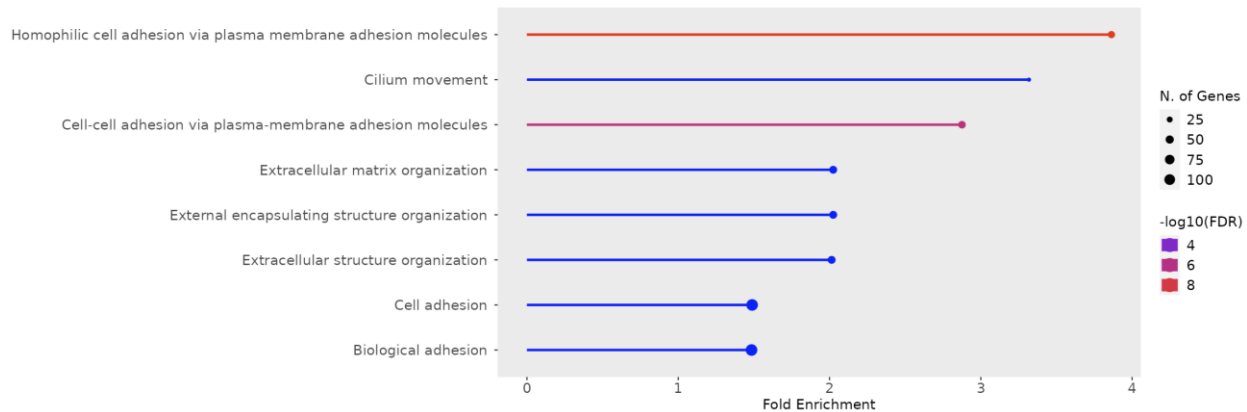


**Figure 52: Fold enrichment analysis of the genes in pathways related to GO Biological process.** The plot shows the enriched pathways from the differentially upregulated genes from the MEL202 BAP1 KD condition.

These findings indicate that BAP1 depletion leads to alterations in the cellular architecture and the structural integrity of the extracellular microenvironment. As BAP1 is a tumor suppressor, its loss likely disrupts cell adhesion dynamics which is consistent with observations in metastatic cancer where altered ECM organization plays a key role in promoting cell detachment, migration and invasion. These processes critically point in the development of aggressivity in cancer in particular UM in which metastasis is a major concern.

The pathway enrichment analysis for molecular functions in **Figure 53** revealed significant enrichment of genes associated with transcriptional regulatory mechanisms, particularly those related to transcription cis-regulatory region binding, sequence-specific DNA binding, and RNA polymerase II-specific DNA binding. This result suggests that the upregulated genes are involved in transcriptional activation, likely compensating for the disruption caused by the loss of BAP1. Furthermore, the upregulation of DNA-binding transcription factors indicates a complex reprogramming of gene expression wherein cells attempt to adapt to the chromatin structural changes induced by BAP1 loss.

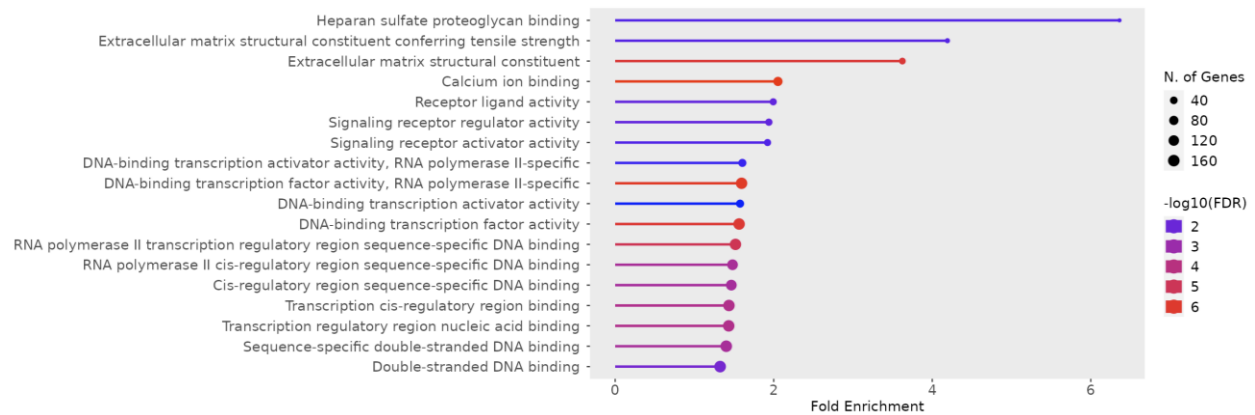


**Figure 53: Fold enrichment analysis of the genes in pathways related to GO Molecular function.** The plot shows the enriched pathways from the differentially upregulated genes from the MEL202 BAP1 KD condition.

It can be inferred from the result that, BAP1 has functions in the regulation of the transcriptional control, with its absence leading to dysregulation in transcriptional machinery especially in RNA polymerase II-mediated transcription. This could explain why BAP1 KD cells exhibit changes in transcription factor activity consistent with BAP1's known role in gene regulation.

**Figure 54** shows the cellular component-related enrichment in the transcription factor AP-1 complex and extracellular matrix-related components. This reinforces the notion that BAP1 depletion disrupts both gene regulation networks and cellular architecture. The AP-1 complex is a well-known regulator of cell transformation and differentiation often being dysregulated in cancer promoting tumor progression, aggressiveness and resistance to treatments (Bejjani et al., 2019). Its upregulation may serve as a compensatory mechanism in the absence of BAP1, promoting cell survival and proliferation in a tumor context. Additionally, the altered extracellular matrix organization supports the invasive and aggressive nature of BAP1-deficient UM cases. Enrichment of the transcription factor activity, DNA-binding, and cell-adhesion-related processes upon BAP1 loss suggests that BAP1 acts as an important regulator of transcription and cellular structure. Our results indicate that in the absence of BAP1, transcription factors, and DNA-binding proteins are upregulated as a compensatory mechanism, likely to maintain transcriptional homeostasis despite disruptions in chromatin organization. Additionally, the observed changes in cell

adhesion and ECM organization reflect the potential oncogenic transformation triggered by BAP1 loss, where altered cell-matrix interactions may be related to tumor progression and metastasis. These findings are relevant to the understanding of uveal melanoma pathogenesis, as BAP1-deficient tumors are often characterized by high metastatic risk.

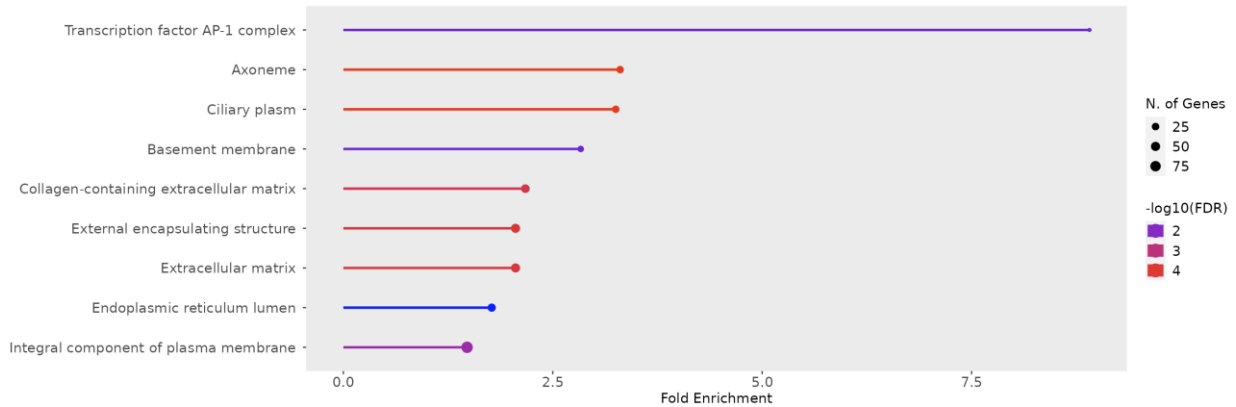


**Figure 54: Fold enrichment analysis of the genes in pathways related to GO Cellular component.** The plot shows the enriched pathways from the differentially upregulated genes from the MEL202 BAP1 KD condition.

#### 4.5.3. Integration of BAP1-binding sites with altered gene expression profiles in MEL202 WT and BAP1-KD cells

To better understand how BAP1 influences the gene expression, we conducted a comprehensive analysis integrating BAP1-binding sites from our ChIP-seq data obtained in MEL202 cells with the RNA-seq data from both MEL202 and MEL202 BAP1 KD conditions. This allowed us to pinpoint the genes that are not only bound by BAP1 but also exhibit differential expression upon BAP1 KD.

For this purpose, we used a filtering strategy as represented in the Sankey diagram in **Figure 55**. The total gene pool which is comprising 12529 genes is firstly split into the DEGs (2784 genes) and non-DEGs (9745 genes). Among the DEGs, we applied the further distinction between upregulated (1445 genes) and downregulated genes (1339 genes) following BAP1 knockdown.

Within the upregulated and downregulated gene sets, we integrated the BAP1-binding profile. Of the 1445 differentially upregulated genes, 295 (20%) were found to be bound

by BAP1, while the remaining 1150 showed no BAP1 binding. Conversely, out of the 1339 downregulated genes, 142 (10%) were associated with BAP1 binding, whereas 1197 were not bound by BAP1. This analysis indicates a stronger association of BAP1 binding with the upregulated gene set. The non-DEG category further shows that 2263 genes are BAP1-bound but not differentially expressed, suggesting BAP1's presence in regions without immediate transcriptional changes. Meanwhile, 7482 non-DEGs do not exhibit BAP1 binding. This comprehensive filtering highlights the subset of DEGs directly impacted by BAP1 binding, providing insights into how BAP1 loss leads to both transcriptional activation and repression possibly influencing the gene expression in UM.

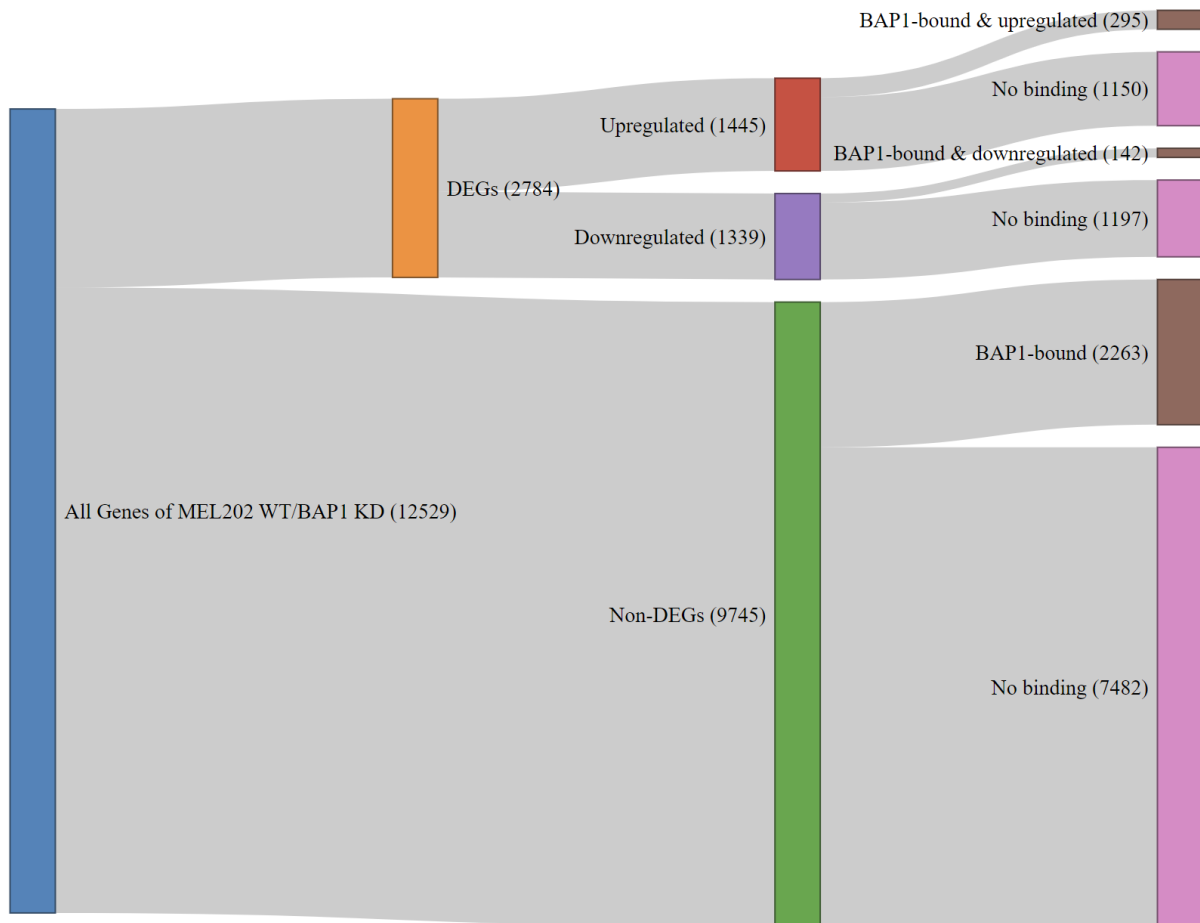


**Figure 55: Sankey diagram shows our filtering strategy for the BAP1-bound DEGs of MEL202 BAP1 WT / BAP1 KD condition.** 295 BAP1-bound differentially upregulated and 142 BAP1-bound differentially downregulated genes are detected.

Next, we focused on the BAP1-bound DEGs from our analysis as presented in the scatter plot in **Figure 56**. Genes such as *HDAC9*, *MBD5*, *MDM2*, and *SOCS2* were among the significantly ( $|\logFC|>1$ ) upregulated genes following BAP1 loss. These genes are involved in a variety of cellular processes, including chromatin remodeling (*HDAC9*), transcriptional regulation (*MDM2*), and cytokine signaling (*SOCS2*). In contrast, genes such as *PMEL*, *DNMT1*, *BRCA1*, *MCM4*, and *FGFR1* were significantly ( $|\logFC|>1$ ) downregulated in the BAP1 KD condition. The downregulation of *DNMT1*, *BRCA1* and *MCM4* is particularly important, because these genes are involved in DNA methylation, repair and replication.

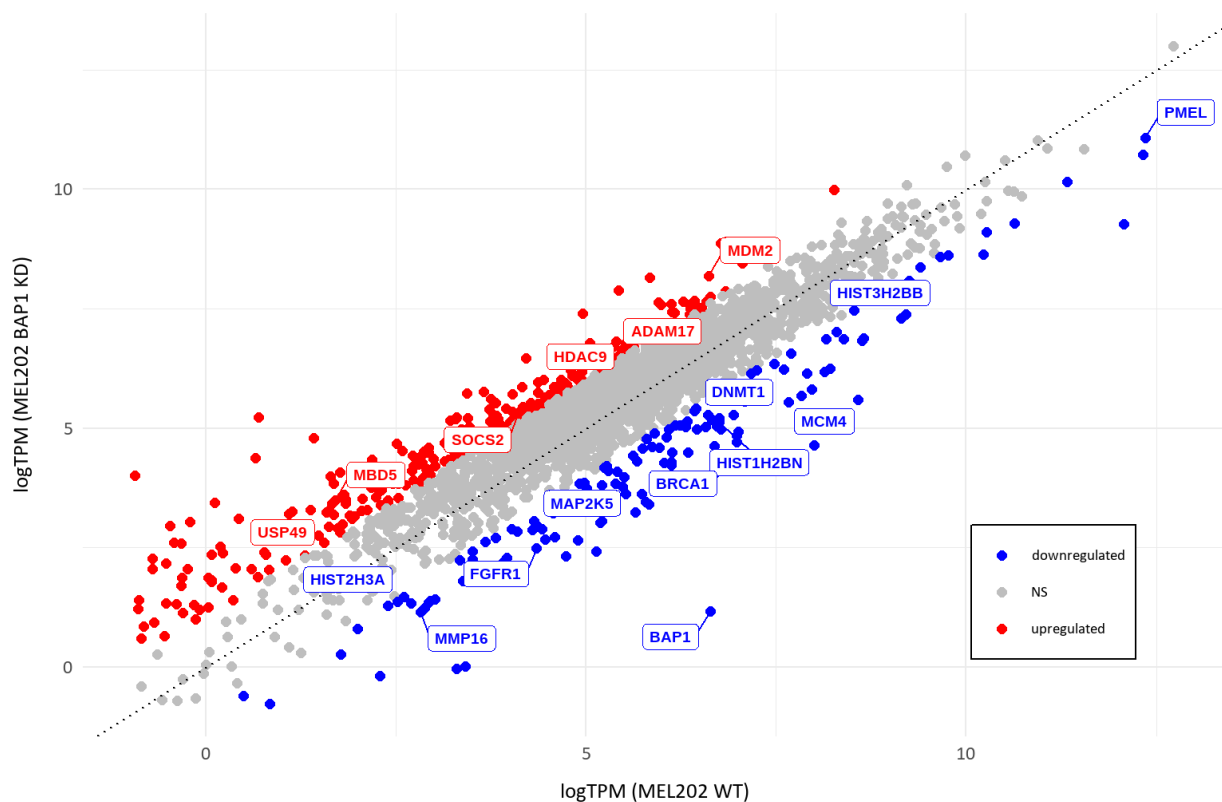


**Figure 56: Scatter plot shows the BAP1-bound DEGs after BAP1 loss in MEL202 cells.** BAP1-bound differentially upregulated genes are shown in red, and BAP1-bound differentially downregulated genes are shown in blue.  $|\logFC|>1$ .

The integration of these findings with the gene expression profiles highlights the crucial role BAP1 plays in maintaining genomic stability and transcriptional regulation. The upregulation or downregulation of BAP1-bound genes in the BAP1 knockdown condition suggests that these genes are actively regulated by the presence or absence of BAP1.

#### 4.5.4. DNA replication and repair pathways of BAP1-bound genes are suppressed upon BAP1 loss

To further elucidate the direct regulatory roles of BAP1 in gene expression of UM cells, we performed the pathway enrichment analyses specifically on the 142 BAP1-bound and differentially downregulated genes in MEL202 cells. This subset of genes provided insight into how BAP1 affects critical cellular processes, particularly those related to DNA replication, repair, maintaining genomic integrity and proper cell cycle progression.

We specifically focused on GO terms for molecular function in the enrichment analysis as shown in **Figure 57**. The enrichment analysis revealed a reduction in the molecular functions associated with DNA helicase activity, DNA polymerase activity, and DNA replication origin binding.

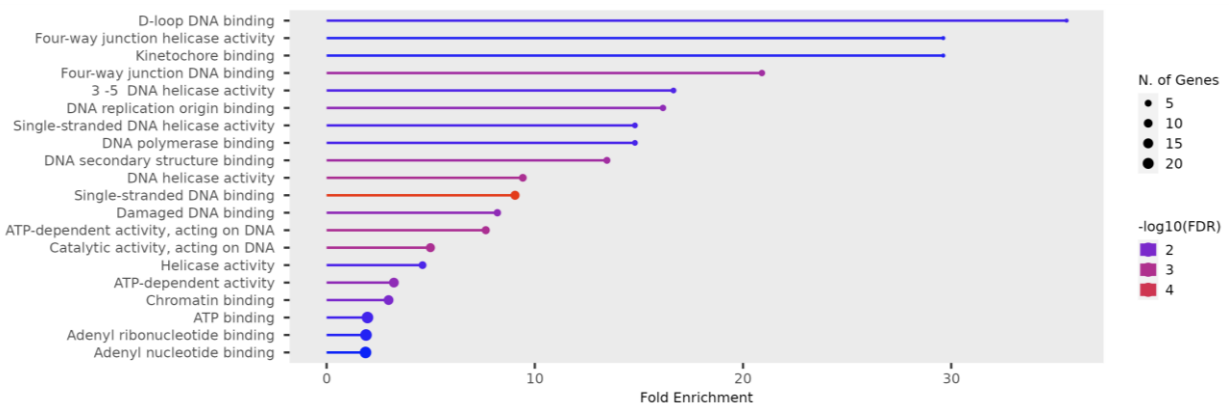


**Figure 57: GO Molecular function pathway enrichment analysis of the differentially downregulated genes (which were annotated with BAP1-binding in MEL202 WT condition).** Downregulated genes are obtained after BAP1 KD.

These findings indicate that BAP1 is involved by binding in the transcriptional regulation of genes critical for DNA unwinding and replication. DNA helicases and polymerases play a pivotal role in unwinding the double helix during replication and facilitating the accurate synthesis of new DNA strands. The depletion of these molecular functions in BAP1 KD cells could lead to replication stress, which is known to contribute to the accumulation of DNA damage and genomic instability in cancer cells. This depletion of replication-related genes supports the hypothesis that BAP1 loss disrupts the integrity of the DNA replication machinery, potentially leading to errors during cell division. Such errors could serve as a

driver of tumor progression and metastasis in the context of UM showing BAP1 mutations are commonly associated with poor outcomes and increased metastatic risk.

To better understand the broader implications of BAP1's regulatory role, a network analysis was performed on the BAP1-bound differentially downregulated genes using ShinyGO (version 0.77) as shown in **Figure 58**.

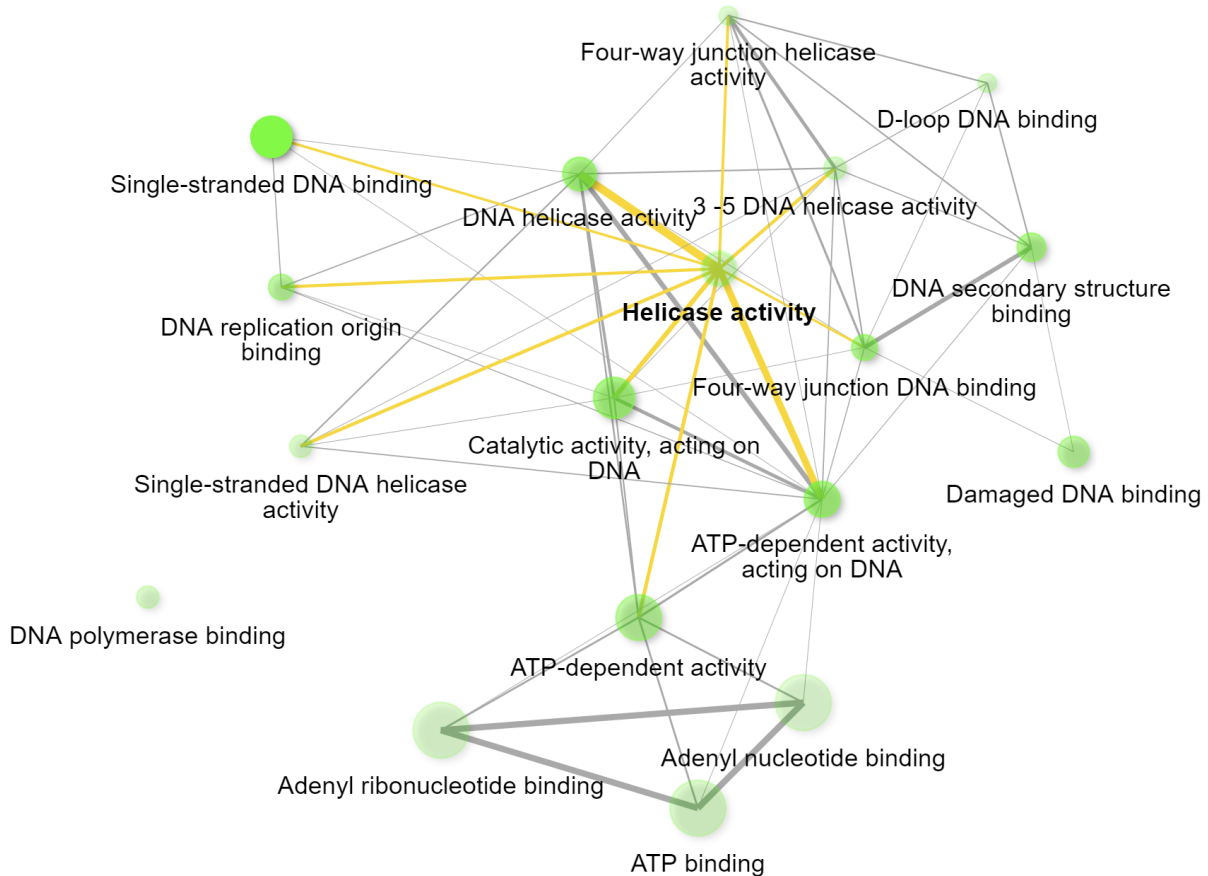


**Figure 58: Network of the enriched gene clusters (annotated with BAP1-binding in MEL202 WT condition) downregulated after BAP1 loss.** Edge cutoff: 0.3.

This analysis demonstrated that the downregulated pathways were not isolated but instead part of a highly interconnected network of gene clusters. Pathways related to chromatin binding, DNA helicase activity, and replication fork protection were strongly interconnected, suggesting a coordinated regulatory mechanism under BAP1's control.

The depletion of chromatin binding-related functions is particularly important because it indicates that BAP1 is essential for maintaining an accessible and functional chromatin



environment conducive to efficient replication and repair. Chromatin remodeling is a critical process for ensuring that the replication machinery can access DNA during the S phase of the cell cycle. Thus, BAP1's role in regulating chromatin accessibility at replication origins may be crucial for preventing replication errors and the subsequent accumulation of mutations. The suppression of DNA replication and repair pathways upon BAP1 loss highlights the tumor suppressor's central role in maintaining genomic stability. BAP1 binds to the promoters of key genes involved in these pathways, and its depletion disrupts their normal expression. This likely leads to impaired replication fork progression, an increase in replication stress, and a failure to efficiently repair DNA damage, all of which are drivers of tumorigenesis.

Given BAP1's known deubiquitinase activity and its role in chromatin remodeling, its loss likely causes epigenetic dysregulation, further compounding the defects in DNA replication and repair. This combination of factors may explain the aggressive nature of BAP1-deficient tumors, which are characterized by high rates of genomic instability and increased metastatic potential.

In conclusion, the loss of BAP1 significantly suppresses critical pathways related to DNA replication and repair, leading to profound disruptions in genomic integrity. These findings highlight the importance of BAP1 in preventing replication stress and maintaining the fidelity of DNA replication, offering new insights into the mechanisms by which BAP1 loss promotes tumor progression in UM.

#### **4.5.5. BAP1 loss upregulates BAP1-bound genes related TF activity, cis-regulation, DNA-binding of transcription factors, and RNA polymerase II**

To further understand the direct transcriptional consequences of BAP1 loss, we conducted the pathway enrichment analysis using GO terms specifically for molecular functions on the 295 differentially upregulated genes that are bound by BAP1 in MEL202 cells. These genes exhibited increased expression levels upon BAP1 KD, suggesting that the loss of BAP1 leads to a de-repression of these transcriptional regulatory pathways.

Our GO pathway enrichment analysis molecular function terms is represented in **Figure 59**. The analysis revealed significant enrichment ( $|\log_{2}FC| > 1$ ) in pathways related to DNA-binding transcription factor activity, RNA polymerase II-specific DNA binding, and transcription regulatory region binding. These findings indicate that BAP1 plays a central role in modulating transcriptional repression at key regulatory sites, such as transcription factor binding regions. Loss of BAP1 disrupts this regulation, resulting in the activation of genes that control transcriptional processes. The upregulation of transcription factors and other DNA-binding proteins suggests a compensatory mechanism in response to the chromatin alterations caused by BAP1 depletion.

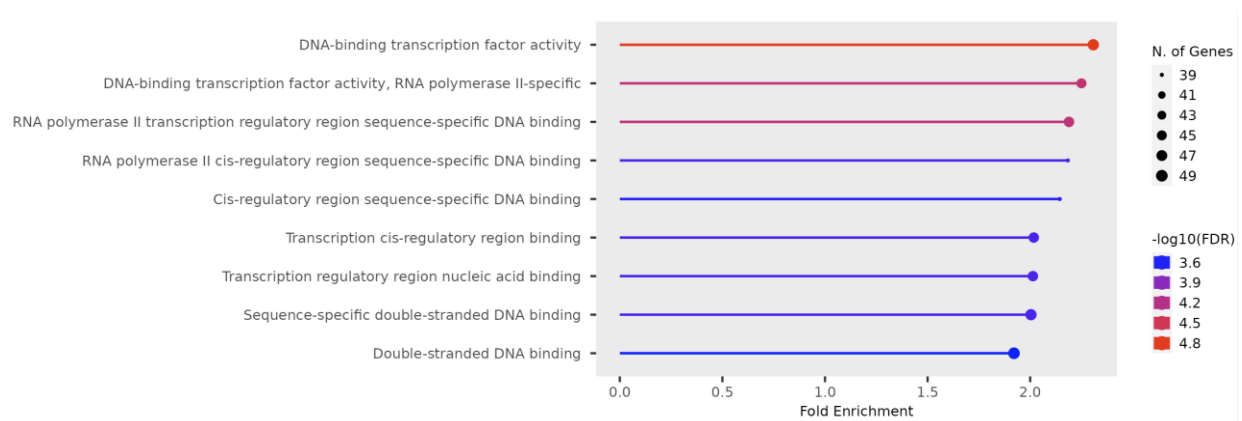


**Figure 59: GO Molecular function pathway enrichment analysis of the differentially upregulated genes (which were annotated with BAP1-binding in MEL202 WT condition).** Upregulated genes are obtained after BAP1 KD.

Additionally, the enrichment in RNA polymerase II binding activity suggests that the loss of BAP1 influences transcription at the level of RNA synthesis, leading to increased RNA polymerase recruitment and activity at previously repressed loci. This is consistent with BAP1's known role as a tumor suppressor that interacts with chromatin remodelers to maintain transcriptional repression in the cells.

A network analysis (**Figure 60**) of these enriched gene clusters was performed to visualize the relationships between the upregulated transcriptional regulatory pathways. This network highlights the significant interconnectedness between transcription factor activity,

cis-regulation, and DNA-binding functions, reinforcing the idea that BAP1 plays a crucial role in orchestrating transcriptional repression at multiple levels.

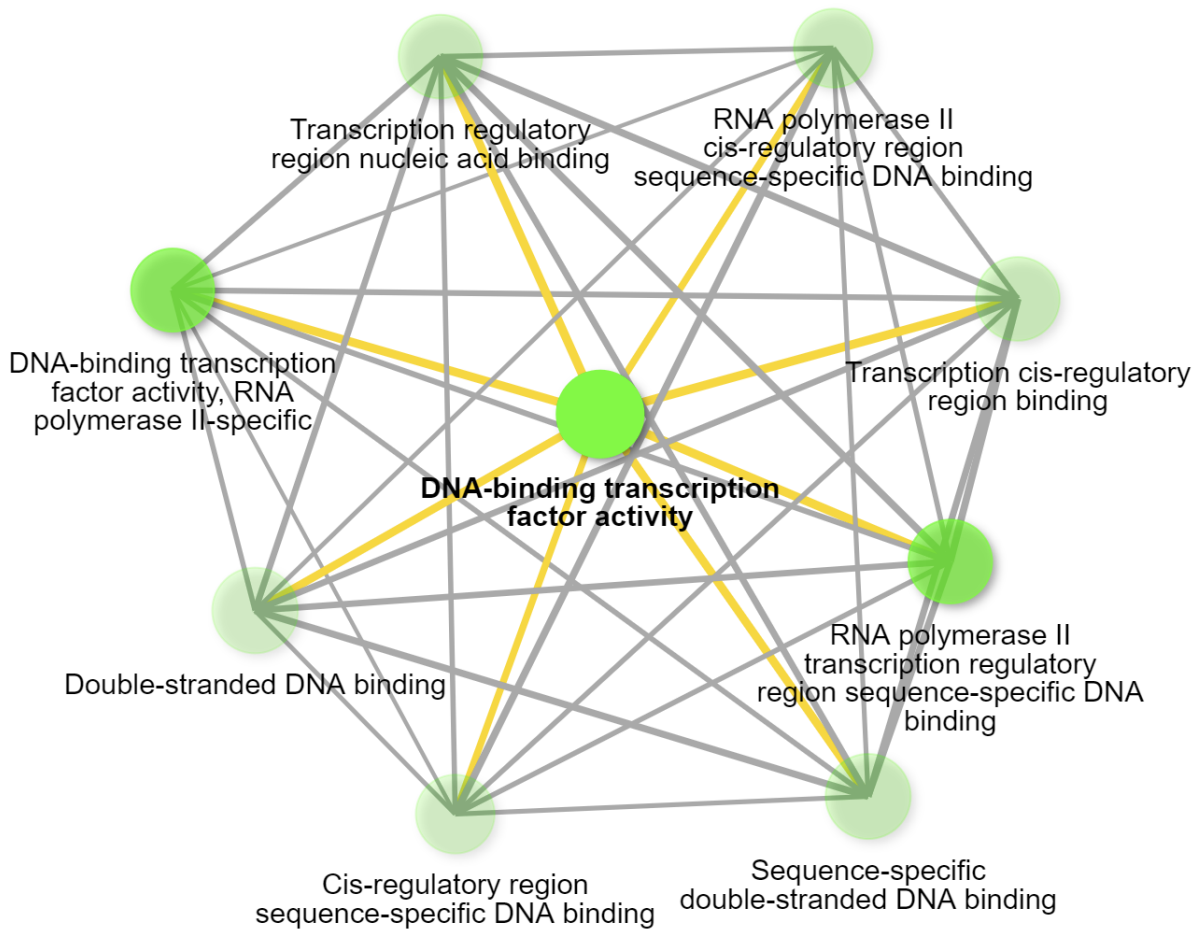


**Figure 60: Network of the enriched gene clusters (annotated with BAP1-binding in MEL202 WT condition) upregulated after BAP1 loss. Edge cutoff: 0.3.**

The results suggest that upon BAP1 loss, a wide array of transcription factors and regulatory regions are freed from repression, leading to broad transcriptional reprogramming in MEL202 cells. This reprogramming could contribute to the oncogenic transformation observed in UM by activating pathways that promote cell proliferation and survival.

The upregulation of genes involved in transcription factor activity and RNA polymerase II binding upon BAP1 loss points to a critical role for BAP1 in maintaining transcriptional homeostasis. The loss of BAP1 likely disrupts the balance between active and repressed

states of chromatin, resulting in the activation of genes that would otherwise remain silent in the WT condition. This transcriptional activation, possibly driven by changes in chromatin accessibility and transcription factor recruitment may likely contribute to the tumorigenesis associated with BAP1-deficient UMs.

#### 4.6. Impact of BAP1 loss through enrichment of TF binding motifs for TFAP2 family and DNA methylation in MEL202 cells

In this section, we investigated how BAP1 loss affects especially genome-wide TF binding motifs in MEL202 UM cells. This analysis provided insight into the regulatory changes triggered by BAP1 loss and their potential relevance to UM progression.

Downregulated genes: 1339 differentially downregulated genes from MEL202 BAP1 KD condition revealed several genomic enrichment sites. **Figure 61** illustrates the genomic distribution of the differentially downregulated genes upon BAP1 loss in MEL202 cells.

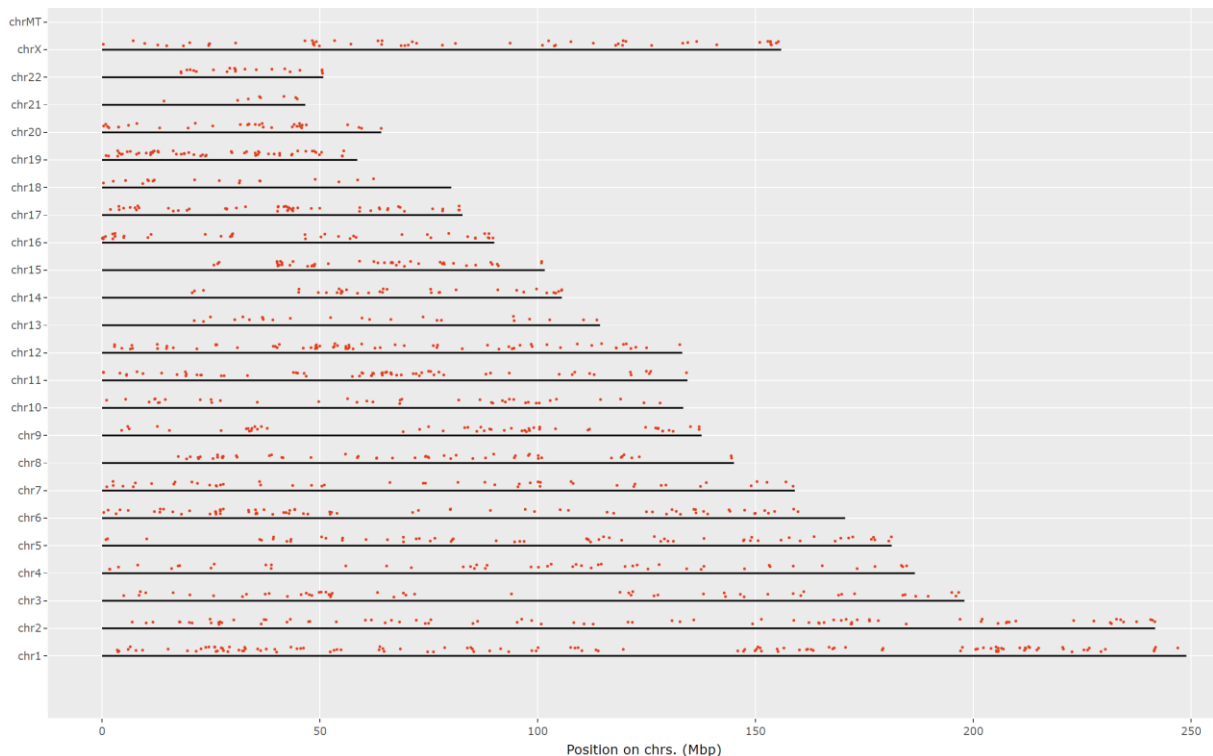


**Figure 61: Genome-enrichment representation of the differentially downregulated genes upon BAP1 loss in MEL202 cells.**

While the red dots represent the downregulated genes, the absence of purple lines suggests that no regions in the genome showed a genomic location-based significant enrichment of these downregulated genes. This indicates that, despite performing a sliding window analysis and applying a hypergeometric test for overrepresentation, the downregulated genes are distributed across the genome without any specific genomic clusters of statistical enrichment. This result points to more dispersed transcriptional repression rather than localized effects in particular genomic regions following BAP1 loss.

Next, we analyzed the enrichment for TF motifs in the promoters of the 1339 differentially downregulated genes. **Table 29** lists these enriched TF binding motifs in the promoters of these differentially downregulated genes after BAP1 loss in MEL202 cells. As we observed, motifs for TCFL5, DNMT1, E2F1, SP1, EGR1, E2F4, E2F6, and others were significantly enriched. This suggests that in the presence of BAP1, these proteins play a prominent role in the regulation of gene expression in MEL202 UM cells.

TCFL5 (bHLH family) shows strong enrichment (P-value: 0.0E+00), suggesting that BAP1 plays a role in regulating genes associated with TCFL5 binding. As a basic helix-loop-helix (bHLH) transcription factor, TCFL5 is involved in cell differentiation and developmental processes (Galan-Martinez et al., 2022). DNMT1 (CxxC family) is a DNA methyltransferase and the significant enrichment (P-value: 0.0E+00) indicates a potential link between BAP1 and epigenetic regulation, specifically in DNA methylation. DNMT1's motif enrichment suggests that BAP1 might have a role in DNMT1-dependent methylation patterns. E2F family (E2F1, E2F4, E2F6) transcription factors, particularly those involved in cell cycle regulation (E2F1) are highly enriched. The E2F family is known to control genes required for DNA replication and cell cycle progression (Xie et al., 2021), aligning with the previously established role of BAP1 in these processes. SP1, SP2 (C2H2 ZF family) zinc finger transcription factors are involved in gene expression regulation related to growth and development (Safe, 2023). The significant enrichment indicates that SP1/SP2 are potentially regulated through BAP1-mediated chromatin changes. TFAP2A/TFAP2C (AP-2 family) TFs are known to be involved in early developmental regulation, cellular differentiation as well as carcinogenesis process (Seberg et al., 2017b, Kolat et al., 2019).

The dual enrichment of TFAP2A and TFAP2C could suggest their “novel” potential roles in the transcriptional reprogramming that occurs upon BAP1 loss the UM.

**Table 29: Enriched TF binding motifs at promoters (600 bp upstream) of the differentially downregulated genes upon BAP1 loss in MEL202 cells.**

Enriched motif in promoter	TF	TF family	P val.	FDR	Score	Note
CACGTG	TCFL5	bHLH	0.0E+00	0.0E+00	1.0E+01	
CCG	DNMT1	CxxC	0.0E+00	0.0E+00	6.0E+00	* Query Gene
GGGCGGGAG	E2F1	E2F	0.0E+00	0.0E+00	1.5E+01	* Query Gene
GGGGGCGGGG	SP1	C2H2 ZF	0.0E+00	0.0E+00	2.0E+01	
GCGGGGCGGGG	EGR1	C2H2 ZF	0.0E+00	0.0E+00	2.2E+01	
GGCGGGAA	E2F4	E2F	0.0E+00	0.0E+00	1.6E+01	
GGGCGGGAA	E2F6	E2F	0.0E+00	0.0E+00	1.2E+01	
GGGGGCGGGGC	SP2	C2H2 ZF	0.0E+00	0.0E+00	2.5E+01	
TGCGGG	ZBTB1	C2H2 ZF	3.8E-15	1.7E-13	7.0E+00	
GGGGGGGGGCC	PATZ1	C2H2 ZF	3.0E-14	1.2E-12	1.4E+01	
GGCGCC	E2F2	E2F	3.4E-14	1.3E-12	1.0E+01	
GCGCAGGCGC	NRF1	Unknown	5.2E-14	1.8E-12	1.7E+01	
CG	CGBP	CxxC	8.3E-14	2.7E-12	3.0E+00	
GGGCGGGGC	KLF5	C2H2 ZF	1.1E-13	3.3E-12	1.3E+01	
GGGCGTG	KLF7	C2H2 ZF	3.6E-13	1.0E-11	9.0E+00	
CCCCGGGC	TFAP2A	AP-2	1.6E-12	4.2E-11	6.0E+00	
CG	TET1	CxxC	5.4E-12	1.3E-10	3.0E+00	
CCCCGGGC	TFAP2C	AP-2	8.0E-12	1.9E-10	7.0E+00	
CACGCG	HES4	bHLH	1.8E-11	3.9E-10	6.0E+00	
CG	MLL	CxxC	1.9E-11	3.9E-10	3.0E+00	
TGCGTGGGCGT	EGR3	C2H2 ZF	3.8E-10	7.4E-09	1.1E+01	
TGCGTGGGCGT	EGR1	C2H2 ZF	3.1E-09	5.8E-08	9.0E+00	
ATGCGTGGGCGG	EGR4	C2H2 ZF	5.9E-09	1.1E-07	1.0E+01	
GGGGGTGG	ZNF281	C2H2 ZF	7.6E-09	1.3E-07	7.0E+00	
GGAGGAGGAGGGGAGGAGG	ZNF263	C2H2 ZF	9.2E-09	1.5E-07	1.4E+01	
TGCGTGGGCG	EGR2	C2H2 ZF	1.4E-08	2.3E-07	9.0E+00	
TGGCCACCAGGGGGCGC	CTCF	C2H2 ZF	1.7E-08	2.7E-07	1.0E+01	
TCGCGCCAAA	E2F1	E2F	3.3E-08	4.9E-07	8.0E+00	* Query Gene
AGATCTCGCGAGA	ZBTB33	C2H2 ZF	5.4E-08	7.7E-07	9.0E+00	
GGGGCGCAGCTGCGTCCC	NHLH1	bHLH	2.9E-07	4.0E-06	1.1E+01	

P-values and FDRs for the majority of the TFs are extremely low indicating a very high level of significance and it highlights that the motifs for these TFs are not randomly present but are statistically overrepresented in the promoters of the affected genes. Also, several TFs, particularly DNMT1, E2F1, and E2F4 show the note "Query Gene" indicating these genes are part of the query dataset and may also be targets of the identified transcription factors.

Upregulated Genes: 1445 differentially upregulated genes from MEL202 BAP1 KD revealed several genomic enrichment sites with interesting statistically significant site. In **Figure 62**, we observe a genome-wide scan for the enriched genomic regions of the differentially upregulated genes in MEL202 cells after BAP1 KD. The red dots represent the genes distributed across various chromosomes, and the purple lines mark regions of statistically significant enrichment. Chromosome 5 shows statistically enriched region, as indicated by the purple line.

Detection of the 2 enriched regions on the chromosome 5 when only 0.01 regions were expected suggests that BAP1 loss leads to an overrepresentation of the affected genes in this chromosomal area. The remaining chromosomes show a more dispersed distribution of red dots (genes), but no other statistically enriched regions were detected. This suggests that while gene expression changes occur across the genome, the specific location of the chromosome 5 appears to be a hotspot for BAP1-regulated genes.

When we zoom in to this region, The genome enrichment analysis revealed a significant enrichment of the PCDHGA gene cluster on chromosome 5, specifically involving 12 genes (*PCDHGA1, 2, 3, 4, 5, 6, 7, 8, 9, 10, 11* and *12*). The protocadherin gamma (PCDHGA) gene family is part of the cadherin superfamily, which is known for its role in cell-cell adhesion. These genes are primarily involved in neuronal connectivity and have been implicated in maintaining cellular architecture and tissue organization (Kirov et al., 2003, Long et al., 2023). In the context of BAP1 loss, the significant enrichment of this gene cluster may suggest that alterations in cell adhesion and cellular communication pathways are critical consequences of BAP1 knockdown.

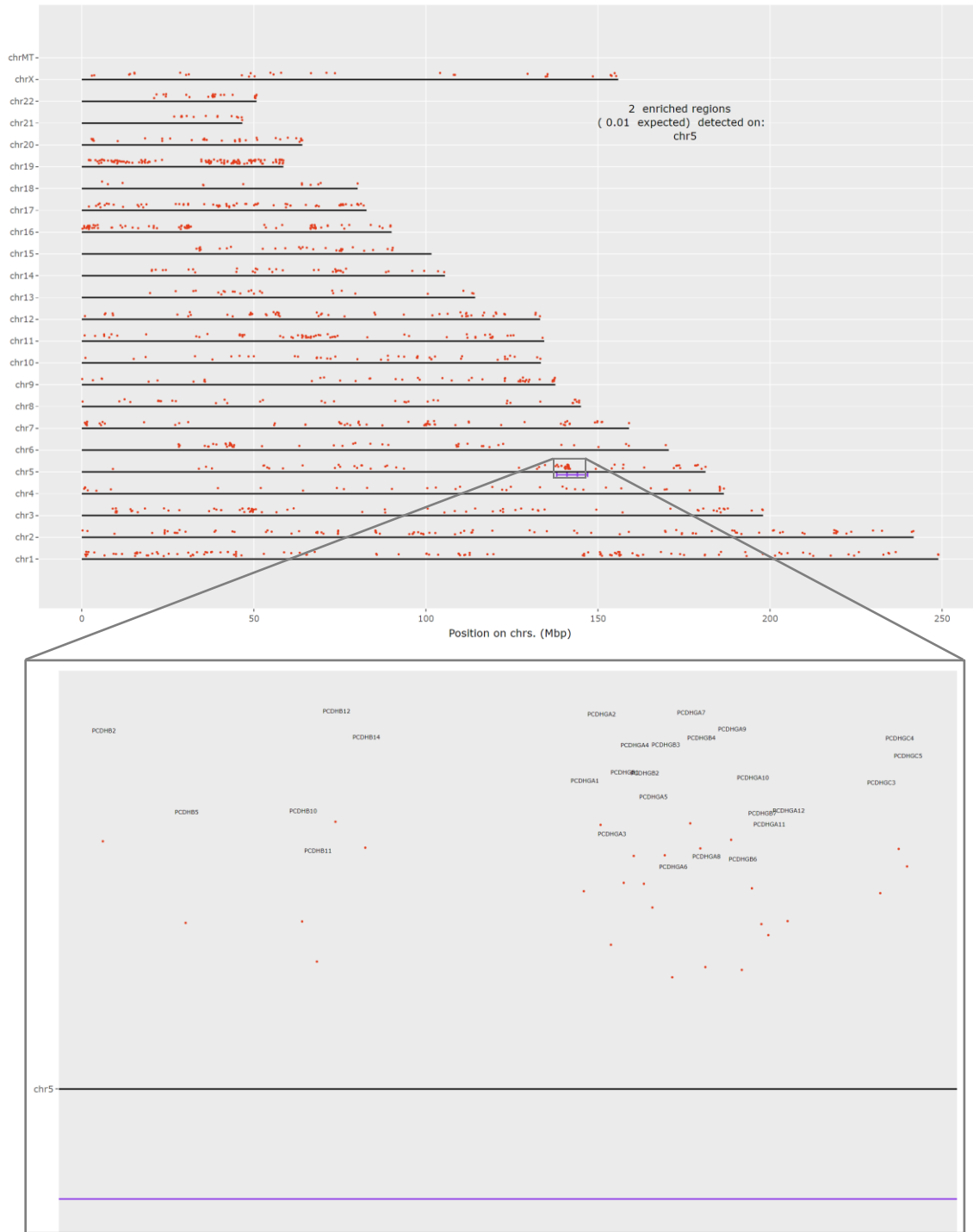


**Figure 62: Genome-enrichment representation of the differentially upregulated genes after BAP1 loss in MEL202 cells.** Genome-wide representation (top), focused frame to the significantly enriched region of PCDHGA gene cluster on the chromosome 5 (below).



**Table 30** lists the enriched TF binding motifs in the promoters of the differentially upregulated genes upon BAP1 loss. The motifs for transcription factors such as DNMT1, TFAP2A, and TFAP2C are highly enriched, as indicated by the P-values and the FDRs.

**Table 30: Enriched TF binding motifs at promoters (600 bp upstream) of the differentially upregulated genes upon BAP1 loss in MEL202 cells.**

Enriched motif in promoter	TF	TF family	P val.	FDR	Score	Note
CCG	→ DNMT1	CxxC	2.9E-15	1.2E-12	5.0E+00	
CG	CGBP	CxxC	1.8E-14	3.6E-12	3.0E+00	
CCCCGGGC	→ TFAP2C	AP-2	4.1E-12	5.7E-10	7.0E+00	
CCCCGGGC	→ TFAP2A	AP-2	7.5E-12	7.7E-10	5.0E+00	
GCCTGAGG	TFAP2E	AP-2	1.4E-10	1.1E-08	6.0E+00	* Query Gene
GCGCAGGCGC	NRF1	Unknown	4.8E-10	3.3E-08	1.4E+01	
GCCGAGGCCT	ZFY	C2H2 ZF	3.5E-09	2.1E-07	1.0E+01	
CACGTG	TCFL5	bHLH	5.3E-09	2.8E-07	6.0E+00	
CG	MLL	CxxC	1.6E-08	7.5E-07	2.0E+00	
CCTGGCAAC	RFX6	RFX	2.0E-08	8.2E-07	4.0E+00	
GGGGGCGGGGC	SP2	C2H2 ZF	2.5E-08	9.3E-07	1.3E+01	
TGCGGG	ZBTB1	C2H2 ZF	4.6E-08	1.6E-06	5.0E+00	
CCGGAAGT	ELK1	Ets	1.0E-07	3.2E-06	6.0E+00	
GTTGCCATGGCAACCG	RFX2	RFX	1.1E-07	3.4E-06	1.0E+01	
GGGCGTG	KLF7	C2H2 ZF	1.7E-07	4.7E-06	6.0E+00	
GGGGCGCAGCTGCGTCCC	NHLH1	bHLH	2.2E-07	5.7E-06	1.0E+01	
GGGGCGCAGCTGCGCCC	NHLH1	bHLH	3.0E-07	7.2E-06	9.0E+00	
GCCCTGGGGC	TFAP2C	AP-2	3.7E-07	8.6E-06	7.0E+00	
CCGGAAG	ELK1	Ets	5.5E-07	1.2E-05	5.0E+00	
GCGGGGGCGGGG	EGR1	C2H2 ZF	8.3E-07	1.7E-05	1.1E+01	* Query Gene
CCGGAAGTG	ELK4	Ets	9.2E-07	1.8E-05	7.0E+00	
CG	KDM2B	CxxC	9.6E-07	1.8E-05	1.0E+00	
GGGGGCGGGG	SP1	C2H2 ZF	1.2E-06	2.1E-05	1.0E+01	
GGCGCC	E2F2	E2F	1.5E-06	2.5E-05	5.0E+00	
GACATGCCCGGGCATGTCC	TP53	p53	2.9E-06	4.8E-05	1.0E+01	
CGAGGCGCAGTGATGCGTAGCGGC	PAX5	Paired box	6.9E-06	1.1E-04	7.0E+00	
GGGCGGGGC	KLF5	C2H2 ZF	7.9E-06	1.2E-04	8.0E+00	* Query Gene
TGCGTGGGCGT	EGR1	C2H2 ZF	1.2E-05	1.7E-04	7.0E+00	* Query Gene
GGGGGGGGGCC	PATZ1	C2H2 ZF	1.4E-05	2.0E-04	8.0E+00	
ATGCGTGGGCGG	EGR4	C2H2 ZF	1.6E-05	2.2E-04	7.0E+00	

DNMT1 (CxxC family, P-value: 2.9E-15, FDR: 1.2E-12) is responsible for maintaining DNA methylation patterns (Svedruzic, 2011). The highest enrichment being the DNMT1 motif may suggest that BAP1 might play a role in controlling epigenetic modifications through the DNA methylation. BAP1 loss could result in epigenetic dysregulation, contributing to gene silencing or activation of oncogenic pathways. TFAP2C and TFAP2A (AP-2 family, TFAP2C P-value: 4.1E-12, FDR: 5.7E-10; TFAP2A P-value: 7.5E-12, FDR: 7.7E-10) AP-2 transcription factors are involved in developmental regulation and cell differentiation. The enrichment of these motifs suggests that TFAP2A and TFAP2C may become more active upon BAP1 loss, driving the transcriptional changes that contribute to the proliferation, migration, and invasiveness of cancer cells. These findings also align with the known role of TFAP2 family members in cancer progression but these are the novel findings in our UM study. CGBBP (CxxC family) motifs are also enriched (P-value: 1.8E-14), suggesting involvement in epigenetic regulation.

#### **4.7. Interplay between BAP1 and TFAP2A/TFAP2C pioneering transcription factors in UM**

A study conducted in our laboratory utilizing bulk-RNAseq data from the UM patients and their CLICK (CLuster Identification via Connectivity Kernels) clustering analysis (Sharan et al., 2003) together whole genome methylation sequencing result of these UM patient samples had identified *TFAP2A* and *TFAP2C* as not only differentially expressed, but also differentially methylated genes that distinguished BAP1-positive Disomy 3 (D3) from BAP1-deficient Monosomy 3 (M3) patient cohorts. These previous findings along with the motif enrichment results from our BAP1 KD experiments in MEL202 cells highlighted the potential significance of TFAP2A and TFAP2C in UM pathogenesis.

The enrichment of TFAP2A and TFAP2C binding motifs upon BAP1 loss suggests that these two transcription factors may play critical roles in the transcriptional dysregulation observed in BAP1-deficient UM cells. Motivated by all these findings, we aimed to explore the interplay between BAP1 and these pioneering transcription factors to further understand their regulatory relationships and potential impact on UM progression.

Gene expression data from our UM patient cohort suggested that D3 patients have higher levels of *TFAP2A* expression while M3 patients have elevated levels of *TFAP2C* expression. Also, we examined the correlations between *BAP1* and *TFAP2A/TFAP2C* gene expressions using the data from The Cancer Genome Atlas (TCGA) involving 80 UM patients (Robertson et al., 2017) on cBioPortal for Cancer Genomics (Cerami et al., 2012, Gao et al., 2013, de Bruijn et al., 2023). **Figure 63** shows a positive correlation between *BAP1* and *TFAP2A* (Spearman: 0.77, Pearson: 0.74) expression, indicating that higher *BAP1* expression (as in the D3 case) is associated with higher *TFAP2A* expression.

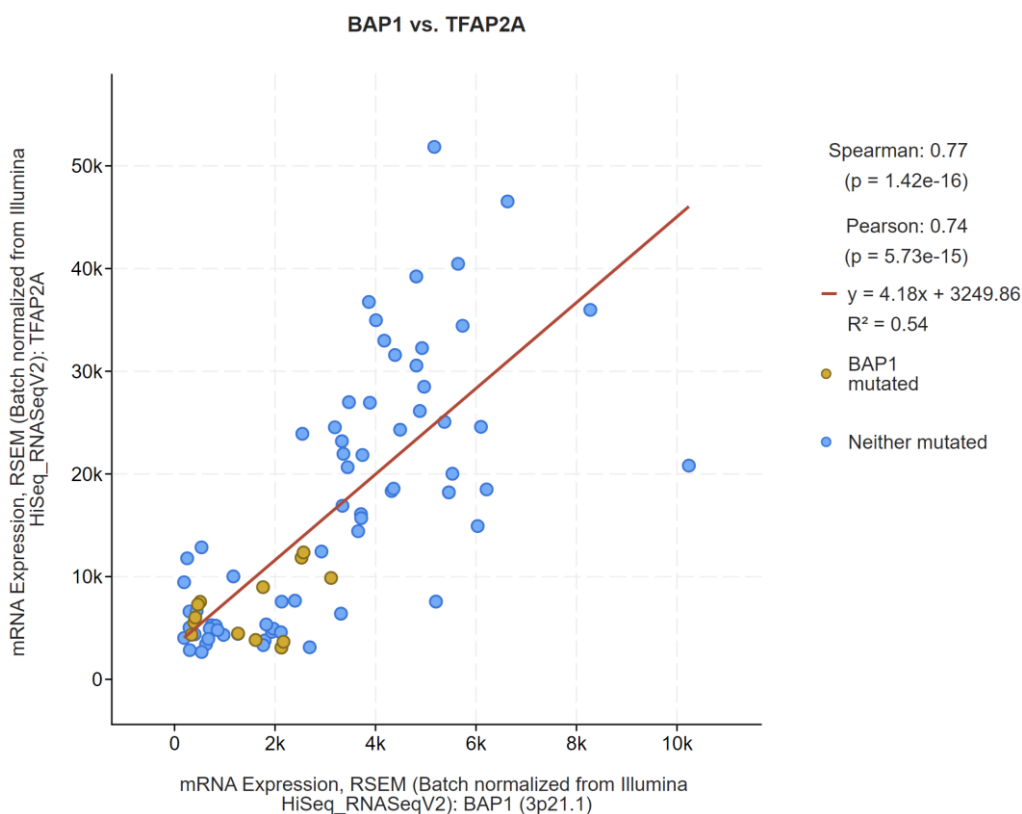


**Figure 63: Positive correlation between *BAP1* and *TFAP2A* gene expressions.** Data showing the gene expression values of 80 UM patients from TCGA database.

Conversely, **Figure 64** illustrates a negative correlation between expressions of *BAP1* and *TFAP2C* (Spearman: -0.49, Pearson: -0.43), suggesting that higher *BAP1* expression correlates with lower *TFAP2C* expression.

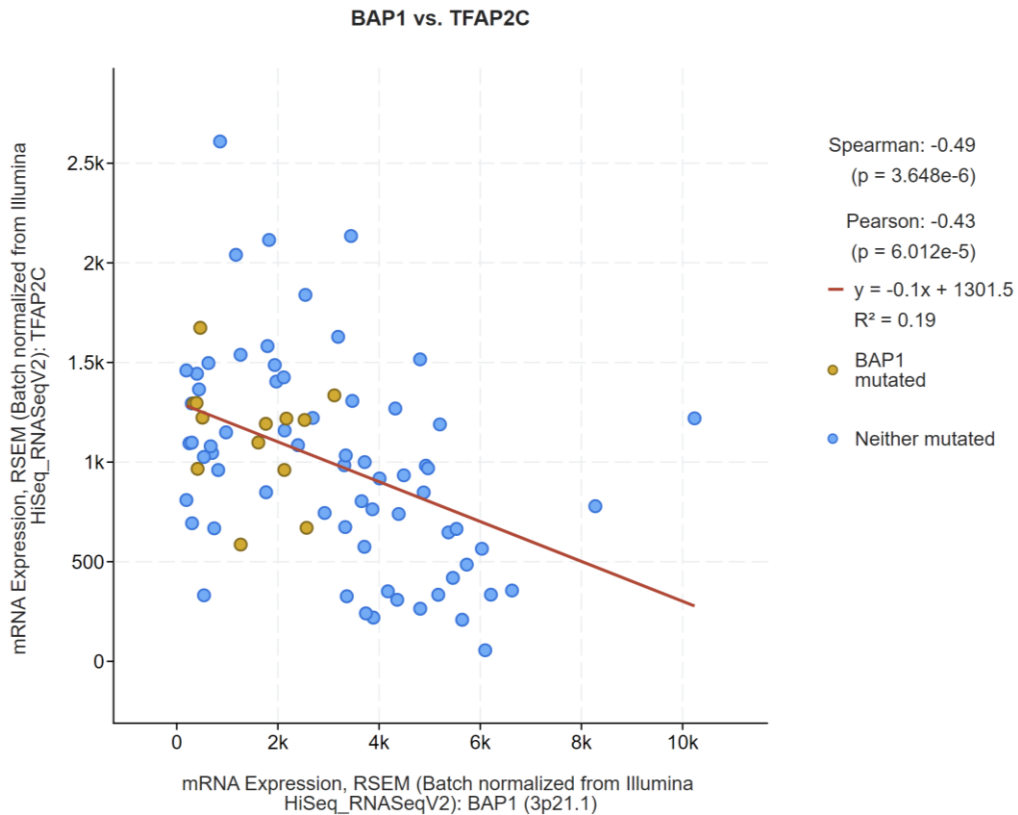


**Figure 64: Negative correlation between *BAP1* and *TFAP2C* gene expressions.** Data showing the gene expression values of 80 UM patients from TCGA database.

#### 4.7.1. Loss of *BAP1* changes *TFAP2A/TFAP2C* occupancies at their target sites

Based on the findings from the UM patients and our experimental UM cell culture system, we expanded the investigation to focus on how *BAP1* loss affects the binding of *TFAP2A* and *TFAP2C* in UM cells. To study the binding interplay between these transcription factors, we performed ChIP-seq in both MEL202 and *BAP1* KD cells.

In this section, we focused on the binding patterns of *TFAP2A* and *TFAP2C* at their target sites. The aim was to firstly categorize the changes of the ChIP-seq signals whether maintained (kept), increased (gained), or lost following *BAP1* knockdown in the MEL202 UM cells.

In **Figure 65A**, we observe that TFAP2A binding is more substantially affected by BAP1 KD compared to TFAP2C (**Figure 65B**) in terms of the maintained binding signals. The heatmap shows that a significant proportion of TFAP2A binding is lost. This loss of TFAP2A occupancy suggests that BAP1 may play a crucial role in stabilizing TFAP2A binding at its target sites, and without BAP1, TFAP2A's ability to bind DNA is decreased. This result suggests that TFAP2A's function may be regulated by the chromatin environment that BAP1 helps maintain. Compared to the WT condition, the absence of BAP1, chromatin remodeling could lead to a more closed or altered state, reducing TFAP2A's access to these target regulatory elements. Also, the loss of TFAP2A binding could lead to the downregulation of genes critical for maintaining cell differentiation and proliferation control.

In contrast, **Figure 65B** illustrates a bigger trend of increased TFAP2C occupancy at its target sites following BAP1 knockdown comparing TFAP2A. This increased binding implies that TFAP2C may become more active or its target genes more accessible in BAP1-deficient cells, particularly at TSS and enhancer regions. The resilience of TFAP2C to BAP1 loss (in terms of the maintained signal amount, comparing TFAP2A) suggests that TFAP2C might be capable of compensatory mechanisms in transcriptional regulation when BAP1 is absent. This enhanced binding could indicate a compensatory role for TFAP2C in maintaining certain gene expression programs, potentially driving cell proliferation, migration, and survival pathways that are critical for UM. TFAP2C may also be involved in activating alternative pathways that support oncogenesis in the absence of BAP1, thus contributing to the aggressive phenotype observed in BAP1-deficient UM.

The differential effects on TFAP2A and TFAP2C binding can also be partially attributed to BAP1's role in chromatin accessibility. BAP1 acts as a chromatin modifier, and its loss could lead to changes in the chromatin landscape that selectively affect transcription factor access.

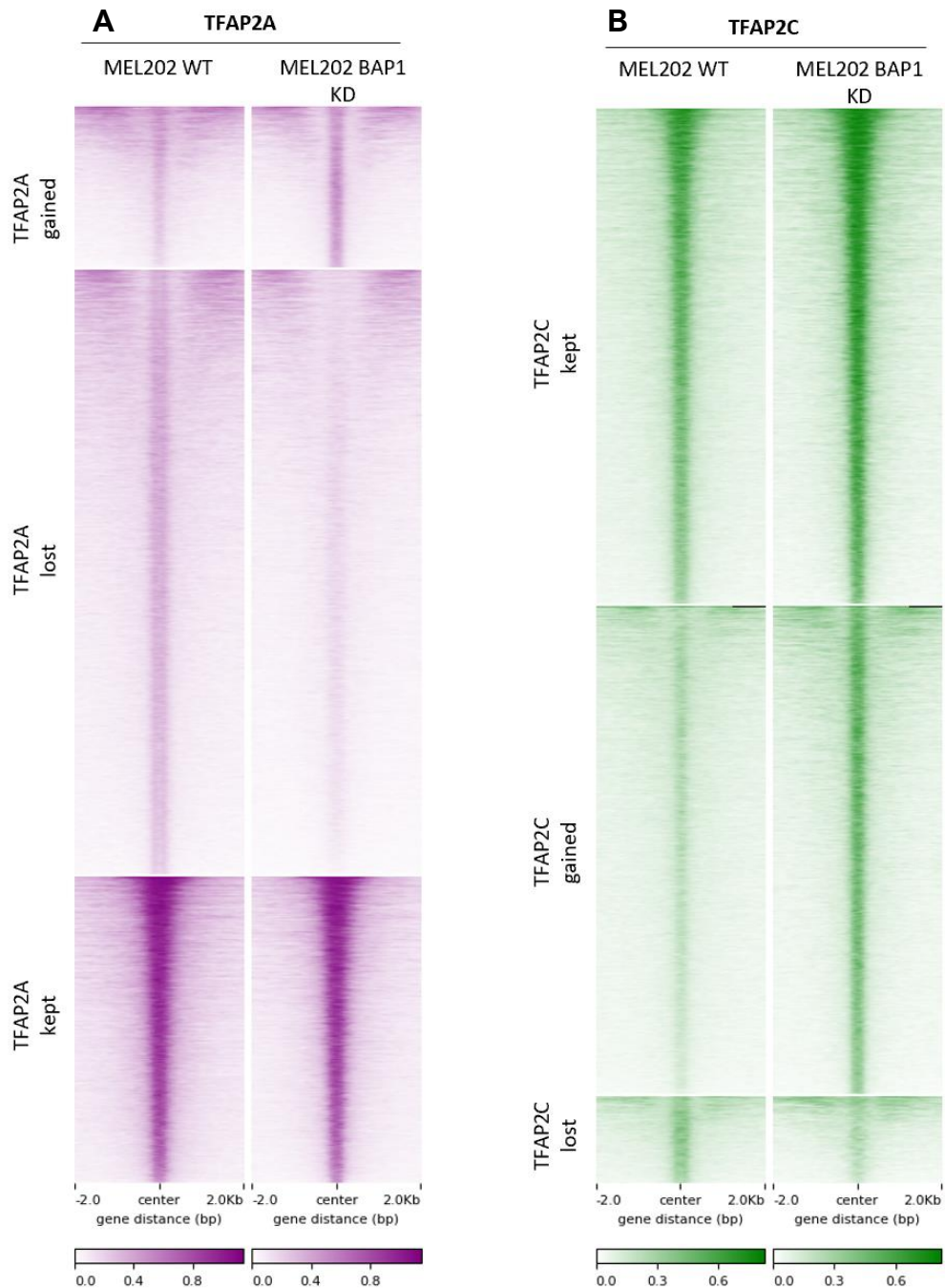


**Figure 65: Heatmaps showing the binding profiles of (A) TFAP2A and (B) TFAP2C between MEL202 WT / BAP1 KD conditions.**

For TFAP2A, BAP1 loss may be leading to chromatin closure preventing TFAP2A from effectively binding its target sites. In contrast, TFAP2C may bind to regions where chromatin remains accessible even in the absence of BAP1, or its binding sites might become more open due to compensatory chromatin remodeling.

While the expression TPM levels of *TFAP2A* (Appendix **Figure 94**) and *TFAP2C* (**Figure 66**) in MEL202 / BAP1 KD conditions do not display a significant change ( $|\log_{2}FC| < 1$ ), this does not detract from the crucial regulatory interplay observed between these TFs.

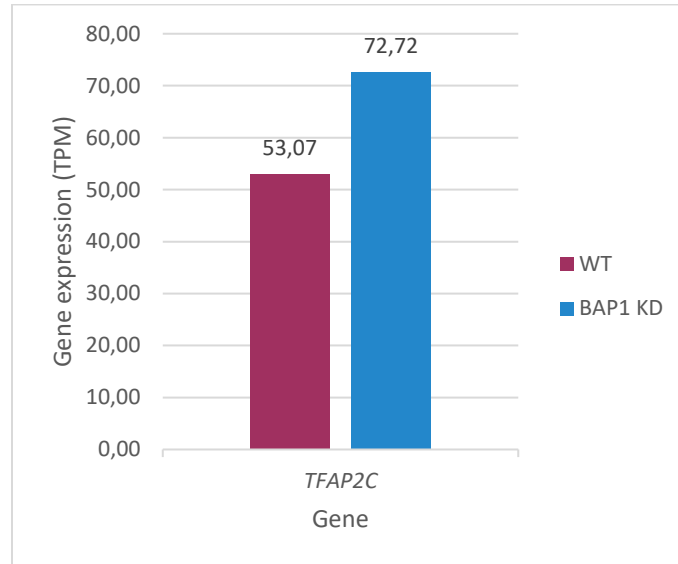


**Figure 66: Change in the TPM gene expressions of *TFAP2C* between MEL202 WT / BAP1 KD conditions.**

Our findings from ChIP-seq data demonstrate that despite modest changes at the mRNA level, *TFAP2A* and *TFAP2C* exhibit substantial differences in chromatin binding upon BAP1 loss. This suggests their functional modulation mainly occurs at the level of transcriptional regulation and chromatin accessibility, rather than being reflected in drastic mRNA fluctuations in MEL202 UM cells. Therefore, the interplay between *TFAP2A* and *TFAP2C* appears to be more associated with their differential binding, influencing the transcriptional landscape in MEL202 UM cells. The shift in binding between *TFAP2A* and *TFAP2C* may also reflect their differential roles in UM. *TFAP2A* has been associated with differentiation and developmental pathways, which could be disrupted by BAP1 loss, leading to de-differentiation and cancer stem cell-like properties. Meanwhile, *TFAP2C*, which is often linked to proliferation and survival pathways, might promote a more aggressive tumor phenotype by driving gene expression programs associated with cell survival and migration. The loss of *TFAP2A* binding and the gain of *TFAP2C* binding could represent a broader transcriptional reprogramming that occurs in BAP1-deficient UM.

#### **4.7.2. Modulation of TFAP2A and TFAP2C pioneering TF binding on BAP1-bound genes in UM cells**

Next, we designed a strategy to understand the TFAP2A / TFAP2C modulation specifically on the BAP1-bound genes comparing the MEL202 / BAP1 KD conditions. Thus, we integrated genes that are annotated as BAP1-bound (from the ChIP-seq experiment) and show the overlap for the binding events of TFAP2A / TFAP2C TFs revealing their binding differences on these genes upon BAP1 loss.

As shown in **Figure 67A** and **Figure 67B**, there are disruptions in transcriptional regulation upon BAP1 KD specifically on TFAP2C binding. While TFAP2A binding profile on the BAP1-bound genes does not show a dramatical change upon BAP1 loss, there is an increase in the binding profile of TFAP2C to the direction of BAP1 KD condition. It highlights the crucial regulatory role that BAP1 may play in modulating TFAP2C's regulation on the chromatin.

A possible hypothesis could be that the loss of BAP1 may lead to an increased opportunity especially for TFAP2C to bind more freely at regions that were previously not bound. This could drive the expression of genes contributing to the aggressive nature of BAP1-deficient UM. Also, BAP1's role as a chromatin modifier suggests that its loss could cause epigenetic alterations, such as changes in histone modifications or DNA methylation patterns, thereby influencing the binding of TFAP2C.

The increased TFAP2C binding, in particular, may weaken the regulation of genes involved in cell adhesion and cell-cell interactions, potentially leading to increased invasiveness. TFAP2A could also contribute to these processes, but in a more stable and less disrupted manner upon BAP1 loss.



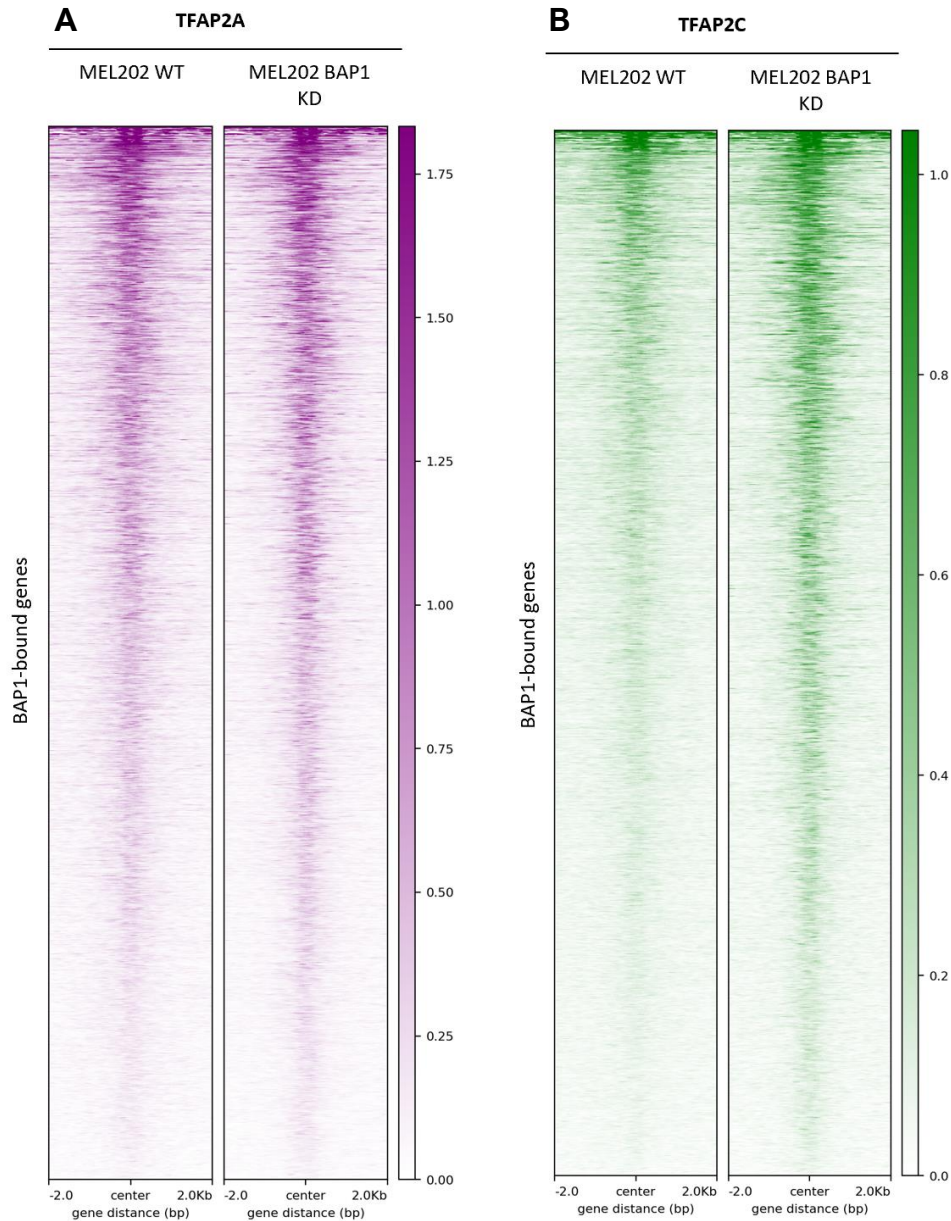


**Figure 67: Heatmaps showing the differences of TFAP2A/TFAP2C binding patterns on the BAP1-bound genes in MEL202 BAP1 WT / KD conditions. (A) Effect of BAP1 loss on the binding of TFAP2A on BAP1-bound genes (n=2700), (B) Effect of BAP1 loss on the binding of TFAP2C on BAP1-bound genes (n=2700).**

To better understand the nature of the chromatin landscape associated with TFAP2C, we mapped its peaks across various chromatin states in WT cells. **Figure 68** shows the distribution of TFAP2C peaks across the chromatin states indicating a significant enrichment at transcription start sites (79%) and enhancers (17%).

This result aligns with our previous hypothesis that attributes the target sites of TFAP2C mostly to regulatory elements of the genes. Next, we observed the majority of TFAP2C peaks across ATAC-seq peaks at mainly accessible sites (89%). This may demonstrate that TFAP2C presents mainly at accessible chromatin regions or this pioneering TF programs its novel binding sites as accessible particularly in UM.

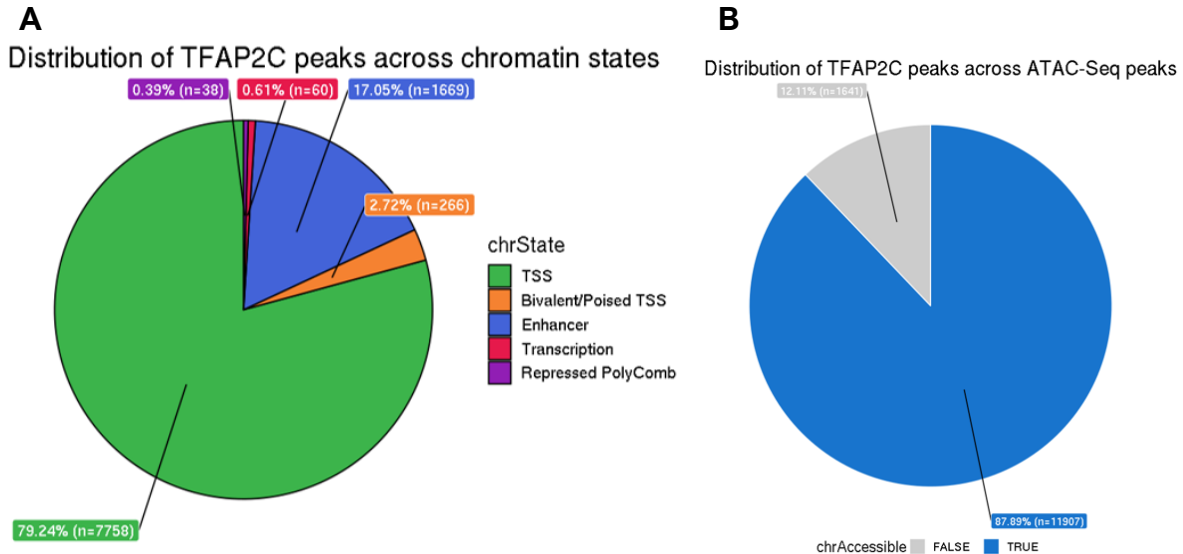






**Figure 68: Distribution of TFAP2C peaks (A) across the chromatin states and (B) ATAC-seq peaks.**

BAP1 and TFAP2C show association to the similar chromatin states and ATAC-seq chromatin accessibility peak distributions, suggesting that they both act on the regulatory elements of the genome. The fact that most of the TFAP2C binding sites are located in accessible chromatin regions (88%) and overlap with TSS and enhancer regions (**Figure 68**) implies that TFAP2C, like BAP1 may be involved in regulating genes that require fine control of the transcription.

Next, we analyzed the TF binding motif of TFAP2C in the WT cells to understand the preferences of its binding patterns. **Table 31** shows the *de novo* motif enrichment result obtained from the HOMER tool.

**Table 31: HOMER *de novo* motif analysis results for TFAP2C-binding sequences.** Cutoff for the p-value set to  $< 1 \times 10^{-15}$ .

Motif	p-value	% of targets	Match
	$1 \times 10^{-89}$	40.67%	AP-2gamma (TFAP2C) (AP2 family TF)
	$1 \times 10^{-36}$	9.02%	NF-Y (CBF) (CCAAT-binding factor)
	$1 \times 10^{-35}$	37.64%	MEF2C (MADS-box TF)
	$1 \times 10^{-27}$	33.31%	ELK1 (ETS family TF)

The motif analysis of TFAP2C-binding sequences (**Table 31**) revealed several significantly enriched transcription factor motifs. Among the most enriched motifs were those for AP-2gamma (TFAP2C) itself, indicating autoregulatory activity, along with motifs for NF-Y (CCAAT-binding factor), MEF2C (MADS-box transcription factor), and ELK1 (ETS family transcription factor). The enrichment of these motifs suggests that TFAP2C may cooperate with these transcription factors to regulate gene expression in specific genomic regions.

We observed a striking enrichment of the ELK1 binding motif in TFAP2C-binding regions. This finding is particularly important because ELK1 is also the highest enriched motif in the BAP1-binding regions identified in our analyses. This striking overlap suggests a potential co-regulatory mechanism, where ELK1 plays a central role in integrating signals from both TFAP2C and BAP1.

ELK1 is a transcription factor within the ETS family, known to be involved in cell proliferation, differentiation, and survival pathways (Buchwalter et al., 2004, Yang and Sharrocks, 2006). This may suggest a possible interplay between BAP1, TFAP2C, and ELK1 in regulation of transcriptional programs. The co-regulation of genes by ELK1 in conjunction with TFAP2C suggests that this axis may control genes involved in essential oncogenic pathways. BAP1's chromatin-modifying function might enhance or repress ELK1-mediated gene transcription, depending on whether BAP1 is present or lost. In

BAP1-deficient cells, where TFAP2C becomes more prominent, ELK1 could shift its role from regulating normal cell growth to driving cancer-promoting pathways. This hypothesis is supported by the overlap of binding patterns between BAP1 and TFAP2C, suggesting that the loss of BAP1 leads to dysregulated binding of transcription factors like TFAP2C using a common ELK1 motif. In summary, the enrichment of ELK1 binding motifs in both BAP1 and TFAP2C-binding regions underscores its potential as a transcriptional regulator that integrates signals from both BAP1 and TFAP2C, influencing gene expression in UM.

#### **4.7.3. Signature of novel TFAP2C-bound genes stratify UM patients based on BAP1 status**

To further explore the significance of BAP1 loss and its interplay with TFAP2C on gene regulation, we integrated the RNA-seq data of MEL202 WT and BAP1 KD cells with ChIP-seq data to identify differentially expressed genes that show differential TFAP2C binding upon BAP1 loss.

Specifically, we filtered for genes that were (1) differentially expressed ( $|\log\text{FC}| > 1$ ) in BAP1 KD cells, (2) bound by BAP1 in the WT condition, and (3) not bound by TFAP2C in the WT condition but bound by TFAP2C in BAP1 KD cells. This filtering process yielded a subset of 80 genes; 19 downregulated and 61 upregulated, suggesting that these genes may be directly influenced by the dynamic shift in TFAP2C binding upon BAP1 loss.

To assess the broader significance of these genes, we performed a hierarchical clustering analysis using RNA-seq expression data from the TCGA UM cohort, encompassing 80 patients. The heatmap generated from this analysis revealed a clustering pattern with distinct patient subgroups emerging based on the expression of these BAP1-TFAP2C target genes as shown in **Figure 69**.

This result suggests that the BAP1-TFAP2C axis may play a critical role in defining molecular subtypes of UM, particularly in the context of BAP1 loss. The emergence of these TFAP2C binding sites upon BAP1 loss suggests that TFAP2C may play a compensatory role in regulating genes that were previously under BAP1 control. This shift likely contributes to the transcriptional reprogramming observed in BAP1-deficient cells.

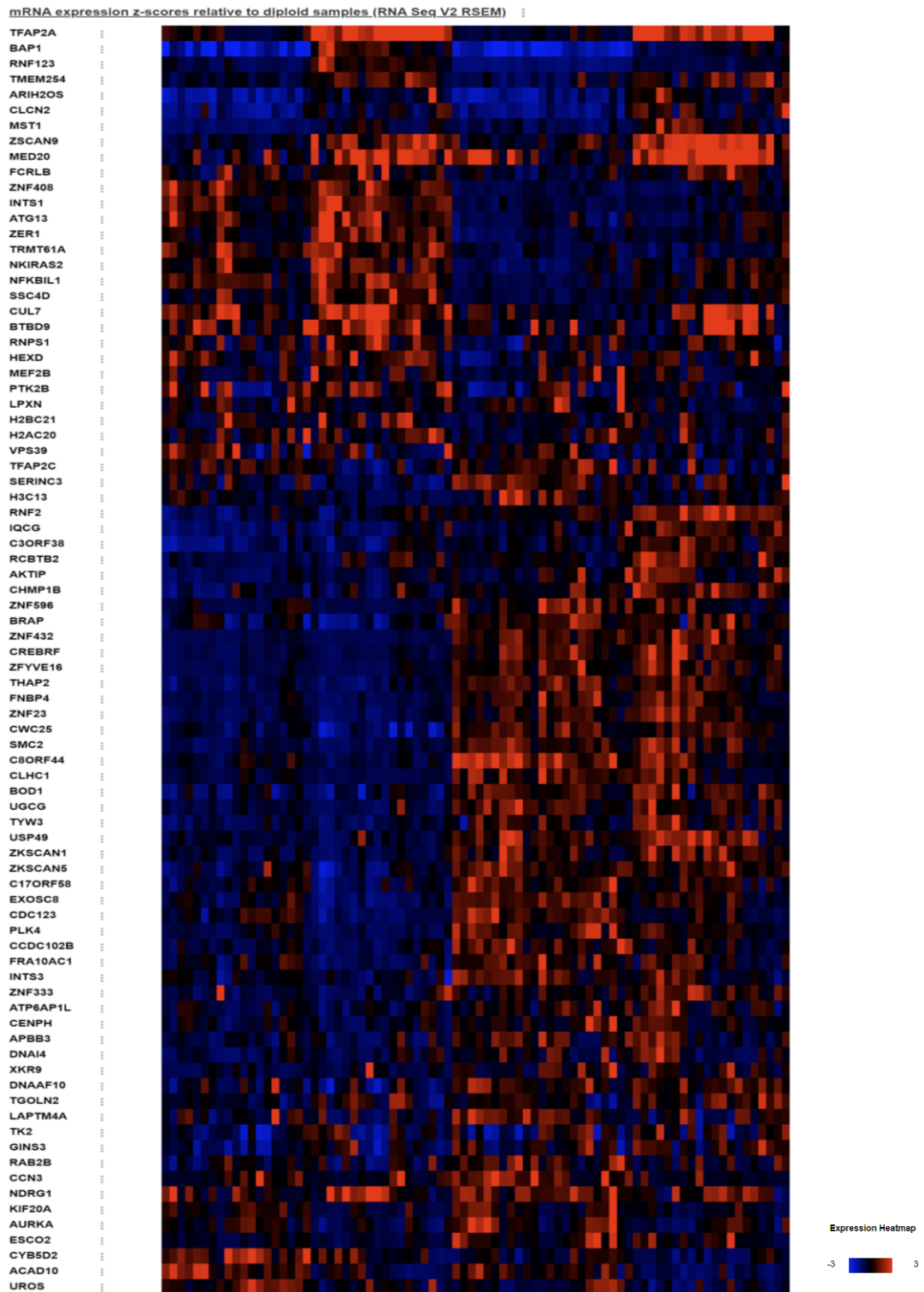


**Figure 69: Clustered heatmap of 80 TCGA uveal melanoma patients based on BAP1-dependent, TFAP2C-bound genes.** Differentially expressed genes ( $|\log_{2}FC| > 1$ ) from MEL202 WT and BAP1 KD conditions were filtered for BAP1-bound genes in WT samples, and further refined to exclude TFAP2C-bound genes in WT but include those bound by TFAP2C in BAP1 KD conditions.

The appearance of these new TFAP2C binding events may be indicative of a broader regulatory shift that occurs when BAP1 is lost, possibly altering key pathways involved in UM progression. The ability of these genes to stratify patients based on their BAP1 status provides further support for the functional relevance of TFAP2C binding in driving gene expression changes following BAP1 loss. This analysis illustrates the impact of BAP1 loss on the transcriptomic landscape, particularly in its modulation of transcription factor binding. The enrichment of the ELK1 motif in both BAP1- and TFAP2C-bound regions further supports the notion of a shared transcriptional network. The hierarchical clustering based on these genes in the TCGA cohort indicates that this regulatory shift has potential clinical implications.

#### **4.8. Chromatin accessibility changes in response to BAP1 loss**

In the previous sections, we aimed to explore the gene regulatory roles of BAP1 and its interplay with the pioneering TFs, focusing on their ability to genome-wide binding mainly TSS and enhancers, and how this binding is modulated by the presence or absence of BAP1. These pioneering TFs play critical roles in regulating gene expression by occupying key regulatory elements in the genome. The loss of BAP1 affects the binding of them, possibly changing the transcriptional programs in UM.

In this section, we aim to extend our investigation towards the perspective of chromatin remodeling in terms of genome-wide chromatin accessibility changes that occur in response to BAP1 loss. By examining alterations focusing at TSS and enhancer regions, we aim to determine how the global chromatin landscape is reprogrammed upon BAP1 knockdown. Here, we assess whether the reduction of BAP1 leads to widespread changes in chromatin openness, which could further impact the recruitment of the transcription factors and the regulation of gene expression. We provide insights into how BAP1 deficiency reshapes the accessibility of the chromatin architecture, contributing to the transcriptional dysregulation observed in BAP1-deficient UM.

#### 4.8.1. Chromatin accessibility decreases at BAP1-bound TSS and enhancer regions

We assessed the chromatin accessibilities using ATAC-seq to evaluate the changes that occur upon BAP1 loss in MEL202 cells. **Figure 70** provides a comprehensive visualization of chromatin accessibility across the genome, clustered by transcription start sites (TSS) and enhancer regions (that were annotated by BAP1-binding) in both BAP1 WT and BAP1 KD conditions. The heatmaps (**Figure 70A** and **Figure 70B**) and the density plots (**Figure 70C** and **Figure 70D**) demonstrate a reduction in the chromatin accessibility at TSS and enhancers of the BAP1-bound genes in the conditions of BAP1 KD.

The TSS heatmaps at the top panels in **Figure 70A** and **Figure 70B** illustrate that chromatin remains relatively more accessible in BAP1 WT cells compared to BAP1 KD cells. This trend is further supported by the density plot in **Figure 70C**, which quantifies the average chromatin accessibility across active TSS regions. While there is a noticeable decrease in accessibility at TSS regions upon BAP1 loss, the magnitude of this decrease is not as dramatic as the changes observed at enhancers. The relatively less pronounced reduction in accessibility at TSS may suggest that BAP1 is more crucial for maintaining chromatin openness at enhancer regions, while TSS regions retain some degree of accessibility due to the presence of other transcription factors or chromatin remodelers that could be compensating for the loss of BAP1 in the UM cells.

In contrast, enhancer regions of the BAP1-bound genes exhibit a more dramatic loss of chromatin accessibility upon BAP1 knockdown. The enhancer heatmaps at the bottom panels in **Figure 70A** and **Figure 70B** and the density plot in **Figure 70D** highlight this significant reduction in the chromatin accessibility, with BAP1 KD cells showing markedly lower levels of chromatin openness compared to WT cells. This observation suggests that BAP1 plays a critical role in maintaining open chromatin states at enhancers, which are key regulatory regions for the gene activation. Enhancers often interact with TSS to facilitate the transcription of genes involved in cell differentiation, proliferation, and survival. Therefore, the loss of accessibility at enhancers upon BAP1 KD likely contributes



to the transcriptional repression of genes that are essential for maintaining the cellular functions of the cells.

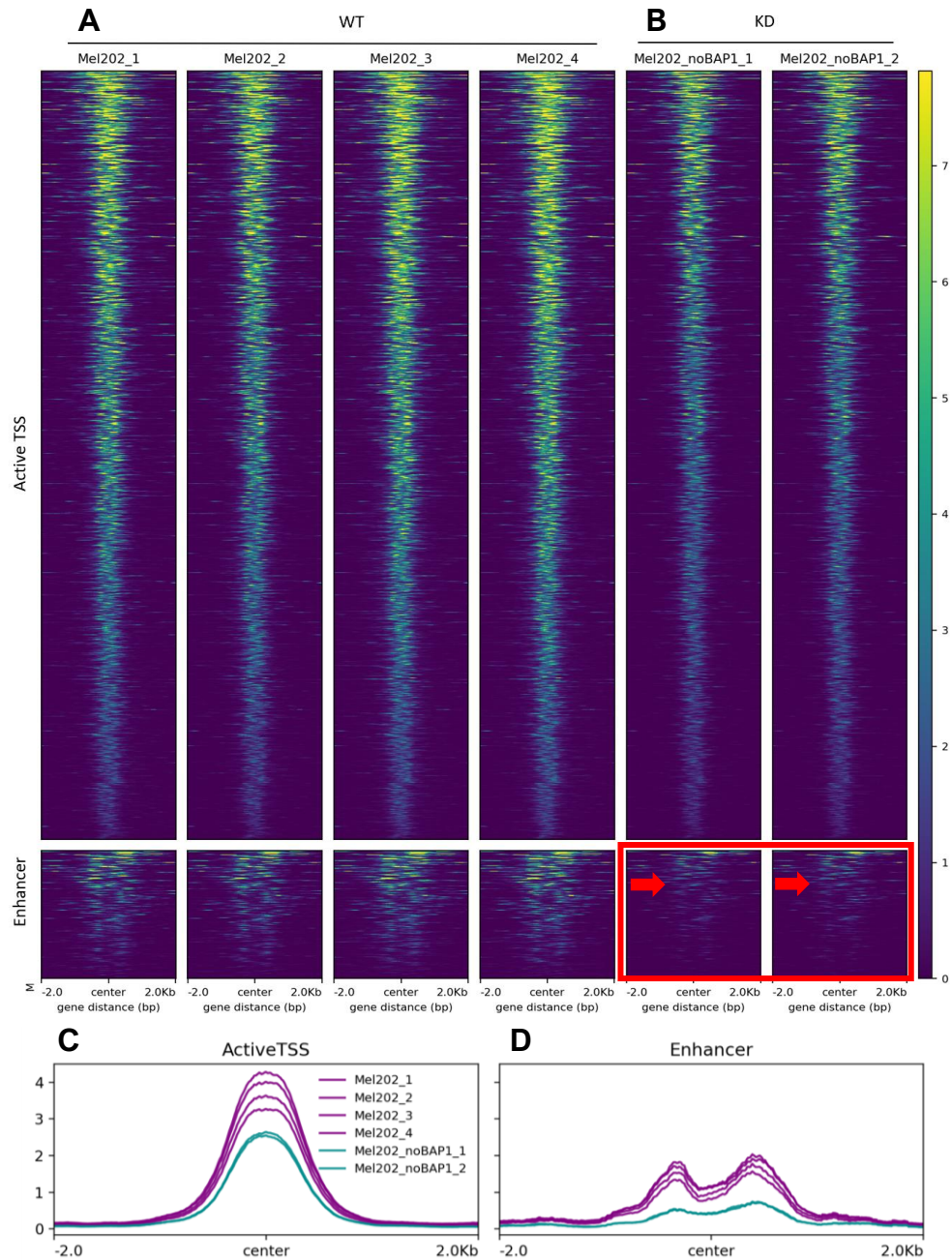


**Figure 70: Chromatin accessibilities decreased at active TSS and Enhancer sites when BAP1 is KD.** (A, B) Heatmaps showing the 4 replicates of MEL202 WT and 2 replicates of MEL202 BAP1 KD conditions are clustered as TSS (top panels) and enhancer (bottom panels). Red arrows within the red rectangle show the reduction of the chromatin accessibility in the KD condition in the 2 replicates. (C, D) Density plot representations of the clusters.



The significant reduction in chromatin accessibility at enhancer regions upon BAP1 loss suggests that BAP1 is essential for keeping these regulatory elements open, enabling the recruitment of transcription factors like TFAP2C as previously discussed. Without BAP1, these enhancers may become less accessible, preventing transcription factors from effectively binding and activating gene expression.

The milder reduction in TSS accessibility indicates that although BAP1 is involved in maintaining accessibility in these regions, its role may be more pronounced at enhancers, which are distant regulatory elements crucial for fine-tuning gene expression. The loss of enhancer accessibility could lead to widespread transcriptional repression, particularly affecting genes involved in critical pathways for cell proliferation and tumor suppression. This could be one of the mechanisms driving the tumorigenic phenotype observed in BAP1-deficient UM cells.

#### **4.8.2. Genome-wide accessibility reductions in Bivalent enhancers following BAP1 loss**

In this section, we explore how BAP1 loss leads to genome-wide reductions in chromatin accessibility, specifically focusing on enhancer regions. Previous analyses have already demonstrated a decrease in chromatin accessibility at active TSS and enhancer regions upon BAP1 KD. To gain further insights into the nature of this loss, we performed a more detailed analysis by stratifying enhancer regions into distinct chromatin states, reflecting their diverse regulatory functions. We classified enhancers into subtypes: Genic Enhancers (Enh\_G1 and Enh\_G2), Active Enhancers (Enh\_A1 and Enh\_A2), Weak Enhancers (Enh\_Wk) and Bivalent Enhancers (Enh\_Biv) (Appendix **Figure 95**).

Bivalent Enhancer (Enh\_Biv) subtype exhibit the most pronounced reduction. **Figure 71** illustrates the heatmap profiles of the chromatin accessibility differences at Bivalent enhancers in the WT and BAP1 KD conditions of UM cells.

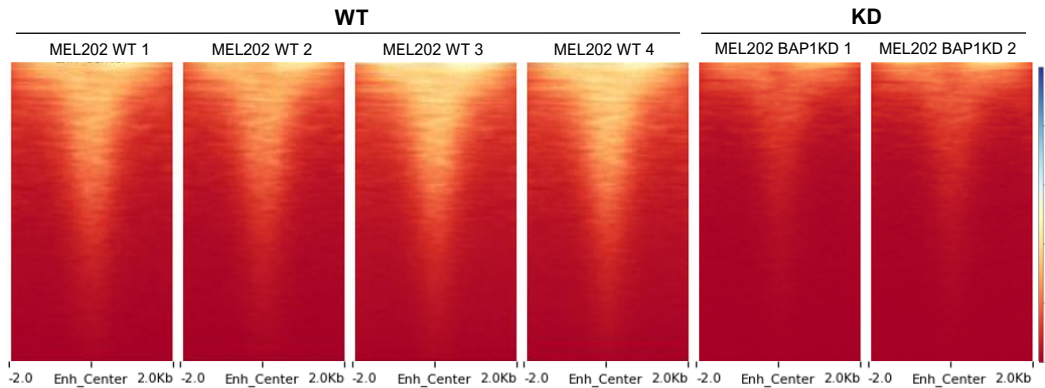


**Figure 71: Chromatin accessibilities shown for the Bivalent Enhancers.** Reduction of the chromatin accessibilities comparing 4 WT, 2 BAP1 KD replicates in MEL202 cells.

Bivalent Enhancers (Enh\_Biv) are characterized by the presence of both active (H3K4me1/3) and repressive (H3K27me3) histone marks, indicating a poised state where the enhancer is primed for activation but remains repressed until specific signals trigger its full activation. These regions are often involved in developmental gene regulation and are crucial for maintaining the balance between gene activation and repression during cellular differentiation (Kumar et al., 2021). The substantial reduction in accessibility at bivalent enhancers upon BAP1 loss suggests that BAP1 plays a critical role in maintaining these enhancers in a poised, accessible state. Without BAP1, these enhancers may become repressed, preventing their activation and leading to the downregulation of genes involved in cell fate decisions and differentiation.

This could contribute to the de-differentiation phenotype often observed in BAP1-deficient tumors, where cells lose their differentiated characteristics and acquire more stem-like, invasive properties. Moreover, the specific loss of accessibility at bivalent enhancers likely disrupts the finely-tuned regulation of genes involved in developmental pathways and cell identity, potentially contributing to the aggressive phenotype seen in BAP1-deficient UM. This suggests that BAP1 functions as a regulator of enhancer activity, and its loss leads to widespread chromatin changes that drive transcriptional dysregulation.

In conclusion, we observed the biggest decrease in chromatin accessibility in the Bivalent enhancers in the KD condition, highlighting the critical role of BAP1 in maintaining chromatin accessibility at these enhancer regions.

#### **4.9. Impact of BAP1 loss on genome-wide histone mark landscape**

We have shown that BAP1 loss leads to alterations in chromatin accessibility, especially at enhancer regions with a reduction in accessibility at bivalent enhancer sites. Also, BAP1 is crucial not only for maintaining open chromatin states but also for the proper regulation of transcription factors like TFAP2A and TFAP2C whose interplay is affected in BAP1-deficient cells. Given these changes in chromatin accessibility, it becomes imperative to examine the epigenetic landscape in BAP1-deficient cells, particularly how histone modifications are altered.

Histone modifications serve as epigenetic signals that define the transcriptional activity of chromatin regions, marking them for activation, repression, or poised states (Zhao et al., 2021). In the context of BAP1 loss, we aimed to explore how histone modifications are altered and how these changes correlate with the transcriptional and chromatin accessibility changes we have observed so far. We performed ChIP-seq experiments focusing on four key histone marks: H3K27ac is associated with active enhancers and TSS regions, H3K4me3 is linked to active promoters, H3K4me1 is associated with enhancer activity particularly marking poised or active enhancers and H3K27me3 is a mark of repressive chromatin particularly involved in the bivalent promoters.

##### **4.9.1. H3K27ac: Divergent effects at TSS and enhancers regions**

We initially aimed to decipher the landscape of H3K27ac, a well-known mark of transcriptionally active regions, including active enhancers and promoter regions. By comparing the distribution and levels of H3K27ac between MEL202 WT and BAP1 KD cells, we aimed to understand how BAP1 loss influences histone acetylation patterns and consequently, transcriptional activity at these key regulatory elements. Our previous analyses have shown a reduction in chromatin accessibility at enhancers and TSS regions in BAP1 KD cells. Here, we explore whether the acetylation of H3K27 at these regions mirrors the changes in chromatin accessibility, particularly at bivalent enhancers, which we previously identified as being particularly sensitive to BAP1 loss. By examining the divergent effects of H3K27ac at both TSS and enhancer regions, we aim to understand

whether BAP1 influences the epigenetic state of these regions, promoting or repressing gene expression through histone acetylation.

**Figure 72** illustrates the changes in H3K27ac levels upon BAP1 loss at mostly changed three chromatin states: active enhancers, flanking TSS regions, and active TSS in MEL202 cells.

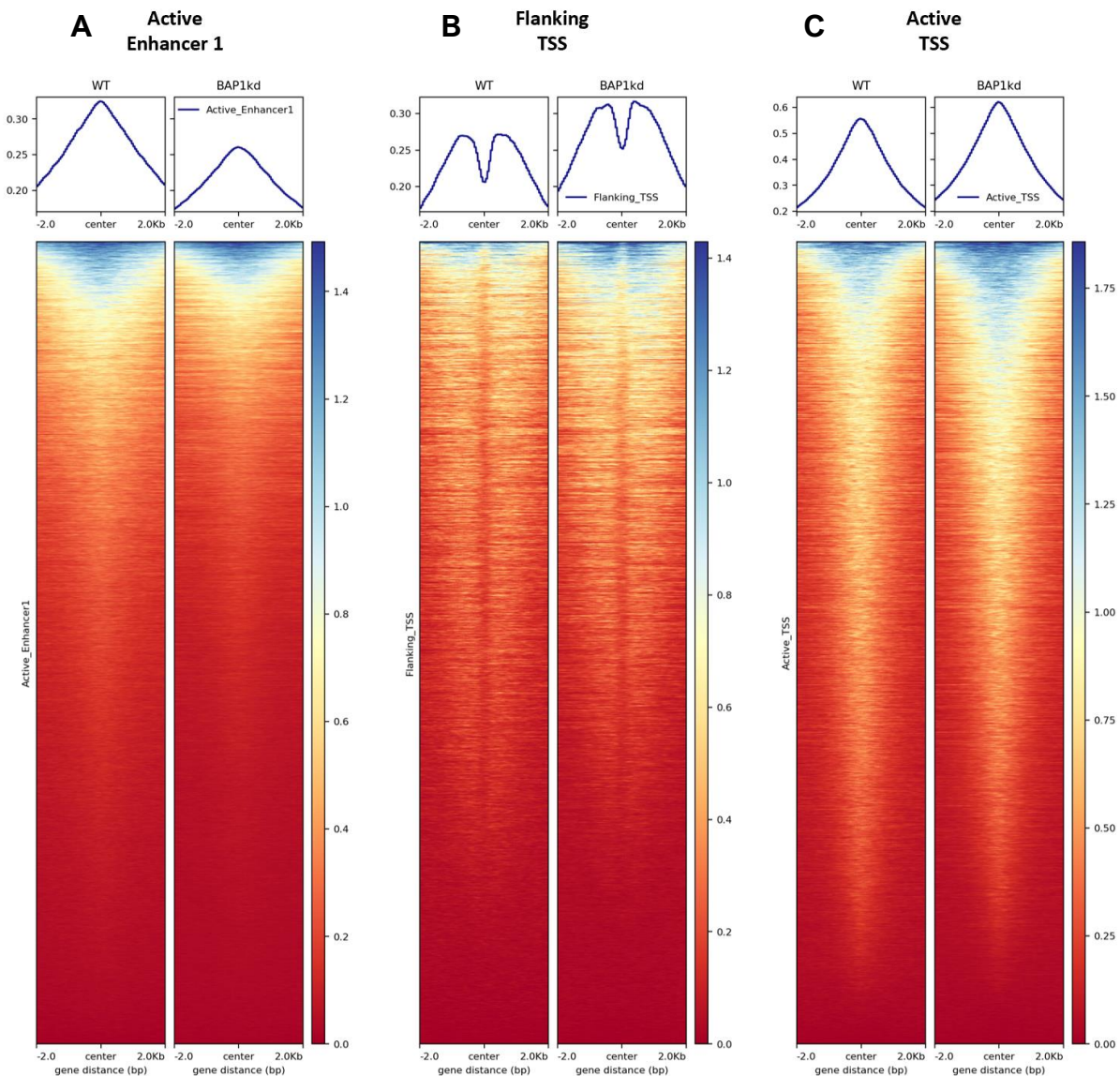


**Figure 72: H3K27ac histone mark profile differences at (A) active enhancers (B) flanking TSS and (C) active TSS sites upon BAP1 loss in MEL202 cells.**

The heatmap and density plot in **Figure 72A** show a reduction in H3K27ac levels at active enhancer regions upon BAP1 KD. In the WT condition, active enhancers exhibit more signals of H3K27ac, which is indicative of their transcriptional activity and their role in gene regulation. However, in BAP1-deficient cells, a decrease in H3K27ac levels is observed, suggesting that BAP1 is essential for maintaining acetylation at these regulatory regions. This decrease in H3K27ac at active enhancers mirrors the reduction in chromatin accessibility previously observed at enhancer regions upon BAP1 loss. The loss of H3K27ac may reflect a repressive chromatin state, resulting in the downregulation of genes controlled by these enhancers. Given the importance of enhancers in regulating biological pathways, the reduction in H3K27ac may contribute to the transcriptional repression of these pathways in BAP1-deficient UM.

Interestingly, **Figure 72B** reveals an opposite trend in H3K27ac distribution at flanking TSS regions. Upon BAP1 KD, an increase in H3K27ac levels is observed in the regions surrounding the TSS. In the WT condition, H3K27ac is already moderately enriched at flanking TSS regions, indicating active transcription. However, following BAP1 loss, this enrichment slightly increases, suggesting that the acetylation of H3K27 is increased around TSS sites, despite the overall loss of chromatin accessibility at these regions. The increase in H3K27ac at flanking TSS regions may represent a compensatory mechanism where transcriptional activity is sustained or enhanced at certain genes in BAP1-deficient cells. This could imply that BAP1 loss results in a selective increase in the activation of TSS-proximal regions, possibly contributing to the upregulation of specific genes. These genes may be involved in oncogenic pathways, allowing BAP1-deficient UM to maintain certain proliferative signals even as broader transcriptional regulation is impaired.

Similarly, **Figure 72C** demonstrates an increase in H3K27ac levels at active TSS upon BAP1 KD. In the WT condition, H3K27ac is enriched at active TSS regions, consistent with its role in promoting active transcription. Upon BAP1 loss, this enrichment is further increased, indicating a heightened acetylation state at the TSS of actively transcribed genes. This observation supports the hypothesis that BAP1 loss may lead to a selective enhancement of transcriptional activity at certain promoter regions, potentially driving the

expression of pro-survival or proliferative genes. The increase in H3K27ac at TSS regions contrasts with the loss of acetylation at enhancers, suggesting that BAP1 may contribute differential regulation of the promoter and enhancer acetylation.

#### 4.9.2. H3K4me3: Active mark suppression at promoters and enhancers

To further understand the epigenetic consequences of BAP1 loss, we next examined the H3K4me3 histone mark, which is predominantly associated with active promoters and TSS regions. H3K4me3 marks are generally enriched at the 5' end of actively transcribed genes, promoting the recruitment of transcriptional machinery and facilitating the initiation of transcription.

**Figure 73** displays the heatmaps and density plots of H3K4me3 across various chromatin states, including active TSS, flanking TSS regions (including up- and downstream), and bivalent TSS regions.

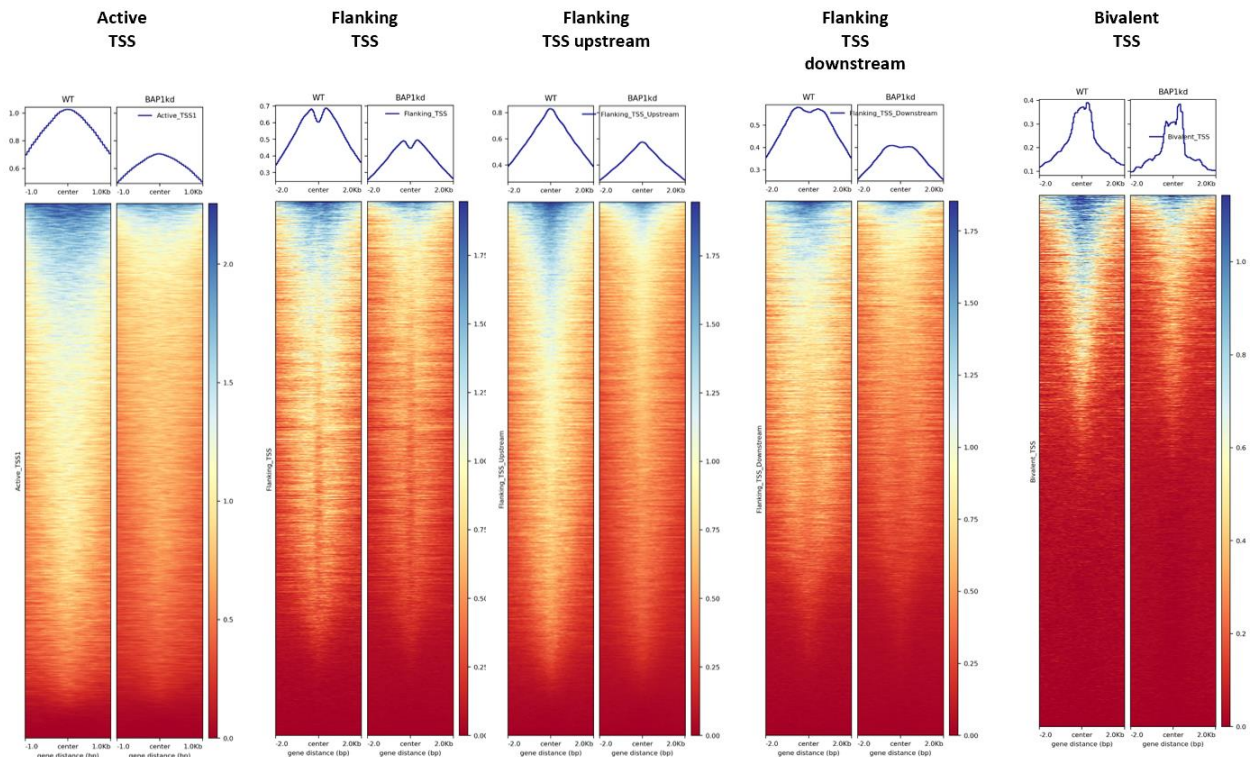


**Figure 73: H3K4me3 histone mark landscapes at active, flanking, and bivalent TSS regions upon BAP1 loss in MEL202 cells.**

Our results indicate a general reduction in H3K4me3 levels upon BAP1 KD, suggesting that BAP1 plays a critical role in maintaining H3K4me3 enrichment at these regulatory regions. As shown in **Figure 73**, the H3K4me3 levels at active TSS and flanking TSS regions significantly decrease upon BAP1 KD. In MEL202 cells, H3K4me3 is highly enriched at active TSS sites (**Figure 73**, left panel), facilitating transcription initiation. However, in the BAP1 KD condition, a substantial reduction in H3K4me3 is observed, suggesting that BAP1 is required to maintain promoter activity through this histone mark. H3K4me3 levels at flanking TSS sites (**Figure 73**, both upstream and downstream) are reduced following BAP1 loss. These reductions indicate that BAP1 loss not only impacts core promoter regions but also surrounding chromatin, which may further contribute to transcriptional repression in BAP1-deficient cells.

Interestingly, **Figure 73** also shows a reduction in H3K4me3 at bivalent TSS regions. Bivalent promoters, marked by both H3K4me3 (active) and H3K27me3 (repressive) histone marks, are poised for activation but remain repressed until specific signals activate them. In the WT condition, H3K4me3 is enriched at bivalent TSS sites, indicating a poised state ready for transcriptional activation. However, upon BAP1 KD, H3K4me3 levels are diminished, suggesting that BAP1 helps maintain the poised state at bivalent promoters, possibly allowing for the timely activation of differentiation-related genes. The loss of H3K4me3 at these sites may lead to gene silencing and the failure of proper differentiation pathways, contributing to the aggressive phenotype of BAP1-deficient UM case.

**Figure 74** highlights the H3K4me3 distribution at genic enhancers. Here, we observe a similar reduction in H3K4me3 levels at these enhancer regions in BAP1 KD cells, further supporting the role of BAP1 in maintaining active histone marks at both enhancers and TSS regions. In WT cells, H3K4me3 has an enrichment at genic enhancers, contributing to their activation and the regulation of nearby genes. However, this enrichment is slightly decreased lost upon BAP1 knockdown, suggesting that BAP1 has a contribution for maintaining the active enhancer state and its loss may lead to decreased enhancer activation and subsequent transcriptional repression.



The reduction in H3K4me3 levels at both promoters and enhancers has profound implications for the transcriptional landscape. H3K4me3 is essential for marking active gene regions, and its loss indicates a shift toward transcriptional repression. This suppression of active histone marks likely contributes to the downregulation of pathways, including those involved in tumor suppression, cell cycle control. The loss of H3K4me3 at bivalent promoters may further intensify this effect by preventing the activation of developmental genes, contributing to the dysregulation in differentiation process promoting invasive phenotype of BAP1-deficient UM cells.

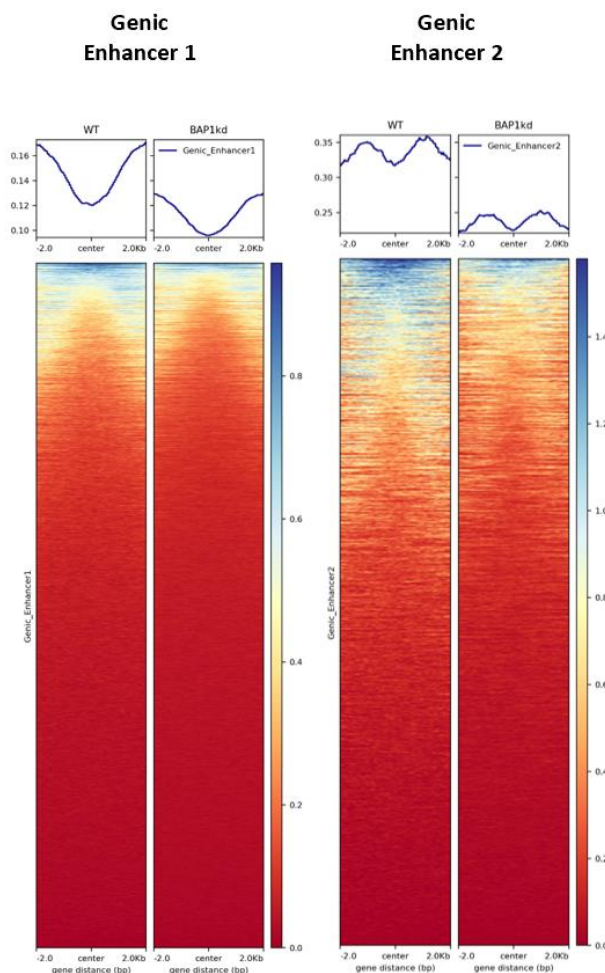


**Figure 74: H3K4me3 histone mark landscapes at genic enhancers.**

As an example for the changes of active histone marks, we selected *DNMT1* gene from the BAP1-bound DEG list from our cell line experiment. We assessed the epigenetic landscape of the gene using ChIP-seq, RNA-seq, and ATAC-seq under both WT and BAP1



KD conditions in MEL202 cells. Our analysis focused on two key histone marks, H3K27ac and H3K4me3, as well as transcription factors TFAP2A and TFAP2C, to evaluate the changes in chromatin state and transcriptional activity following BAP1 loss (**Figure 75**).

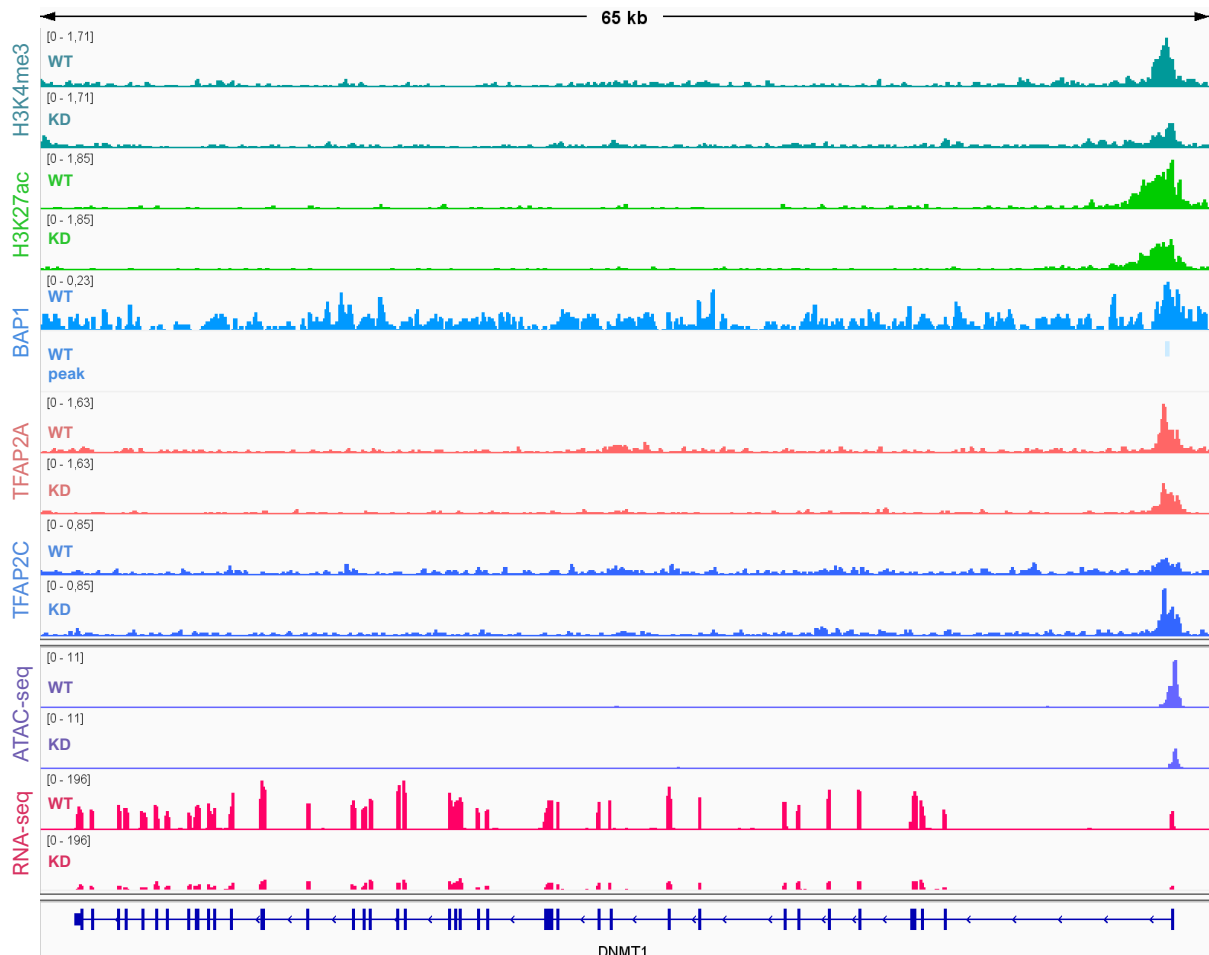


**Figure 75: Representative image from the IGV browser showing ChIP-seq (H3K4me3, H3K27ac, H3K4me1, BAP1, TFAP2A, TFAP2C), RNA-seq and ATAC-seq results of *DNMT1* gene in MEL202 WT and BAP1 KD conditions.**

H3K27ac active enhancer mark and H3K4me3 active promoter show a decrease in the KD condition around the *DNMT1* promoter region possibly reflecting reduced transcriptional efficiency or a shift in the chromatin state towards a more poised or repressed state. BAP1 ChIP-seq data revealed binding of BAP1 at the *DNMT1* promoter in WT condition, further emphasizing BAP1's regulatory role in maintaining chromatin accessibility and transcriptional activity at this locus. Upon BAP1 KD, we observed a corresponding

decrease in chromatin accessibility as indicated by ATAC-seq signals, supporting the idea that BAP1 is essential for maintaining an open chromatin configuration. This decrease in accessibility is consistent with the downregulation of *DNMT1* transcription, as seen in the RNA-seq data, which shows reduced expression of *DNMT1* in the BAP1-deficient cells.

TFAP2A and TFAP2C binding patterns further elucidate the potential regulatory impact of BAP1 loss. Under WT and KD conditions, TFAP2A binding was detectable at the *DNMT1* locus, having slight decrease upon BAP1 loss. On the other hand, we observed increased TFAP2C binding after BAP1 knockdown, indicating a potential compensatory mechanism or shift in the transcriptional regulation. This binding switch may reflect the loss of BAP1's stabilizing influence on chromatin architecture.

These results highlight the complex interplay between BAP1, histone modifications, and TFAP2A / TFAP2C transcription factors in regulating *DNMT1* expression. The decreased H3K27ac and H3K4me3 levels and altered TFAP2C binding suggest that BAP1 loss induces a chromatin environment favoring transcriptional repression potentially leading to dysregulated gene expression.

#### **4.9.3. H3K4me1: Reductions predominantly at enhancer sites**

We further investigated the H3K4me1 histone mark, which is primarily associated with enhancer activity. H3K4me1 marks are enriched at enhancers, particularly at poised enhancers, where they signal regulatory regions that are primed for transcriptional activation but may not yet be fully active. This mark plays a critical role in the activation of enhancers and their ability to regulate target gene expression.

**Figure 76** shows the heatmaps and density plots of H3K4me1 levels at active enhancers and genic enhancers in MEL202 and BAP1 KD cells. The data demonstrate a decrease in H3K4me1 levels at these enhancer regions upon BAP1 KD, suggesting that BAP1 plays a role in maintaining the poised and active enhancer states.

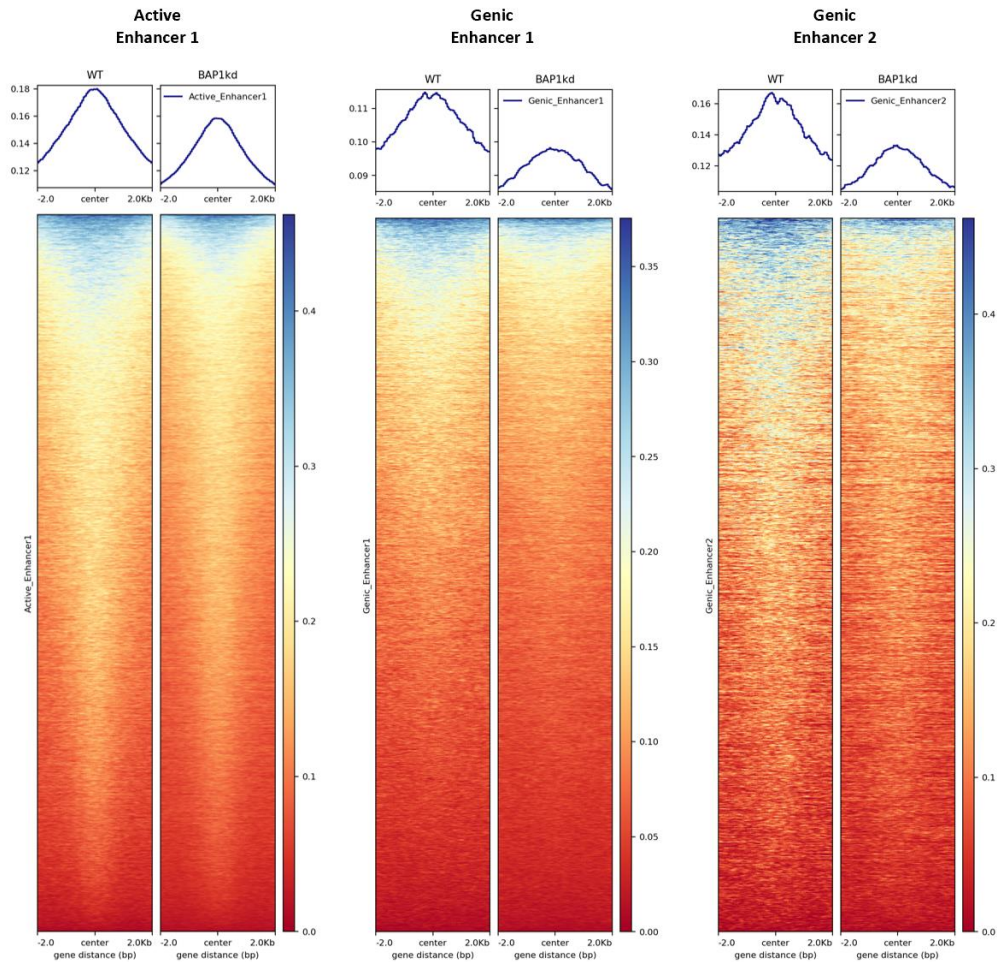


**Figure 76: H3K4me1 histone mark profiles show decreased patterns at enhancers upon BAP1 loss.**

The left panel of **Figure 76** illustrates the changes in H3K4me1 at active enhancers. In WT MEL202 cells, H3K4me1 is robustly enriched at these enhancers, indicating that these regions are primed for activation or are already contributing to gene expression regulation. However, following BAP1 knockdown, a reduction in H3K4me1 is observed at these enhancers. This reduction in H3K4me1 suggests that BAP1 is essential for maintaining the active state of enhancers or for ensuring that enhancers remain poised for activation. The loss of H3K4me1 at active enhancers may lead to dysregulation of the genes regulated by these enhancers, contributing to the transcriptional silencing of critical pathways.

H3K4me1 levels at genic enhancers (**Figure 76**, middle and right panels) also show a decrease upon BAP1 loss. Genic enhancers play a vital role in regulating gene expression by interacting with promoters and facilitating transcriptional activation. In the WT condition,

H3K4me1 is enriched at genic enhancers, marking that these regions are poised to regulate gene expression. However, in BAP1 KD cells, this enrichment decreased, suggesting a lesser extent of activation of the genic enhancers. The reduction in H3K4me1 at genic enhancers likely leads to the loss of transcriptional regulation at target genes. Since genic enhancers also regulate genes involved in cell identity and tumor suppression, the reduction of H3K4me1 could have profound effects on tumor progression in BAP1-deficient UM cells.

The reduction in H3K4me1 levels across active and genic enhancers suggests that BAP1 loss impairs the ability of enhancers to remain poised or active, leading to a loss of transcriptional activation. Enhancers marked by H3K4me1 are often critical for controlling long-range gene regulation, influencing genes located far from the enhancer itself. The reduction in H3K4me1 likely disrupts this regulatory network, causing widespread dysregulation in gene expression.

#### **4.9.4. H3K27me3: Subtle increases at bivalent promoters**

In this section, we analyzed the repressive histone mark H3K27me3, which is deposited by Polycomb Repressive Complex 2 (PRC2) and plays a key role in gene silencing and chromatin compaction. H3K27me3 is frequently found at bivalent promoters, which are marked by both active (H3K4me3) and repressive (H3K27me3) histone marks. These promoters are poised for activation but remain repressed until specific signals trigger their activation.

The data presented in **Figure 77** demonstrate that H3K27me3 levels increase slightly at bivalent TSS regions following BAP1 knockdown. In the WT condition, bivalent promoters maintain a balance between activation and repression, upon BAP1 loss, the increase in H3K27me3 could suggest a reinforcement of the repressive chromatin state, potentially preventing the activation of the related genes regulated by these promoters.

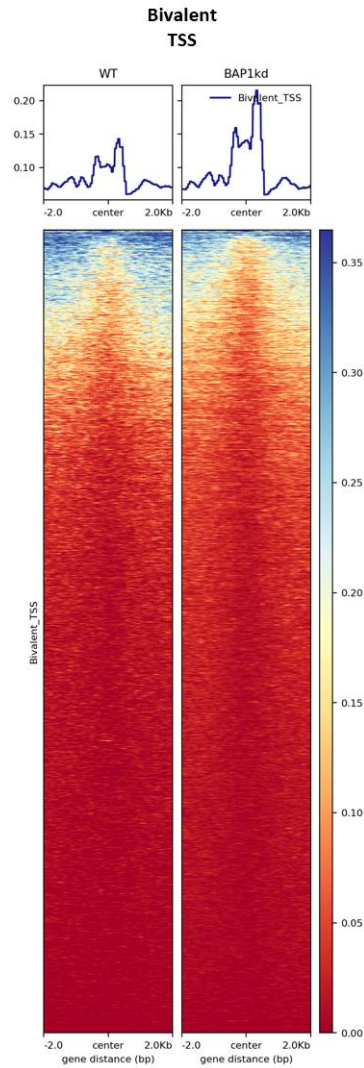


**Figure 77: H3K27me3 repressive histone mark profile showing a decrease at bivalent TSS upon BAP1 loss.**

Bivalent promoters are critical regulatory regions that often control genes involved in cell fate determination and developmental pathways. The subtle increase in H3K27me3 at these sites indicates a shift toward gene silencing, which could prevent the proper activation of tumor suppressor genes or differentiation pathways.

The increase in H3K27me3 at bivalent promoters may be driven by the Polycomb Repressive Complex 2 (PRC2), which is responsible for depositing this mark. In BAP1-deficient cells, the loss of BAP1's regulatory influence may result in PRC2 overactivity, leading to the increased deposition of H3K27me3. This would reinforce gene repression at bivalent promoters, thereby preventing the expression of key regulatory genes that

could counteract tumorigenesis. This increase in H3K27me3 at bivalent promoters suggests that BAP1 loss tilts the balance at these regulatory elements toward a repressive chromatin state. This could result in the failure of critical genes to become activated. As H3K27me3 is associated with long-term gene silencing, the increase in this mark at bivalent promoters may have significant consequences for the epigenetic landscape of BAP1-deficient UM, promoting an environment conducive to tumor progression.

The observed increase in H3K27me3 at bivalent promoters sets the stage for understanding the antagonistic effect of Polycomb Repressive Complex 1 (PRC1) member RING1B, which is the focus of the next section. While PRC2 is responsible for depositing H3K27me3, PRC1, and specifically RING1B, plays a crucial role in maintaining gene repression through chromatin compaction and ubiquitination of histones. The increase in H3K27me3 upon BAP1 loss may enhance PRC1 activity, leading to further repression of key genes.

#### **4.10. Antagonistic effect of PRC1 member RING1B reveals differential genome-wide occupancy**

In this section, we aim to explore the antagonistic relationship between BAP1 and the Polycomb Repressive Complex 1 (PRC1) member RING1B (RNF2). RING1B is part of the PRC1 and is known to maintain repressive chromatin states through the ubiquitination of histone H2A at lysine 119 (H2AK119ub) (Tamburri et al., 2020). Given the role of BAP1 in chromatin regulation and its previously observed counteractions with Polycomb proteins (Conway et al., 2021), we performed ChIP-seq experiments to assess the genomic distribution of RING1B. Our goal was to determine the influences of the binding patterns of RING1B, potentially leading to differential regulation of gene expression and chromatin accessibility.

Our analysis of RING1B binding distribution across different chromatin states in MEL202 WT reveals significant enrichment of RING1B at the repressed Polycomb regions and bivalent/poised TSS sites, consistent with the known role of RING1B in gene repression.

**Figure 78A** shows that RING1B binding sites are predominantly located in repressed Polycomb regions (63.2%). Also, Enhancers (13.51%), TSS (10.31%), and Bivalent promoters (9.13%) were marked by RING1B.

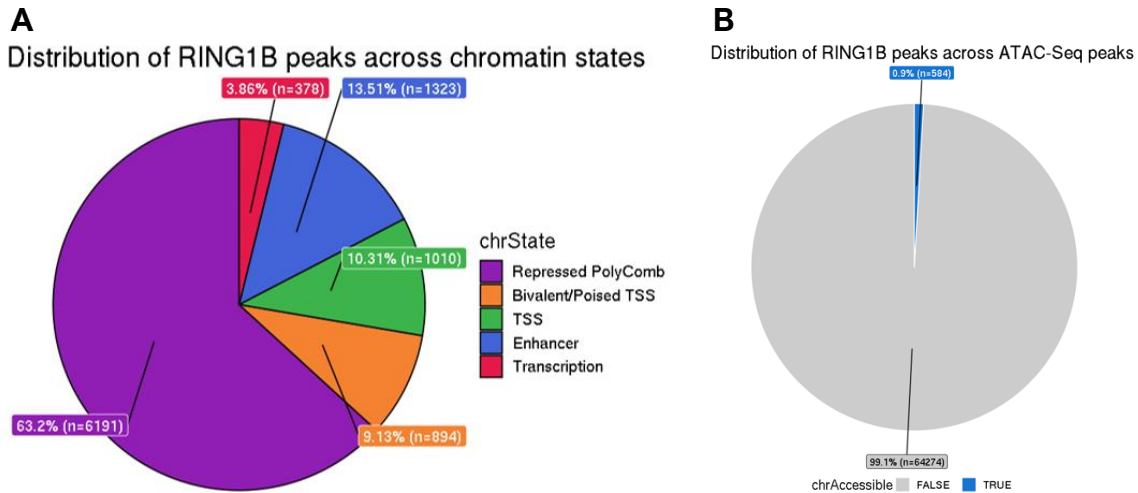


**Figure 78: Distribution of RING1B peaks (A) across the chromatin states, (B) ATAC-seq peaks.**

This suggests that RING1B plays an essential role in maintaining the repressed state of Polycomb target genes in the UM cells. ATAC-seq analysis (**Figure 78B**) reveals that the vast majority of RING1B-bound regions are located in inaccessible chromatin states (99.1%), further supporting the role of RING1B in maintaining repressive chromatin structures and silencing gene expression. These findings are in alignment with the increased H3K27me3 levels observed earlier at bivalent promoters, where RING1B likely interacts with PRC2-deposited H3K27me3 to reinforce gene repression.

While the expression TPM level of *RING1B* (Appendix **Figure 94**) does not display a significant change ( $|\log_{2}FC| < 1$ ) in the BAP1 KD condition, this does not detract from the crucial regulatory interplay observed. We further explored the binding counteraction of BAP1 and RING1B. **Figure 79** illustrates a heatmap showing the binding patterns of BAP1 and RING1B in MEL202 WT cells. The data highlight regions where BAP1 and RING1B binding overlap, as well as regions where their binding patterns are distinct. In WT cells, the very small region where BAP1 and RING1B binding overlap is consistent with the functional antagonism between these two proteins. While BAP1 may facilitate chromatin decompaction and gene activation, RING1B likely promotes chromatin compaction and

gene repression. The presence of unique binding sites for both BAP1 and RING1B suggests that BAP1 and RING1B may exert distinct regulatory effects at specific genomic loci, potentially competing for control over certain regions of chromatin.



**Figure 79: Counteracting binding patterns of PRC1-member RING1B in the antagonism of BAP1 in MEL202 cells.**



This antagonism between BAP1 and RING1B could regulate key pathways involved in tumorigenesis and cell fate determination in UM. In summary, the findings from **Figure 79** suggest that BAP1 and RING1B have antagonistic roles in regulating chromatin states and gene expression. The loss of BAP1 also disrupts this balance. The antagonism could be particularly important at bivalent promoters, where RING1B might outcompete BAP1 for chromatin binding, tipping the balance toward gene repression. The antagonistic BAP1-RING1B interplay also appears to regulate the activity of critical genes in BAP1-deficient UM.

## Chapter 5: Discussion

Uveal melanoma (UM) is the most common primary intraocular malignancy in adults and presents significant clinical challenges due to its aggressive metastatic potential and limited therapeutic options. This malignancy arises from melanocytes within the uveal tract of the eye, which originate from neural crest cells (NCCs). The distinct biological behavior of these melanocytes, compared to their cutaneous counterparts, can be attributed to their unique developmental pathways and migration patterns during embryogenesis. The developmental origins and epigenetic modifications of uveal melanocytes contribute to their heterogeneity and susceptibility to oncogenic transformation. Such variations may underlie the diverse oncogenic drivers observed in UM and are influenced by both genetic and epigenetic factors.

Studies have shown that the plasticity of melanocytes, driven by stem cell-like properties and neural lineage markers, is associated with the heterogeneity, treatment resistance, and varying clinical outcomes observed in melanoma (Larribere et al., 2018, Larribere and Utikal, 2019, Johannessen et al., 2013). These characteristics highlight UM as a complex and unique malignancy that warrants a deeper understanding of its underlying molecular mechanisms.

At the genomic level, UM is characterized by mutations in the driver genes *GNAQ* and *GNA11*, which are pivotal in the early stages of UM development. However, the progression and metastatic potential of UM are driven by secondary mutations in genes such as *BAP1*, *SF3B1*, and *EIF1AX*. Among these, *BAP1* mutations, along with Monosomy 3, are strongly correlated with poor prognosis and increased metastatic risk, particularly to the liver, which is the site of metastasis in up to 90% of metastatic UM cases. This high metastatic propensity highlights the urgent need to identify novel molecular targets and pathways that contribute to UM progression.

This thesis explores the gene regulatory networks and epigenetic landscapes affected by *BAP1* loss in UM, aiming to provide insights into the mechanisms that drive the aggressive nature of this cancer. Specifically, we examined genome-wide transcriptional changes,

histone modifications, chromatin accessibility, and transcription factor binding in BAP1-wild type versus BAP1-knockdown conditions to identify critical molecular pathways influenced by BAP1 loss.

Our findings not only elucidate how BAP1 regulates transcriptional and epigenetic reprogramming in UM but also highlight the novel interplay between pioneering transcription factors and chromatin accessibility upon BAP1 loss. This work identifies key molecular pathways that could serve as therapeutic targets, offering new avenues for research and treatment strategies in BAP1-mutant uveal melanoma.

### **5.1. Aim 1: Genome-wide effects of BAP1 loss on gene expression, chromatin accessibility and histone mark profiles in UM cells**

To comprehensively understand the role of BAP1 in regulating gene expression and epigenetic factors, we investigated the genome-wide effects of BAP1 loss on the transcriptional profiles, chromatin accessibility, and histone modifications in UM cells. As a known tumor suppressor and epigenetic regulator, BAP1 depletion is associated with changes in gene expression (Masclef et al., 2021, Fursova et al., 2021) and epigenetic regulation (Conway et al., 2021, Mo et al., 2021) that may drive tumorigenesis. Here, we systematically explored how BAP1 deficiency reshapes these molecular landscapes, providing insights into the mechanistic underpinnings of its tumor-suppressive functions in UM.

In our study, we modeled the MEL202 UM cell line and validated the presence of BAP1 protein in these cells using Western blotting with the BAP1 (sc-28383, C4) antibody clone. While the theoretical molecular weight of BAP1 is approximately 91 kDa, we observed a band around 100 kDa. This slight difference in the observed molecular weight could be attributed to several factors, including the type of protein ladder used and variations in gel running conditions. Additionally, the manufacturer's datasheet indicates BAP1 bands in the 90 - 100 kDa range across different experimental conditions and cell lines (Appendix **Figure 86** and Appendix **Figure 87**), supporting the observed shift in its apparent size. BAP1 is also known to undergo post-translational modifications, such as phosphorylation

and ubiquitination, which can alter its molecular weight and affect its migration pattern in SDS-PAGE gels. Also, the observed localization pattern of BAP1 is consistent with the profile of BAP1 via its nuclear localization signal, confirming its presence in MEL202 cells and supporting the validity of the experimental approach used in our study.

#### **5.1.1. Modulation of gene expression and transcriptomic programs in BAP1-deficient UM**

BAP1 (BRCA1-associated protein 1) is a tumor suppressor and epigenetic regulator, whose loss is associated with poor prognosis especially in the Monosomy 3 subtype of UM carrying a high metastatic risk. Previous studies have suggested BAP1's roles in chromatin modification (Scheuermann et al., 2010), regulation of gene expression (Okino et al., 2015), regulation of cell cycle (Machida et al., 2009) and genomic stability (Zhao et al., 2017, Nishikawa et al., 2009). Our findings reinforce these studies. Further, we show the way that BAP1 predominantly binds to active regulatory regions especially TSS and enhancers in MEL202 UM cells.

Moreover, we show that BAP1 has a major association with CpG islands (CGIs) compared to other CpG regions such as shores, shelves, and inter-CGI (open sea) regions. The spatial distribution of BAP1 across the genome suggests that it plays a critical role in regulating gene expression at CGI-enriched sites, potentially acting as an epigenetic modulator to maintain the transcriptional integrity of these regions, as represented in **Figure 80**. This suggests that BAP1 is integral to controlling gene expression programs on CpG islands potentially suppressing the aggressive characteristics not only transcriptionally but also epigenetically, reinforcing its critical tumor-suppressive functions in UM.

Loss of BAP1 led to transcriptional dysregulation in MEL202 cells, with a total of 1339 differentially downregulated and 1445 differentially upregulated genes identified (**Figure 44**). Differentially downregulated genes were predominantly enriched in pathways associated with cell cycle control and DNA damage response, both of which are critical for maintaining genomic integrity and preventing uncontrolled proliferation.

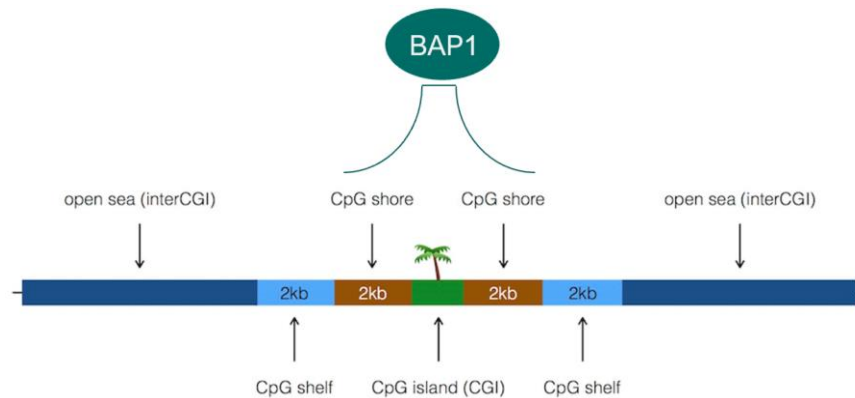


**Figure 80: Location of the BAP1 binding sites majorly at CGIs compared to CpG shore, shelf, and inter CGI regions on the genome.** Adapted from (Cavalcante, 2017).

As we showed in the plot, *BRCA1* which is a crucial gene in homologous recombination repair was significantly downregulated aligning with previous findings showing BAP1's involvement in maintaining genomic stability (Savage and Harkin, 2015). The reduction in *RAD51* expression further supports the notion of impaired DNA repair mechanisms in BAP1-deficient cells (Zhao et al., 2017). Also, *DNMT1* DNA methyltransferase showed decreased expression, suggesting potential dysregulation of DNA methylation patterns in the absence of BAP1. This can contribute to widespread epigenetic reprogramming, thereby promoting a more oncogenic phenotype. *MITF* is a master regulator of melanocyte development and its downregulation suggests that BAP1 may play a role in maintaining melanocytic identity and differentiation (Seberg et al., 2017a). The concurrent decrease in *FGFR1* and *LGR4*, both of which are involved in growth factor signaling may indicate that BAP1 loss disrupts signaling pathways crucial for cell proliferation and survival (Krook et al., 2021, Ordaz-Ramos et al., 2021).

Conversely, upregulated genes were significantly enriched in pathways related to transcription factor activity and DNA-binding processes, which are often linked to transcriptional reprogramming events during tumor progression. For example, *HDAC9*, *HDAC5* and *SATB1* are both involved in chromatin remodeling and gene regulation showed increased expression suggesting a shift towards a more repressive chromatin state (Zhao et al., 2021). This observation aligns with the enhanced expression of *KLF9* and *CPEB4*, transcriptional regulators are known to promote cell survival and

differentiation under stress conditions (Zhong et al., 2018, Wang et al., 2018). The upregulation of *JUN* and *TXNIP* indicates that BAP1 loss may lead to the activation of stress response pathways and redox homeostasis (Deng et al., 2023). JUN is a component of the AP-1 transcription factor complex and it is known to be involved in cell proliferation, differentiation and apoptosis further highlighting the aggressive phenotype observed in BAP1-deficient UM cells (Lin et al., 2023).

Our pathway network analysis further validated that these transcriptional changes are part of an interconnected regulatory network influenced by BAP1. The observed downregulation of cell cycle and DNA repair-related genes upon BAP1 loss may reflect a disrupted genomic stability mechanism, predisposing cells to increased genomic instability and promoting oncogenesis. Conversely, the upregulation of transcription factor activity and DNA-binding genes suggests a compensatory response to the loss of BAP1, possibly driving alternative transcriptional programs that favor tumor progression. Thus, these findings align with the literature on BAP1 in maintaining genome stability (Kwon et al., 2023) and suggest that its loss triggers widespread transcriptional reprogramming in UM.

Then, we compared our findings from the DEGs of MEL202 / BAP1 KD condition with the UM patient cohort to assess the relevance of our cell line model to the clinical UM samples and to understand whether the gene expression changes observed in MEL202 cells upon BAP1 loss reflect similar alterations in the UM patient cohort. Establishing this overlap allowed us to identify which genes are affected by BAP1 loss across different settings, thereby providing a better understanding of BAP1's role in UM pathogenesis in both *in vitro* and clinical contexts. We observed an overlap of 126 DEGs of which 15 were consistently upregulated and 55 were consistently downregulated in both the cell line and the patient cohort. These shared gene expression changes may suggest that the MEL202 BAP1 KD cell model partially recapitulates certain transcriptional alterations observed in the BAP1-deficient UM patient cohort.

Common differentially downregulated genes both in MEL202 BAP1 KD cell line condition and BAP1-deficient (M3) UM patient cohort shown in **Figure 46** provided us with valuable

insights into the roles of genes such as *FGF2*, *GATA4*, *MIA*, *RASD1*, *HTN1* which are implicated in diverse cellular processes including growth signaling, transcriptional regulation, tumor suppression, and stress response pathways. *FGF2* (Fibroblast Growth Factor 2) is essential for cell proliferation, angiogenesis, and wound healing. Its downregulation upon BAP1 loss could disrupt normal cell proliferation and survival, contributing to the more aggressive phenotype observed in BAP1-deficient UM cells (Wang et al., 2022). The reduced *FGF2* expression in M3 patients would mirror the findings in MEL202 BAP1 KD, further reinforcing its role in tumor suppression. *GATA4* is a member of the GATA transcription factor family and is involved in cell differentiation as well as organ development (Gong et al., 2018). In the context of UM, its downregulation may impair the transcriptional regulation of critical pathways of cell differentiation and response to stress. *MIA* (Melanoma Inhibitory Activity) is known to inhibit melanoma growth and progression (Sasahira et al., 2018). The observed reduction in both MEL202 KD cells and M3 patients likely removes this inhibitory effect, allowing for uncontrolled melanoma progression. *RASD1* (Ras-related dexamethasone-induced 1) is involved in MAPK signaling and stress response (Gao et al., 2017). Its downregulation following BAP1 KD suggests a dysregulation in MAPK signaling, which could alter the cellular stress response and contribute to tumor progression in UM. *HTN1* (Histatin 1) is known for its role in wound healing and antimicrobial activity, downregulation of this gene could reduce the tissue's ability to repair damage, thus facilitating tumor invasiveness (Torres et al., 2018).

Common differentially upregulated genes observed in both the MEL202 BAP1 KD cell line condition and the BAP1-deficient (M3) UM patient cohort, as illustrated in **Figure 47**, revealed critical insights into the roles of genes such as *CLIC2*, *GNAT3*, *MAP2*, and *RAPGEF4*. These genes are associated with diverse biological processes, including ion transport, signal transduction, cytoskeletal organization, and cell proliferation, all of which are potentially contributing to tumor-promoting signaling pathways in the absence of BAP1. *RAPGEF4* (Rap guanine nucleotide exchange factor 4) is involved in regulating cyclic AMP (cAMP) signaling pathways which are critical for controlling cellular growth and differentiation (Sugawara et al., 2016). Its upregulation upon BAP1 loss might enhance

cAMP-mediated tumor-promoting signals in UM, thus contributing to UM cell survival and proliferation. *MAP2* (Microtubule-associated protein 2) is a cytoskeletal protein that stabilizes microtubules, essential for cell structure and division (Dehmelt and Halpain, 2005). Its upregulation in BAP1-deficient cells suggests a role in enhancing cell motility, a key aspect of tumor metastasis. *GNAT3* (Guanine nucleotide-binding protein G(T) subunit alpha-3) plays a role in signal transduction processes, particularly within sensory systems (Hoffman et al., 2021). While its direct role in UM is less clear, its significant upregulation may indicate an involvement in abnormal signaling pathways. *CLIC2* (Chloride intracellular channel 2) is involved in chloride ion transport and has been implicated in the regulation of cell cycle and apoptosis (Ozaki et al., 2022). The increased expression of *CLIC2* in BAP1 KD and M3 patients suggests that it might help maintain tumor cell homeostasis, allowing UM cells to evade apoptosis and promote survival.

While these overlaps in the differentially up and down regulated genes indicate that certain gene expression changes are shared between the cell line and patient cohort, it is important to acknowledge the limitations of this model. Firstly, the MEL202 cell line originates from a primary malignancy and represents a primary tumor context, whereas our UM patient cohort was derived from metastatic UM tissues. Moreover, the patient samples were obtained from tumor tissues, which include infiltrating immune cells and tumor microenvironment components which are the factors that are absent in an *in vitro* cell culture model. Additionally, the patient-derived samples inherently reflect the complexities of *in vivo* conditions, such as cellular interactions and signaling within the microenvironment. As a result, the observed overlap in DEGs between the MEL202 model and patient samples. While we compared the DEGs from both conditions, still they may not fully capture the diverse regulatory networks active in the UM patient cohort tumors. Despite these constraints, our findings highlight the shared transcriptional changes that are relevant across both models, suggesting that MEL202 BAP1 KD cells can serve as a useful but limited system to study BAP1 loss in UM, with the potential to inform about specific regulatory mechanisms conserved in BAP1-deficient UM cases.



### 5.1.2. Gene expression changes annotated with BAP1-binding

While the previous section discussed the general transcriptomic changes upon BAP1 and the overlap between the MEL202 cell line and UM patient cohort, this section focuses specifically on the DEGs of MEL202 cells directly bound by BAP1. This distinction allows us to delineate the transcriptional impact of BAP1-binding and how its loss leads to the dysregulation of these specific genes and their associated pathways.

To gain a deeper understanding of the direct impact of BAP1-binding on gene regulation in UM, we examined the expression profiles of genes that are bound by BAP1 under WT conditions but become differentially expressed upon BAP1 KD as presented in **Figure 56**. Downregulation of the BAP1-bound genes such as *PMEL*, *DNMT1*, *BRCA1*, *MCM4*, and *FGFR1* as well as histone core subunit-related genes *HIST3H2BB*, *HIST1H2BN*, *HIST2H3A* in BAP1-deficient MEL202 cells highlights the profound influence of BAP1-binding on regulating key cellular processes, including chromatin remodeling, transcriptional regulation, and DNA repair. Their suppression upon BAP1 loss could contribute to the increased genomic instability typically observed in UM and other cancers associated with BAP1 mutations. On the other hand, upregulation of genes such as *HDAC9*, *MBD5*, *MDM2*, and *SOCS2* might suggest compensatory mechanisms that cells activate in response to chromatin or transcriptional disruptions caused by BAP1 depletion. For example, MDM2 is a key regulator of p53 and its increased expression could point to a stress response triggered by the loss of BAP1's tumor suppressive functions.

The observation that BAP1-bound genes are not simply passive markers but actively respond to BAP1's loss points to a broader mechanism of transcriptional dysregulation in UM. This alteration in gene expression profiles could contribute to a shift in the transcriptional landscape, thereby promoting tumor progression and highlighting the potential oncogenic consequences of BAP1 loss in UM cells.

### **5.1.3. Chromatin accessibility, histone modification landscape and repressive chromatin states**

BAP1's impact on gene regulation extends beyond transcriptional activity to chromatin structure, influencing both chromatin accessibility and histone modifications. Epigenetic alterations such as histone modifications and chromatin compaction are known to emerge early in cancer development and accumulate as the disease progresses (Fraga et al., 2005). Our study demonstrates that BAP1 loss leads to genome-wide changes in chromatin accessibility and histone modifications, particularly at transcription start sites and enhancer regions, which are critical regulatory elements for gene expression.

Upon BAP1 loss, ATAC-seq analysis revealed a significant reduction in chromatin accessibility, especially at enhancer regions, indicating that BAP1 is essential for maintaining an open chromatin state at these regulatory regions. Enhancers are key elements that control gene expression by facilitating the interaction between distal regulatory elements and promoters, thereby promoting transcriptional activation (Hon et al., 2009). The genome-wide reduction in enhancer accessibility observed in BAP1-deficient cells likely leads to the silencing of genes involved in cellular differentiation, proliferation, and survival, contributing to the aggressive phenotype of UM. This is consistent with the transcriptional reprogramming seen in BAP1-deficient tumors, where disruption of enhancer function alters the expression of genes associated with tumor suppression and progression.

In addition to chromatin accessibility, BAP1 loss results in widespread changes in histone modifications. Histone marks such as H3K27ac, H3K4me1, H3K4me3, and H3K27me3 displayed differential patterns upon BAP1 loss. The active enhancer mark H3K27ac was significantly reduced at enhancer regions but increased at TSS in BAP1-deficient cells. This shift suggests a potential regulatory transition from enhancer-driven transcription to a more promoter-centric mechanism, which may further contribute to transcriptional dysregulation in BAP1 KD conditions. Similarly, H3K4me1 and H3K4me3 levels were reduced at both enhancer and promoter regions, indicating a loss of active chromatin marks and reinforcing a repressive chromatin environment in BAP1-deficient UM cells.

These changes suggest that BAP1 loss disrupts the balance between active and repressive chromatin states, leading to a more repressive chromatin landscape that favors oncogenic pathways.

Another key finding is the subtle increase in H3K27me3, particularly at bivalent promoters. Bivalent promoters are typically associated with genes involved in cell fate determination and development, and the increased deposition of H3K27me3 suggests that BAP1 normally counters the activity of Polycomb Repressive Complex 2 (PRC2) in these regions. The increased levels of H3K27me3 in BAP1-deficient cells likely contribute to the stable repression of key genes, which could further drive tumor progression by hindering differentiation pathways.

The antagonistic relationship between BAP1 and PRC1 is further supported by the binding patterns of RING1B, a core component of PRC1. RING1B preferentially binds to repressive chromatin regions also marked by H3K27me3. Without BAP1, excessive PRC1 recruitment promotes a repressive chromatin landscape, which in turn drives the transcriptional silencing of tumor suppressor genes and other key regulatory pathways.

#### **5.1.4. Impact on the enhancer subtypes**

Given the pivotal role of enhancers in regulating gene expression, BAP1 loss has a profound impact on different enhancer subtypes, leading to their compaction and altered activity. Enhancers can be categorized into subtypes such as active, weak, genic, and bivalent enhancers, each with distinct roles in gene regulation. Importantly, we observed that the reduction in chromatin accessibility was not uniform across all enhancer types. Bivalent enhancers, which are poised to either activate or repress gene transcription depending on cellular signals, showed the most pronounced reduction in accessibility following BAP1 loss.

Bivalent enhancers are typically associated with genes involved in development and differentiation, and their repression upon BAP1 loss likely pushes these genes towards a stably repressed state, silencing crucial developmental pathways. This observation suggests that BAP1 is necessary for maintaining an open chromatin state at bivalent

enhancers, and its absence leads to chromatin compaction, reinforcing a transcriptionally repressive environment that could promote oncogenic transformation. The differential effect on bivalent enhancers highlights the complexity of BAP1's regulatory role and underscores its importance in fine-tuning gene expression at key regulatory elements.

## **5.2. Aim 2: BAP1 modifies the interplay of TFs in UM**

BAP1's role as a tumor suppressor and epigenetic regulator extends to its impact on key transcription factors such as TFAP2A and TFAP2C, both of which have been implicated in UM pathogenesis. Our investigation revealed that BAP1 modulates the balance between these two pioneering transcription factors in both UM patients and experimental UM cell culture models. This suggests that BAP1 influences the transcriptional landscape in UM by altering the binding profiles of TFAP2A and TFAP2C at regulatory regions, reshaping gene expression programs that drive tumor progression.

### **5.2.1. Enriched TF binding motifs based on the transcriptional regulation in BAP1-deficient UM cells**

To understand how BAP1 loss affects transcriptional regulation, we performed a TF motif enrichment analysis at the promoters of differentially up- and downregulated genes following BAP1 KD in MEL202 cells. The analysis revealed significant enrichment of motifs for various TFs including DNMT1, TFAP2A, and TFAP2C suggesting that these TFs may play critical roles in the transcriptional reprogramming observed in BAP1-deficient UM cells. This led us to hypothesize a potential regulatory interplay between BAP1 and these TFs.

When we analyzed the enriched TF motifs at the promoters of 1339 differentially downregulated genes, we observed enrichment of TCFL5, DNMT1, and E2F family members. Based on our observations from the enrichments of the TF families, we may project the more general pathways. The strong enrichment of E2F family members, which are key regulators of the G1/S transition in the cell cycle, further underscores the role of BAP1 in maintaining normal cell cycle progression. The downregulation of genes

associated with these TF motifs could explain the replication stress and cell cycle arrest observed upon BAP1 loss. The enrichment of DNMT1 binding motifs links BAP1 loss to changes in DNA methylation, which is consistent with BAP1's known role in chromatin remodeling. Loss of proper methylation control may lead to transcriptional silencing of tumor suppressor genes, contributing to tumor progression. Dual enrichment levels of TFAP2A and TFAP2C suggest that these TFs may play a role in transcriptional changes that drive tumorigenesis. Their involvement in cell adhesion and differentiation pathways could have a role in the aggressive behavior and metastatic potential observed in BAP1-deficient UM tumors. The findings suggest that BAP1 potentially plays a role in regulating transcriptional networks involved in cell cycle control, DNA methylation, and developmental pathways. The loss of BAP1 likely disrupts these networks, leading to widespread transcriptional reprogramming that could contribute to the tumor progression.

Our analysis also extended to the enriched TF motifs at the promoters of 1445 differentially upregulated genes. Motif enrichment of DNMT1, TFAP2A, and TFAP2C in the promoter regions of upregulated genes indicate that these factors may become more prominent in regulating gene expression in the absence of BAP1. This suggests that the loss of BAP1 leads to widespread changes in epigenetic control and indicates the potential importance of transcriptional regulation (through TFAP2A/C), contributing to tumorigenesis in UM. We also did genome-enrichment of these upregulated genes and found the gene cluster for protocadherin gamma gene cluster on Chromosome 5 as the "hot spot". One possible explanation is that BAP1 loss may induce epigenetic or transcriptional reprogramming that increases the transcriptional activity of the PCDHGA cluster, leading to overexpression of these genes. This dysregulation in cell adhesion genes could contribute to a pro-metastatic phenotype, where changes in cell-cell adhesion dynamics enable tumor cells to detach and invade surrounding tissues more effectively. Such a mechanism aligns with the characteristics observed in BAP1-deficient UM.

The observed motif enrichments for TFAP2A and TFAP2C prompted us to further investigate how BAP1 loss impacts their expression and binding. Our analysis of patient-derived UM samples demonstrated that TFAP2A expression is elevated in BAP1-positive

Disomy 3 (D3) patients, whereas TFAP2C expression is increased in BAP1-deficient Monosomy 3 (M3) patients. This inverse relationship suggests that BAP1 may exert its tumor-suppressive function partly by maintaining a regulatory balance between TFAP2A and TFAP2C. Specifically, BAP1 appears to support TFAP2A-mediated transcriptional programs, which are associated with differentiation and tumor suppression, while suppressing TFAP2C-driven pathways linked to cell proliferation and tumor progression.

Also, we validated our UM cohort by comparing the public dataset from TCGA UM cohort and observed the strong positive correlation between *BAP1* and *TFAP2A* expression in the UM patient data (**Figure 63**) suggests that BAP1 positively regulates TFAP2A activity, reinforcing its role in maintaining normal cellular function. Conversely, the negative correlation between *BAP1* and *TFAP2C* expression (**Figure 64**) indicates that BAP1 loss leads to a shift toward TFAP2C-dominated transcriptional regulation. This shift likely contributes to the aggressive phenotype observed in BAP1-deficient tumors by promoting transcriptional programs that favor oncogenesis.

### **5.2.2. Altered TFAP2A and TFAP2C binding upon BAP1 loss**

Our CHIP-seq analysis in MEL202 UM cells provided further insight into how BAP1 loss affects the binding of TFAP2A and TFAP2C. Upon BAP1 knockdown, we observed a significant loss of TFAP2A binding at its target sites, suggesting that BAP1 is crucial for stabilizing TFAP2A binding. This loss of binding could be attributed to changes in the chromatin landscape, as BAP1 is known to facilitate an open chromatin state that allows TFAP2A access to its target sites. Without BAP1, the chromatin may adopt a more repressive configuration, preventing TFAP2A from efficiently binding to and regulating key genes involved in cell differentiation and proliferation control.

In contrast, TFAP2C binding increased in BAP1-deficient cells, particularly at regulatory regions such as TSS and enhancers. This increased binding suggests that TFAP2C becomes more active in the absence of BAP1. It may potentially compensate for the loss of TFAP2A by driving alternative transcriptional programs. The differential effects of BAP1 loss on TFAP2A and TFAP2C binding highlight the complex regulatory interplay between

these factors. While TFAP2A appears to require BAP1 for stable chromatin binding, TFAP2C may be less dependent on BAP1 and may even take advantage of the altered chromatin environment to bind more freely to its target sites.

The increased TFAP2C binding at regulatory regions in BAP1-deficient cells suggests that TFAP2C may play a compensatory role in maintaining certain gene expression programs, potentially driving cell proliferation, migration, and survival pathways critical for UM progression. This is consistent with TFAP2C's known role in oncogenesis, where it has been implicated in promoting tumor growth and metastasis. The resilience of TFAP2C binding despite BAP1 loss further underscores its potential as a key regulator of transcriptional reprogramming in BAP1-deficient UM cells.

### **5.2.3. The role of ELK1 in the BAP1-TFAP2C axis**

One of the most striking findings from our motif enrichment analysis was the significant overlap between ELK1 motifs in both BAP1- and TFAP2C-bound regions. ELK1 is a member of the ETS transcription factor family and it is known to regulate genes involved in cell proliferation and differentiation. The enrichment of ELK1 motifs in both BAP1 and TFAP2C binding sites suggests that ELK1 may serve as a regulator integrating signals from both players.

Given that ELK1 was the most enriched motif in BAP1- and one of the most enrichment motifs in TFAP2C-bound regions, we can further suggest that BAP1 and TFAP2C co-regulate a shared set of target genes through ELK1. In BAP1-deficient cells, where TFAP2C shows more active binding, ELK1 may shift from a role in maintaining cellular processes to more oncogenic pathways. This shift could contribute to the phenotype observed in BAP1-deficient UM. The co-enrichment of ELK1 motifs in BAP1 and TFAP2C binding regions highlights its potential as a player in the transcriptional dysregulation caused by BAP1 loss.

#### **5.2.4. Novel TFAP2C-bound genes and patient stratification**

To further investigate the significance of the interplay between BAP1 and TFAP2C, we identified a subset of genes that were differentially expressed in BAP1-deficient cells and showed differential TFAP2C binding. These genes were not bound by TFAP2C in BAP1 WT conditions but became bound with TFAP2C upon BAP1 loss, suggesting that TFAP2C gains access to new regulatory regions in the absence of BAP1. Hierarchical clustering of these genes in a cohort of 80 UM patients from TCGA database revealed distinct subgroups of patients stratified based on their BAP1 status.

This finding underscores the potential clinical relevance of the BAP1-TFAP2C axis in UM. The ability of these genes to stratify patients based on BAP1 status suggests that TFAP2C may serve as a biomarker for patient subtyping and prognosis. Moreover, the identification of these novel TFAP2C-bound genes opens new avenues for therapeutic targeting, particularly in BAP1-deficient UM patients, where disrupting the TFAP2C-ELK1 interaction could provide a strategy to inhibit tumor progression.

In conclusion, our study highlights the critical role of BAP1 in modulating the transcriptional interplay between TFAP2A and TFAP2C, with implications for understanding the transcriptional reprogramming that drives UM progression. The enrichment of ELK1 motifs in both BAP1 and TFAP2C binding regions suggests a shared transcriptional network that may be disrupted in BAP1-deficient tumors. These findings provide new insights into the molecular mechanisms underlying UM.

#### **5.3. Aim 3: Potential contribution of molecular changes to the disease progression observed in BAP1-mutant UM**

Our findings demonstrate the profound influence of BAP1 on chromatin accessibility and histone modifications, underscoring its role as a regulator of gene expression in UM. Loss of BAP1 disrupts the equilibrium between active and repressive chromatin states. This shift results in a repressive chromatin environment conducive to tumor progression. By maintaining active chromatin marks such as H3K27ac, H3K4me1, and H3K4me3 at both



enhancers and promoters, BAP1 functions as a safeguard against the silencing of key tumor suppressor genes and other regulatory elements critical for cellular homeostasis.

In BAP1-deficient cells, we observed a significant reduction in enhancer accessibility, a key feature of gene regulation that is tightly linked to tumor-suppressive pathways. Enhancers are crucial regulatory elements that drive the expression of genes involved in cellular differentiation, proliferation, and survival. The widespread loss of chromatin accessibility at enhancers in BAP1 KD cells may lead to the transcriptional silencing of genes required for maintaining cellular homeostasis, thus promoting tumorigenesis.

Additionally, the increase in repressive histone marks, such as H3K27me<sub>3</sub>, at bivalent promoters in BAP1-deficient cells provides further insight into the mechanisms driving tumor progression. Bivalent promoters, often associated with developmental genes that control cell fate, are poised between activation and repression. The accumulation of H3K27me<sub>3</sub> in these regions suggests that in the absence of BAP1, PRC1 and PRC2 gain a dominant role in silencing key developmental genes. This repression may drive a de-differentiated state, characteristic of cancer stem cell-like properties, contributing to the aggressive and metastatic behavior observed in BAP1-mutant UM.

The representation in **Figure 81** illustrates the proposed scheme of BAP1's act in an open chromatin state, particularly at regulatory elements like promoters. Without BAP1, the chromatin becomes more repressive, facilitating the recruitment of Polycomb repressive complexes (PRC1 and PRC2), which further drive the deposition of repressive histone marks such as H3K27me<sub>3</sub>. This shift towards repressive chromatin states supports a transcriptional program that favors tumorigenesis, highlighting the critical role of BAP1 in epigenetic regulation in UM.

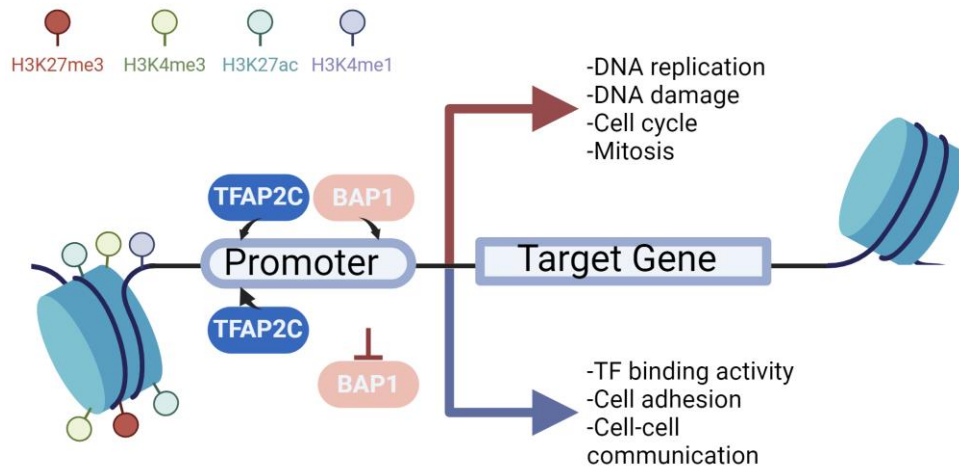


**Figure 81: Schematic representation of the roles of BAP1 along with TFAP2C in regulation of the target genes.** MEL202 BAP1 WT condition (upside), MEL202 BAP1 loss condition (downside), (Created with BioRender)

#### 5.4. Clinical implications and future directions

The molecular insights uncovered in this study not only enhance our understanding of BAP1's role in UM pathogenesis but also open potential therapeutic avenues for treatment. Given the impact of BAP1 loss on chromatin accessibility and histone modifications, targeting the epigenetic regulators affected by this loss may present a potential strategy. Therapies designed to modulate chromatin structure such as histone deacetylase (HDAC) inhibitors or Polycomb repressive complex (PRC) inhibitors could potentially restore a more normal chromatin state in BAP1-deficient UM cells. These therapies may reactivate silenced tumor suppressor genes, offering a novel approach to combat the aggressive behavior associated with BAP1 mutations.

TFAP2A and TFAP2C, two transcription factors identified as players in the BAP1-deficient UM landscape. Targeting the transcriptional networks regulated by these factors, particularly in the context of their interplay with BAP1, could disrupt the transcriptional reprogramming driving UM progression.

Moving forward, it will be essential to further investigate the precise mechanisms by which BAP1 interacts with chromatin remodelers and transcription factors to maintain epigenetic control. Understanding these interactions could help refine therapeutic strategies aimed

at restoring BAP1's tumor-suppressive functions. Moreover, exploring the BAP1-PRC axis, particularly the role of PRC1 and PRC2 in gene silencing, may yield new targets that could prevent or reverse the epigenetic changes driving UM progression.

The findings from this study also provide a foundation for future research into the clinical relevance of BAP1 mutations in patient stratification and prognosis. The distinct molecular signatures observed in BAP1-deficient cells suggest that BAP1 status could serve as a biomarker for identifying high-risk UM patients. This stratification could guide the use of epigenetic therapies and other targeted treatments, particularly in patients harboring BAP1 mutations.

## **5.5. Conclusions**

In this study, we provide a comprehensive view of how BAP1 loss alters the epigenetic landscape in UM, leading to transcriptional reprogramming that promotes tumor progression. Using genome-wide multi-omics approaches such as RNA-seq, ATAC-seq, and ChIP-seq, we showed that the interplay of pioneering transcription factors, chromatin modifications, and regulatory elements affected by BAP1 loss highlights the complexity of the molecular changes driving UM pathogenesis. By elucidating the role of BAP1 in maintaining chromatin accessibility and preventing the accumulation of repressive histone marks, we have uncovered new insights into the epigenetic mechanisms that contribute to the aggressive nature of BAP1-deficient UM.

Further research is needed to validate these findings in larger patient cohorts and explore the therapeutic potential of targeting the BAP1-PRC axis, transcription factors like TFAP2A and TFAP2C, and chromatin-modifying enzymes. Ultimately, these discoveries can provide valuable insights for a better understanding of the transcriptional programs and gene regulatory networks, development of epigenetic therapies aimed at restoring normal gene expression patterns and improving outcomes for UM patients with BAP1 mutations.

## Bibliography

- AALTO, Y., ERIKSSON, L., SEREGARD, S., LARSSON, O. & KNUUTILA, S. 2001. Concomitant loss of chromosome 3 and whole arm losses and gains of chromosome 1, 6, or 8 in metastasizing primary uveal melanoma. *Invest Ophthalmol Vis Sci*, 42, 313-7.
- ABDEL-RAHMAN, M. H., PILARSKI, R., CEBULLA, C. M., MASSENGILL, J. B., CHRISTOPHER, B. N., BORU, G., HOVLAND, P. & DAVIDORF, F. H. 2011. Germline BAP1 mutation predisposes to uveal melanoma, lung adenocarcinoma, meningioma, and other cancers. *J Med Genet*, 48, 856-9.
- ALEXANDER, H. 2019. *What's the difference between UVA and UVB rays?* [Online]. The University of Texas MD Anderson Cancer Center. Available: <https://www.mdanderson.org/publications/focused-on-health/what-s-the-difference-between-uva-and-uvb-rays-.h15-1592991.html> [Accessed].
- ALSAFADI, S., HOUY, A., BATTISTELLA, A., POPOVA, T., WASSEF, M., HENRY, E., TIRODE, F., CONSTANTINO, A., PIPERNO-NEUMANN, S., ROMAN-ROMAN, S., DUTERTRE, M. & STERN, M. H. 2016. Cancer-associated SF3B1 mutations affect alternative splicing by promoting alternative branchpoint usage. *Nat Commun*, 7, 10615.
- AMARO, A., GANGEMI, R., PIAGGIO, F., ANGELINI, G., BARISIONE, G., FERRINI, S. & PFEFFER, U. 2017. The biology of uveal melanoma. *Cancer Metastasis Rev*, 36, 109-140.
- AOKI, H., YAMADA, Y., HARA, A. & KUNISADA, T. 2009. Two distinct types of mouse melanocyte: differential signaling requirement for the maintenance of non-cutaneous and dermal versus epidermal melanocytes. *Development*, 136, 2511-21.
- AOUDE, L. G., VAJDIC, C. M., KRICKER, A., ARMSTRONG, B. & HAYWARD, N. K. 2013. Prevalence of germline BAP1 mutation in a population-based sample of uveal melanoma cases. *Pigment Cell Melanoma Res*, 26, 278-9.
- AUDIA, J. E. & CAMPBELL, R. M. 2016. Histone Modifications and Cancer. *Cold Spring Harb Perspect Biol*, 8, a019521.
- AUGSBURGER, J. J., CORREA, Z. M. & SHAIKH, A. H. 2009. Effectiveness of treatments for metastatic uveal melanoma. *Am J Ophthalmol*, 148, 119-27.
- BABCHIA, N., CALIPEL, A., MOURIAUX, F., FAUSSAT, A. M. & MASCARELLI, F. 2010. The PI3K/Akt and mTOR/P70S6K signaling pathways in human uveal melanoma cells: interaction with B-Raf/ERK. *Invest Ophthalmol Vis Sci*, 51, 421-9.
- BARBOUR, H., DAOU, S., HENDZEL, M. & AFFAR, E. B. 2020. Polycomb group-mediated histone H2A monoubiquitination in epigenome regulation and nuclear processes. *Nat Commun*, 11, 5947.
- BASTIAN, B. C. 2014. The molecular pathology of melanoma: an integrated taxonomy of melanocytic neoplasia. *Annu Rev Pathol*, 9, 239-71.
- BAXTER, L. L. & PAVAN, W. J. 2003. Pmel17 expression is Mitf-dependent and reveals cranial melanoblast migration during murine development. *Gene Expr Patterns*, 3, 703-7.
- BAYLIN, S. B. & JONES, P. A. 2011. A decade of exploring the cancer epigenome - biological and translational implications. *Nat Rev Cancer*, 11, 726-34.

- BAYLIN, S. B. & JONES, P. A. 2016. Epigenetic Determinants of Cancer. *Cold Spring Harb Perspect Biol*, 8.
- BAYLIN, S. B. & OHM, J. E. 2006. Epigenetic gene silencing in cancer - a mechanism for early oncogenic pathway addiction? *Nat Rev Cancer*, 6, 107-16.
- BEADLING, C., JACOBSON-DUNLOP, E., HODI, F. S., LE, C., WARRICK, A., PATTERSON, J., TOWN, A., HARLOW, A., CRUZ, F., 3RD, AZAR, S., RUBIN, B. P., MULLER, S., WEST, R., HEINRICH, M. C. & CORLESS, C. L. 2008. KIT gene mutations and copy number in melanoma subtypes. *Clin Cancer Res*, 14, 6821-8.
- BEJJANI, F., EVANNO, E., ZIBARA, K., PIECHACZYK, M. & JARIEL-ENCONTRE, I. 2019. The AP-1 transcriptional complex: Local switch or remote command? *Biochim Biophys Acta Rev Cancer*, 1872, 11-23.
- BEN-PORATH, I. & CEDAR, H. 2001. Epigenetic crosstalk. *Mol Cell*, 8, 933-5.
- BERGER, M. F., HODIS, E., HEFFERNAN, T. P., DERIBE, Y. L., LAWRENCE, M. S., PROTOPOPOV, A., IVANOVA, E., WATSON, I. R., NICKERSON, E., GHOSH, P., ZHANG, H., ZEID, R., REN, X., CIBULSKIS, K., SIVACHENKO, A. Y., WAGLE, N., SUCKER, A., SOUGNEZ, C., ONOFRIO, R., AMBROGIO, L., AUCLAIR, D., FENNEL, T., CARTER, S. L., DRIER, Y., STOJANOV, P., SINGER, M. A., VOET, D., JING, R., SAKSENA, G., BARRETINA, J., RAMOS, A. H., PUGH, T. J., STRANSKY, N., PARKIN, M., WINCKLER, W., MAHAN, S., ARDLIE, K., BALDWIN, J., WARGO, J., SCHADENDORF, D., MEYERSON, M., GABRIEL, S. B., GOLUB, T. R., WAGNER, S. N., LANDER, E. S., GETZ, G., CHIN, L. & GARRAWAY, L. A. 2012. Melanoma genome sequencing reveals frequent PREX2 mutations. *Nature*, 485, 502-6.
- BHATIA, S., MOON, J., MARGOLIN, K. A., WEBER, J. S., LAO, C. D., OTHUS, M., APARICIO, A. M., RIBAS, A. & SONDAK, V. K. 2012. Phase II trial of sorafenib in combination with carboplatin and paclitaxel in patients with metastatic uveal melanoma: SWOG S0512. *PLoS One*, 7, e48787.
- BIGGAR, K. K. & LI, S. S. 2015. Non-histone protein methylation as a regulator of cellular signalling and function. *Nat Rev Mol Cell Biol*, 16, 5-17.
- BIRD, A. 2007. Perceptions of epigenetics. *Nature*, 447, 396-8.
- BODMER, W., BIELAS, J. H. & BECKMAN, R. A. 2008. Genetic instability is not a requirement for tumor development. *Cancer Res*, 68, 3558-60; discussion 3560-1.
- BONAVENTURE, J., DOMINGUES, M. J. & LARUE, L. 2013. Cellular and molecular mechanisms controlling the migration of melanocytes and melanoma cells. *Pigment Cell Melanoma Res*, 26, 316-25.
- BOUTROS, A., CROCE, E., FERRARI, M., GILI, R., MASSARO, G., MARCONCINI, R., ARECCO, L., TANDA, E. T. & SPAGNOLO, F. 2024. The treatment of advanced melanoma: Current approaches and new challenges. *Crit Rev Oncol Hematol*, 196, 104276.
- BRENNER, M. & HEARING, V. J. 2008. The protective role of melanin against UV damage in human skin. *Photochem Photobiol*, 84, 539-49.
- BUCHWALTER, G., GROSS, C. & WASYLYK, B. 2004. Ets ternary complex transcription factors. *Gene*, 324, 1-14.

- BURNS, A. 1811. Observations on the Surgical Anatomy of the Head and Neck: Illustrated by Cases and Engravings. *Edinburgh: Bryce & Co.*, 349-360.
- BUSHNELL, B., ROOD, J. & SINGER, E. 2017. BBMerge - Accurate paired shotgun read merging via overlap. *PLoS One*, 12, e0185056.
- CAMPAGNE, A., LEE, M. K., ZIELINSKI, D., MICHAUD, A., LE CORRE, S., DINGLI, F., CHEN, H., SHAHIDIAN, L. Z., VASSILEV, I., SERVANT, N., LOEW, D., PASMANT, E., POSTEL-VINAY, S., WASSEF, M. & MARGUERON, R. 2019. BAP1 complex promotes transcription by opposing PRC1-mediated H2A ubiquitylation. *Nat Commun*, 10, 348.
- CANCER GENOME ATLAS, N. 2015. Genomic Classification of Cutaneous Melanoma. *Cell*, 161, 1681-96.
- CAPORALI, S., BUTERA, A. & AMELIO, I. 2022. BAP1 in cancer: epigenetic stability and genome integrity. *Discov Oncol*, 13, 117.
- CARBONE, M., FERRIS, L. K., BAUMANN, F., NAPOLITANO, A., LUM, C. A., FLORES, E. G., GAUDINO, G., POWERS, A., BRYANT-GREENWOOD, P., KRAUSZ, T., HYJEK, E., TATE, R., FRIEDBERG, J., WEIGEL, T., PASS, H. I. & YANG, H. 2012. BAP1 cancer syndrome: malignant mesothelioma, uveal and cutaneous melanoma, and MBAITs. *J Transl Med*, 10, 179.
- CARNEIRO, F., KRUIHOF, B. P., BALANI, K., AGARWAL, A., GAUSSIN, V. & KOS, L. 2015. Relationships between melanocytes, mechanical properties and extracellular matrix composition in mouse heart valves. *J Long Term Eff Med Implants*, 25, 17-26.
- CARVAJAL, R. D., PIPERNO-NEUMANN, S., KAPITEIJN, E., CHAPMAN, P. B., FRANK, S., JOSHUA, A. M., PIULATS, J. M., WOLTER, P., COCQUYT, V., CHMIELOWSKI, B., EVANS, T. R. J., GASTAUD, L., LINETTE, G., BERKING, C., SCHACHTER, J., RODRIGUES, M. J., SHOUSHARI, A. N., CLEMETT, D., GHIORGHIU, D., MARIANI, G., SPRATT, S., LOVICK, S., BARKER, P., KILGOUR, E., LAI, Z., SCHWARTZ, G. K. & NATHAN, P. 2018. Selumetinib in Combination With Dacarbazine in Patients With Metastatic Uveal Melanoma: A Phase III, Multicenter, Randomized Trial (SUMIT). *J Clin Oncol*, 36, 1232-1239.
- CARVAJAL, R. D., SACCO, J. J., JAGER, M. J., ESCHELMAN, D. J., OLOFSSON BAGGE, R., HARBOUR, J. W., CHIENG, N. D., PATEL, S. P., JOSHUA, A. M. & PIPERNO-NEUMANN, S. 2023. Advances in the clinical management of uveal melanoma. *Nat Rev Clin Oncol*, 20, 99-115.
- CARVAJAL, R. D., SCHWARTZ, G. K., TEZEL, T., MARR, B., FRANCIS, J. H. & NATHAN, P. D. 2017. Metastatic disease from uveal melanoma: treatment options and future prospects. *Br J Ophthalmol*, 101, 38-44.
- CASSOUX, N., RODRIGUES, M. J., PLANCHER, C., ASSELAIN, B., LEVY-GABRIEL, C., LUMBROSO-LE ROUIC, L., PIPERNO-NEUMANN, S., DENDALE, R., SASTRE, X., DESJARDINS, L. & COUTURIER, J. 2014. Genome-wide profiling is a clinically relevant and affordable prognostic test in posterior uveal melanoma. *Br J Ophthalmol*, 98, 769-74.
- CASTRO-PEREZ, E., SINGH, M., SADANGI, S., MELA-SANCHEZ, C. & SETALURI, V. 2023. Connecting the dots: Melanoma cell of origin, tumor cell plasticity, trans-differentiation, and drug resistance. *Pigment Cell Melanoma Res*, 36, 330-347.

- CAVALCANTE, R. G. 2017. *annotatr: Making sense of genomic regions* [Online]. Available: <http://bioconductor.statistik.tu-dortmund.de/packages/3.5/bioc/vignettes/annotatr/inst/doc/annotatr-vignette.html> [Accessed].
- CAZZOLA, M., ROSSI, M., MALCOVATI, L. & ASSOCIAZIONE ITALIANA PER LA RICERCA SUL CANCRO GRUPPO ITALIANO MALATTIE, M. 2013. Biologic and clinical significance of somatic mutations of SF3B1 in myeloid and lymphoid neoplasms. *Blood*, 121, 260-9.
- CEDAR, H. & BERGMAN, Y. 2012. Programming of DNA methylation patterns. *Annu Rev Biochem*, 81, 97-117.
- CENTENO, P. P., PAVET, V. & MARAIS, R. 2023. The journey from melanocytes to melanoma. *Nat Rev Cancer*, 23, 372-390.
- CERAMI, E., GAO, J., DOGRUSOZ, U., GROSS, B. E., SUMER, S. O., AKSOY, B. A., JACOBSEN, A., BYRNE, C. J., HEUER, M. L., LARSSON, E., ANTIPIN, Y., REVA, B., GOLDBERG, A. P., SANDER, C. & SCHULTZ, N. 2012. The cBio cancer genomics portal: an open platform for exploring multidimensional cancer genomics data. *Cancer Discov*, 2, 401-4.
- CHANG, S. H., WORLEY, L. A., ONKEN, M. D. & HARBOUR, J. W. 2008. Prognostic biomarkers in uveal melanoma: evidence for a stem cell-like phenotype associated with metastasis. *Melanoma Res*, 18, 191-200.
- CHEN, X., WU, Q., DEPEILLE, P., CHEN, P., THORNTON, S., KALIRAI, H., COUPLAND, S. E., ROOSE, J. P. & BASTIAN, B. C. 2017. RasGRP3 Mediates MAPK Pathway Activation in GNAQ Mutant Uveal Melanoma. *Cancer Cell*, 31, 685-696 e6.
- CHEN, Y., LUN, A. T. & SMYTH, G. K. 2016. From reads to genes to pathways: differential expression analysis of RNA-Seq experiments using Rsubread and the edgeR quasi-likelihood pipeline. *F1000Res*, 5, 1438.
- CHENG, Y., HE, C., WANG, M., MA, X., MO, F., YANG, S., HAN, J. & WEI, X. 2019. Targeting epigenetic regulators for cancer therapy: mechanisms and advances in clinical trials. *Signal Transduct Target Ther*, 4, 62.
- CHOKHACHI BARADARAN, P., KOZOVSKA, Z., FURDOVA, A. & SMOLKOVA, B. 2020. Targeting Epigenetic Modifications in Uveal Melanoma. *Int J Mol Sci*, 21.
- CHRISTENSEN, B. C., KELSEY, K. T., ZHENG, S., HOUSEMAN, E. A., MARSIT, C. J., WRENSCH, M. R., WIEMELS, J. L., NELSON, H. H., KARAGAS, M. R., KUSHI, L. H., KWAN, M. L. & WIENCKE, J. K. 2010. Breast cancer DNA methylation profiles are associated with tumor size and alcohol and folate intake. *PLoS Genet*, 6, e1001043.
- CHUA, V., LAPADULA, D., RANDOLPH, C., BENOVIC, J. L., WEDEGAERTNER, P. B. & APLIN, A. E. 2017. Dysregulated GPCR Signaling and Therapeutic Options in Uveal Melanoma. *Mol Cancer Res*, 15, 501-506.
- CICHOREK, M., WACHULSKA, M. & STASIEWICZ, A. 2013a. Heterogeneity of neural crest-derived melanocytes. *Open Life Sciences*, 8, 315-330.
- CICHOREK, M., WACHULSKA, M., STASIEWICZ, A. & TYMINSKA, A. 2013b. Skin melanocytes: biology and development. *Postepy Dermatol Alergol*, 30, 30-41.

- CIRENAJWIS, H., LAUSS, M., EKEDAHL, H., TORNGREN, T., KVIST, A., SAAL, L. H., OLSSON, H., STAAF, J., CARNEIRO, A., INGVAR, C., HARBST, K., HAYWARD, N. K. & JONSSON, G. 2017. NF1-mutated melanoma tumors harbor distinct clinical and biological characteristics. *Mol Oncol*, 11, 438-451.
- CLARK, W. H., JR., ELDER, D. E. & VAN HORN, M. 1986. The biologic forms of malignant melanoma. *Hum Pathol*, 17, 443-50.
- CONWAY, E., ROSSI, F., FERNANDEZ-PEREZ, D., PONZO, E., FERRARI, K. J., ZANOTTI, M., MANGANARO, D., RODIGHIERO, S., TAMBURRI, S. & PASINI, D. 2021. BAP1 enhances Polycomb repression by counteracting widespread H2AK119ub1 deposition and chromatin condensation. *Mol Cell*, 81, 3526-3541 e8.
- CORREA, Z. M. 2016. Assessing Prognosis in Uveal Melanoma. *Cancer Control*, 23, 93-8.
- COSTA, P., SALES, S. L. A., PINHEIRO, D. P., PONTES, L. Q., MARANHÃO, S. S., PESSOA, C. D. O., FURTADO, G. P. & FURTADO, C. L. M. 2023. Epigenetic reprogramming in cancer: From diagnosis to treatment. *Front Cell Dev Biol*, 11, 1116805.
- COUPLAND, S. E., LAKE, S. L., ZESCHNIGK, M. & DAMATO, B. E. 2013. Molecular pathology of uveal melanoma. *Eye (Lond)*, 27, 230-42.
- D'MELLO, S. A., FINLAY, G. J., BAGULEY, B. C. & ASKARIAN-AMIRI, M. E. 2016. Signaling Pathways in Melanogenesis. *Int J Mol Sci*, 17.
- DAMATO, B. 2010. Does ocular treatment of uveal melanoma influence survival? *Br J Cancer*, 103, 285-90.
- DAMATO, B. & COUPLAND, S. E. 2009a. A reappraisal of the significance of largest basal diameter of posterior uveal melanoma. *Eye*.
- DAMATO, B. & COUPLAND, S. E. 2009b. Translating uveal melanoma cytogenetics into clinical care. *Arch Ophthalmol*, 127, 423-9.
- DAMATO, B., DOPIERALA, J. A. & COUPLAND, S. E. 2010. Genotypic profiling of 452 choroidal melanomas with multiplex ligation-dependent probe amplification. *Clin Cancer Res*, 16, 6083-92.
- DAMATO, B. E., DUKES, J., GOODALL, H. & CARVAJAL, R. D. 2019. Tebentafusp: T Cell Redirection for the Treatment of Metastatic Uveal Melanoma. *Cancers (Basel)*, 11.
- DANECEK, P., BONFIELD, J. K., LIDDLE, J., MARSHALL, J., OHAN, V., POLLARD, M. O., WHITWHAM, A., KEANE, T., MCCARTHY, S. A., DAVIES, R. M. & LI, H. 2021. Twelve years of SAMtools and BCFtools. *Gigascience*, 10.
- DARMAN, R. B., SEILER, M., AGRAWAL, A. A., LIM, K. H., PENG, S., AIRD, D., BAILEY, S. L., BHAVSAR, E. B., CHAN, B., COLLA, S., CORSON, L., FEALA, J., FEKKES, P., ICHIKAWA, K., KEANEY, G. F., LEE, L., KUMAR, P., KUNII, K., MACKENZIE, C., MATIJEVIC, M., MIZUI, Y., MYINT, K., PARK, E. S., PUYANG, X., SELVARAJ, A., THOMAS, M. P., TSAI, J., WANG, J. Y., WARMUTH, M., YANG, H., ZHU, P., GARCIA-MANERO, G., FURMAN, R. R., YU, L., SMITH, P. G. & BUONAMICI, S. 2015. Cancer-Associated SF3B1 Hotspot Mutations Induce Cryptic 3' Splice Site Selection through Use of a Different Branch Point. *Cell Rep*, 13, 1033-45.



- DARWICHE, N. 2020. Epigenetic mechanisms and the hallmarks of cancer: an intimate affair. *Am J Cancer Res*, 10, 1954-1978.
- DE BRUIJN, I., KUNDRA, R., MASTROGIACOMO, B., TRAN, T. N., SIKINA, L., MAZOR, T., LI, X., OCHOA, A., ZHAO, G., LAI, B., ABESHOUSE, A., BAICEANU, D., CIFTCI, E., DOGRUSOZ, U., DUFILIE, A., ERKOC, Z., GARCIA LARA, E., FU, Z., GROSS, B., HAYNES, C., HEATH, A., HIGGINS, D., JAGANNATHAN, P., KALLETLA, K., KUMARI, P., LINDSAY, J., LISMAN, A., LEENKNEGT, B., LUKASSE, P., MADELA, D., MADUPURI, R., VAN NIEROP, P., PLANTALECH, O., QUACH, J., RESNICK, A. C., RODENBURG, S. Y. A., SATRAVADA, B. A., SCHAEFFER, F., SHERIDAN, R., SINGH, J., SIROHI, R., SUMER, S. O., VAN HAGEN, S., WANG, A., WILSON, M., ZHANG, H., ZHU, K., RUSK, N., BROWN, S., LAVERY, J. A., PANAGEAS, K. S., RUDOLPH, J. E., LENOUE-NEWTON, M. L., WARNER, J. L., GUO, X., HUNTER-ZINCK, H., YU, T. V., PILAI, S., NICHOLS, C., GARDOS, S. M., PHILIP, J., AACR PROJECT GENIE BPC CORE TEAM, A. P. G. C., KEHL, K. L., RIELY, G. J., SCHRAG, D., LEE, J., FIANDALO, M. V., SWEENEY, S. M., PUGH, T. J., SANDER, C., CERAMI, E., GAO, J. & SCHULTZ, N. 2023. Analysis and Visualization of Longitudinal Genomic and Clinical Data from the AACR Project GENIE Biopharma Collaborative in cBioPortal. *Cancer Res*, 83, 3861-3867.
- DE LANGE, M. J., VAN PELT, S. I., VERSLUIS, M., JORDANOVA, E. S., KROES, W. G., RUIVENKAMP, C., VAN DER BURG, S. H., LUYTEN, G. P., VAN HALL, T., JAGER, M. J. & VAN DER VELDEN, P. A. 2015. Heterogeneity revealed by integrated genomic analysis uncovers a molecular switch in malignant uveal melanoma. *Oncotarget*, 6, 37824-35.
- DEBOEVER, C., GHIA, E. M., SHEPARD, P. J., RASSENTI, L., BARRETT, C. L., JEPSEN, K., JAMIESON, C. H., CARSON, D., KIPPS, T. J. & FRAZER, K. A. 2015. Transcriptome sequencing reveals potential mechanism of cryptic 3' splice site selection in SF3B1-mutated cancers. *PLoS Comput Biol*, 11, e1004105.
- DEHMELT, L. & HALPAIN, S. 2005. The MAP2/Tau family of microtubule-associated proteins. *Genome Biol*, 6, 204.
- DENG, J., PAN, T., LIU, Z., MCCARTHY, C., VICENCIO, J. M., CAO, L., ALFANO, G., SUWAIDAN, A. A., YIN, M., BEATSON, R. & NG, T. 2023. The role of TXNIP in cancer: a fine balance between redox, metabolic, and immunological tumor control. *Br J Cancer*, 129, 1877-1892.
- DI CESARE, S., MALONEY, S., FERNANDES, B. F., MARTINS, C., MARSHALL, J. C., ANTECKA, E., ODASHIRO, A. N., DAWSON, W. W. & BURNIER, M. N., JR. 2009. The effect of blue light exposure in an ocular melanoma animal model. *J Exp Clin Cancer Res*, 28, 48.
- DI CROCE, L. & HELIN, K. 2013. Transcriptional regulation by Polycomb group proteins. *Nat Struct Mol Biol*, 20, 1147-55.
- DOGRUSOZ, M., BAGGER, M., VAN DUINEN, S. G., KROES, W. G., RUIVENKAMP, C. A., BOHRINGER, S., ANDERSEN, K. K., LUYTEN, G. P., KIILGAARD, J. F. & JAGER, M. J. 2017a. The Prognostic Value of AJCC Staging in Uveal Melanoma Is Enhanced by Adding Chromosome 3 and 8q Status. *Invest Ophthalmol Vis Sci*, 58, 833-842.
- DOGRUSOZ, M. & JAGER, M. J. 2018. Genetic prognostication in uveal melanoma. *Acta Ophthalmol*, 96, 331-347.

- DOGRUSOZ, M., JAGER, M. J. & DAMATO, B. 2017b. Uveal Melanoma Treatment and Prognostication. *Asia Pac J Ophthalmol (Phila)*, 6, 186-196.
- DOHERTY, R. E., ALFAWAZ, M., FRANCIS, J., LIJKA-JONES, B. & SISLEY, K. 2018. Genetics of Uveal Melanoma. In: SCOTT, J. F. & GERSTENBLITH, M. R. (eds.) *Noncutaneous Melanoma*. Brisbane (AU): Codon Publications.
- DULL, T., ZUFFEREY, R., KELLY, M., MANDEL, R. J., NGUYEN, M., TRONO, D. & NALDINI, L. 1998. A third-generation lentivirus vector with a conditional packaging system. *J Virol*, 72, 8463-71.
- DUPIN, E., CALLONI, G., REAL, C., GONCALVES-TRENTIN, A. & LE DOUARIN, N. M. 2007. Neural crest progenitors and stem cells. *C R Biol*, 330, 521-9.
- DURANTE, M. A., RODRIGUEZ, D. A., KURTENBACH, S., KUZNETSOV, J. N., SANCHEZ, M. I., DECATUR, C. L., SNYDER, H., FEUN, L. G., LIVINGSTONE, A. S. & HARBOUR, J. W. 2020. Single-cell analysis reveals new evolutionary complexity in uveal melanoma. *Nat Commun*, 11, 496.
- EASWARAN, H., TSAI, H. C. & BAYLIN, S. B. 2014. Cancer epigenetics: tumor heterogeneity, plasticity of stem-like states, and drug resistance. *Mol Cell*, 54, 716-27.
- ECHEGARAY, J. J., MEDINA, C. A., BISCOTTI, C. V., PLESEC, T. & SINGH, A. D. 2019. Multifocal Primary Uveal Melanoma: Clinical and Molecular Characteristics. *Ocul Oncol Pathol*, 5, 8-12.
- EHLERS, J. P. & HARBOUR, J. W. 2005. NBS1 expression as a prognostic marker in uveal melanoma. *Clin Cancer Res*, 11, 1849-53.
- EHLERS, J. P., WORLEY, L., ONKEN, M. D. & HARBOUR, J. W. 2005. DDEF1 is located in an amplified region of chromosome 8q and is overexpressed in uveal melanoma. *Clin Cancer Res*, 11, 3609-13.
- EHLERS, J. P., WORLEY, L., ONKEN, M. D. & HARBOUR, J. W. 2008. Integrative genomic analysis of aneuploidy in uveal melanoma. *Clin Cancer Res*, 14, 115-22.
- ELDER, D. E., BASTIAN, B. C., CREE, I. A., MASSI, D. & SCOLYER, R. A. 2020. The 2018 World Health Organization Classification of Cutaneous, Mucosal, and Uveal Melanoma: Detailed Analysis of 9 Distinct Subtypes Defined by Their Evolutionary Pathway. *Arch Pathol Lab Med*, 144, 500-522.
- ETEGHADI, A., EBRAHIMI, M. & KESHEL, S. H. 2024. New immunotherapy approaches as the most effective treatment for uveal melanoma. *Crit Rev Oncol Hematol*, 194, 104260.
- EWENS, K. G., KANETSKY, P. A., RICHARDS-YUTZ, J., AL-DAHMAH, S., DE LUCA, M. C., BIANCIOTTO, C. G., SHIELDS, C. L. & GANGULY, A. 2013. Genomic profile of 320 uveal melanoma cases: chromosome 8p-loss and metastatic outcome. *Invest Ophthalmol Vis Sci*, 54, 5721-9.
- EWENS, K. G., KANETSKY, P. A., RICHARDS-YUTZ, J., PURRAZZELLA, J., SHIELDS, C. L., GANGULY, T. & GANGULY, A. 2014. Chromosome 3 status combined with BAP1 and EIF1AX mutation profiles are associated with metastasis in uveal melanoma. *Invest Ophthalmol Vis Sci*, 55, 5160-7.
- FAHRNER, J. A., EGUCHI, S., HERMAN, J. G. & BAYLIN, S. B. 2002. Dependence of histone modifications and gene expression on DNA hypermethylation in cancer. *Cancer Res*, 62, 7213-8.
- FALLICO, M., RACITI, G., LONGO, A., REIBALDI, M., BONFIGLIO, V., RUSSO, A., CALTABIANO, R., GATTUSO, G., FALZONE, L. & AVITABILE, T. 2021. Current molecular and clinical insights into uveal melanoma (Review). *Int J Oncol*, 58.

- FARRIA, A., LI, W. & DENT, S. Y. 2015. KATs in cancer: functions and therapies. *Oncogene*, 34, 4901-13.
- FIELD, M. G., DECATUR, C. L., KURTENBACH, S., GEZGIN, G., VAN DER VELDEN, P. A., JAGER, M. J., KOZAK, K. N. & HARBOUR, J. W. 2016. PRAME as an Independent Biomarker for Metastasis in Uveal Melanoma. *Clin Cancer Res*, 22, 1234-42.
- FIELD, M. G., DURANTE, M. A., ANBUNATHAN, H., CAI, L. Z., DECATUR, C. L., BOWCOCK, A. M., KURTENBACH, S. & HARBOUR, J. W. 2018. Punctuated evolution of canonical genomic aberrations in uveal melanoma. *Nat Commun*, 9, 116.
- FIELD, M. G., KUZNETSOV, J. N., BUSSIES, P. L., CAI, L. Z., ALAWA, K. A., DECATUR, C. L., KURTENBACH, S. & HARBOUR, J. W. 2019. BAP1 Loss Is Associated with DNA Methylomic Repatterning in Highly Aggressive Class 2 Uveal Melanomas. *Clin Cancer Res*, 25, 5663-5673.
- FRAGA, M. F., BALLESTAR, E., VILLAR-GAREA, A., BOIX-CHORNET, M., ESPADA, J., SCHOTTA, G., BONALDI, T., HAYDON, C., ROPERO, S., PETRIE, K., IYER, N. G., PEREZ-ROSADO, A., CALVO, E., LOPEZ, J. A., CANO, A., CALASANZ, M. J., COLOMER, D., PIRIS, M. A., AHN, N., IMHOF, A., CALDAS, C., JENUWEIN, T. & ESTELLER, M. 2005. Loss of acetylation at Lys16 and trimethylation at Lys20 of histone H4 is a common hallmark of human cancer. *Nat Genet*, 37, 391-400.
- FRIEDBERG, E. C. 2003. DNA damage and repair. *Nature*, 421, 436-40.
- FUJIWARA, S., NAGAI, H., JIMBO, H., JIMBO, N., TANAKA, T., INOIE, M. & NISHIGORI, C. 2018. Gene Expression and Methylation Analysis in Melanomas and Melanocytes From the Same Patient: Loss of NPM2 Expression Is a Potential Immunohistochemical Marker for Melanoma. *Front Oncol*, 8, 675.
- FURNEY, S. J., PEDERSEN, M., GENTIEN, D., DUMONT, A. G., RAPINAT, A., DESJARDINS, L., TURAJLIC, S., PIPERNO-NEUMANN, S., DE LA GRANGE, P., ROMAN-ROMAN, S., STERN, M. H. & MARAIS, R. 2013. SF3B1 mutations are associated with alternative splicing in uveal melanoma. *Cancer Discov*, 3, 1122-1129.
- FURSOVA, N. A., TURBERFIELD, A. H., BLACKLEDGE, N. P., FINDLATER, E. L., LASTUVKOVA, A., HUSEYIN, M. K., DOBRINIC, P. & KLOSE, R. J. 2021. BAP1 constrains pervasive H2AK119ub1 to control the transcriptional potential of the genome. *Genes Dev*, 35, 749-770.
- GALAN-MARTINEZ, J., BERENQUER, I., DEL CARMEN MAZA, M., STAMATAKIS, K., GIRONES, N. & FRESNO, M. 2022. TCFL5 deficiency impairs the pachytene to diplotene transition during spermatogenesis in the mouse. *Sci Rep*, 12, 10956.
- GANESH, K. & MASSAGUE, J. 2021. Targeting metastatic cancer. *Nat Med*, 27, 34-44.
- GAO, J., AKSOY, B. A., DOGRUSOZ, U., DRESDNER, G., GROSS, B., SUMER, S. O., SUN, Y., JACOBSEN, A., SINHA, R., LARSSON, E., CERAMI, E., SANDER, C. & SCHULTZ, N. 2013. Integrative analysis of complex cancer genomics and clinical profiles using the cBioPortal. *Sci Signal*, 6, p11.
- GAO, S., JIN, L., LIU, G., WANG, P., SUN, Z., CAO, Y., SHI, H., LIU, X., SHI, Q., ZHOU, X. & YU, R. 2017. Overexpression of RASD1 inhibits glioma cell migration/invasion and inactivates the AKT/mTOR signaling pathway. *Sci Rep*, 7, 3202.
- GE, S. X., JUNG, D. & YAO, R. 2020. ShinyGO: a graphical gene-set enrichment tool for animals and plants. *Bioinformatics*, 36, 2628-2629.

- GENTIEN, D., SABERI-ANSARI, E., SERVANT, N., JOLLY, A., DE LA GRANGE, P., NEMATI, F., LIOT, G., SAULE, S., TEISSANDIER, A., BOURC'HIS, D., GIRARD, E., WONG, J., MASLIAH-PLANCHON, J., NARMANLI, E., LIU, Y., TORUN, E., GOULANCOURT, R., RODRIGUES, M., GAUDE, L. V., REYES, C., BAZIRE, M., CHENEGROS, T., HENRY, E., RAPINAT, A., BOHEC, M., BAULANDE, S., M'KACHER, R., JEANDIDIER, E., NICOLAS, A., CIRIELLO, G., MARGUERON, R., DECAUDIN, D., CASSOUX, N., PIPERNO-NEUMANN, S., STERN, M. H., GIBCUS, J. H., DEKKER, J., HEARD, E., ROMAN-ROMAN, S. & WATERFALL, J. J. 2023. Multi-omics comparison of malignant and normal uveal melanocytes reveals molecular features of uveal melanoma. *Cell Rep*, 42, 113132.
- GERAMI, P., POURYAZDANPARAST, P., VEMULA, S. & BASTIAN, B. C. 2010. Molecular analysis of a case of nevus of ota showing progressive evolution to melanoma with intermediate stages resembling cellular blue nevus. *Am J Dermatopathol*, 32, 301-305.
- GIBSON, D. G., YOUNG, L., CHUANG, R. Y., VENTER, J. C., HUTCHISON, C. A., 3RD & SMITH, H. O. 2009. Enzymatic assembly of DNA molecules up to several hundred kilobases. *Nat Methods*, 6, 343-5.
- GITHUB. 2018. *Picard toolkit* [Online]. Broad Institute, GitHub repository: Broad Institute. Available: <http://broadinstitute.github.io/picard/> [Accessed].
- GKIALA, A. & PALIOURA, S. 2020. Conjunctival Melanoma: Update on Genetics, Epigenetics and Targeted Molecular and Immune-Based Therapies. *Clin Ophthalmol*, 14, 3137-3152.
- GOLDBERG, A. D., ALLIS, C. D. & BERNSTEIN, E. 2007. Epigenetics: a landscape takes shape. *Cell*, 128, 635-8.
- GOLDGEIER, M. H., KLEIN, L. E., KLEIN-ANGERER, S., MOELLMANN, G. & NORDLUND, J. J. 1984. The distribution of melanocytes in the leptomeninges of the human brain. *J Invest Dermatol*, 82, 235-8.
- GONG, Y., ZHANG, L., ZHANG, A., CHEN, X., GAO, P. & ZENG, Q. 2018. GATA4 inhibits cell differentiation and proliferation in pancreatic cancer. *PLoS One*, 13, e0202449.
- GOZANI, O., POTASHKIN, J. & REED, R. 1998. A potential role for U2AF-SAP 155 interactions in recruiting U2 snRNP to the branch site. *Mol Cell Biol*, 18, 4752-60.
- GREENMAN, C., STEPHENS, P., SMITH, R., DALGLIESH, G. L., HUNTER, C., BIGNELL, G., DAVIES, H., TEAGUE, J., BUTLER, A., STEVENS, C., EDKINS, S., O'MEARA, S., VASTRIK, I., SCHMIDT, E. E., AVIS, T., BARTHORPE, S., BHAMRA, G., BUCK, G., CHOUDHURY, B., CLEMENTS, J., COLE, J., DICKS, E., FORBES, S., GRAY, K., HALLIDAY, K., HARRISON, R., HILLS, K., HINTON, J., JENKINSON, A., JONES, D., MENZIES, A., MIRONENKO, T., PERRY, J., RAINE, K., RICHARDSON, D., SHEPHERD, R., SMALL, A., TOFTS, C., VARIAN, J., WEBB, T., WEST, S., WIDAA, S., YATES, A., CAHILL, D. P., LOUIS, D. N., GOLDSTRAW, P., NICHOLSON, A. G., BRASSEUR, F., LOOIJENGA, L., WEBER, B. L., CHIEW, Y. E., DEFAZIO, A., GREAVES, M. F., GREEN, A. R., CAMPBELL, P., BIRNEY, E., EASTON, D. F., CHENEVIX-TRENCH, G., TAN, M. H., KHOO, S. K., TEH, B. T., YUEN, S. T., LEUNG, S. Y., WOOSTER, R., FUTREAL, P. A. & STRATTON, M. R. 2007. Patterns of somatic mutation in human cancer genomes. *Nature*, 446, 153-8.
- GRICHNIK, J. M., ROSS, A. L., SCHNEIDER, S. L., SANCHEZ, M. I., ELLER, M. S. & HATZISTERGOS, K. E. 2014. How, and from which cell sources, do nevi really develop? *Exp Dermatol*, 23, 310-3.

- GRIEWANK, K. G., KOELSCHE, C., VAN DE NES, J. A. P., SCHRIMPF, D., GESSI, M., MOLLER, I., SUCKER, A., SCOLYER, R. A., BUCKLAND, M. E., MURALI, R., PIETSCH, T., VON DEIMLING, A. & SCHADENDORF, D. 2018. Integrated Genomic Classification of Melanocytic Tumors of the Central Nervous System Using Mutation Analysis, Copy Number Alterations, and DNA Methylation Profiling. *Clin Cancer Res*, 24, 4494-4504.
- GRIEWANK, K. G., YU, X., KHALILI, J., SOZEN, M. M., STEMPKE-HALE, K., BERNATCHEZ, C., WARDELL, S., BASTIAN, B. C. & WOODMAN, S. E. 2012. Genetic and molecular characterization of uveal melanoma cell lines. *Pigment Cell Melanoma Res*, 25, 182-7.
- GUPTA, G. P. & MASSAGUE, J. 2006. Cancer metastasis: building a framework. *Cell*, 127, 679-95.
- GUPTA, M. P., LANE, A. M., DEANGELIS, M. M., MAYNE, K., CRABTREE, M., GRAGOUDAS, E. S. & KIM, I. K. 2015. Clinical Characteristics of Uveal Melanoma in Patients With Germline BAP1 Mutations. *JAMA Ophthalmol*, 133, 881-7.
- HAASS, N. K., SMALLEY, K. S., LI, L. & HERLYN, M. 2005. Adhesion, migration and communication in melanocytes and melanoma. *Pigment Cell Res*, 18, 150-9.
- HAN, A., PURWIN, T. J. & APLIN, A. E. 2021. Roles of the BAP1 Tumor Suppressor in Cell Metabolism. *Cancer Res*, 81, 2807-2814.
- HANAHAN, D. 2022. Hallmarks of Cancer: New Dimensions. *Cancer Discov*, 12, 31-46.
- HANAHAN, D. & WEINBERG, R. A. 2000. The Hallmarks of Cancer. *Cell*, 100, 57-70.
- HANAHAN, D. & WEINBERG, R. A. 2011. Hallmarks of cancer: the next generation. *Cell*, 144, 646-74.
- HARBOUR, J. W. 2012. The genetics of uveal melanoma: an emerging framework for targeted therapy. *Pigment Cell Melanoma Res*, 25, 171-81.
- HARBOUR, J. W. & CHEN, R. 2013. The DecisionDx-UM Gene Expression Profile Test Provides Risk Stratification and Individualized Patient Care in Uveal Melanoma. *PLoS Curr*, 5.
- HARBOUR, J. W., ONKEN, M. D., ROBERSON, E. D., DUAN, S., CAO, L., WORLEY, L. A., COUNCIL, M. L., MATATALL, K. A., HELMS, C. & BOWCOCK, A. M. 2010. Frequent mutation of BAP1 in metastasizing uveal melanomas. *Science*, 330, 1410-3.
- HARBOUR, J. W., ROBERSON, E. D., ANBUNATHAN, H., ONKEN, M. D., WORLEY, L. A. & BOWCOCK, A. M. 2013. Recurrent mutations at codon 625 of the splicing factor SF3B1 in uveal melanoma. *Nat Genet*, 45, 133-5.
- HARRIS, M. L., BAXTER, L. L., LOFTUS, S. K. & PAVAN, W. J. 2010. Sox proteins in melanocyte development and melanoma. *Pigment Cell Melanoma Res*, 23, 496-513.
- HARRIS, M. L. & ERICKSON, C. A. 2007. Lineage specification in neural crest cell pathfinding. *Dev Dyn*, 236, 1-19.
- HAWKINS, R. D., HON, G. C., YANG, C., ANTOSIEWICZ-BOURGET, J. E., LEE, L. K., NGO, Q. M., KLUGMAN, S., CHING, K. A., EDSALL, L. E., YE, Z., KUAN, S., YU, P., LIU, H., ZHANG, X., GREEN, R. D., LOBANENKOV, V. V., STEWART, R., THOMSON, J. A. & REN, B. 2011. Dynamic chromatin states in human ES cells reveal potential regulatory sequences and genes involved in pluripotency. *Cell Res*, 21, 1393-409.

- HAYWARD, N. K., WILMOTT, J. S., WADDELL, N., JOHANSSON, P. A., FIELD, M. A., NONES, K., PATCH, A. M., KAKAVAND, H., ALEXANDROV, L. B., BURKE, H., JAKROT, V., KAZAKOFF, S., HOLMES, O., LEONARD, C., SABARINATHAN, R., MULARONI, L., WOOD, S., XU, Q., WADDELL, N., TEMBE, V., PUPO, G. M., DE PAOLI-ISEPPI, R., VILAIN, R. E., SHANG, P., LAU, L. M. S., DAGG, R. A., SCHRAMM, S. J., PRITCHARD, A., DUTTON-REGISTER, K., NEWELL, F., FITZGERALD, A., SHANG, C. A., GRIMMOND, S. M., PICKETT, H. A., YANG, J. Y., STRETCH, J. R., BEHREN, A., KEFFORD, R. F., HERSEY, P., LONG, G. V., CEBON, J., SHACKLETON, M., SPILLANE, A. J., SAW, R. P. M., LOPEZ-BIGAS, N., PEARSON, J. V., THOMPSON, J. F., SCOLYER, R. A. & MANN, G. J. 2017. Whole-genome landscapes of major melanoma subtypes. *Nature*, 545, 175-180.
- HEIKANTS, R. C., NIEVEEN, M., HART, K. C., TEUNISSE, A. & JOCHEMSEN, A. G. 2018. Targeting MDMX and PKCdelta to improve current uveal melanoma therapeutic strategies. *Oncogenesis*, 7, 33.
- HEINTZMAN, N. D., HON, G. C., HAWKINS, R. D., KHERADPOUR, P., STARK, A., HARP, L. F., YE, Z., LEE, L. K., STUART, R. K., CHING, C. W., CHING, K. A., ANTOSIEWICZ-BOURGET, J. E., LIU, H., ZHANG, X., GREEN, R. D., LOBANENKOV, V. V., STEWART, R., THOMSON, J. A., CRAWFORD, G. E., KELLIS, M. & REN, B. 2009. Histone modifications at human enhancers reflect global cell-type-specific gene expression. *Nature*, 459, 108-12.
- HEINZ, S., BENNER, C., SPANN, N., BERTOLINO, E., LIN, Y. C., LASLO, P., CHENG, J. X., MURRE, C., SINGH, H. & GLASS, C. K. 2010. Simple combinations of lineage-determining transcription factors prime cis-regulatory elements required for macrophage and B cell identities. *Mol Cell*, 38, 576-89.
- HIGDON, C. W., MITRA, R. D. & JOHNSON, S. L. 2013. Gene expression analysis of zebrafish melanocytes, iridophores, and retinal pigmented epithelium reveals indicators of biological function and developmental origin. *PLoS One*, 8, e67801.
- HITCHMAN, T. D., BAYSHTOK, G., CERAUDO, E., MOORE, A. R., LEE, C., JIA, R., WANG, N., PACHAI, M. R., SHOUSHARI, A. N., FRANCIS, J. H., GUAN, Y., CHEN, J., CHANG, M. T., TAYLOR, B. S., SAKMAR, T. P., HUBER, T., CHI, P. & CHEN, Y. 2021. Combined Inhibition of Galpha(q) and MEK Enhances Therapeutic Efficacy in Uveal Melanoma. *Clin Cancer Res*, 27, 1476-1490.
- HOFFMAN, M. T., KEMP, S. B., SALAS-ESCABILLAS, D. J., ZHANG, Y., STEELE, N. G., THE, S., LONG, D., BENITZ, S., YAN, W., MARGOLSKEE, R. F., BEDNAR, F., PASCA DI MAGLIANO, M., WEN, H. J. & CRAWFORD, H. C. 2021. The Gustatory Sensory G-Protein GNAT3 Suppresses Pancreatic Cancer Progression in Mice. *Cell Mol Gastroenterol Hepatol*, 11, 349-369.
- HOGG, S. J., BEAVIS, P. A., DAWSON, M. A. & JOHNSTONE, R. W. 2020. Targeting the epigenetic regulation of antitumour immunity. *Nat Rev Drug Discov*, 19, 776-800.
- HOLLIDAY, R. 1987. The inheritance of epigenetic defects. *Science*, 238, 163-70.
- HOLT, J. B., SANGUEZA, O. P., LEVINE, E. A., SHEN, P., BERGMAN, S., GEISINGER, K. R. & CREAGER, A. J. 2004. Nodal melanocytic nevi in sentinel lymph nodes. Correlation with melanoma-associated cutaneous nevi. *Am J Clin Pathol*, 121, 58-63.
- HOMSI, J., BEDIKIAN, A. Y., PAPADOPOULOS, N. E., KIM, K. B., HWU, W. J., MAHONEY, S. L. & HWU, P. 2010. Phase 2 open-label study of weekly docosahexaenoic acid-paclitaxel in patients with metastatic uveal melanoma. *Melanoma Res*, 20, 507-10.

- HON, G. C., HAWKINS, R. D. & REN, B. 2009. Predictive chromatin signatures in the mammalian genome. *Hum Mol Genet*, 18, R195-201.
- HONG, L., SIMON, J. D. & SARNA, T. 2006. Melanin structure and the potential functions of uveal melanosomes. *Pigment Cell Res*, 19, 465-6.
- HOUTZAGERS, L. E., WIERENGA, A. P. A., RUYSS, A. A. M., LUYTEN, G. P. M. & JAGER, M. J. 2020. Iris Colour and the Risk of Developing Uveal Melanoma. *Int J Mol Sci*, 21.
- HU, D. N. 2000. Regulation of growth and melanogenesis of uveal melanocytes. *Pigment Cell Res*, 13 Suppl 8, 81-6.
- HU, D. N., MCCORMICK, S. A., SEEDOR, J. A., RITTERBAND, D. C. & SHAH, M. K. 2007. Isolation, purification and cultivation of conjunctival melanocytes. *Exp Eye Res*, 84, 655-62.
- HU, D. N., SIMON, J. D. & SARNA, T. 2008. Role of ocular melanin in ophthalmic physiology and pathology. *Photochem Photobiol*, 84, 639-44.
- HUGHES, M. S., ZAGER, J., FARIES, M., ALEXANDER, H. R., ROYAL, R. E., WOOD, B., CHOI, J., MCCLUSKEY, K., WHITMAN, E., AGARWALA, S., SISKIN, G., NUTTING, C., TOOMEY, M. A., WEBB, C., BERESNEV, T. & PINGPANK, J. F. 2016. Results of a Randomized Controlled Multicenter Phase III Trial of Percutaneous Hepatic Perfusion Compared with Best Available Care for Patients with Melanoma Liver Metastases. *Ann Surg Oncol*, 23, 1309-19.
- HUGHES, S., DAMATO, B. E., GIDDINGS, I., HISCOTT, P. S., HUMPHREYS, J. & HOULSTON, R. S. 2005. Microarray comparative genomic hybridisation analysis of intraocular uveal melanomas identifies distinctive imbalances associated with loss of chromosome 3. *Br J Cancer*, 93, 1191-6.
- IKEHATA, H. & ONO, T. 2011. The mechanisms of UV mutagenesis. *J Radiat Res*, 52, 115-25.
- INOUE, K. & FRY, E. A. 2017. Haploinsufficient tumor suppressor genes. *Adv Med Biol*, 118, 83-122.
- ITO, S., D'ALESSIO, A. C., TARANOVA, O. V., HONG, K., SOWERS, L. C. & ZHANG, Y. 2010. Role of Tet proteins in 5mC to 5hmC conversion, ES-cell self-renewal and inner cell mass specification. *Nature*, 466, 1129-33.
- IWAMOTO, S., BURROWS, R. C., GROSSNIKLAUS, H. E., ORCUTT, J., KALINA, R. E., BOEHM, M., BOTHWELL, M. A. & SCHMIDT, R. 2002. Immunophenotype of conjunctival melanomas: comparisons with uveal and cutaneous melanomas. *Arch Ophthalmol*, 120, 1625-9.
- JAGER, M. J., MAGNER, J. A., KSANDER, B. R. & DUBOVY, S. R. 2016. Uveal Melanoma Cell Lines: Where do they come from? (An American Ophthalmological Society Thesis). *Trans Am Ophthalmol Soc*, 114, T5.
- JAGER, M. J., SHIELDS, C. L., CEBULLA, C. M., ABDEL-RAHMAN, M. H., GROSSNIKLAUS, H. E., STERN, M. H., CARVAJAL, R. D., BELFORT, R. N., JIA, R., SHIELDS, J. A. & DAMATO, B. E. 2020. Uveal melanoma. *Nat Rev Dis Primers*, 6, 24.
- JAYASINGHE, R. G., CAO, S., GAO, Q., WENDL, M. C., VO, N. S., REYNOLDS, S. M., ZHAO, Y., CLIMENTE-GONZALEZ, H., CHAI, S., WANG, F., VARGHESE, R., HUANG, M., LIANG, W. W., WYCZALKOWSKI, M. A., SENGUPTA, S., LI, Z., PAYNE, S. H., FENYO, D., MINER, J. H., WALTER, M. J., CANCER GENOME ATLAS RESEARCH, N., VINCENT, B., EYRAS, E., CHEN, K.,

- SHMULEVICH, I., CHEN, F. & DING, L. 2018. Systematic Analysis of Splice-Site-Creating Mutations in Cancer. *Cell Rep*, 23, 270-281 e3.
- JENSEN, D. E., PROCTOR, M., MARQUIS, S. T., GARDNER, H. P., HA, S. I., CHODOSH, L. A., ISHOV, A. M., TOMMERUP, N., VISSING, H., SEKIDO, Y., MINNA, J., BORODOVSKY, A., SCHULTZ, D. C., WILKINSON, K. D., MAUL, G. G., BARLEV, N., BERGER, S. L., PRENDERGAST, G. C. & RAUSCHER, F. J., 3RD 1998. BAP1: a novel ubiquitin hydrolase which binds to the BRCA1 RING finger and enhances BRCA1-mediated cell growth suppression. *Oncogene*, 16, 1097-112.
- JENUWEIN, T. & ALLIS, C. D. 2001. Translating the histone code. *Science*, 293, 1074-80.
- JOHANNESSEN, C. M., JOHNSON, L. A., PICCIONI, F., TOWNES, A., FREDERICK, D. T., DONAHUE, M. K., NARAYAN, R., FLAHERTY, K. T., WARGO, J. A., ROOT, D. E. & GARRAWAY, L. A. 2013. A melanocyte lineage program confers resistance to MAP kinase pathway inhibition. *Nature*, 504, 138-42.
- JOHANSSON, P., AOUDE, L. G., WADT, K., GLASSON, W. J., WARRIER, S. K., HEWITT, A. W., KIILGAARD, J. F., HEEGAARD, S., ISAACS, T., FRANCHINA, M., INGVAR, C., VERMEULEN, T., WHITEHEAD, K. J., SCHMIDT, C. W., PALMER, J. M., SYMMONS, J., GERDES, A. M., JONSSON, G. & HAYWARD, N. K. 2016. Deep sequencing of uveal melanoma identifies a recurrent mutation in PLCB4. *Oncotarget*, 7, 4624-31.
- JOHANSSON, P. A., BROOKS, K., NEWELL, F., PALMER, J. M., WILMOTT, J. S., PRITCHARD, A. L., BROIT, N., WOOD, S., CARLINO, M. S., LEONARD, C., KOUFARIOTIS, L. T., NATHAN, V., BEASLEY, A. B., HOWLIE, M., DAWSON, R., RIZOS, H., SCHMIDT, C. W., LONG, G. V., HAMILTON, H., KIILGAARD, J. F., ISAACS, T., GRAY, E. S., ROLFE, O. J., PARK, J. J., STARK, A., MANN, G. J., SCOLYER, R. A., PEARSON, J. V., VAN BAREN, N., WADDELL, N., WADT, K. W., MCGRATH, L. A., WARRIER, S. K., GLASSON, W. & HAYWARD, N. K. 2020. Whole genome landscapes of uveal melanoma show an ultraviolet radiation signature in iris tumours. *Nature Communications*, 11, 2408.
- JOHNSON, A. F., NGUYEN, H. T. & VEITIA, R. A. 2019. Causes and effects of haploinsufficiency. *Biol Rev Camb Philos Soc*, 94, 1774-1785.
- JOHNSON, C. P., KIM, I. K., ESMAELI, B., AMIN-MANSOUR, A., TREACY, D. J., CARTER, S. L., HODIS, E., WAGLE, N., SEEPO, S., YU, X., LANE, A. M., GRAGOUDAS, E. S., VAZQUEZ, F., NICKERSON, E., CIBULSKIS, K., MCKENNA, A., GABRIEL, S. B., GETZ, G., VAN ALLEN, E. M., T HOEN, P. A. C., GARRAWAY, L. A. & WOODMAN, S. E. 2017. Systematic genomic and translational efficiency studies of uveal melanoma. *PLoS One*, 12, e0178189.
- JONES, P. A. 2012. Functions of DNA methylation: islands, start sites, gene bodies and beyond. *Nat Rev Genet*, 13, 484-92.
- KESHET, I., LIEMAN-HURWITZ, J. & CEDAR, H. 1986. DNA methylation affects the formation of active chromatin. *Cell*, 44, 535-43.
- KHAN, S. A., ALMALKI, W. H., ARORA, S. & KESHARWANI, P. 2024. Recent approaches for the treatment of uveal melanoma: Opportunities and challenges. *Crit Rev Oncol Hematol*, 193, 104218.
- KHATTAK, M. A., FISHER, R., HUGHES, P., GORE, M. & LARKIN, J. 2013. Ipilimumab activity in advanced uveal melanoma. *Melanoma Res*, 23, 79-81.



- KILIC, E., VAN GILS, W., LODDER, E., BEVERLOO, H. B., VAN TIL, M. E., MOOY, C. M., PARIDAENS, D., DE KLEIN, A. & LUYTEN, G. P. 2006. Clinical and cytogenetic analyses in uveal melanoma. *Invest Ophthalmol Vis Sci*, 47, 3703-7.
- KIM, S. & KAANG, B. K. 2017. Epigenetic regulation and chromatin remodeling in learning and memory. *Exp Mol Med*, 49, e281.
- KING, A., GOTTLIEB, E., BROOKS, D. G., MURPHY, M. P. & DUNAIEF, J. L. 2004. Mitochondria-derived reactive oxygen species mediate blue light-induced death of retinal pigment epithelial cells. *Photochem Photobiol*, 79, 470-5.
- KIROV, G., GEORGIEVA, L., WILLIAMS, N., NIKOLOV, I., NORTON, N., TONCHEVA, D., O'DONOVAN, M. & OWEN, M. J. 2003. Variation in the protocadherin gamma A gene cluster. *Genomics*, 82, 433-40.
- KIVELA, T., SUCIU, S., HANSSON, J., KRUIT, W. H., VUORISTO, M. S., KLOKE, O., GORE, M., HAHKA-KEMPPINEN, M., PARVINEN, L. M., KUMPULAINEN, E., HUMBLET, Y. & PYRHONEN, S. 2003. Bleomycin, vincristine, lomustine and dacarbazine (BOLD) in combination with recombinant interferon alpha-2b for metastatic uveal melanoma. *Eur J Cancer*, 39, 1115-20.
- KIVELA, T. T. 2018. The first description of the complete natural history of uveal melanoma by two Scottish surgeons, Allan Burns and James Wardrop. *Acta Ophthalmol*, 96, 203-214.
- KNUDSON, A. G. 2001. Two genetic hits (more or less) to cancer. *Nat Rev Cancer*, 1, 157-62.
- KNUDSON, A. G. 2002. Cancer genetics. *Am J Med Genet*, 111, 96-102.
- KOLAT, D., KALUZINSKA, Z., BEDNAREK, A. K. & PLUCIENNIK, E. 2019. The biological characteristics of transcription factors AP-2alpha and AP-2gamma and their importance in various types of cancers. *Biosci Rep*, 39.
- KOOPMANS, A. E., VAARWATER, J., PARIDAENS, D., NAUS, N. C., KILIC, E., DE KLEIN, A. & ROTTERDAM OCULAR MELANOMA STUDY, G. 2013. Patient survival in uveal melanoma is not affected by oncogenic mutations in GNAQ and GNA11. *Br J Cancer*, 109, 493-6.
- KOUZARIDES, T. 2007. Chromatin modifications and their function. *Cell*, 128, 693-705.
- KROOK, M. A., REESER, J. W., ERNST, G., BARKER, H., WILBERDING, M., LI, G., CHEN, H. Z. & ROYCHOWDHURY, S. 2021. Fibroblast growth factor receptors in cancer: genetic alterations, diagnostics, therapeutic targets and mechanisms of resistance. *Br J Cancer*, 124, 880-892.
- KULESA, P. M., KASEMEIER-KULESA, J. C., TEDDY, J. M., MARGARYAN, N. V., SEFTOR, E. A., SEFTOR, R. E. & HENDRIX, M. J. 2006. Reprogramming metastatic melanoma cells to assume a neural crest cell-like phenotype in an embryonic microenvironment. *Proc Natl Acad Sci U S A*, 103, 3752-7.
- KULIS, M. & ESTELLER, M. 2010. DNA methylation and cancer. *Adv Genet*, 70, 27-56.
- KUMAR, D., CINGHU, S., OLDFIELD, A. J., YANG, P. & JOTHI, R. 2021. Decoding the function of bivalent chromatin in development and cancer. *Genome Res*, 31, 2170-2184.
- KURAS, M. 2023. Exploring the Complex and Multifaceted Interplay between Melanoma Cells and the Tumor Microenvironment. *Int J Mol Sci*, 24.

- KWON, J., LEE, D. & LEE, S. A. 2023. BAP1 as a guardian of genome stability: implications in human cancer. *Exp Mol Med*, 55, 745-754.
- LABUN, K., MONTAGUE, T. G., GAGNON, J. A., THYME, S. B. & VALEN, E. 2016. CHOPCHOP v2: a web tool for the next generation of CRISPR genome engineering. *Nucleic Acids Res*, 44, W272-6.
- LABUN, K., MONTAGUE, T. G., KRAUSE, M., TORRES CLEUREN, Y. N., TJELDNE, H. & VALEN, E. 2019. CHOPCHOP v3: expanding the CRISPR web toolbox beyond genome editing. *Nucleic Acids Res*, 47, W171-W174.
- LALONDE, E., EWENS, K., RICHARDS-YUTZ, J., EBRAHIMZEDEH, J., TERA, M., GONSALVES, C. F., SATO, T., SHIELDS, C. L. & GANGULY, A. 2022. Improved Uveal Melanoma Copy Number Subtypes Including an Ultra-High-Risk Group. *Ophthalmol Sci*, 2, 100121.
- LAMAS, N. J., MARTEL, A., NAHON-ESTEVE, S., GOFFINET, S., MACOCCO, A., BERLOLOTTO, C., LASSALLE, S. & HOFMAN, P. 2021. Prognostic Biomarkers in Uveal Melanoma: The Status Quo, Recent Advances and Future Directions. *Cancers (Basel)*, 14.
- LAMOREUX, M. L., WAKAMATSU, K. & ITO, S. 2001. Interaction of major coat color gene functions in mice as studied by chemical analysis of eumelanin and pheomelanin. *Pigment Cell Res*, 14, 23-31.
- LANDREVILLE, S., AGAPOVA, O. A., MATATALL, K. A., KNEASS, Z. T., ONKEN, M. D., LEE, R. S., BOWCOCK, A. M. & HARBOUR, J. W. 2012. Histone deacetylase inhibitors induce growth arrest and differentiation in uveal melanoma. *Clin Cancer Res*, 18, 408-16.
- LANGMEAD, B. & SALZBERG, S. L. 2012. Fast gapped-read alignment with Bowtie 2. *Nat Methods*, 9, 357-9.
- LAPADULA, D. & BENOVIC, J. L. 2021. Targeting Oncogenic Galpha(q11) in Uveal Melanoma. *Cancers (Basel)*, 13.
- LARRIBERE, L., KUPHAL, S., SACHPEKIDIS, C., SACHINDRA, HUSER, L., BOSSERHOFF, A. & UTIKAL, J. 2018. Targeted Therapy-Resistant Melanoma Cells Acquire Transcriptomic Similarities with Human Melanoblasts. *Cancers (Basel)*, 10.
- LARRIBERE, L. & UTIKAL, J. 2019. Stem Cell-Derived Models of Neural Crest Are Essential to Understand Melanoma Progression and Therapy Resistance. *Front Mol Neurosci*, 12, 111.
- LAWRENCE, M. S., STOJANOV, P., POLAK, P., KRYUKOV, G. V., CIBULSKIS, K., SIVACHENKO, A., CARTER, S. L., STEWART, C., MERMEL, C. H., ROBERTS, S. A., KIEZUN, A., HAMMERMAN, P. S., MCKENNA, A., DRIER, Y., ZOU, L., RAMOS, A. H., PUGH, T. J., STRANSKY, N., HELMAN, E., KIM, J., SOUGNEZ, C., AMBROGIO, L., NICKERSON, E., SHEFLER, E., CORTES, M. L., AUCLAIR, D., SAKSENA, G., VOET, D., NOBLE, M., DICARA, D., LIN, P., LICHTENSTEIN, L., HEIMAN, D. I., FENNELL, T., IMIELINSKI, M., HERNANDEZ, B., HODIS, E., BACA, S., DULAK, A. M., LOHR, J., LANDAU, D. A., WU, C. J., MELENDEZ-ZAJGLA, J., HIDALGO-MIRANDA, A., KOREN, A., MCCARROLL, S. A., MORA, J., CROMPTON, B., ONOFRIO, R., PARKIN, M., WINCKLER, W., ARDLIE, K., GABRIEL, S. B., ROBERTS, C. W. M., BIEGEL, J. A., STEGMAIER, K., BASS, A. J., GARRAWAY, L. A., MEYERSON, M., GOLUB, T. R., GORDENIN, D. A., SUNYAEV, S., LANDER, E. S. & GETZ, G. 2013. Mutational heterogeneity in cancer and the search for new cancer-associated genes. *Nature*, 499, 214-218.

- LEE, W. H., MORTON, R. A., EPSTEIN, J. I., BROOKS, J. D., CAMPBELL, P. A., BOVA, G. S., HSIEH, W. S., ISAACS, W. B. & NELSON, W. G. 1994. Cytidine methylation of regulatory sequences near the p16 class glutathione S-transferase gene accompanies human prostatic carcinogenesis. *Proc Natl Acad Sci U S A*, 91, 11733-7.
- LEYVRAZ, S., PIPERNO-NEUMANN, S., SUCIU, S., BAURAIN, J. F., ZDZIENICKI, M., TESTORI, A., MARSHALL, E., SCHEULEN, M., JOUARY, T., NEGRIER, S., VERMORKEN, J. B., KAEMPGEN, E., DURANDO, X., SCHADENDORF, D., GURUNATH, R. K. & KEILHOLZ, U. 2014. Hepatic intra-arterial versus intravenous fotemustine in patients with liver metastases from uveal melanoma (EORTC 18021): a multicentric randomized trial. *Ann Oncol*, 25, 742-746.
- LI, Y., JIA, R. & GE, S. 2017. Role of Epigenetics in Uveal Melanoma. *Int J Biol Sci*, 13, 426-433.
- LIN, J. Y. & FISHER, D. E. 2007. Melanocyte biology and skin pigmentation. *Nature*, 445, 843-50.
- LIN, X., CHEN, J. D., WANG, C. Y., CAI, Z., ZHAN, R., YANG, C., ZHANG, L. Y., LI, L. Y., XIAO, Y., CHEN, M. K. & WU, M. 2023. Cooperation of MLL1 and Jun in controlling H3K4me3 on enhancers in colorectal cancer. *Genome Biol*, 24, 268.
- LOGAN, P., BERNABEU, M., FERREIRA, A. & BURNIER, M. N., JR. 2015. Evidence for the Role of Blue Light in the Development of Uveal Melanoma. *J Ophthalmol*, 2015, 386986.
- LONG, R. M., ONG, H., WANG, W. X., KOMIRISHETTY, P., ARETI, A., CHANDRASEKHAR, A., LAROUCHE, M., LEFEBVRE, J. L. & ZOCHODNE, D. W. 2023. The Role of Protocadherin gamma in Adult Sensory Neurons and Skin Reinnervation. *J Neurosci*, 43, 8348-8366.
- LOPES, V. S., WASMEIER, C., SEABRA, M. C. & FUTTER, C. E. 2007. Melanosome maturation defect in Rab38-deficient retinal pigment epithelium results in instability of immature melanosomes during transient melanogenesis. *Mol Biol Cell*, 18, 3914-27.
- LORING, J. F. & ERICKSON, C. A. 1987. Neural crest cell migratory pathways in the trunk of the chick embryo. *Dev Biol*, 121, 220-36.
- LOUIE, B. H. & KURZROCK, R. 2020. BAP1: Not just a BRCA1-associated protein. *Cancer Treat Rev*, 90, 102091.
- LOVE, M. I., HUBER, W. & ANDERS, S. 2014. Moderated estimation of fold change and dispersion for RNA-seq data with DESeq2. *Genome Biol*, 15, 550.
- MAAT, W., VAN DER VELDEN, P. A., OUT-LUITING, C., PLUG, M., DIRKS-MULDER, A., JAGER, M. J. & GRUIS, N. A. 2007. Epigenetic inactivation of RASSF1a in uveal melanoma. *Invest Ophthalmol Vis Sci*, 48, 486-90.
- MACHIDA, Y. J., MACHIDA, Y., VASHISHT, A. A., WOHLSCHEGEL, J. A. & DUTTA, A. 2009. The deubiquitinating enzyme BAP1 regulates cell growth via interaction with HCF-1. *J Biol Chem*, 284, 34179-88.
- MAHENDRARAJ, K., LAU, C. S., LEE, I. & CHAMBERLAIN, R. S. 2016. Trends in incidence, survival, and management of uveal melanoma: a population-based study of 7,516 patients from the Surveillance, Epidemiology, and End Results database (1973-2012). *Clin Ophthalmol*, 10, 2113-2119.

- MANCARELLA, D. & PLASS, C. 2021. Epigenetic signatures in cancer: proper controls, current challenges and the potential for clinical translation. *Genome Med*, 13, 23.
- MARKL, I. D., CHENG, J., LIANG, G., SHIBATA, D., LAIRD, P. W. & JONES, P. A. 2001. Global and gene-specific epigenetic patterns in human bladder cancer genomes are relatively stable in vivo and in vitro over time. *Cancer Res*, 61, 5875-84.
- MARSHALL, J. C., GORDON, K. D., MCCAULEY, C. S., DE SOUZA FILHO, J. P. & BURNIER, M. N. 2006. The effect of blue light exposure and use of intraocular lenses on human uveal melanoma cell lines. *Melanoma Res*, 16, 537-41.
- MARTIN, M. 2011. Cutadapt removes adapter sequences from high-throughput sequencing reads. *EMBnet.journal*, 17.
- MARTIN, M., MASSHOFER, L., TEMMING, P., RAHMANN, S., METZ, C., BORNFELD, N., VAN DE NES, J., KLEIN-HITPASS, L., HINNEBUSCH, A. G., HORSTHEMKE, B., LOHMANN, D. R. & ZESCHNIGK, M. 2013. Exome sequencing identifies recurrent somatic mutations in EIF1AX and SF3B1 in uveal melanoma with disomy 3. *Nat Genet*, 45, 933-6.
- MASCLEF, L., AHMED, O., ESTAVOYER, B., LARRIVEE, B., LABRECQUE, N., NIJNIK, A. & AFFAR, E. B. 2021. Roles and mechanisms of BAP1 deubiquitinase in tumor suppression. *Cell Death Differ*, 28, 606-625.
- MASTRONIKOLIS, S., ADAMOPOULOU, M., PAPOULIAKOS, S., MANOLI, A., KATSINIS, S., MAKRI, O., MONASTIRIOTI, A. E., TSIAMBAS, E. & GEORGAKOPOULOS, C. 2021. Mutational landscape in Uveal Melanoma. *J BUON*, 26, 1194-1197.
- MATATALL, K. A., AGAPOVA, O. A., ONKEN, M. D., WORLEY, L. A., BOWCOCK, A. M. & HARBOUR, J. W. 2013. BAP1 deficiency causes loss of melanocytic cell identity in uveal melanoma. *BMC Cancer*, 13, 371.
- MCCARTHY, D. J., CHEN, Y. & SMYTH, G. K. 2012. Differential expression analysis of multifactor RNA-Seq experiments with respect to biological variation. *Nucleic Acids Res*, 40, 4288-97.
- MEERS, M. P., TENENBAUM, D. & HENIKOFF, S. 2019. Peak calling by Sparse Enrichment Analysis for CUT&RUN chromatin profiling. *Epigenetics Chromatin*, 12, 42.
- MEHDIPOUR, P., CHEN, R. & DE CARVALHO, D. D. 2021. The next generation of DNMT inhibitors. *Nat Cancer*, 2, 1000-1001.
- MERHAVI, E., COHEN, Y., AVRAHAM, B. C., FRENKEL, S., CHOWERS, I., PE'ER, J. & GOLDENBERG-COHEN, N. 2007. Promoter methylation status of multiple genes in uveal melanoma. *Invest Ophthalmol Vis Sci*, 48, 4403-6.
- MIDDLETON, M. R., MCALPINE, C., WOODCOCK, V. K., CORRIE, P., INFANTE, J. R., STEVEN, N. M., EVANS, T. R. J., ANTHONY, A., SHOUSHARI, A. N., HAMID, O., GUPTA, A., VARDEU, A., LEACH, E., NAIDOO, R., STANHOPE, S., LEWIS, S., HURST, J., O'KELLY, I. & SZNOL, M. 2020. Tebentafusp, A TCR/Anti-CD3 Bispecific Fusion Protein Targeting gp100, Potently Activated Antitumor Immune Responses in Patients with Metastatic Melanoma. *Clin Cancer Res*, 26, 5869-5878.

- MO, Q., WAN, L., SCHELL, M. J., JIM, H., TWOROGGER, S. S. & PENG, G. 2021. Integrative Analysis Identifies Multi-Omics Signatures That Drive Molecular Classification of Uveal Melanoma. *Cancers (Basel)*, 13.
- MOCHIZUKI, M., SUGITA, S. & KAMOI, K. 2013. Immunological homeostasis of the eye. *Prog Retin Eye Res*, 33, 10-27.
- MOORE, A. R., CERAUDO, E., SHER, J. J., GUAN, Y., SHOUSHARI, A. N., CHANG, M. T., ZHANG, J. Q., WALCZAK, E. G., KAZMI, M. A., TAYLOR, B. S., HUBER, T., CHI, P., SAKMAR, T. P. & CHEN, Y. 2016. Recurrent activating mutations of G-protein-coupled receptor CYSLTR2 in uveal melanoma. *Nat Genet*, 48, 675-80.
- MOORE, A. R., RAN, L., GUAN, Y., SHER, J. J., HITCHMAN, T. D., ZHANG, J. Q., HWANG, C., WALZAK, E. G., SHOUSHARI, A. N., MONETTE, S., MURALI, R., WIESNER, T., GRIEWANK, K. G., CHI, P. & CHEN, Y. 2018. GNA11 Q209L Mouse Model Reveals RasGRP3 as an Essential Signaling Node in Uveal Melanoma. *Cell Rep*, 22, 2455-2468.
- MORT, R. L., JACKSON, I. J. & PATTON, E. E. 2015. The melanocyte lineage in development and disease. *Development*, 142, 1387.
- MURALI, R., WIESNER, T. & SCOLYER, R. A. 2013. Tumours associated with BAP1 mutations. *Pathology*, 45, 116-26.
- NAM, A. S., CHALIGNE, R. & LANDAU, D. A. 2021. Integrating genetic and non-genetic determinants of cancer evolution by single-cell multi-omics. *Nat Rev Genet*, 22, 3-18.
- NARITA, T., WEINERT, B. T. & CHOUDHARY, C. 2019. Functions and mechanisms of non-histone protein acetylation. *Nat Rev Mol Cell Biol*, 20, 156-174.
- NASTI, T. H. & TIMARES, L. 2015. MC1R, eumelanin and pheomelanin: their role in determining the susceptibility to skin cancer. *Photochem Photobiol*, 91, 188-200.
- NAUS, N. C., VAN DRUNEN, E., DE KLEIN, A., LUYTEN, G. P., PARIDAENS, D. A., ALERS, J. C., KSANDER, B. R., BEVERLOO, H. B. & SLATER, R. M. 2001. Characterization of complex chromosomal abnormalities in uveal melanoma by fluorescence in situ hybridization, spectral karyotyping, and comparative genomic hybridization. *Genes Chromosomes Cancer*, 30, 267-73.
- NGUYEN, J. Q. N., DRABAREK, W., YAVUZYIGITOGU, S., MEDICO SALSENCH, E., VERDIJK, R. M., NAUS, N. C., DE KLEIN, A., KILIC, E. & BROSENS, E. 2020. Spliceosome Mutations in Uveal Melanoma. *Int J Mol Sci*, 21.
- NI, W., PEREZ, A. A., SCHREINER, S., NICOLET, C. M. & FARNHAM, P. J. 2020. Characterization of the ZFX family of transcription factors that bind downstream of the start site of CpG island promoters. *Nucleic Acids Res*, 48, 5986-6000.
- NISHIKAWA, H., WU, W., KOIKE, A., KOJIMA, R., GOMI, H., FUKUDA, M. & OHTA, T. 2009. BRCA1-associated protein 1 interferes with BRCA1/BARD1 RING heterodimer activity. *Cancer Res*, 69, 111-9.
- NORDIN, A., ZAMBANINI, G., PAGELLA, P. & CANTU, C. 2023. The CUT&RUN suspect list of problematic regions of the genome. *Genome Biol*, 24, 185.

- NY, L., JESPERSEN, H., KARLSSON, J., ALSEN, S., FILGES, S., ALL-ERIKSSON, C., ANDERSSON, B., CARNEIRO, A., HELGADOTTIR, H., LEVIN, M., LJUSLINDER, I., OLOFSSON BAGGE, R., SAH, V. R., STIERNER, U., STAHLBERG, A., ULLENHAG, G., NILSSON, L. M. & NILSSON, J. A. 2021. The PEMDAC phase 2 study of pembrolizumab and entinostat in patients with metastatic uveal melanoma. *Nat Commun*, 12, 5155.
- O'RAHILLY, R. & MULLER, F. 2007. The development of the neural crest in the human. *J Anat*, 211, 335-51.
- OKINO, Y., MACHIDA, Y., FRANKLAND-SEARBY, S. & MACHIDA, Y. J. 2015. BRCA1-associated protein 1 (BAP1) deubiquitinase antagonizes the ubiquitin-mediated activation of FoxK2 target genes. *J Biol Chem*, 290, 1580-91.
- ONKEN, M. D., EHLERS, J. P., WORLEY, L. A., MAKITA, J., YOKOTA, Y. & HARBOUR, J. W. 2006. Functional gene expression analysis uncovers phenotypic switch in aggressive uveal melanomas. *Cancer Res*, 66, 4602-9.
- ONKEN, M. D., WORLEY, L. A., CHAR, D. H., AUGSBURGER, J. J., CORREA, Z. M., NUDLEMAN, E., AABERG, T. M., JR., ALTAWHEEL, M. M., BARDENSTEIN, D. S., FINGER, P. T., GALLIE, B. L., HAROCOPOS, G. J., HOVLAND, P. G., MCGOWAN, H. D., MILMAN, T., MRUTHYUNJAYA, P., SIMPSON, E. R., SMITH, M. E., WILSON, D. J., WIROSTKO, W. J. & HARBOUR, J. W. 2012. Collaborative Ocular Oncology Group report number 1: prospective validation of a multi-gene prognostic assay in uveal melanoma. *Ophthalmology*, 119, 1596-603.
- ONKEN, M. D., WORLEY, L. A., EHLERS, J. P. & HARBOUR, J. W. 2004. Gene expression profiling in uveal melanoma reveals two molecular classes and predicts metastatic death. *Cancer Res*, 64, 7205-9.
- ONKEN, M. D., WORLEY, L. A. & HARBOUR, J. W. 2010a. Association between gene expression profile, proliferation and metastasis in uveal melanoma. *Curr Eye Res*, 35, 857-63.
- ONKEN, M. D., WORLEY, L. A., LONG, M. D., DUAN, S., COUNCIL, M. L., BOWCOCK, A. M. & HARBOUR, J. W. 2008. Oncogenic mutations in GNAQ occur early in uveal melanoma. *Invest Ophthalmol Vis Sci*, 49, 5230-4.
- ONKEN, M. D., WORLEY, L. A., PERSON, E., CHAR, D. H., BOWCOCK, A. M. & HARBOUR, J. W. 2007. Loss of heterozygosity of chromosome 3 detected with single nucleotide polymorphisms is superior to monosomy 3 for predicting metastasis in uveal melanoma. *Clin Cancer Res*, 13, 2923-7.
- ONKEN, M. D., WORLEY, L. A., TUSCAN, M. D. & HARBOUR, J. W. 2010b. An accurate, clinically feasible multi-gene expression assay for predicting metastasis in uveal melanoma. *J Mol Diagn*, 12, 461-8.
- ONO, K., HATA, K., NAKAMURA, E., ISHIHARA, S., KOBAYASHI, S., NAKANISHI, M., YOSHIDA, M., TAKAHATA, Y., MURAKAMI, T., TAKENOSHITA, S., KOMORI, T., NISHIMURA, R. & YONEDA, T. 2021. Dmrt2 promotes transition of endochondral bone formation by linking Sox9 and Runx2. *Commun Biol*, 4, 326.
- ORDAZ-RAMOS, A., ROSALES-GALLEGOS, V. H., MELENDEZ-ZAJGLA, J., MALDONADO, V. & VAZQUEZ-SANTILLAN, K. 2021. The Role of LGR4 (GPR48) in Normal and Cancer Processes. *Int J Mol Sci*, 22.

- OZAKI, S., MIKAMI, K., KUNIEDA, T. & TANAKA, J. 2022. Chloride Intracellular Channel Proteins (CLICs) and Malignant Tumor Progression: A Focus on the Preventive Role of CLIC2 in Invasion and Metastasis. *Cancers (Basel)*, 14.
- PANDIANI, C., BERANGER, G. E., LECLERC, J., BALLOTTI, R. & BERTOLOTTO, C. 2017. Focus on cutaneous and uveal melanoma specificities. *Genes Dev*, 31, 724-743.
- PARRELLA, P., CABALLERO, O. L., SIDRANSKY, D. & MERBS, S. L. 2001. Detection of c-myc amplification in uveal melanoma by fluorescent in situ hybridization. *Invest Ophthalmol Vis Sci*, 42, 1679-84.
- PATEL, K. A., EDMONDSON, N. D., TALBOT, F., PARSONS, M. A., RENNIE, I. G. & SISLEY, K. 2001. Prediction of prognosis in patients with uveal melanoma using fluorescence in situ hybridisation. *Br J Ophthalmol*, 85, 1440-4.
- PILARSKI, R., CEBULLA, C. M., MASSENGILL, J. B., RAI, K., RICH, T., STRONG, L., MCGILLIVRAY, B., ASRAT, M. J., DAVIDORF, F. H. & ABDEL-RAHMAN, M. H. 2014. Expanding the clinical phenotype of hereditary BAP1 cancer predisposition syndrome, reporting three new cases. *Genes Chromosomes Cancer*, 53, 177-82.
- PLASSERAUD, K. M., COOK, R. W., TSAI, T., SHILDKROT, Y., MIDDLEBROOK, B., MAETZOLD, D., WILKINSON, J., STONE, J., JOHNSON, C., OELSCHLAGER, K. & AABERG, T. M. 2016. Clinical Performance and Management Outcomes with the DecisionDx-UM Gene Expression Profile Test in a Prospective Multicenter Study. *J Oncol*, 2016, 5325762.
- PONS, F., PLANA, M., CAMINAL, J. M., PERA, J., FERNANDES, I., PEREZ, J., GARCIA-DEL-MURO, X., MARCOVAL, J., PENIN, R., FABRA, A. & PIULATS, J. M. 2011. Metastatic uveal melanoma: is there a role for conventional chemotherapy? - A single center study based on 58 patients. *Melanoma Res*, 21, 217-22.
- POPOVA, T., HEBERT, L., JACQUEMIN, V., GAD, S., CAUX-MONCOUTIER, V., DUBOIS-D'ENGHIEN, C., RICHAUDEAU, B., RENAUDIN, X., SELLERS, J., NICOLAS, A., SASTRE-GARAU, X., DESJARDINS, L., GYAPAY, G., RAYNAL, V., SINILNIKOVA, O. M., ANDRIEU, N., MANIE, E., DE PAUW, A., GESTA, P., BONADONA, V., MAUGARD, C. M., PENET, C., AVRIL, M. F., BARILLOT, E., CABARET, O., DELATTRE, O., RICHARD, S., CARON, O., BENFODDA, M., HU, H. H., SOUFIR, N., BRESSAC-DE PAILLERETS, B., STOPPA-LYONNET, D. & STERN, M. H. 2013. Germline BAP1 mutations predispose to renal cell carcinomas. *Am J Hum Genet*, 92, 974-80.
- PRESCHER, G., BORNFELD, N., FRIEDRICH, W., SEEGER, S. & BECHER, R. 1995. Cytogenetics of twelve cases of uveal melanoma and patterns of nonrandom anomalies and isochromosome formation. *Cancer Genet Cytogenet*, 80, 40-6.
- PRESCHER, G., BORNFELD, N., HIRCHE, H., HORSTHEMKE, B., JOCKEL, K. H. & BECHER, R. 1996. Prognostic implications of monosomy 3 in uveal melanoma. *Lancet*, 347, 1222-5.
- QUINLAN, A. R. & HALL, I. M. 2010. BEDTools: a flexible suite of utilities for comparing genomic features. *Bioinformatics*, 26, 841-2.
- QUINTERO-RONDEROS, P. & MONTOYA-ORTIZ, G. 2012. Epigenetics and autoimmune diseases. *Autoimmune Dis*, 2012, 593720.

- RAMIREZ, F., RYAN, D. P., GRUNING, B., BHARDWAJ, V., KILPERT, F., RICHTER, A. S., HEYNE, S., DUNDAR, F. & MANKE, T. 2016. deepTools2: a next generation web server for deep-sequencing data analysis. *Nucleic Acids Res*, 44, W160-5.
- RANDHAWA, M., HUFF, T., VALENCIA, J. C., YOUNOSSI, Z., CHANDHOKE, V., HEARING, V. J. & BARANOVA, A. 2009. Evidence for the ectopic synthesis of melanin in human adipose tissue. *FASEB J*, 23, 835-43.
- RASTRELLI, M., TROPEA, S., ROSSI, C. R. & ALAIBAC, M. 2014. Melanoma: epidemiology, risk factors, pathogenesis, diagnosis and classification. *In Vivo*, 28, 1005-11.
- RAZIN, A. & RIGGS, A. D. 1980. DNA methylation and gene function. *Science*, 210, 604-10.
- REDDY, B. Y., MILLER, D. M. & TSAO, H. 2017. Somatic driver mutations in melanoma. *Cancer*, 123, 2104-2117.
- RIBAS, A. & FLAHERTY, K. T. 2011. BRAF targeted therapy changes the treatment paradigm in melanoma. *Nat Rev Clin Oncol*, 8, 426-33.
- RICHARDS, E. J. & ELGIN, S. C. 2002. Epigenetic codes for heterochromatin formation and silencing: rounding up the usual suspects. *Cell*, 108, 489-500.
- RIGGS, A. D. 1975. X inactivation, differentiation, and DNA methylation. *Cytogenet Cell Genet*, 14, 9-25.
- RINDERLE, C., CHRISTENSEN, H. M., SCHWEIGER, S., LEHRACH, H. & YASPO, M. L. 1999. AIRE encodes a nuclear protein co-localizing with cytoskeletal filaments: altered sub-cellular distribution of mutants lacking the PHD zinc fingers. *Hum Mol Genet*, 8, 277-90.
- ROBERTSON, A. G., SHIH, J., YAU, C., GIBB, E. A., OBA, J., MUNGALL, K. L., HESS, J. M., UZUNANGELOV, V., WALTER, V., DANILOVA, L., LICHTENBERG, T. M., KUCHERLAPATI, M., KIMES, P. K., TANG, M., PENSON, A., BABUR, O., AKBANI, R., BRISTOW, C. A., HOADLEY, K. A., IYPE, L., CHANG, M. T., NETWORK, T. R., CHERNIACK, A. D., BENZ, C., MILLS, G. B., VERHAAK, R. G. W., GRIEWANK, K. G., FELAU, I., ZENKLUSEN, J. C., GERSHENWALD, J. E., SCHOENFIELD, L., LAZAR, A. J., ABDEL-RAHMAN, M. H., ROMAN-ROMAN, S., STERN, M. H., CEBULLA, C. M., WILLIAMS, M. D., JAGER, M. J., COUPLAND, S. E., ESMAELI, B., KANDOTH, C. & WOODMAN, S. E. 2017. Integrative Analysis Identifies Four Molecular and Clinical Subsets in Uveal Melanoma. *Cancer Cell*, 32, 204-220 e15.
- ROBINSON, M. D., MCCARTHY, D. J. & SMYTH, G. K. 2010. edgeR: a Bioconductor package for differential expression analysis of digital gene expression data. *Bioinformatics*, 26, 139-40.
- RODRIGUES, M., KONING, L., COUPLAND, S. E., JOCHEMSEN, A. G., MARAIS, R., STERN, M. H., VALENTE, A., BARNHILL, R., CASSOUX, N., EVANS, A., GALLOWAY, I., JAGER, M. J., KAPITEIJN, E., ROMANOWSKA-DIXON, B., RYLL, B., ROMAN-ROMAN, S., PIPERNO-NEUMANN, S. & CONSORTIUM, U. M. C. 2019. So Close, yet so Far: Discrepancies between Uveal and Other Melanomas. A Position Paper from UM Cure 2020. *Cancers (Basel)*, 11.
- RODRIGUEZ-VIDAL, C., FERNANDEZ-DIAZ, D., FERNANDEZ-MARTA, B., LAGO-BAAMEIRO, N., PARDO, M., SILVA, P., PANIAGUA, L., BLANCO-TEIJEIRO, M. J., PINEIRO, A. & BANDE, M. 2020. Treatment of Metastatic Uveal Melanoma: Systematic Review. *Cancers (Basel)*, 12.



- RODRIGUEZ, A., DUENAS-GONZALEZ, A. & DELGADO-PELAYO, S. 2016. Clinical presentation and management of uveal melanoma. *Mol Clin Oncol*, 5, 675-677.
- ROSS-INNES, C. S., STARK, R., TESCHENDORFF, A. E., HOLMES, K. A., ALI, H. R., DUNNING, M. J., BROWN, G. D., GOJIS, O., ELLIS, I. O., GREEN, A. R., ALI, S., CHIN, S. F., PALMIERI, C., CALDAS, C. & CARROLL, J. S. 2012. Differential oestrogen receptor binding is associated with clinical outcome in breast cancer. *Nature*, 481, 389-93.
- ROYER-BERTRAND, B., TORSSELLO, M., RIMOLDI, D., EL ZAOUI, I., CISAROVA, K., PESCHINI-GOBERT, R., RAYNAUD, F., ZOGRAFOS, L., SCHALENBOURG, A., SPEISER, D., NICOLAS, M., VALLAT, L., KLEIN, R., LEYVRAZ, S., CIRIELLO, G., RIGGI, N., MOULIN, A. P. & RIVOLTA, C. 2016. Comprehensive Genetic Landscape of Uveal Melanoma by Whole-Genome Sequencing. *Am J Hum Genet*, 99, 1190-1198.
- SACCO, J. J., JACKSON, R., CORRIE, P., DANSON, S., EVANS, T. R. J., OCHSENREITHER, S., KUMAR, S., GOODMAN, A., LARKIN, J., KARYDIS, I., STEVEN, N., LORIGAN, P., PLUMMER, R., PATEL, P., PSARELLI, E., OLSSON-BROWN, A., SHAW, H., LEYVRAZ, S., HANDLEY, L., RAWCLIFFE, C. & NATHAN, P. 2024. A three-arm randomised phase II study of the MEK inhibitor selumetinib alone or in combination with paclitaxel in metastatic uveal melanoma. *Eur J Cancer*, 202, 114009.
- SAFE, S. 2023. Specificity Proteins (Sp) and Cancer. *Int J Mol Sci*, 24.
- SAINI, A. K., NANDA, J. S., LORSCH, J. R. & HINNEBUSCH, A. G. 2010. Regulatory elements in eIF1A control the fidelity of start codon selection by modulating tRNA(i)(Met) binding to the ribosome. *Genes Dev*, 24, 97-110.
- SARNA, T., BURKE, J. M., KORYTOWSKI, W., ROZANOWSKA, M., SKUMATZ, C. M., ZAREBA, A. & ZAREBA, M. 2003. Loss of melanin from human RPE with aging: possible role of melanin photooxidation. *Exp Eye Res*, 76, 89-98.
- SASAHIRA, T., BOSSERHOFF, A. K. & KIRITA, T. 2018. The importance of melanoma inhibitory activity gene family in the tumor progression of oral cancer. *Pathol Int*, 68, 278-286.
- SAVAGE, K. I. & HARKIN, D. P. 2015. BRCA1, a 'complex' protein involved in the maintenance of genomic stability. *FEBS J*, 282, 630-46.
- SCHADENDORF, D., VAN AKKOOI, A. C. J., BERKING, C., GRIEWANK, K. G., GUTZMER, R., HAUSCHILD, A., STANG, A., ROESCH, A. & UGUREL, S. 2018. Melanoma. *Lancet*, 392, 971-984.
- SCHEUERMANN, J. C., DE AYALA ALONSO, A. G., OKTABA, K., LY-HARTIG, N., MCGINTY, R. K., FRATERMAN, S., WILM, M., MUIR, T. W. & MULLER, J. 2010. Histone H2A deubiquitinase activity of the Polycomb repressive complex PR-DUB. *Nature*, 465, 243-7.
- SCHOLES, A. G., DAMATO, B. E., NUNN, J., HISCOTT, P., GRIERSON, I. & FIELD, J. K. 2003. Monosomy 3 in uveal melanoma: correlation with clinical and histologic predictors of survival. *Invest Ophthalmol Vis Sci*, 44, 1008-11.
- SEBERG, H. E., VAN OTTERLOO, E. & CORNELL, R. A. 2017a. Beyond MITF: Multiple transcription factors directly regulate the cellular phenotype in melanocytes and melanoma. *Pigment Cell Melanoma Res*, 30, 454-466.

- SEBERG, H. E., VAN OTTERLOO, E., LOFTUS, S. K., LIU, H., BONDE, G., SOMPALLAE, R., GILDEA, D. E., SANTANA, J. F., MANAK, J. R., PAVAN, W. J., WILLIAMS, T. & CORNELL, R. A. 2017b. TFAP2 paralogs regulate melanocyte differentiation in parallel with MITF. *PLoS Genet*, 13, e1006636.
- SELIGSON, D. B., HORVATH, S., MCBRIAN, M. A., MAH, V., YU, H., TZE, S., WANG, Q., CHIA, D., GOODGLICK, L. & KURDISTANI, S. K. 2009. Global levels of histone modifications predict prognosis in different cancers. *Am J Pathol*, 174, 1619-28.
- SELIGSON, D. B., HORVATH, S., SHI, T., YU, H., TZE, S., GRUNSTEIN, M. & KURDISTANI, S. K. 2005. Global histone modification patterns predict risk of prostate cancer recurrence. *Nature*, 435, 1262-6.
- SHAIN, A. H., BAGGER, M. M., YU, R., CHANG, D., LIU, S., VEMULA, S., WEIER, J. F., WADT, K., HEEGAARD, S., BASTIAN, B. C. & KIILGAARD, J. F. 2019. The genetic evolution of metastatic uveal melanoma. *Nat Genet*, 51, 1123-1130.
- SHAIN, A. H. & BASTIAN, B. C. 2016. From melanocytes to melanomas. *Nat Rev Cancer*, 16, 345-58.
- SHARAN, R., MARON-KATZ, A. & SHAMIR, R. 2003. CLICK and EXPANDER: a system for clustering and visualizing gene expression data. *Bioinformatics*, 19, 1787-99.
- SHEN, H. & LAIRD, P. W. 2013. Interplay between the cancer genome and epigenome. *Cell*, 153, 38-55.
- SHIELDS, C. L., KALIKI, S., SHAH, S. U., LUO, W., FURUTA, M. & SHIELDS, J. A. 2012. Iris melanoma: features and prognosis in 317 children and adults. *J AAPOS*, 16, 10-6.
- SHIELDS, J. A. & SHIELDS, C. L. 2015. Management of posterior uveal melanoma: past, present, and future: the 2014 Charles L. Schepens lecture. *Ophthalmology*, 122, 414-28.
- SHIRLEY, M. D., TANG, H., GALLIONE, C. J., BAUGHER, J. D., FRELIN, L. P., COHEN, B., NORTH, P. E., MARCHUK, D. A., COMI, A. M. & PEVSNER, J. 2013. Sturge-Weber syndrome and port-wine stains caused by somatic mutation in GNAQ. *N Engl J Med*, 368, 1971-9.
- SHOUSHTARI, A. N. & CARVAJAL, R. D. 2014. GNAQ and GNA11 mutations in uveal melanoma. *Melanoma Res*, 24, 525-34.
- SILVA-RODRIGUEZ, P., FERNANDEZ-DIAZ, D., BANDE, M., PARDO, M., LOIDI, L. & BLANCO-TEIJEIRO, M. J. 2022. GNAQ and GNA11 Genes: A Comprehensive Review on Oncogenesis, Prognosis and Therapeutic Opportunities in Uveal Melanoma. *Cancers (Basel)*, 14.
- SIMON, J. D., PELES, D., WAKAMATSU, K. & ITO, S. 2009. Current challenges in understanding melanogenesis: bridging chemistry, biological control, morphology, and function. *Pigment Cell Melanoma Res*, 22, 563-79.
- SINGH, A. D., SHIELDS, C. L., SHIELDS, J. A. & DE POTTER, P. 1996. Bilateral primary uveal melanoma. Bad luck or bad genes? *Ophthalmology*, 103, 256-62.
- SINGH, A. D., TURELL, M. E. & TOPHAM, A. K. 2011. Uveal melanoma: trends in incidence, treatment, and survival. *Ophthalmology*, 118, 1881-5.
- SINGH, N., SINGH, R., BOWEN, R. C., ABDEL-RAHMAN, M. H. & SINGH, A. D. 2021. Uveal Melanoma in BAP1 Tumor Predisposition Syndrome: Estimation of Risk. *Am J Ophthalmol*, 224, 172-177.

- SISLEY, K., PARSONS, M. A., GARNHAM, J., POTTER, A. M., CURTIS, D., REES, R. C. & RENNIE, I. G. 2000. Association of specific chromosome alterations with tumour phenotype in posterior uveal melanoma. *Br J Cancer*, 82, 330-8.
- SISLEY, K., RENNIE, I. G., COTTAM, D. W., POTTER, A. M., POTTER, C. W. & REES, R. C. 1990. Cytogenetic findings in six posterior uveal melanomas: involvement of chromosomes 3, 6, and 8. *Genes Chromosomes Cancer*, 2, 205-9.
- SISLEY, K., RENNIE, I. G., PARSONS, M. A., JACQUES, R., HAMMOND, D. W., BELL, S. M., POTTER, A. M. & REES, R. C. 1997. Abnormalities of chromosomes 3 and 8 in posterior uveal melanoma correlate with prognosis. *Genes Chromosomes Cancer*, 19, 22-8.
- SITIWIN, E., MADIGAN, M. C., GRATTON, E., CHEREPANOFF, S., CONWAY, R. M., WHAN, R. & MACMILLAN, A. 2019. Shedding light on melanins within in situ human eye melanocytes using 2-photon microscopy profiling techniques. *Sci Rep*, 9, 18585.
- SLINEY, D. H. 2002. How light reaches the eye and its components. *Int J Toxicol*, 21, 501-9.
- SLOMINSKI, A., TOBIN, D. J., SHIBAHARA, S. & WORTSMAN, J. 2004. Melanin pigmentation in mammalian skin and its hormonal regulation. *Physiol Rev*, 84, 1155-228.
- SLOMINSKI, A., ZMIJEWSKI, M. A. & PAWELEK, J. 2012. L-tyrosine and L-dihydroxyphenylalanine as hormone-like regulators of melanocyte functions. *Pigment Cell Melanoma Res*, 25, 14-27.
- SMIT, K. N., BOERS, R., VAARWATER, J., BOERS, J., BRANDS, T., MENSINK, H., VERDIJK, R. M., VAN, I. W. F. J., GRIBNAU, J., DE KLEIN, A. & KILIC, E. 2022. Genome-wide aberrant methylation in primary metastatic UM and their matched metastases. *Sci Rep*, 12, 42.
- SMITH, J. R., PE'ER, J., BELFORT, R. N., CARDOSO, F., CARVAJAL, R. D., CARVALHO, C., COUPLAND, S. E., DESJARDINS, L., FRANCIS, J. H., GALLIE, B. L., GOMBOS, D. S., GROSSNIKLAUS, H. E., HEEGAARD, S., JAGER, M. J., KALIKI, S., KSANDER, B. R., MAEURER, M., MORENO, E., PULIDO, J. S., RYLL, B., SINGH, A. D., ZHAO, J., PARREIRA, A., WILSON, D. J. & O'BRIEN, J. M. 2019. Proceedings of the Association for Research in Vision and Ophthalmology and Champalimaud Foundation Ocular Oncogenesis and Oncology Conference. *Transl Vis Sci Technol*, 8, 9.
- SQUATRITO, M., VANOLI, F., SCHULTZ, N., JASIN, M. & HOLLAND, E. C. 2012. 53BP1 is a haploinsufficient tumor suppressor and protects cells from radiation response in glioma. *Cancer Res*, 72, 5250-60.
- STARK, R. B., G. 2013. DiffBind: differential binding analysis of ChIP-Seq peak data. Available: <https://bioconductor.statistik.tu-dortmund.de/packages/2.13/bioc/vignettes/DiffBind/inst/doc/DiffBind.pdf>.
- STEHELIN, D., VARMUS, H. E., BISHOP, J. M. & VOGT, P. K. 1976. DNA related to the transforming gene(s) of avian sarcoma viruses is present in normal avian DNA. *Nature*, 260, 170-3.
- STRAHL, B. D. & ALLIS, C. D. 2000. The language of covalent histone modifications. *Nature*, 403, 41-5.
- STRATTON, M. R., CAMPBELL, P. J. & FUTREAL, P. A. 2009. The cancer genome. *Nature*, 458, 719-24.
- STURM, V. & RICHARD, G. 2007. [The prevalence of bilateral malignant uveal melanoma]. *Klin Monbl Augenheilkd*, 224, 770-4.

- SUGAWARA, K., SHIBASAKI, T., TAKAHASHI, H. & SEINO, S. 2016. Structure and functional roles of Epac2 (Rapgef4). *Gene*, 575, 577-83.
- SVEDRUZIC, Z. M. 2011. Dnmt1 structure and function. *Prog Mol Biol Transl Sci*, 101, 221-54.
- TAKEDA, K., TAKAHASHI, N. H. & SHIBAHARA, S. 2007. Neuroendocrine functions of melanocytes: beyond the skin-deep melanin maker. *Tohoku J Exp Med*, 211, 201-21.
- TAMBURRI, S., LAVARONE, E., FERNANDEZ-PEREZ, D., CONWAY, E., ZANOTTI, M., MANGANARO, D. & PASINI, D. 2020. Histone H2AK119 Mono-Ubiquitination Is Essential for Polycomb-Mediated Transcriptional Repression. *Mol Cell*, 77, 840-856 e5.
- TAUBE, J. M., BEGUM, S., SHI, C., ESHLEMAN, J. R. & WESTRA, W. H. 2009. Benign nodal nevi frequently harbor the activating V600E BRAF mutation. *Am J Surg Pathol*, 33, 568-71.
- TESTA, J. R., CHEUNG, M., PEI, J., BELOW, J. E., TAN, Y., SEMENTINO, E., COX, N. J., DOGAN, A. U., PASS, H. I., TRUSA, S., HESDORFFER, M., NASU, M., POWERS, A., RIVERA, Z., COMERTPAY, S., TANJI, M., GAUDINO, G., YANG, H. & CARBONE, M. 2011. Germline BAP1 mutations predispose to malignant mesothelioma. *Nat Genet*, 43, 1022-5.
- THEVENEAU, E. & MAYOR, R. 2012. Neural crest delamination and migration: from epithelium-to-mesenchyme transition to collective cell migration. *Dev Biol*, 366, 34-54.
- TORRES-CABALA, C. A., WANG, W. L., TRENT, J., YANG, D., CHEN, S., GALBINCEA, J., KIM, K. B., WOODMAN, S., DAVIES, M., PLAZA, J. A., NASH, J. W., PRIETO, V. G., LAZAR, A. J. & IVAN, D. 2009. Correlation between KIT expression and KIT mutation in melanoma: a study of 173 cases with emphasis on the acral-lentiginous/mucosal type. *Mod Pathol*, 22, 1446-56.
- TORRES, P., CASTRO, M., REYES, M. & TORRES, V. A. 2018. Histatins, wound healing, and cell migration. *Oral Dis*, 24, 1150-1160.
- TSCHENTSCHER, F., HUSING, J., HOLTER, T., KRUSE, E., DRESEN, I. G., JOCKEL, K. H., ANASTASSIOU, G., SCHILLING, H., BORNFELD, N., HORSTHEMKE, B., LOHMANN, D. R. & ZESCHNIGK, M. 2003. Tumor classification based on gene expression profiling shows that uveal melanomas with and without monosomy 3 represent two distinct entities. *Cancer Res*, 63, 2578-84.
- TSHERNIAK, A., VAZQUEZ, F., MONTGOMERY, P. G., WEIR, B. A., KRYUKOV, G., COWLEY, G. S., GILL, S., HARRINGTON, W. F., PANTEL, S., KRILL-BURGER, J. M., MEYERS, R. M., ALI, L., GOODALE, A., LEE, Y., JIANG, G., HSIAO, J., GERATH, W. F. J., HOWELL, S., MERKEL, E., GHANDI, M., GARRAWAY, L. A., ROOT, D. E., GOLUB, T. R., BOEHM, J. S. & HAHN, W. C. 2017. Defining a Cancer Dependency Map. *Cell*, 170, 564-576 e16.
- VADER, M. J. C., MADIGAN, M. C., VERSLUIS, M., SULEIMAN, H. M., GEZGIN, G., GRUIS, N. A., OUT-LUITING, J. J., BERGMAN, W., VERDIJK, R. M., JAGER, M. J. & VAN DER VELDEN, P. A. 2017. GNAQ and GNA11 mutations and downstream YAP activation in choroidal nevi. *Br J Cancer*, 117, 884-887.
- VALASTYAN, S. & WEINBERG, R. A. 2011. Tumor metastasis: molecular insights and evolving paradigms. *Cell*, 147, 275-92.
- VALENTINI, E., ZAMPIERI, M., MALAVOLTA, M., BACALINI, M. G., CALABRESE, R., GUASTAFIERRO, T., REALE, A., FRANCESCHI, C., HERVONEN, A., KOLLER, B., BERNHARDT, J., SLAGBOOM, P. E.,

- TOUSSAINT, O., SIKORA, E., GONOS, E. S., BREUSING, N., GRUNE, T., JANSEN, E., DOLLE, M. E., MORENO-VILLANUEVA, M., SINDLINGER, T., BURKLE, A., CICCARONE, F. & CAIAFA, P. 2016. Analysis of the machinery and intermediates of the 5hmC-mediated DNA demethylation pathway in aging on samples from the MARK-AGE Study. *Aging (Albany NY)*, 8, 1896-1922.
- VAN DEN BOSCH, T., VAN BEEK, J. G., VAARWATER, J., VERDIJK, R. M., NAUS, N. C., PARIDAENS, D., DE KLEIN, A. & KILIC, E. 2012. Higher percentage of FISH-determined monosomy 3 and 8q amplification in uveal melanoma cells relate to poor patient prognosis. *Invest Ophthalmol Vis Sci*, 53, 2668-74.
- VAN DER KOOIJ, M. K., SPEETJENS, F. M., VAN DER BURG, S. H. & KAPITEIJN, E. 2019. Uveal Versus Cutaneous Melanoma; Same Origin, Very Distinct Tumor Types. *Cancers (Basel)*, 11.
- VAN DER VELDE, A., FAN, K., TSUJI, J., MOORE, J. E., PURCARO, M. J., PRATT, H. E. & WENG, Z. 2021. Annotation of chromatin states in 66 complete mouse epigenomes during development. *Commun Biol*, 4, 239.
- VAN DER VELDEN, P. A., METZELAAR-BLOK, J. A., BERGMAN, W., MONIQUE, H., HURKS, H., FRANTS, R. R., GRUIS, N. A. & JAGER, M. J. 2001. Promoter hypermethylation: a common cause of reduced p16(INK4a) expression in uveal melanoma. *Cancer Res*, 61, 5303-6.
- VAN RAAMSDONK, C. D., BEZROOKOVE, V., GREEN, G., BAUER, J., GAUGLER, L., O'BRIEN, J. M., SIMPSON, E. M., BARSH, G. S. & BASTIAN, B. C. 2009. Frequent somatic mutations of GNAQ in uveal melanoma and blue naevi. *Nature*, 457, 599-602.
- VAN RAAMSDONK, C. D., GRIEWANK, K. G., CROSBY, M. B., GARRIDO, M. C., VEMULA, S., WIESNER, T., OBENAU, A. C., WACKERNAGEL, W., GREEN, G., BOUVIER, N., SOZEN, M. M., BAIMUKANOVA, G., ROY, R., HEGUY, A., DOLGALEV, I., KHANIN, R., BUSAM, K., SPEICHER, M. R., O'BRIEN, J. & BASTIAN, B. C. 2010. Mutations in GNA11 in uveal melanoma. *N Engl J Med*, 363, 2191-9.
- VENKATACHALAM, S., SHI, Y. P., JONES, S. N., VOGEL, H., BRADLEY, A., PINKEL, D. & DONEHOWER, L. A. 1998. Retention of wild-type p53 in tumors from p53 heterozygous mice: reduction of p53 dosage can promote cancer formation. *EMBO J*, 17, 4657-67.
- VENTII, K. H., DEVI, N. S., FRIEDRICH, K. L., CHERNOVA, T. A., TIGHIOUART, M., VAN MEIR, E. G. & WILKINSON, K. D. 2008. BRCA1-associated protein-1 is a tumor suppressor that requires deubiquitinating activity and nuclear localization. *Cancer Res*, 68, 6953-62.
- VIDEIRA, I. F., MOURA, D. F. & MAGINA, S. 2013. Mechanisms regulating melanogenesis. *An Bras Dermatol*, 88, 76-83.
- VISCONTE, V., MAKISHIMA, H., JANKOWSKA, A., SZPURKA, H., TRAINA, F., JEREZ, A., O'KEEFE, C., ROGERS, H. J., SEKERES, M. A., MACIEJEWSKI, J. P. & TIU, R. V. 2012. SF3B1, a splicing factor is frequently mutated in refractory anemia with ring sideroblasts. *Leukemia*, 26, 542-5.
- VIVET-NOGUER, R., TARIN, M., ROMAN-ROMAN, S. & ALSAFADI, S. 2019. Emerging Therapeutic Opportunities Based on Current Knowledge of Uveal Melanoma Biology. *Cancers (Basel)*, 11.
- VOGELSTEIN, B. & KINZLER, K. W. 2004. Cancer genes and the pathways they control. *Nat Med*, 10, 789-99.

- VOGELSTEIN, B., PAPADOPOULOS, N., VELCULESCU, V. E., ZHOU, S., DIAZ, L. A., JR. & KINZLER, K. W. 2013. Cancer genome landscapes. *Science*, 339, 1546-58.
- WADDINGTON, C. H. 2012. The epigenotype. 1942. *Int J Epidemiol*, 41, 10-3.
- WADE, N. J. & FINGER, S. 2001. The eye as an optical instrument: from camera obscura to Helmholtz's perspective. *Perception*, 30, 1157-77.
- WAJAPEYEE, N. & GUPTA, R. 2021. Epigenetic Alterations and Mechanisms That Drive Resistance to Targeted Cancer Therapies. *Cancer Res*, 81, 5589-5595.
- WALPOLE, S., PRITCHARD, A. L., CEBULLA, C. M., PILARSKI, R., STAUTBERG, M., DAVIDORF, F. H., DE LA FOUCHARDIERE, A., CABARET, O., GOLMARD, L., STOPPA-LYONNET, D., GARFIELD, E., NJAUW, C. N., CHEUNG, M., TURUNEN, J. A., REPO, P., JARVINEN, R. S., VAN DOORN, R., JAGER, M. J., LUYTEN, G. P. M., MARINKOVIC, M., CHAU, C., POTRONY, M., HOIOM, V., HELGADOTTIR, H., PASTORINO, L., BRUNO, W., ANDREOTTI, V., DALMASSO, B., CICCARESE, G., QUEIROLO, P., MASTRACCI, L., WADT, K., KIILGAARD, J. F., SPEICHER, M. R., VAN POPPELEN, N., KILIC, E., AL-JAMAL, R. T., DIANZANI, I., BETTI, M., BERGMANN, C., SANTAGATA, S., DAHIYA, S., TAIBJEE, S., BURKE, J., POPLAWSKI, N., O'SHEA, S. J., NEWTON-BISHOP, J., ADLARD, J., ADAMS, D. J., LANE, A. M., KIM, I., KLEBE, S., RACHER, H., HARBOUR, J. W., NICKERSON, M. L., MURALI, R., PALMER, J. M., HOWLIE, M., SYMMONS, J., HAMILTON, H., WARRIER, S., GLASSON, W., JOHANSSON, P., ROBLES-ESPINOZA, C. D., OSSIO, R., DE KLEIN, A., PUIG, S., GHIORZO, P., NIELSEN, M., KIVELA, T. T., TSAO, H., TESTA, J. R., GERAMI, P., STERN, M. H., PAILLERETS, B. B., ABDEL-RAHMAN, M. H. & HAYWARD, N. K. 2018. Comprehensive Study of the Clinical Phenotype of Germline BAP1 Variant-Carrying Families Worldwide. *J Natl Cancer Inst*, 110, 1328-1341.
- WALTER, D. M., VENANCIO, O. S., BUZA, E. L., TOBIAS, J. W., DESHPANDE, C., GUDIEL, A. A., KIM-KISELAK, C., CICCHINI, M., YATES, T. J. & FELDSER, D. M. 2017. Systematic In Vivo Inactivation of Chromatin-Regulating Enzymes Identifies Setd2 as a Potent Tumor Suppressor in Lung Adenocarcinoma. *Cancer Res*, 77, 1719-1729.
- WANG, A., PAPNEJA, A., HYRCZA, M., AL-HABEEB, A. & GHAZARIAN, D. 2016. Gene of the month: BAP1. *J Clin Pathol*, 69, 750-3.
- WANG, H. X., QIN, R., MAO, J., HUANG, Q. L., HONG, F., LI, F., GONG, Z. Y., XU, T., YAN, Y., CHAO, S. H., ZHANG, S. K. & CHEN, J. X. 2018. CPEB4 regulates glioblastoma cell proliferation and predicts poor outcome of patients. *Clin Neurol Neurosurg*, 169, 92-97.
- WANG, Y., SUN, Q., YE, Y., SUN, X., XIE, S., ZHAN, Y., SONG, J., FAN, X., ZHANG, B., YANG, M., LV, L., HOSAKA, K., YANG, Y. & NIE, G. 2022. FGF-2 signaling in nasopharyngeal carcinoma modulates pericyte-macrophage crosstalk and metastasis. *JCI Insight*, 7.
- WARDROP, J. 1809. Practical Observations on the Mode of Making the Incision of the Cornea. *Edinb Med Surg J*, 5, 1-7.
- WELCHMAN, R. L., GORDON, C. & MAYER, R. J. 2005. Ubiquitin and ubiquitin-like proteins as multifunctional signals. *Nat Rev Mol Cell Biol*, 6, 599-609.
- WESPISER, M., NEIDHARDT, E. & NEGRIER, S. 2023. Uveal melanoma: In the era of new treatments. *Cancer Treat Rev*, 119, 102599.

- WHITE, V. A., CHAMBERS, J. D., COURTRIGHT, P. D., CHANG, W. Y. & HORSMAN, D. E. 1998. Correlation of cytogenetic abnormalities with the outcome of patients with uveal melanoma. *Cancer*, 83, 354-9.
- WIESNER, T., OBENAU, A. C., MURALI, R., FRIED, I., GRIEWANK, K. G., ULZ, P., WINDPASSINGER, C., WACKERNAGEL, W., LOY, S., WOLF, I., VIALE, A., LASH, A. E., PIRUN, M., SOCCI, N. D., RUTTEN, A., PALMEDO, G., ABRAMSON, D., OFFIT, K., OTT, A., BECKER, J. C., CERRONI, L., KUTZNER, H., BASTIAN, B. C. & SPEICHER, M. R. 2011. Germline mutations in BAP1 predispose to melanocytic tumors. *Nat Genet*, 43, 1018-21.
- WILSON, Y. M., RICHARDS, K. L., FORD-PERRISS, M. L., PANTHIER, J. J. & MURPHY, M. 2004. Neural crest cell lineage segregation in the mouse neural tube. *Development*, 131, 6153-62.
- WILTING, R. H. & DANNENBERG, J. H. 2012. Epigenetic mechanisms in tumorigenesis, tumor cell heterogeneity and drug resistance. *Drug Resist Updat*, 15, 21-38.
- WILTSHIRE, R. N., ELNER, V. M., DENNIS, T., VINE, A. K. & TRENT, J. M. 1993. Cytogenetic analysis of posterior uveal melanoma. *Cancer Genet Cytogenet*, 66, 47-53.
- WINSLOW, T. 2007. *Uveal Melanoma* [Online]. National Cancer Institute. Available: <https://www.cancer.gov/publications/dictionaries/cancer-terms/def/uveal-melanoma> [Accessed].
- WIRIYASERMKUL, P., MORIYAMA, S. & NAGAMORI, S. 2020. Membrane transport proteins in melanosomes: Regulation of ions for pigmentation. *Biochim Biophys Acta Biomembr*, 1862, 183318.
- WOLCHOK, J. D., WEBER, J. S., MAIO, M., NEYNS, B., HARMANKAYA, K., CHIN, K., CYKOWSKI, L., DE PRIL, V., HUMPHREY, R. & LEBBE, C. 2013. Four-year survival rates for patients with metastatic melanoma who received ipilimumab in phase II clinical trials. *Ann Oncol*, 24, 2174-80.
- WOLF, S. F., JOLLY, D. J., LUNNEN, K. D., FRIEDMANN, T. & MIGEON, B. R. 1984. Methylation of the hypoxanthine phosphoribosyltransferase locus on the human X chromosome: implications for X-chromosome inactivation. *Proc Natl Acad Sci U S A*, 81, 2806-10.
- WU, X. N., SHI, T. T., HE, Y. H., WANG, F. F., SANG, R., DING, J. C., ZHANG, W. J., SHU, X. Y., SHEN, H. F., YI, J., GAO, X. & LIU, W. 2017. Methylation of transcription factor YY2 regulates its transcriptional activity and cell proliferation. *Cell Discov*, 3, 17035.
- XIE, D., PEI, Q., LI, J., WAN, X. & YE, T. 2021. Emerging Role of E2F Family in Cancer Stem Cells. *Front Oncol*, 11, 723137.
- YAMAGUCHI, Y. & HEARING, V. J. 2014. Melanocytes and their diseases. *Cold Spring Harb Perspect Med*, 4.
- YANG, S. H. & SHARROCKS, A. D. 2006. Convergence of the SUMO and MAPK pathways on the ETS-domain transcription factor Elk-1. *Biochem Soc Symp*, 121-9.
- YANG, Y., ZHANG, M. & WANG, Y. 2022. The roles of histone modifications in tumorigenesis and associated inhibitors in cancer therapy. *Journal of the National Cancer Center*, 2, 277-290.
- YAVUZYIGITOGU, S., KOOPMANS, A. E., VERDIJK, R. M., VAARWATER, J., EUSSEN, B., VAN BODEGOM, A., PARIDAENS, D., KILIC, E., DE KLEIN, A. & ROTTERDAM OCULAR MELANOMA

- STUDY, G. 2016a. Uveal Melanomas with SF3B1 Mutations: A Distinct Subclass Associated with Late-Onset Metastases. *Ophthalmology*, 123, 1118-28.
- YAVUZYIGITOGU, S., MENSINK, H. W., SMIT, K. N., VAARWATER, J., VERDIJK, R. M., BEVERLOO, B., BRUGGENWIRTH, H. T., VAN MARION, R., DUBBINK, H. J., PARIDAENS, D., NAUS, N. C., DE KLEIN, A., KILIC, E. & ROTTERDAM OCULAR MELANOMA STUDY, G. 2016b. Metastatic Disease in Polyploid Uveal Melanoma Patients Is Associated With BAP1 Mutations. *Invest Ophthalmol Vis Sci*, 57, 2232-9.
- YOSHIDA, K., SANADA, M., SHIRAISHI, Y., NOWAK, D., NAGATA, Y., YAMAMOTO, R., SATO, Y., SATO-OTSUBO, A., KON, A., NAGASAKI, M., CHALKIDIS, G., SUZUKI, Y., SHIOSAKA, M., KAWAHATA, R., YAMAGUCHI, T., OTSU, M., OBARA, N., SAKATA-YANAGIMOTO, M., ISHIYAMA, K., MORI, H., NOLTE, F., HOFMANN, W. K., MIYAWAKI, S., SUGANO, S., HAFERLACH, C., KOEFFLER, H. P., SHIH, L. Y., HAFERLACH, T., CHIBA, S., NAKAUCHI, H., MIYANO, S. & OGAWA, S. 2011. Frequent pathway mutations of splicing machinery in myelodysplasia. *Nature*, 478, 64-9.
- YOUN, A., KIM, K. I., RABADAN, R., TYCKO, B., SHEN, Y. & WANG, S. 2018. A pan-cancer analysis of driver gene mutations, DNA methylation and gene expressions reveals that chromatin remodeling is a major mechanism inducing global changes in cancer epigenomes. *BMC Med Genomics*, 11, 98.
- YU, G., WANG, L. G. & HE, Q. Y. 2015. ChIPseeker: an R/Bioconductor package for ChIP peak annotation, comparison and visualization. *Bioinformatics*, 31, 2382-3.
- YU, H., KUMAR, S. M., KOSSENKOV, A. V., SHOWE, L. & XU, X. 2010. Stem cells with neural crest characteristics derived from the bulge region of cultured human hair follicles. *J Invest Dermatol*, 130, 1227-36.
- YU, L., ZHOU, D., ZHANG, G., REN, Z., LUO, X., LIU, P., PLOUFFE, S. W., MENG, Z., MOROISHI, T., LI, Y., ZHANG, Y., BROWN, J. H., LIU, S. & GUAN, K. L. 2022. Co-occurrence of BAP1 and SF3B1 mutations in uveal melanoma induces cellular senescence. *Mol Oncol*, 16, 607-629.
- ZECCA, L., CASELLA, L., ALBERTINI, A., BELLEI, C., ZUCCA, F. A., ENGELEN, M., ZADLO, A., SZEWCZYK, G., ZAREBA, M. & SARNA, T. 2008. Neuromelanin can protect against iron-mediated oxidative damage in system modeling iron overload of brain aging and Parkinson's disease. *J Neurochem*, 106, 1866-75.
- ZENG, Y. & CHEN, T. 2019. DNA Methylation Reprogramming during Mammalian Development. *Genes (Basel)*, 10.
- ZHAO, S., ALLIS, C. D. & WANG, G. G. 2021. The language of chromatin modification in human cancers. *Nat Rev Cancer*, 21, 413-430.
- ZHAO, W., STEINFELD, J. B., LIANG, F., CHEN, X., MARANON, D. G., JIAN MA, C., KWON, Y., RAO, T., WANG, W., SHENG, C., SONG, X., DENG, Y., JIMENEZ-SAINZ, J., LU, L., JENSEN, R. B., XIONG, Y., KUPFER, G. M., WIESE, C., GREENE, E. C. & SUNG, P. 2017. BRCA1-BARD1 promotes RAD51-mediated homologous DNA pairing. *Nature*, 550, 360-365.
- ZHILNIKOVA, M. V., TROITSKAYA, O. S., NOVAK, D. D., ATAMANOV, V. V. & KOVAL, O. A. 2024. Uveal Melanoma: Molecular and Genetic Mechanisms of Development and Therapeutic Approaches. *Molecular Biology*, 58, 165-177.



ZHONG, Z., ZHOU, F., WANG, D., WU, M., ZHOU, W., ZOU, Y., LI, J., WU, L. & YIN, X. 2018. Expression of KLF9 in pancreatic cancer and its effects on the invasion, migration, apoptosis, cell cycle distribution, and proliferation of pancreatic cancer cell lines. *Oncol Rep*, 40, 3852-3860.

# Appendix

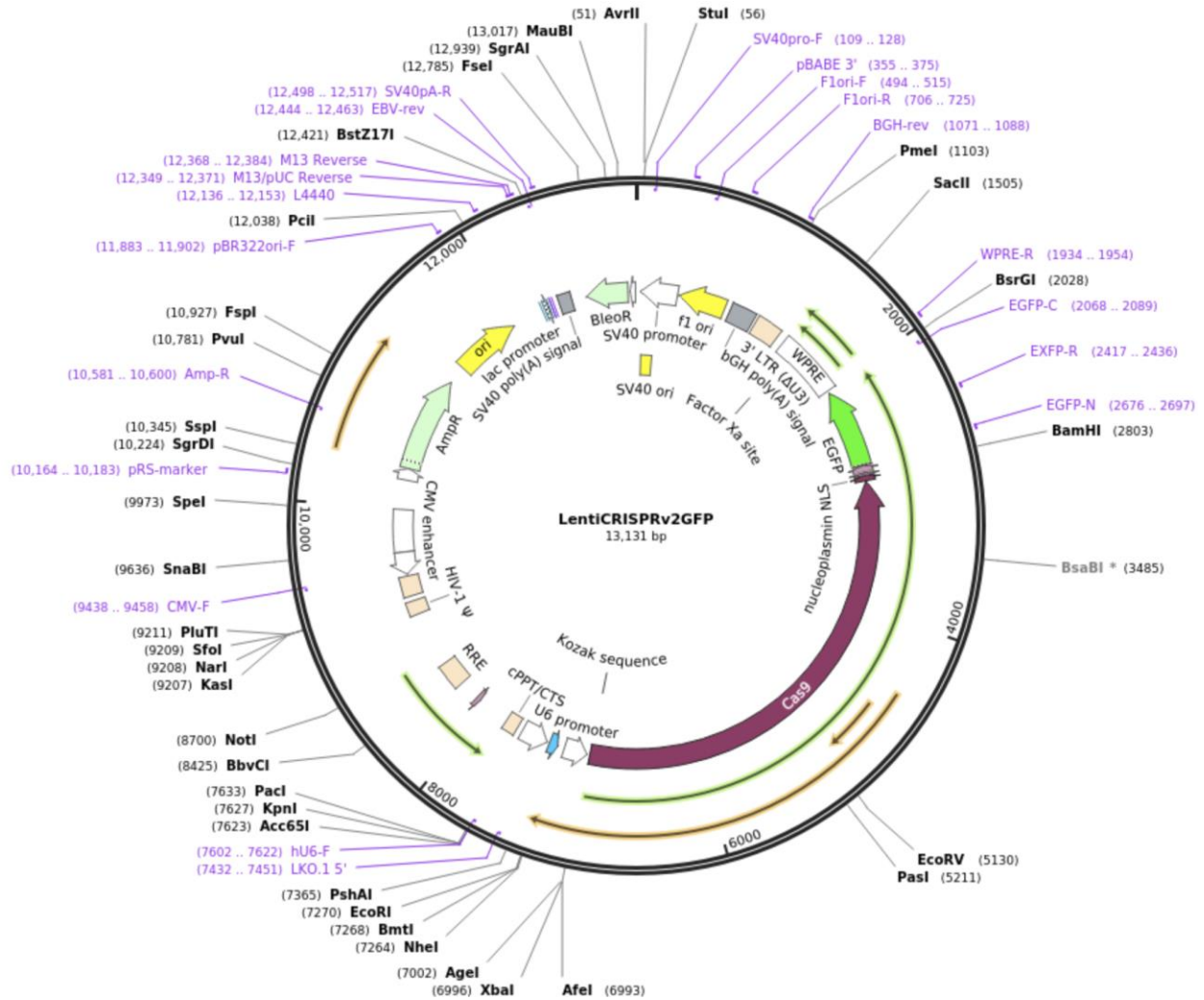


Figure 82: Plasmid map of LentiCRISPRv2GFP vector. (Walter et al., 2017).

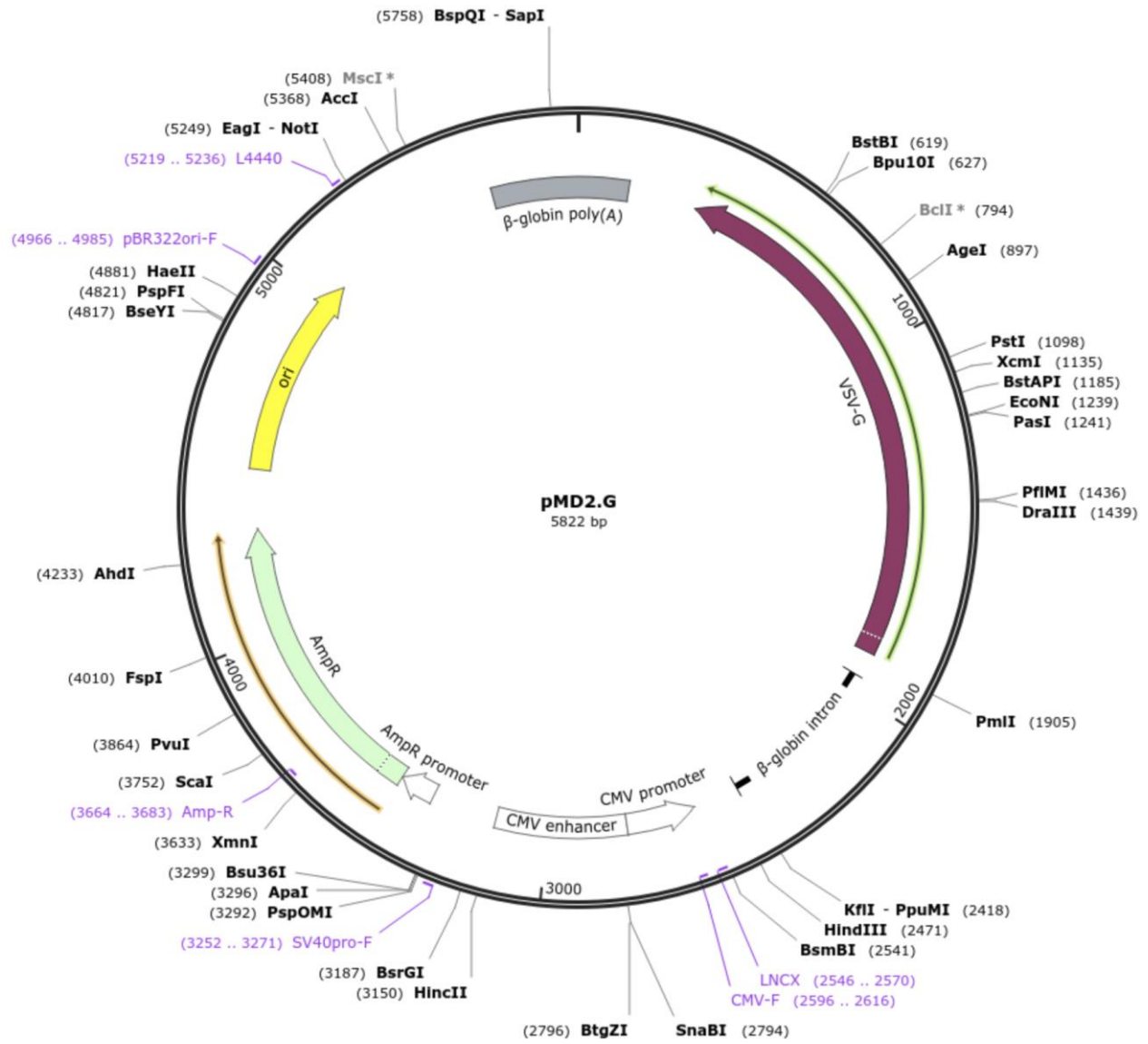


Figure 83: Plasmid map of pMD2.G vector.

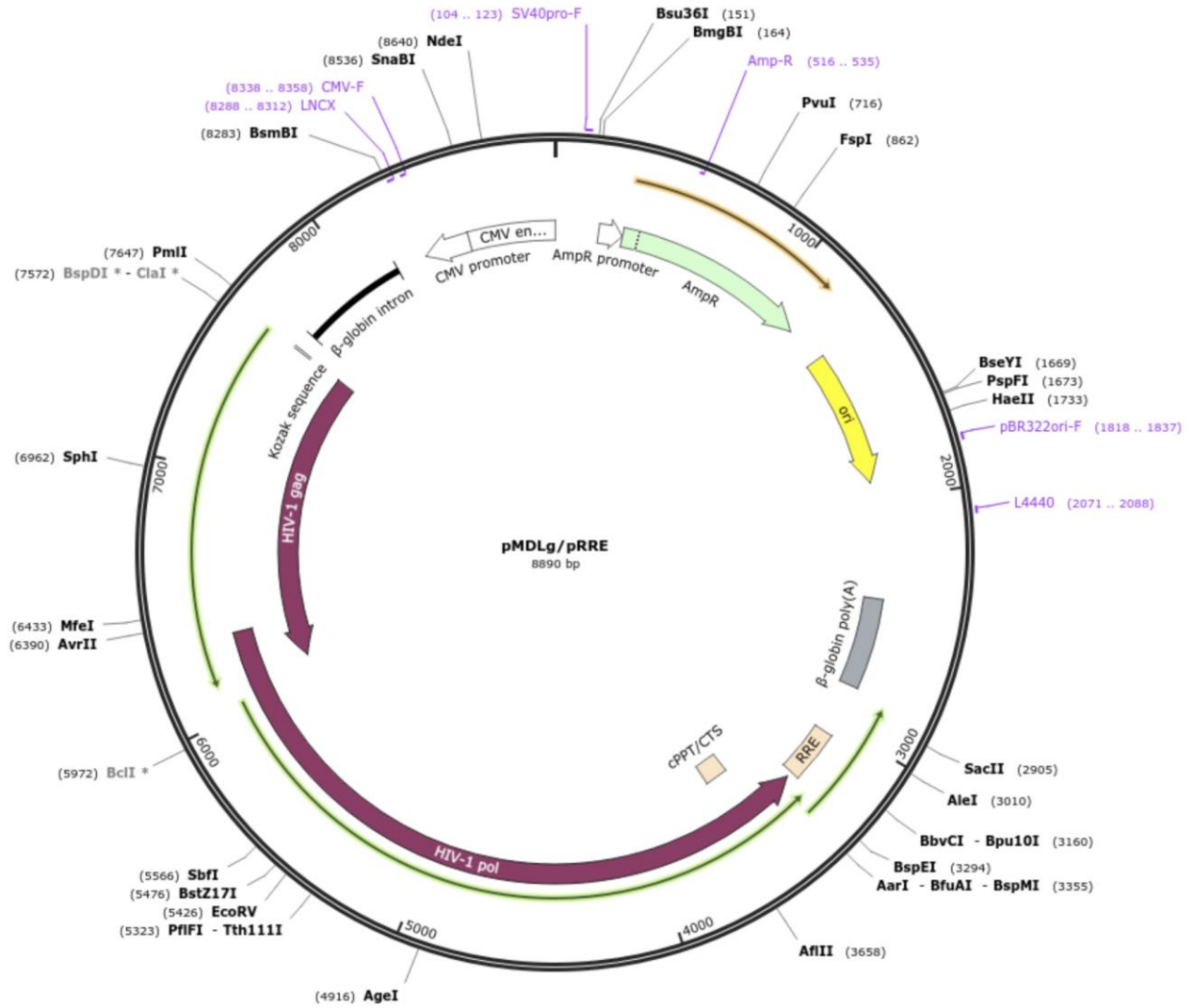


Figure 84: Plasmid map of pMDLg/pRRE vector. (Dull et al., 1998).

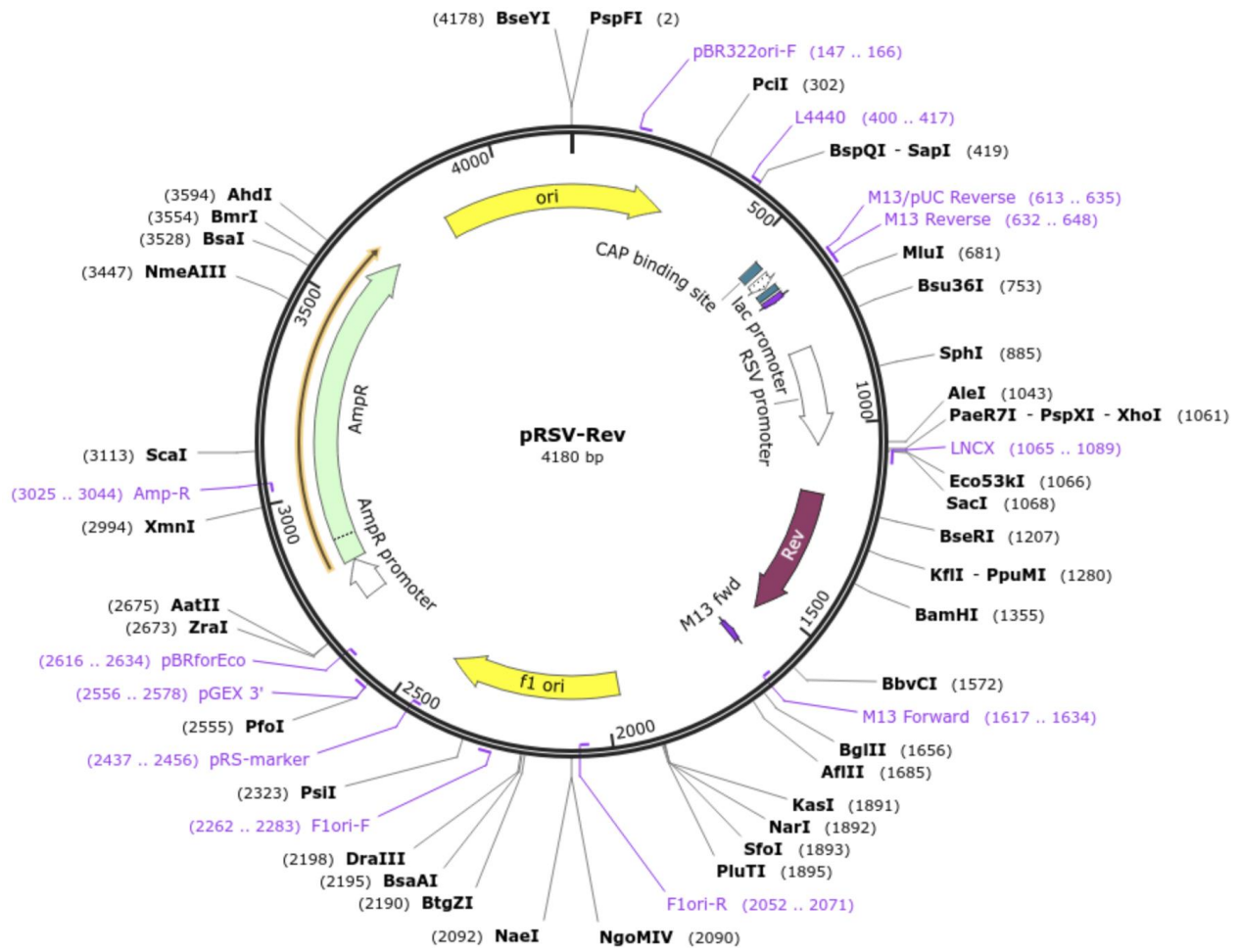
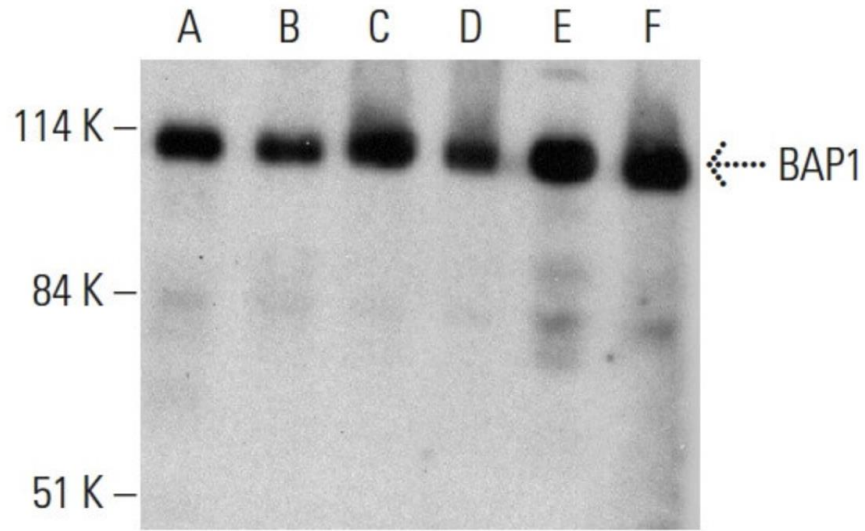
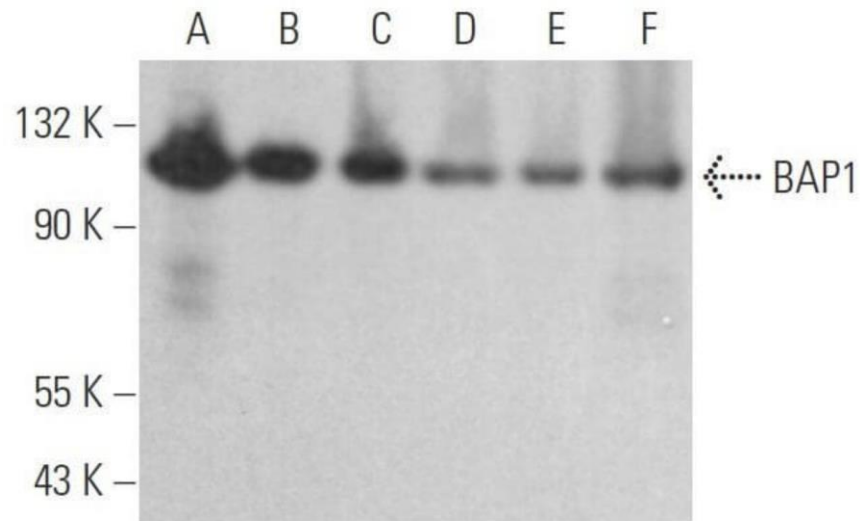


Figure 85: Plasmid map of pRSV-Rev vector. (Dull et al., 1998).



**Figure 86: Antibody manufacturer's Western blot result for BAP1 (C-4 clone) expression in (A) KNRK, (B) PC-3, (C) A-431, (D) MCF7, (E) Jurkat and (F) THP-1 whole cell lysates.** [https://www.scbt.com/p/bap1-antibody-c-4?srsId=AfmBOopjaSo8KuuAoaY\\_cY8Rjnt5nWzWg0BM5Uq1JmE5uNMUbPJdEf1](https://www.scbt.com/p/bap1-antibody-c-4?srsId=AfmBOopjaSo8KuuAoaY_cY8Rjnt5nWzWg0BM5Uq1JmE5uNMUbPJdEf1)



**Figure 87: Antibody manufacturer's Western blot result of BAP1 (C-4 clone) in (A) KNRK and (B) PC-3 whole cell lysates and (C) A-431, (D) HeLa, (E) MCF7 and (F) Jurkat nuclear extracts.** [https://www.scbt.com/p/bap1-antibody-c-4?srsId=AfmBOopjaSo8KuuAoaY\\_cY8Rjnt5nWzWg0BM5Uq1JmE5uNMUbPJdEf1](https://www.scbt.com/p/bap1-antibody-c-4?srsId=AfmBOopjaSo8KuuAoaY_cY8Rjnt5nWzWg0BM5Uq1JmE5uNMUbPJdEf1)

BD FACSDiva 8.0.1

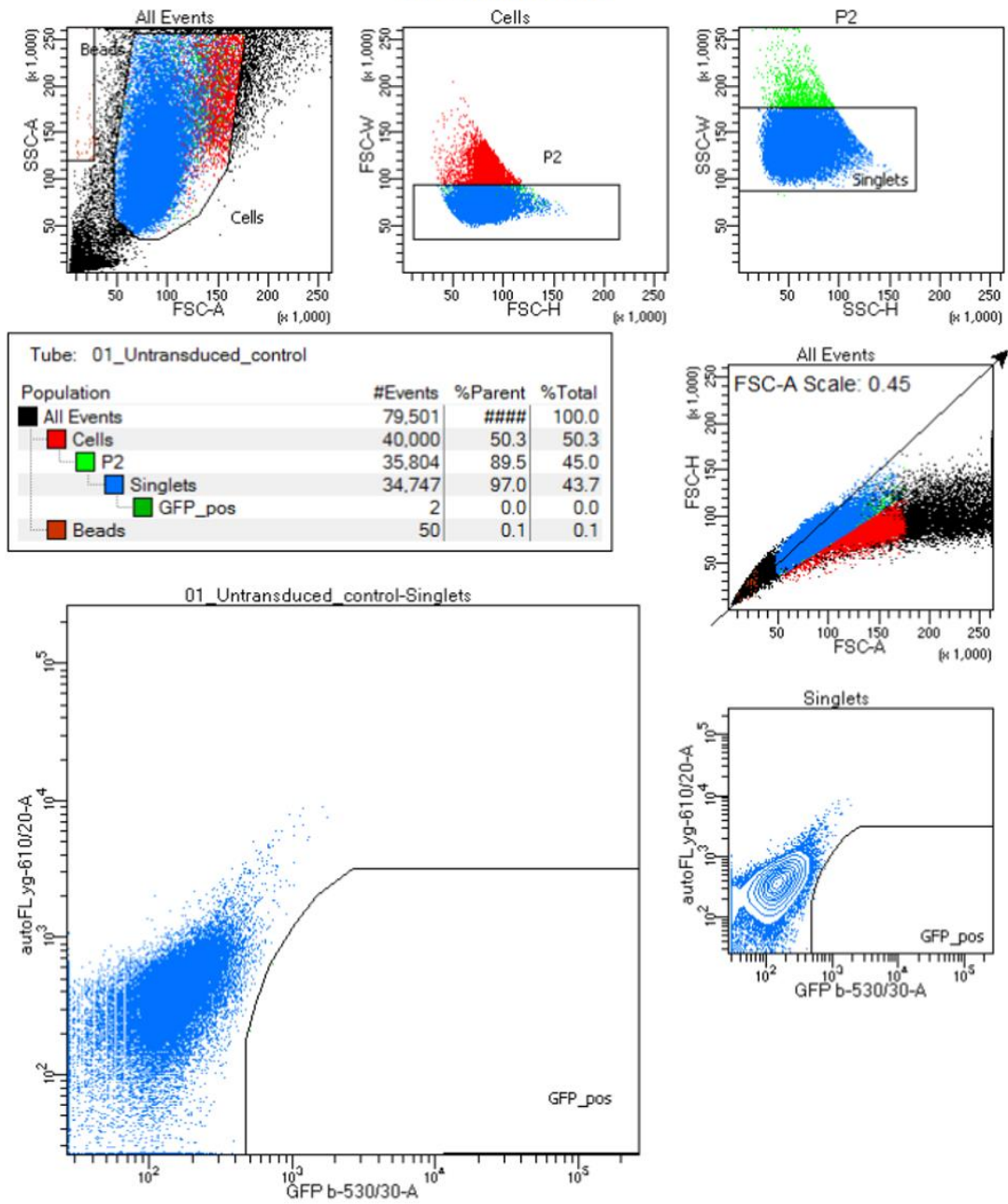
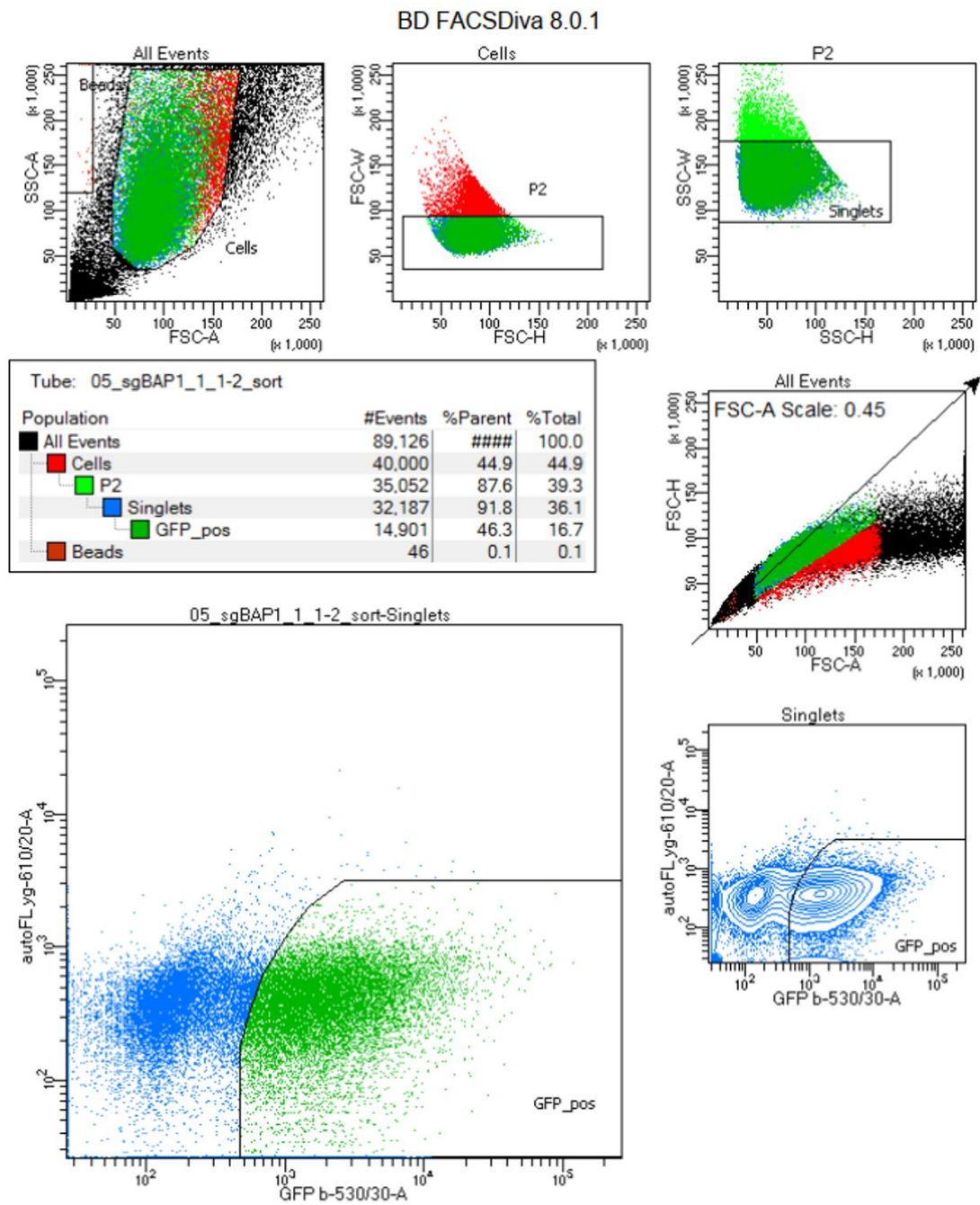


Figure 88: FACS settings and gating strategy for the untransduced MEL202 cells as negative control.





**Figure 89: FACS settings and gating strategy for the transduced MEL202 cells with sgBAP1\_1-Cas9-GFP construct.**



BD FACSDiva 8.0.1

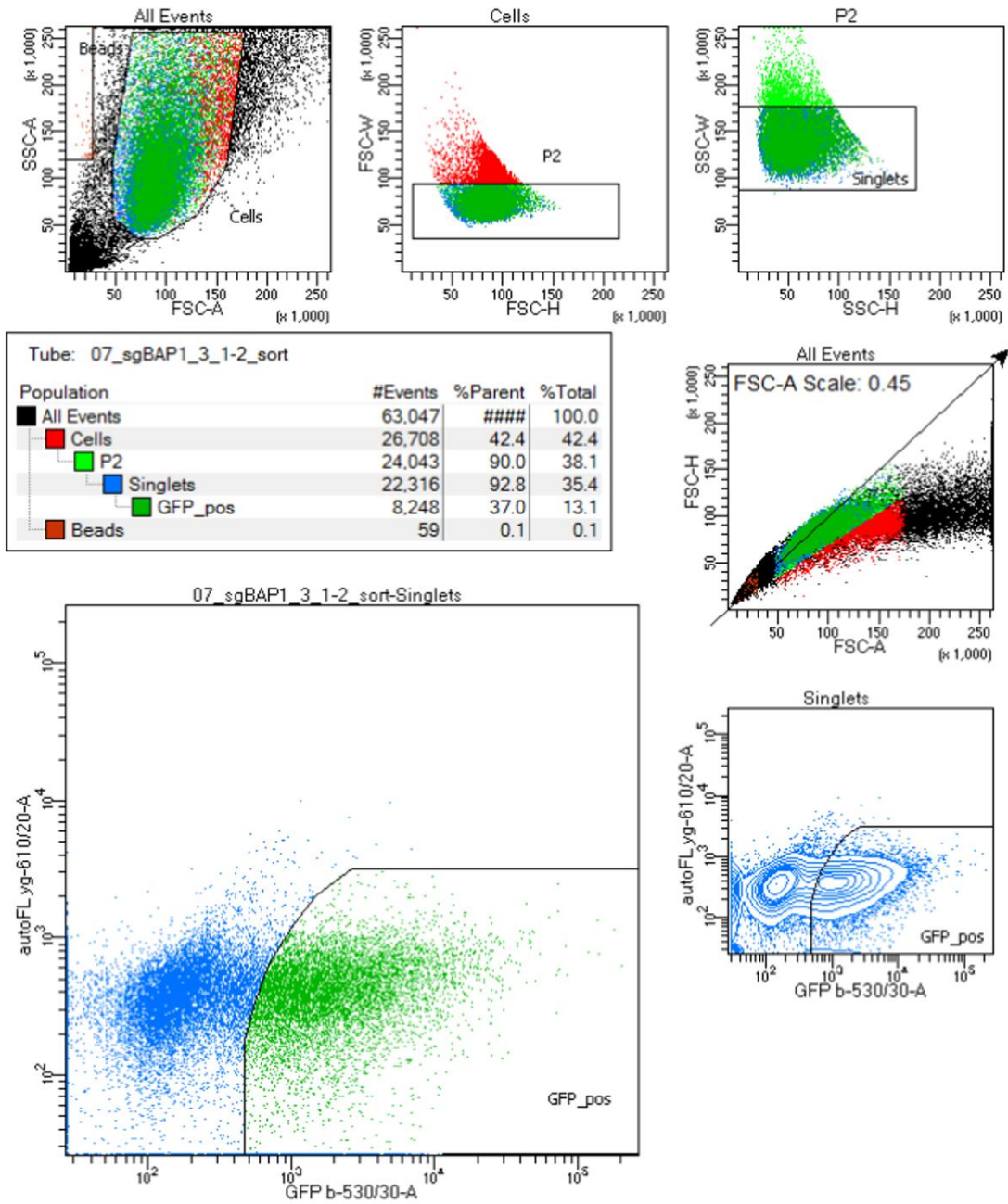
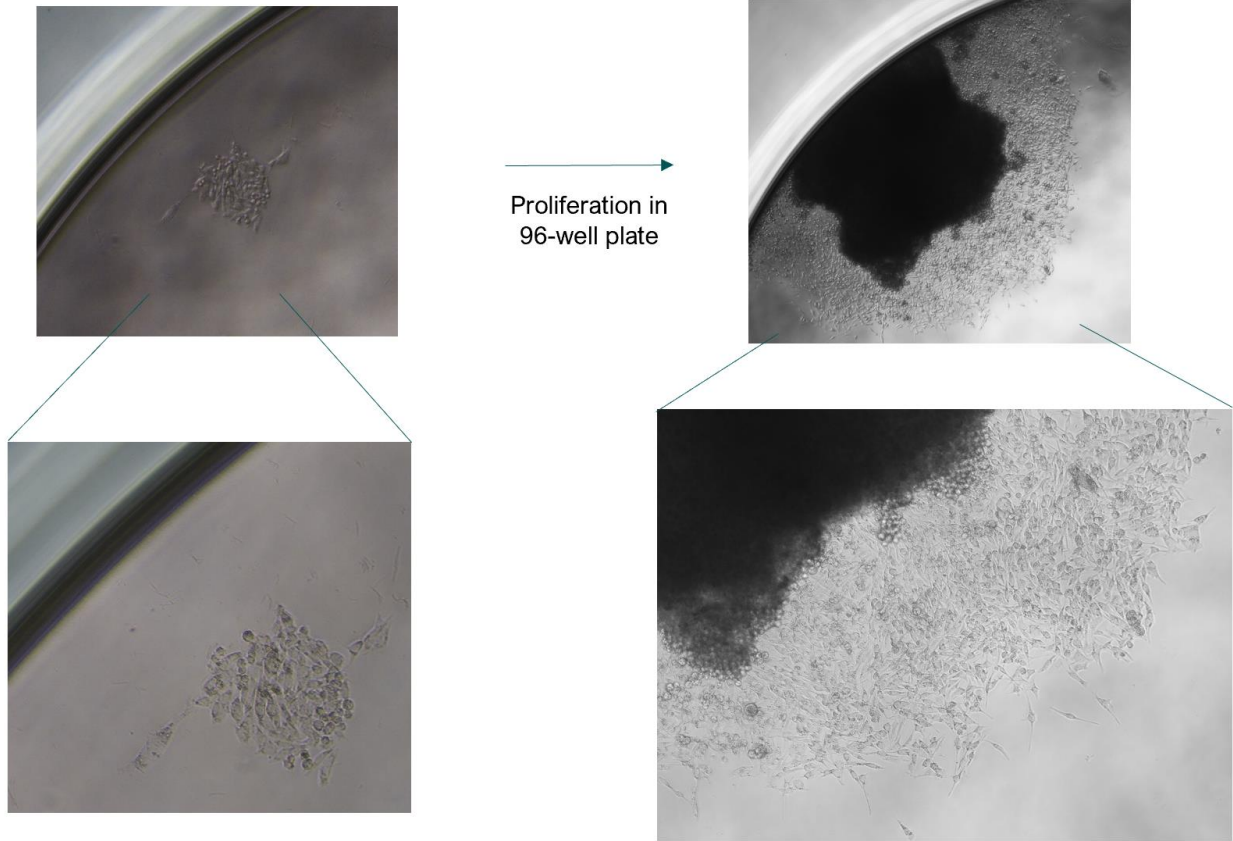
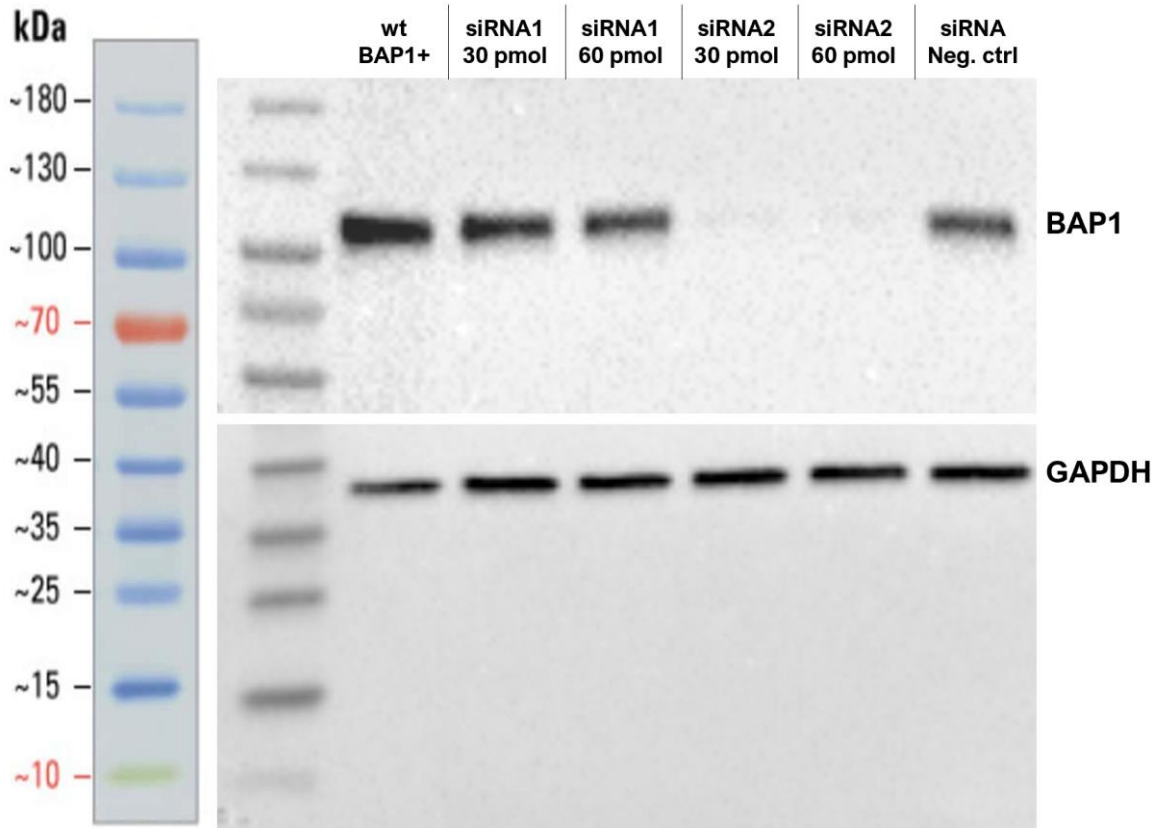


Figure 90: FACS settings and gating strategy for the transduced MEL202 cells with sgBAP1\_3-Cas9-GFP construct.



**Figure 91: Monoclonal growth after one month of the transduced MEL202 cells with sgBAP1\_1-Cas9-GFP construct.**



**Figure 92: Western blot result for replicates of siRNA-mediated BAP1 knockdown experiment in MEL202 cells, showing the effects of two different siRNAs targeting BAP1 and optimization of their amounts.** siRNA1: Silencer® Select Pre-Designed siRNA, ID: s15820. siRNA2: Silencer® Select Pre-Designed siRNA, ID: s15822. siRNA Neg. ctrl: Silencer™ Select Negative Control No. 1 siRNA.

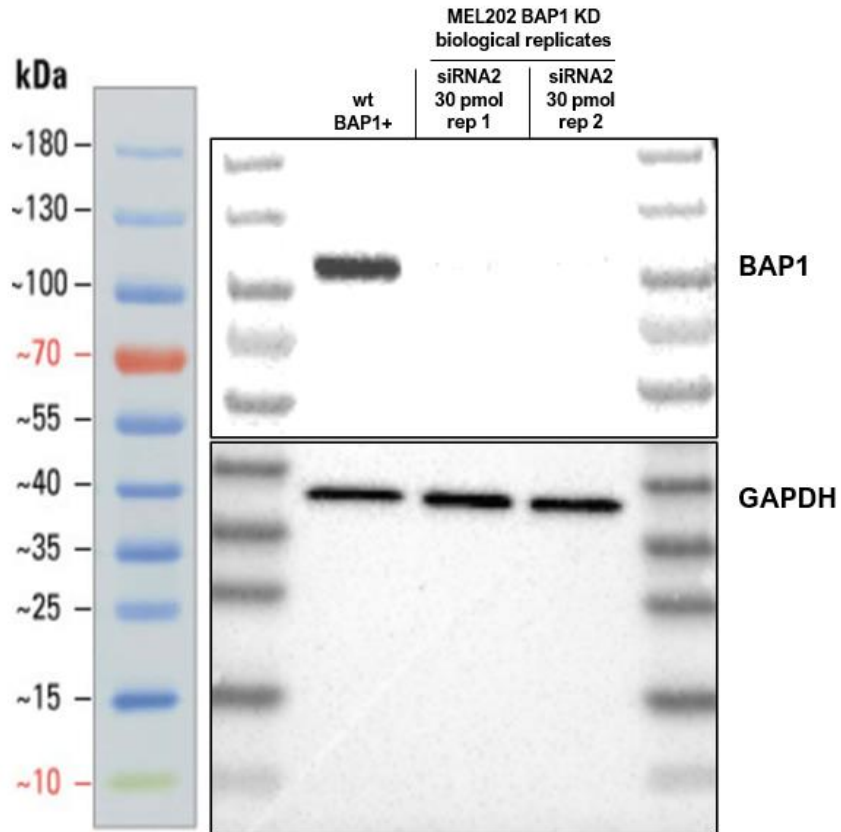


**Figure 93: Different replicates of the siRNA-mediated BAP1 knockdown experiment in MEL202 cells, showing two different replicates using optimized siRNA amount. siRNA2: Silencer® Select Pre-Designed siRNA, ID: s15822.**

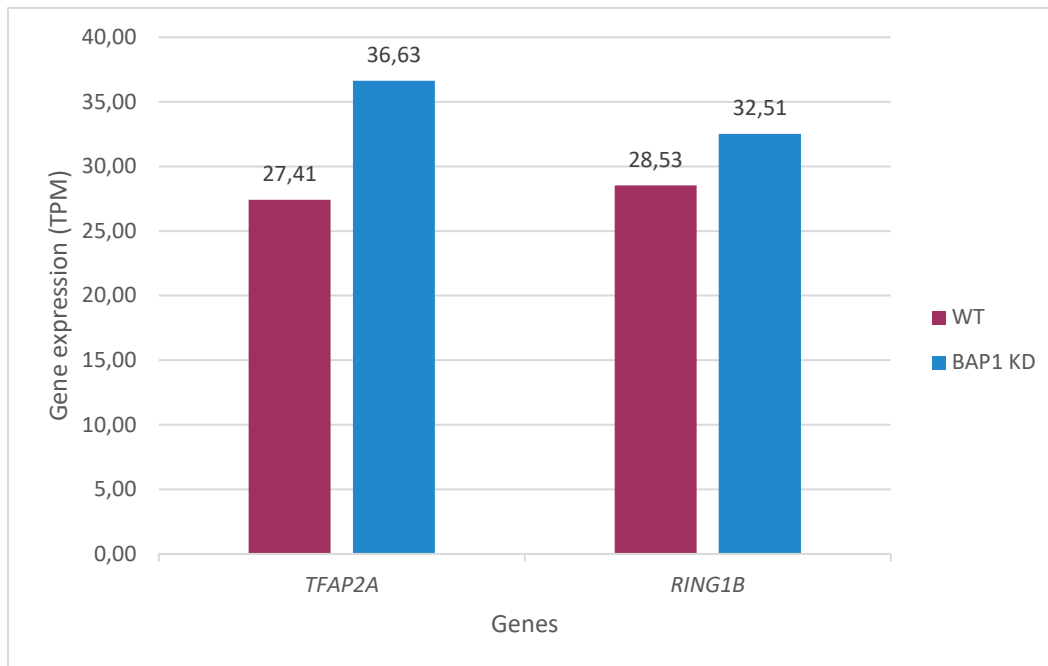


**Figure 94: Changes in the TPM gene expressions of *TFAP2A* and *RING1B* between MEL202 WT / BAP1 KD conditions.**

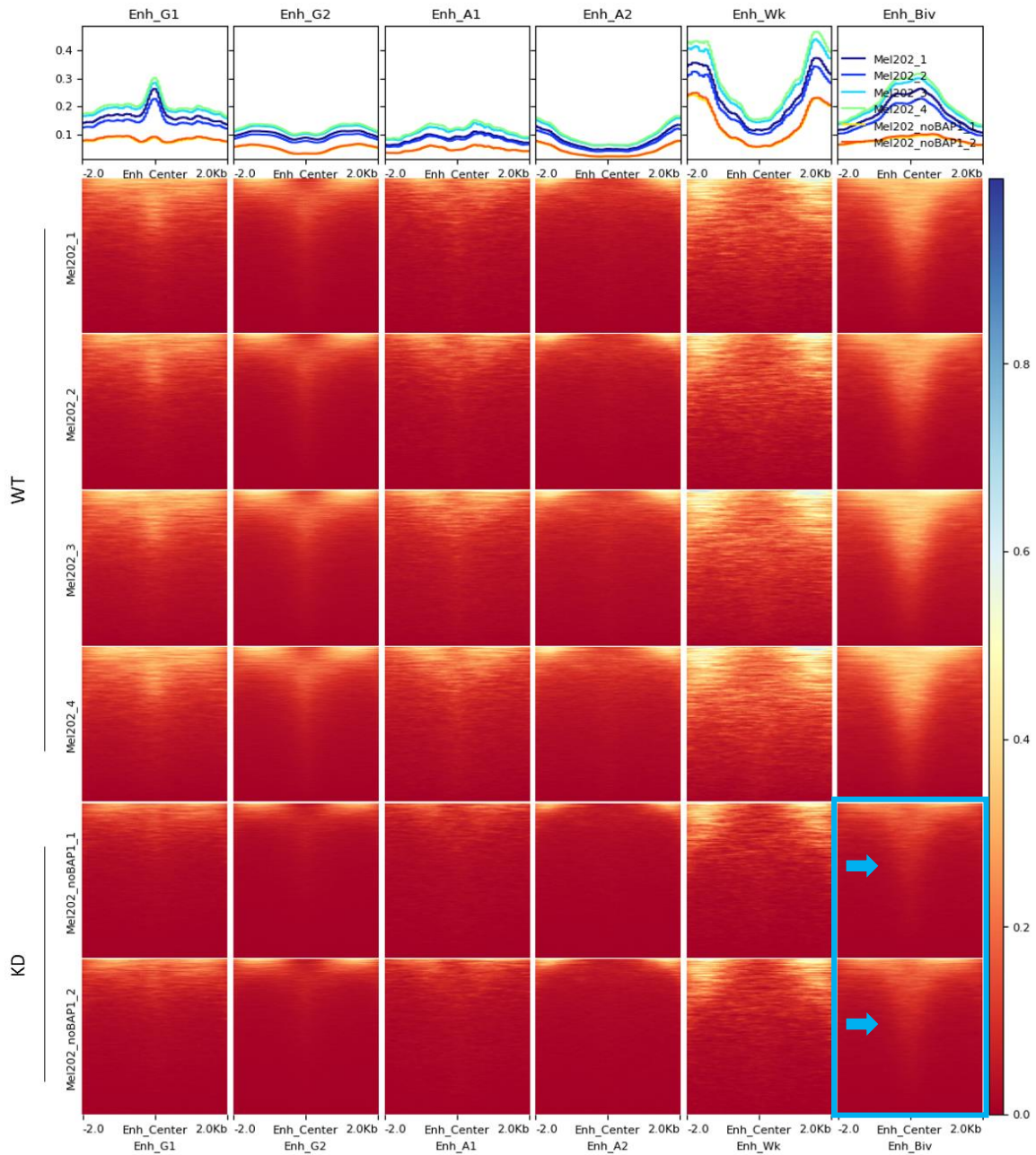


**Figure 95: Chromatin accessibilities shown for the all Enhancer site groups.** Blue arrows within the blue rectangle show the reduction of the chromatin accessibility in the KD condition in the 2 replicates.